KYTHERA

An Extended Duration Robotic Lander Mission to Venus

AE3200: Design Synthesis Exercise

Group 12

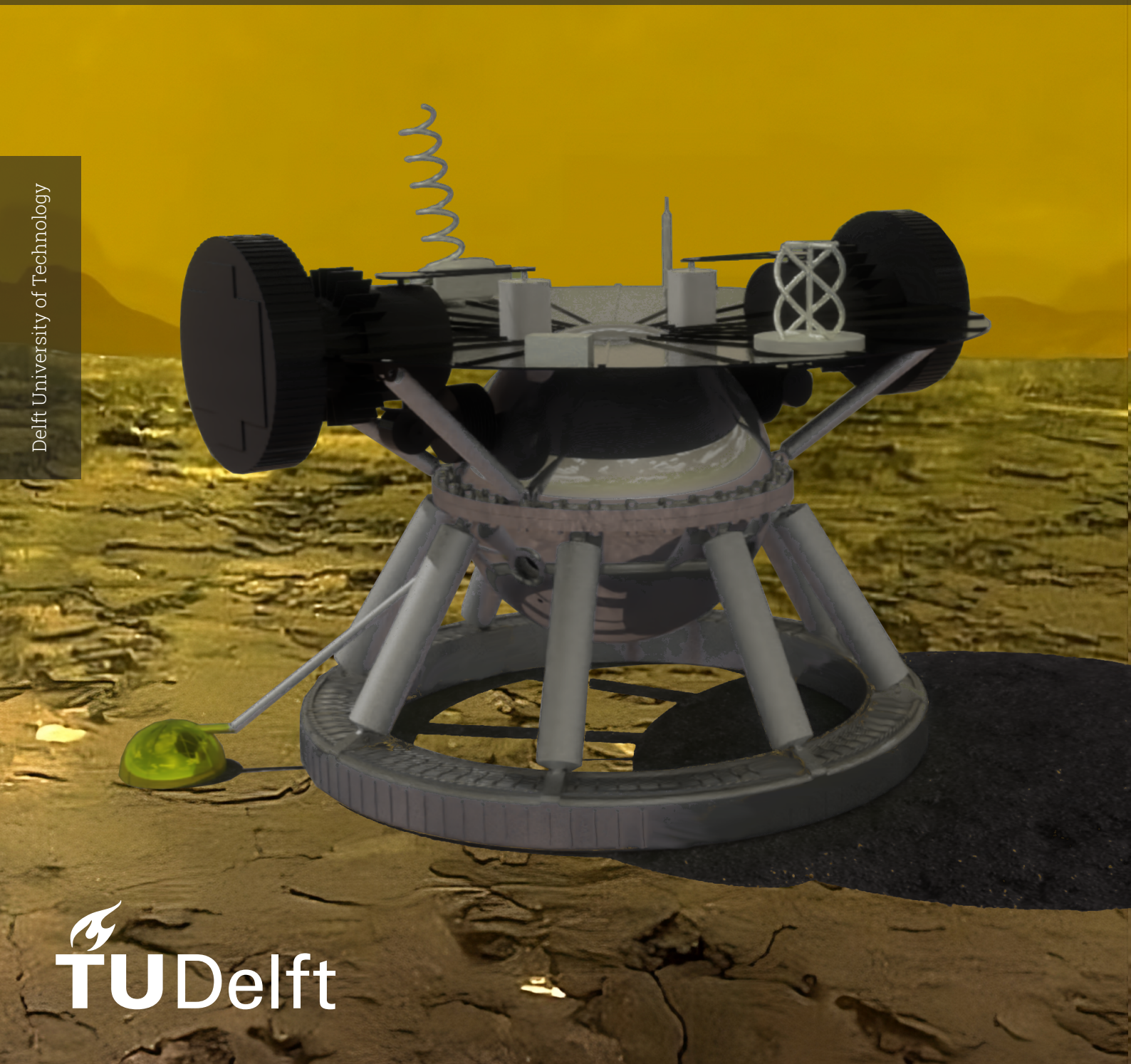

Delft University of Technology

TU Delft

KYTHERA

An Extended Duration Robotic Lander Mission to Venus

by

Group 12

Student Name	Student Number
Gergely Farkas	5739187
Ameline Geldolf	5693063
Luka Lorenci	5749921
Raphael Methner	5523699
Maurizio Pavel	5797144
Laasya Priya Potharaju	5692768
Silvio Topper	5069580
Jutta Van Gestel	5734487
Thomas Wijgerse	5307503
Michael Xin	5687543

Tutor:	Dr. E. S. Steenstra
Coaches:	Dr. E. J. O. Schrama, Y.-C. Lin
Teaching Assistant:	A. Van Parys
Project Duration:	April, 2025 - June, 2025
Faculty:	Faculty of Aerospace Engineering, Delft

Cover: CAD Model of the Lander. Background is a merger of images from Mark Garlick / Science Photo Library / Getty Images and Petapixel / Donald Mitchell / Jason Major

Style: TU Delft Report Style

TU Delft

Contents

Executive Overview

Introduction

Venus is not only Earth's closest planetary neighbor, but also the most similar planet that we know of. Even so, the surface conditions could not be further apart, with Venus being the hottest planet in the Solar System. Exploration to the bottom of its crushing atmosphere has been very limited, and hasn't been attempted since Vega 2 in 1985. This is why KYTHERA is going back to the hellish landscape; and with improved technology, it will operate for more than 6 Earth months. This report will describe how this highly challenging and unique mission will be fulfilled, as well as the preliminary design of the vehicle that will execute it.

Mission Motivation and Objectives

An important part of any project is its identity, which stems from its mission and goals. Top-level requirements are constructed first, combining user requirements with mission requirements and system requirements. These represent the requirements set forth by the Project Guide as well as the scientific community and are used to lead the project into the best direction.

KYTHERA's objectives revolve around the much-needed investigations of Venus's lower atmosphere and surface, which have been prohibited by the thick cloud cover. New information pertaining to the geological makeup of Venus could help the scientific community better understand its formation, and, indirectly, Earth's history. It is for this reason that KYTHERA aims to perform the most detailed surface and lower atmospheric measurements yet, and survive on Venus for extended durations of time.

For the construction of its identity, the KYTHERA team formulated a Mission Need and Project Objective Statement, flowing from user requirements and the team's objectives and intentions:

Mission Need Statement: *To expand our understanding of Venus's evolution by collecting and returning data on its lower atmospheric, seismic, and geochemical properties over at least 200 Earth days.*

Project Objective Statement: *To design a system capable of conducting long-duration in-situ measurements of the Venusian lower atmosphere and surface by 10 students in 10 weeks.*

KYTHERA aims to conduct seismic and atmospheric chemical analyses, study surface rock composition, and operate on Venus for at least 200 Earth days. It must land in the volcanic plains, weigh no more than 350 kg, and stay within a 200 million euro budget.

Market Analysis

In the market analysis the Strengths, Weaknesses, Opportunities and Threats to the KYTHERA mission were identified and analyzed. Furthermore, all the stakeholders were identified where the primary stakeholders were found to be the Venus orbiter team, the space agency and the mission operators. The geological, seismological and atmospheric science opportunities were discovered.
Lastly, comparable missions were analyzed. These include the past Venera missions, Venera-17, VOICE, AREE, Venus Life Finder, DAVINCI and SAEVe. Among all of those the KYTHERA mission was found to be unique mostly because of its mission duration of 200 days. This makes the variety of scientific data that will be collected extra valuable. Furthermore, the lander has an advanced and unique power and thermal control subsystem.

Sustainable Development Strategy

Sustainable development has been defined for the purpose of this project as "development that meets the needs of the present without compromising the ability of further generations to meet their own need". For KYTHERA, sustainability will be a trade-off criteria, but it will not be a major one. It is a very challenging mission with a tight design space, and putting too high of a weight to sustainability would likely drive the performance of the chosen components to an unacceptable extent - it would, indeed, turn out to be killing.

Nevertheless, for the materials used on the lander, manufacturing safety and environmental hazard was considered. Some materials did show superior performance despite being unsustainable, in which case protective equipment, safety briefings, and proper disposal of material scraps will be needed as mitigation.

Looking at the future, in case many more landers will be sent to Venus, sustainability should be greatly improved. For example, a Venus-compliant alternative for Plutonium-based power generation should be found. Since KYTHERA is the

first of its kind, some unsustainable choices were made, which the team acknowledges.

Next to sustainability being taken into account in the design were relevant, KYTHERA will also contribute by sustainability by providing knowledge about Venus' evolution, which might help understand Earth's evolution. This is relevant considering Venus' strong greenhouse effect.

Summary of Previous Trade-offs

This chapter will review the work done in previous reports, namely the Baseline and the Midterm reports.

Mission Architecture Selection

To initiate the design phase, five conceptual architectures were considered: a lander with orbiter, lander with balloon, single lander, multiple landers, and a rover. Each option was evaluated in the context of KYTHERA's mission objectives. A trade-off analysis was then conducted using weighted criteria, including mass, cost, technology readiness level (TRL), reliability, and performance. Among these, cost and performance were assigned the highest weights, while mass and TRL received the lowest. Based on this evaluation, the single lander emerged as the most favorable option, achieving the highest overall score by a considerable margin.

After the tradeoff was finished, a sensitivity analysis was performed by changing the weights of each criterion and then removing one criterion at a time. It was found that the single stationary lander was a robust winner.

Landing Site Selection

One of the most important questions of any mission to the surface of another celestial body is where exactly it will land. However, the limited information about Venus's surface makes this a challenge. The only available information about its surface are from Venera landers and radar mapping missions. From radar data it was possible to discern between distinct geological units, of which the most common is the so-called regional plains, upper unit, or rp1. Its low to moderate surface deformations and its widespread distribution make this terrain the best choice for a safe and scientifically interesting landing site.

Due to communications concerns, the landing site has been chosen to be above 65° N or below 65° S. Additionally, preference was given to sites elevated at high altitudes above the Venus reference level of 0 m, close to active geological features or in the vicinity of canali.

Two finalist candidates were selected. These are circles of 100 km radius, centered at: 69.6° North, 33.0° West (Lakshmi Planum) and 68.75° South, 19.7° West (Lada Terra). Lakshmi Planum is located at 3000 m above Lada Terra, but the former is closer to active tectonic features. As a tradeoff between the two proved inconclusive, it is recommended that in future design steps a working group is established to first set a more thorough methodology for determining safe landing sites and then searching for more landing areas. Lakshmi Planum has been arbitrarily chosen as a primary landing site for the time being.

Systems Engineering

System engineering is critical for the KYTHERA mission as it provides a structured and interdisciplinary approach to designing complex systems. This chapter detailed the work that went into organizing the design process of each component of the lander, as well as planning for post-DSE phases of the project.

Requirements Management

System engineering also plays a crucial role in ensuring stakeholder satisfaction, where top-level requirements are managed through the requirement compliance matrix (RCM), which tracks the status of each requirement and whether they have been met. In this way, accountability and transparency are ensured throughout the mission duration. Subsystem-level requirements need to be verified; this follows from the SMART criteria. The requirement verification methods are given alongside their respective IDs, abiding by the European Corporation for Space Standardization (ECSS).

System Architecture

The system architecture section displays how all the subsystems on the KYTHERA lander interact and where they are installed. Firstly, an N2 diagram is generated, which shows all inputs in parallel and all outputs, as well as how their inputs and outputs overlap with one another. The next diagram used to show relationships between the subsystems is the mechanical block diagram, which shows different connection types between different subsystems. Next, the electrical block diagram displays the electrical power flow between all the components in the lander. Finally, the software block diagram shows all the software and programs required on board and how they interact with each other and external components.

Key Interfaces

For the KYTHERA lander to function well, it is required that key interfaces are defined to ensure seamless integration and reliable inter-operation. The primary mechanical interfaces include the structural connection points between the lander and

the descent system, designed to withstand high entry forces and thermal loads. Electrical interfaces are critical for power distribution and data exchange between subsystems such as avionics, sensors, and the antenna. Thermal interfaces must accommodate both active and passive systems to protect internal components from Venus's hostile environment. External interfaces were also defined, namely connections to the accompanying orbiter that need to be separated, and interfaces required for fueling and other ground operations. Interfaces also include points where different subsystems interact in the process of designing, i.e. where the sizing outputs of one component affect the sizing of another. These have to be kept track off such that everything works well together when the full design is integrated.

Design Phases

The development of the KYTHERA mission is divided into distinct design phases. The ESA design phases are followed, dividing the process in phases A to F. These range from the conceptual design of a mission, to detailed design of the vehicle, all the way to the final operation and decommissioning of the system. This forward looking approach enables the design team to accurately spread the use of resources over time to where they are most needed. Furthermore, every mission design phase is gated by reviews and decision points. This makes sure that every part of the design process has a chance to incorporate feedback and giving ample opportunities to tweak the design and re-baseline schedules. Only moving to the next design phase after these reviews are successful makes sure that any problems are caught early, reducing program risk.

Budgets

To define the scope of the project in terms of maximum allowed mass, power, and cost, engineering budgets are created. These set a maximum for these values and allocate them over different subsystems. This makes sure that all subsystem leads are on the same page on these values in their design. The initial allocation in these budgets is made by estimating the required or wanted values. This was done by looking at relevant examples and by following industry best practices. These engineering budgets are a guide, and were iterated on if necessary. For example, if certain subsystems appeared to require less mass than initially estimated, or vice versa.

Risk Analysis and Management

Risk Analysis and Management was carried out continuously throughout the project. Using this method, risks were identified early in the project. By investigating what risks are most impactful and likely, limited project resources can be allocated efficiently to reduce the overall risk to the development or operation of the system. Furthermore, by identifying risks early, the chance of major redesigns being required during late stages of development is reduced. Risks were identified for all subsystems, and on a system level. For the most critical risks, mitigation strategies were developed. With these mitigation strategies in place, the criticality and severity of these risks were reevaluated. Both the unmitigated and mitigated risks are plotted in risk maps and can be found in their respective subsections.

Subsystems

Entry, Descent and Landing

To deliver the KYTHERA lander to the surface of Venus from Earth, a primary and a backup interplanetary transfer window was selected with arrival dates of 28/Jun/2036 for for the primary, and 25/Jan/2038 for the backup transfer opportunity, respectively. At both of these arrival times, the landing site will be situated on the sunlit side of Venus, therefore optical mapping of the landing ellipse is possible.

The lander, encased in the EDL system (i.e. the entry capsule) will be transported to Venus on a transfer stage. A direct entry procedure will be followed, meaning that the lander will perform atmospheric entry directly from the interplanetary transfer trajectory. The lander and the transfer stage separate approximately two days before entry, after which coasting begins. The transfer stage will use its propulsion system to change its course and perform propulsive capture with a final 24 h period, 0.821 eccentricity polar orbit, where it will function as a communications relay to the lander.

During coast, the EDL system will be supported by a Coasting Stage (CoS). A radiative Cruise Heat Rejection System (CHRS) and an Attitude Control and Determination System (ADCS) will be integrated into the CoS. The CHRS keeps the internal temperature below 60 °C and the ADCS utilizes star trackers and a set of thrusters to control the attitude of the system. The thrusters of the ADCS will also be used to make trajectory corrections and to spin up the capsule to 13.5 RPM before separating from the EDL system. The CoS will be separated 50 minutes before entry.

In transit and coast, a looped heat pipe will be used to transport heat away from the generators. A 56 kg block of paraffin will be used to keep the internal temperature below 65 °C between CoS separation and aeroshell separation.

A baseline design for the entry capsule was made by scaling and modifying the geometry of the Stardust Sample Return Capsule. The scaling factor was 2.7, resulting in a maximum radius of 109.7 cm. The aeroshell angle was increased from 60° to 85° to accommodate the drag plate. The main heat shield half cone angle remained at 60°. These design changes imply that additional aerodynamic and stability analyses will be needed in the next design steps and the feasibility of spin

stabilization need to be reassessed.

The Thermal Protection System (TPS) was sized using a parametric entry trajectory solver and TPS thickness estimator tool developed, named Parametric Entry Trajectory Simulator for Venus (PETS4V). The program was verified and validated by comparison to program output to reference data. PETS4V uses NASA's Venus-GRAM to calculate atmospheric properties during the entry. The Sutton-Graves and Tauber-Sutton (for Venus) relations were used to estimate entry heating. Semi-empirical Mass Estimation Relationships (MERs) were used to estimate the required TPS thickness. Out of the materials considered, only Carbon-Phenolic Atop Carbon-Carbon (CP/ACC) was found feasible for the main heat shield. This is the same material that was used on the Pioneer-Venus probes. For the aeroshell, Acusil-II was selected despite its marginally worse mass performance due to its easier and potentially safer manufacturability. The final heat shield is 8 cm and the aeroshell is 3 cm thick. A safe entry corridor was identified between -11° and -12.8° entry flight path angles for entry speeds lower than 12 km/s.

After the craft has slowed down sufficiently and does not need to be protected from intense heating anymore. A drogue and a Disk-Band-Gap parachute will be deployed at high subsonic speeds to facilitate the separation of the main heat shield and aeroshell deployment. The parachute deployment sequence will begin between 154 and 209 seconds after entry, and will last up to 6 minutes. The lander will reach the ground approximately 42 minutes after the atmospheric interface.

The reliability of the EDL system is conservatively estimated to be at least 91%. This will increase in later stages of the design as more qualification testing is done.

There are still many missing features that could be implemented to improve PETS4V, such as 3D capability. One of the considered heat shield materials, Phenolic Impregnated Carbon Ablator (PICA) was not considered as an aeroshell ablator. However, it could be a promising material for aeroshell applications and it is recommended to conduct research into PICA as a backshell TPS material.

Payload

Detailed design was performed for the various subsystems of the lander. This work in presented in the following sections.

EDL Instruments

During EDL a camera will map the landing site once the heat shield is rejected. The camera selected for this is the KLT-CMFL143004-IMX317 V1.0 equipped with the Sony IMX317 CMOS sensor. In order for the EDL camera to not overheat, it will be surrounded by a paraffin wax phase change material.
Furthermore, the attitude and acceleration of the lander during EDL will be monitored by the LN-200S Internal Measurement Unit developed by Northrop Grumman. This IMU contains three gyroscopes and three accelerometers and will be placed inside the coldbox because of operating temperature limits.

Seismometer

For seismological research, the miniaturized MEMS-based seismometer developed by the NASA HOTTech program is implemented. This specific model has been designed to withstand the harsh surface conditions. It is deployed using an arm powered by a pre-loaded spring damper mechanism. To ensure it is not deployed on a rock or some other obstacle, a system has been implemented that allows for a different deployment location.

Camera

The lander is equipped with four cameras inside its coldbox that reach out to some wide angle lenses through the hotbox using optical fiber cables. These allow the scientist on Earth to visualize the terrain and then choose preferred targets for the chemical analysis of the terrain, as well as making sure that the seismometer is deployed correctly.

Atmospheric Chemical Analysis

Chemical analyses of Venus's atmosphere have been limited to high altitudes due to the opaqueness of its cloud cover. Thus, there is a high demand in further investigation of atmospheric composition and evolution through time. KYTHERA intends to satisfy this need by conducting chemical analyses every 12 hours after landing.

The instrument chosen for this task is a modified instrument already planned to fly on another Venus mission, the DAVINCI mission. The instrument is the Venus Mass Spectrometer, or the VMS, merged with the Venus Tunable Laser Spectrometer, or VTLS for short. The VMS is composed of two major components, the Quadrupole Mass Spectrometer (QMS), and the Noble Gas Trap (NGT). The instruments all work in synchrony to detect, measure and analyze molecules between 1.5 and 535.5 Da to a very high precision.

The instrument was adapted for prolonged operation on Venus's surface by hardening it against higher pressures and temperatures. Additionally, non-sustainable design solutions were eliminated, such as the phase-change cooling of the NGT. The end result is an instrument that can function for the entire length of the mission and that can return valuable data for the scientific community back on Earth.

Geological Chemical Analysis

At the beginning of the KYTHERA mission 20 individual chemical analysis of Venus rock surface material will be conducted. This will be done remotely with the use of Laser Induced Breakdown Spectroscopy and Raman Spectroscopy. LIBS enables the detection of major, minor and trace (low atomic number) elements whereas Raman detects minerals. This means that the instruments highly complement each other. The NASA SuperCam LIBS and Raman spectrometer instruments were found to be the most suitable for this mission. In SuperCam LIBS and Raman are integrated to save for example weight. The geological instruments will be placed inside the coldbox to meet their operating and surviving temperatures. Because the CCD's of the spectrometers on SuperCam had negative operating temperatures new ones were selected by the team and replaced. They are operational up to 30 °C and survive until 50 °C.

The geological analyzer consists of three main instruments: a laser, telescope and a spectrometer unit. The laser will be used to send laser signals through the telescope to the target rock material. After that the telescope will receive the radiation coming back and it will be distributed among the spectrometers for analysis. There will be a laser and telescope in front of every window, which means that there will be four of each, and one spectrometer unit. For each geochemical analysis only one of the lasers and telescopes will be working at a time.

Radiometer, Pressure Sensor, Thermometer and Wind Sensor

The radiometer, pressure sensor, thermometer and the wind sensor are additional instruments of which the team thinks they add extra value to the mission. Radiation measurements will be conducted by the LLISSE radiometer from the outside of the lander. This radiometer is being developed by NASA and was designed for the Venus environment.

Furthermore, the ambient pressure will be measured by the High-Temperature Silicon Carbide (SiC) Pressure Sensor developed by NASA Glenn, which has been proven to work on Venus conditions. The pressure will also be measured inside the coldbox. For this the Keller PAA-33X was selected. This instrument will also serve as a thermometer for the coldbox. The ambient Venus temperature will be measured by a type B thermocouple. It has an excellent high-temperature performance and chemical resistance, but it will still be housed inside a protective sheath made of Inconel or platinum-rhodium to make sure it can be operational for the whole mission. Furthermore, careful calibration of the thermocouple compensation electronics are needed.

For the wind sensor the miniature drag-force anemometer that is being developed by NASA was selected. This wind sensor is designed specifically Venus conditions and is lightweight and has a low power-consumption, which makes it the most suitable option for this mission. It determines the wind speed and direction by measuring the strain in the cantilever beam that is caused by the wind.

Power and Thermal Control

The environment of the Venus surface is one of the harshest in the solar system. The surface temperature can go up to 464 °C and the pressure is up to 93 bar. The surface atmosphere is also rich in carbon dioxide and contains SO_2, making a corrosion-resistant design necessary. Thermal control in any spacecraft can be achieved either passively or actively. Active cooling refers to cooling methods that use electric or mechanical energy or those that are powered through the movement of fluids. In spacecraft design, it is normally desired to only implement passive cooling methods if possible to reduce the power, mass, complexity, and cost of the system. However, given the harsh environment of Venus, it was concluded early that active cooling methods would be necessary for the lander to survive for a long-duration. The Venera landers launched by the Soviet Union throughout the 1960s to 1980s did not have any significant active cooling units and the longest surviving mission at the Venus surface lasted just under 2 hours. The main cooling function will thus be achieved through the use of active coolers, and passive cooling methods will also be implemented to supplement the cooling function and reduce the workload of the active cooling system.

Next to the thermal control, the power subsystem is also an important aspect for any spacecraft. Electricity is required to power the instruments onboard. The main components of the power subsystem includes primary power, secondary power, and distribution systems. In simple terms, the primary power is responsible for generating electricity, the secondary power stores electricity and is to be used when the demand of electricity is high and the power provided by the primary source is inefficient, and the distribution systems distributes and regulates the electric power going into each component. As will be explained in the report, a single Stirling cycle based system can be used to provide both active cooling and power generation. For this reason, the power and thermal control is considered to be a single subsystem for KYTHERA.

A Stirling cycle based system is used for active thermal control and electric power generation for KYTHERA. The working principles is as follows: A set of seven GPHS (General purpose heat source) modules which houses plutonium-238 supplies thermal energy to the Stirling generator. The Stirling generator converts this to mechanical energy via movements of pistons and displacers. This is connected mechanically to two chain sprockets via a crankshaft; one of them is connected to an alternator that generates electricity from the rotational motion of the crankshaft and the chain sprocket, the other is connected to the piston and displacer of a Stirling cooler that performs the active cooling for KYTHERA. This set up allows the active cooling to be achieved purely mechanically, without the use of any direct electric power. As the working temperature of the GPHS modules is up to 1200 °C, they need to be well insulated and placed far away from the rest of

the lander structure as much as possible. For this reason, the Stirling generators are placed on the drag plate. Two units of the Stirling generators and coolers are used and are placed at an 180 degree angle from each other.

In order to achieve cooling without requiring megawatts of power, a passive thermal control strategy needed to be designed. No traditional insulation will be used. Instead, KYTHERA's two-shell design will be used to the advantage of thermal control. Both the hotbox and the coldbox will have a vacuum environment. Through vacuum, no conductive or convective heat transfer take place, meaning the only heat leaks of concern are those through radiation and through any mechanical connections between the two boxes. To maintain this vacuum, getters will be implemented, which react with gasses and turn them into solid materials or adsorb them. The total heat leak, using this two-shell vacuum configuration, is 174.3 W. To minimize radiative heat leak (i.e. minimize hotbox size) while still allowing the two boxes to be connected to each other, the hotbox size was constrained to 64 cm in diameter. That is, the difference between the coldbox and hotbox radius is 3 cm.

Communications

A monofilar right-hand circularly polarized (RHCP) axial-mode helical antenna has been selected as the primary high-gain antenna (HGA) for the lander. To extend relay duration and improve reliability, a secondary low-gain quadrifilar helical antenna (QHA) is also employed. Both antennas are mounted on the drag plate, directly exposed to the ambient conditions of the Venusian surface.

The antenna is mounted with a fixed offset of 20.4°, and has a motor stage attached to the mounting that allows for antenna rotation on its vertical axis by $\pm 180°$. This mobility allows orientation of the antenna towards Venus's north pole, which is where the apoapsis of the orbit will be to ensure maximum relay window duration. The half-power beamwidth of the HGA is around 42.49° and enables a relay time of around 12.7 hours per 24-hour full orbit. The QHA will also be mounted on the drag plate, opposite the HGA. It provides limited coverage but will still be able to transmit data to the orbiter for 1.9 hours per orbit. Both antennas are connected to a shared transceiver capable of toggling between transmission and reception modes. The transceiver is housed within the actively cooled coldbox and actively maintained at 30°C.

The total uplink data volume per orbit is approximately 6 MB. The same antennas are used for downlink, with the downlink data rate constrained to 400 bits per second to preserve a high link margin and ensure robust data delivery. Both uplink and downlink channels use Binary Phase Shift Keying (BPSK) modulation, along with concatenated Forward Error Correction (FEC) composed of a Reed–Solomon outer code and a convolutional inner code.

Material selection is driven by the need to balance thermal stability, mechanical strength, electrical conductivity, and corrosion resistance in the extreme Venusian environment.

Command and Data Handling

To make sure all the data produced by the different instruments on board is collected, processed, stored and packaged correctly, and that commands that are sent to the lander are implemented properly, a well designed command and data handling (CDH) system is required. The three main elements of this system are the central processing unit (CPU), the volatile memory and the non-volatile memory. The exact models chosen for the lander are a GR740, a DDR3 and a NAND Flash, in the respective order. The team has analyzed all the different data rates, and created a visual map of their flow within the CDH subsystem in the Command and Data Handling Block Diagram. Furthermore, advanced compression algorithms are used by the lander to optimize the use of the limited amount of data that can be sent back.

Structures and Materials

The structures and materials subsystem design starts wit the identification of different loads KYTHERA will experience. These loads include the launch, EDL, landing impact, and static loads that KYTHERA will experience throughout its mission duration. Once these loads were established, the next steps were performed concurrently.

The materials selection of the components of the lander was either done by the subsystem engineers themselves, or by the Materials Engineer. Criteria such as strength, stiffness, transmission transparency, mass, cost, corrosion resistance, sustainability and manufacturability were considered. Additionally, all materials in contact with the Venus atmosphere needed to survive the 464 °C temperature, and all structural materials needed to have a fracture toughness of at least 15 MPa $m^{1/2}$. An overview of which material is used on which component was made in a table. Additionally, a material properties table was constructed listing the selected materials.

The component design was done concurrently with the material selection. The inner sphere was designed first by arranging the payload in a way such that they fit well inside a sphere. The sphere was then dimensioned using literature. This also provided a sizing constraint, in specific a diameter constraint, for the outer sphere. Based on this, the outer sphere thickness and structure was designed. Then, the legs and impact ring were sized using an iterative design. After the sizing for all the components were decided, loading diagrams for the leg components were generated and the natural frequency was calculated.

Following this, a sensitivity analysis and next steps for more accurate design were detailed. The sensitivity analysis

highlights the driving factors for the design and the extent of viability for the current design, while the next steps section details the steps need to be taken for furthering the design after DSE. In the next steps of the design, the structure can still be optimized via a FEM analysis. Some of the materials choices may need to be revised to improve performance.

Integrated Design

The integrated design chapter brought together the subsystems described above into one place. It details the main elements91 of the lander which have been created a result of the needs of the subsystems. The overall configuration of the lander superficially resembles that of previous designs, including the Veneras, but that is because Venus's strict conditions impose an optimum design that all concepts use.

The coldbox is the actively cooled compartment at the core of the lander. It is 58 cm in diameter, weighs 8 kg by itself and houses all the payload and instruments within a highly reflective anti-infrared foil covering.

The hotbox is the outer shell of the lander that provides the structural strength needed to maintain vacuum inside the lander. It is made of Inconel 718, has a diameter of 64 cm and weighs 56 kg. It has numerous holes and cutouts for instruments, cabling and cooling attachments.

The instruments that are housed within the coldbox have access to the outside via windows and atmospheric inlet ports. The geochemical analyzers and the cameras are placed in a symmetric arrangement of 4, giving maximum coverage of the landing site.

The drag plate is used as a mounting point for the power generation system as well as the antennas for the communications system. The heaviest components, the Stirling generators and GPHS units, are placed symmetrically and diametrically opposite of each other to reduce asymmetrical effects.

The EDL system is connected to the lander itself via the use of detachable struts and a cup from the heatshield to the hotbox. This is to reduce the load on the landing ring during the peak acceleration phase of entry and to more uniformly distribute loading during this time.

Conclusion

This report has shown the preliminary design of KYTHERA shown in Figure 1, an extended duration robotic lander mission to the surface of Venus. It has shown both the big-picture view of the lander, and the details of the subsystems that make it up. With all this work finished, it is possible to proceed to the next design stage, and eventually to a 2036 launch towards Venus.

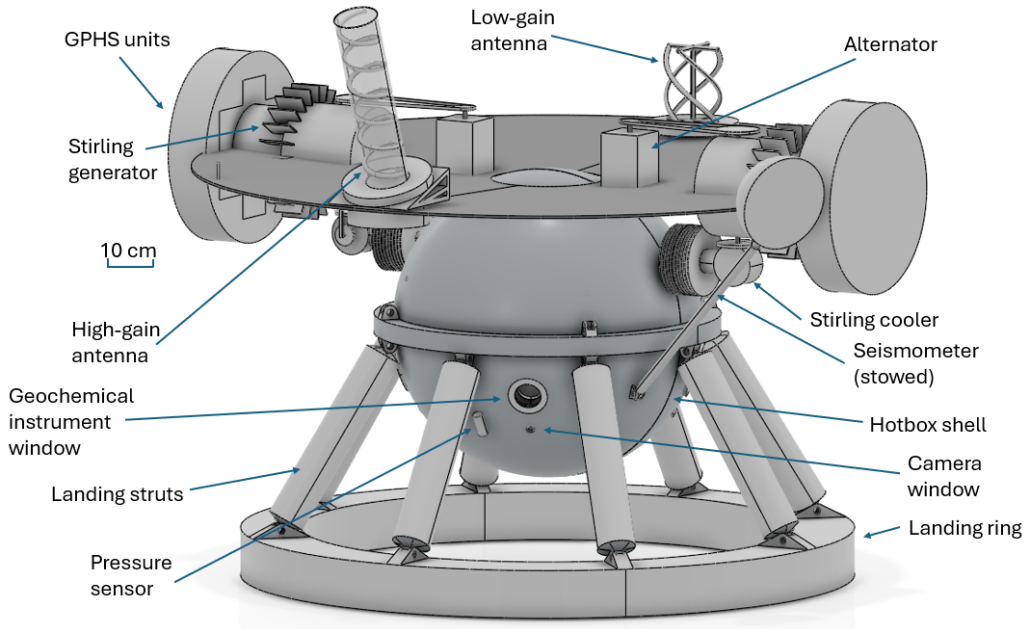

Figure 1: KYTHERA overall configuration.

Nomenclature

Abbreviations

ACA	Atmospheric Chemical Analyzer
ADCS	Attitude Determination and Control System
AM	Amplitude Modulation
AREE	Automaton Rover for Extreme Environments
AS	Aeroshell
ASRG	Advanced Stirling Radioisotope Generator
AWGN	Additive White Gaussian Noise
BER	Bit Error Rate
BPSK	Binary Phase Shift Keying
CAD	Computer-Aided Design
CCD	Charge-Coupled Device
CDH	Command and Data Handling subsystem
CDR	Critical Design Review
CG	Center of Gravity
CHRS	Cruise Heat Rejection System
CMOS	Complementary Metal-Oxide Semiconductor
COM	Communications subsystem
ConOps	Concept of Operations
CoS	Coasting Stage
COSPAR	Commitee on Space Research
CP/ACC	Carbon-Phenolic Atop Carbon-Carbon ablator
CPU	Central Processing Unit
CTE	Coefficient of Thermal Expansion
DAVINCI	Deep Atmosphere Venus Investigation of Noble gases, Chemistry and Imaging
DBG	Disk-Band-Gap parachute
DC	Direct Current
DOT	Design Option Tree
DSE	Design Synthesis Excercise
DSMC	Direct-Simulation Monte Carlo
DSN	Deep Space Network
DTE	Direct-to-Earth link
EDL	Entry, Descent and Landing
EIRP	Effective Isotropic Radiative Power dBm
ESTRACT	European Space Tracking network
FBS	Function Breakdown Structure
FEC	Forward Error Connection
FEM	Finite-Element Method
FFD	Function Flow Diagram
FIAT	Fully Implicit Ablation and Thermal Analysis program
FM	Frequency Modulation
GCA	Geological Chemical Analyzer
GEER	Glenn Extreme Environment Rig
GPHS	General Purpose Heat Source
GRAM	Global Reference Atmospheric Model
HGA	High-Gain Antenna
HPBW	Half-Power Beam Width
HS	Heat Shield
IMU	Inertial Measurement Unit
IR	Infrared
ITLR	Initial Top-Level Requirement
LAURA	Langley Aerothermodynamic Upwind Relaxation Algorithm
LDPC	Low-Density Parity-Check
LGA	Low-Gain Antenna
LHP	Looped Heat Pipe
LIBS	Laser-Induced Breakdown Spectroscopy
LLISSE	Long-Lived In-Situ Solar System Explorer
LOS	Line-Of-Sight
LVO	Link-via-Orbiter
MCR	Mission Close-out Review
MEMS	Micro-Electro-Mechanical System
MER	Mass Estimation Relationship
MIT	Massachusetts Institute of Technology
MR	Mission Requirement
MVCRS	Multi-staged Vapor-Compression Refrigeration System
MWRS	Microwave Radiation Sounder
N/A	Not Applicable
N/D	No Data
NGT	Noble Gas Trap
NIR	Near-Infrared
NMS	Neutral Mass Spectrometer
OLF	One-Leg-Failure
PAY	Payload subsystem
PCM	Phase-Change Material
PD&D	Project Development and Design logic
PDR	Preliminary Design Review
PETS4V	Parametric Entry Trajectory Simulator for Venus
PICA	Phenolic Impregnated Carbon Ablator
PLL	Phase-Locked Loop
PM	Phase Modulation
POW	Power subsystem
QHA	Quadrifilar Helical Antenna
QMS	Quadrupole Mass Spectrometer
QPSK	Quadrature Phase Shift Keying
RC	Requirement Compliancy
RHCP	Right-Hand Circularly Polarized antenna
RK4	Runge-Kutta 4 method
RPM	Revolution-Per-Minute
RSG	Radioisotope Stirling Generator
RTD	Resistance Temperature Detector
RTG	Radioisotope Thermoelectric Generator
SAEVe	Seismic and Atmospheric Exploration of Venus
SAM	Sampling At Mars
SDS	Safety Data Sheet
SE&I	Systems Engineering & Integration
SIRCA	Silicone Impregnated Refractory Ceramic Ablator
SMAD	Space Mission Analysis and Design (book)
SMART	Specific, Measurable, Achievable, Relevant, Timely
SMS	Structures & Materials
SNR	Signal to Noise Ratio
SNR	Signal-to-Noise Ratio
SOC	Science Operations Center
SR	System Requirement
SRC	Sample Return Capsule
SU	Spectrometer Unit
SWOT	Strengths, Weaknesses, Opportunities, Threats
TBD	To-Be Determined
TDD	Time-Division Duplexing Scheme
THM	Thermal Management subsystem
TPS	Thermal Protection System
TRL	Technology Readiness Level
TT&C	Telemetry, Tracking and Command System
UHF	Ultra-High Frequency
UR	User Requirement
UVN-MSI	Ultraviolet-Visible-Near Infrared Multispectral Imager
VCHP	Variable Conductance Heat Pipe
VEXAG	Venus Exploration Analysis Group
VME	Venus Mobile Explorer
VMS	Venus Mass Spectrometer
VOICE	Venus Volcano Imaging and Climate Explorer
VTLS	Venus Tunable Laser Spectrometer
XRF	X-Ray Fluorescence

Greek Symbols

α	Half-cone angle	$^\circ$
δ	Impact ring height	m
ϵ	Emissivity	-
η	Drag plate mounting parameter	-
γ_E	Entry flight path angle	$^\circ$
λ	Reliability time constant	s^{-1}
ν	Poisson's ratio	
ω	Angular velocity	$\mathrm{rad\,s}^{-1}$
ρ	Density	$\mathrm{kg\,m}^{-3}$
σ	Strength/stress	MPa
σ_*	Stefan-Boltzmann constant	$5.67 \cdot 10^{-8}\ \frac{\mathrm{W}}{\mathrm{m^2K}}$
$\tan\delta$	Material dissipation factor	-
τ	Time	s
θ	Leg angle from horizontal	$^\circ$
ε_r	Material dielectric constant	-
ζ	Drag plate angle	$^\circ$

Latin Symbols

Δp	Pressure difference	bar
Δx	Conductance length	m
Δx_{wind}	Maximum displacement due to wind	km
$\dot{q}$	(Total) cold-wall heat flux	$\mathrm{W\,cm}^{-2}$
κ	Thermal conductivity	$\frac{\mathrm{W}}{\mathrm{m\cdot K}}$
A	Area	m^2
a	Deceleration	
B	Channel bandwidth	Hz
C	Column buckling constant	-
c	Distance from neutral axis	m
C_D	Coefficient of drag	-
C_m	cost per Unit Mass	
D	Outer diameter	m
d	Inner diameter	m
DS	Dynamic shock factor	-
E	Young's modulus	GPa
E_b/N_o	Energy-per-bit to noise-power spectral density ratio	dB
F	Radiative heat transfer factor	-
F_{crush}	Crush force	N
FS	Factor of Safety	
G	Gain	dB, dBm, dBi
g	Surface gravity of Venus	$\mathrm{m\,s}^{-2}$
g_0	Surface gravity of Earth	$9.81\,\mathrm{m\,s}^{-2}$
h	Height	m
I	Second moment of area	m^4
K	Sutton-Graves constant for Venus' atmosphere	$1.896 \cdot 10^{-8}\ \frac{\mathrm{Ws}^3}{\mathrm{cm^2kg^{0.5}m}}$
k_{eff}	Effective stiffness	$\mathrm{N\,m}^{-1}$
k_{foam}	Impact ring stiffness	$\mathrm{N\,m}^{-1}$
k_{leg}	Leg stiffness	$\mathrm{N\,m}^{-1}$
KE	Kinetic energy	J
Kn	Knudsen number	-
L	Loss	dB, dBm, dBi
M	Mach number	-
m	Mass	kg
n	Number of legs	-
N_0	Noise Power Spectral Density	Hz
P	Power	W, dB, dBm
p_{cr}	Critical buckling pressure	bar
R	Resistance	Ω
$R(t)$	Reliability as a function of time	-
r_{base}	Capsule base radius	m
r_{max}	Maximum capsule radius	m
R_N	Nose radius	m
T	Temperature	K
t	Thickness	cm, mm
U	Voltage	V
V	Velocity	$\mathrm{m\,s}^{-1}$
v	Volume	m^3
V_{wind}	Wind speed	$\mathrm{m\,s}^{-1}$
V_E	Entry velocity	$\mathrm{km\,s}^{-1}$
x_{CG}	Center of gravity location	m

Subscripts

∞	Free-stream value
1	Innermost surface
2	Outermost surface
a	Wheel a
AS	Aeroshell
atm	Atmospheric
b	Wheel b
c	Compression
cond	Conductive
conv	Convective
cs	Cross-sectional
DP	Drag plate
EDL	Entry, Descent and Landing
eff	Effective
foam	Material foam
HB	Hotbox
HS	Heat shield
in	Inside/Coldbox
max	Maximum
original	Original material
out	Outside
p	Pointing
pol	Polarization
rad	Radiative
RX	Received/receiver
t	Tangential
td	Touchdown
TPS	Thermal Protection System
TX	Transmitted/transmitter
ult	Ultimate
y	Yield

1

Introduction

For centuries, humans have looked at the evening sky and wondered at the brilliant star they named Venus, after the goddess of beauty and love. Little did they know of the truly hellish landscape lying beneath the acidic clouds covering the entire planet in a thick blanket. So perilous is venturing beyond the haze that no attempt has been made since the Soviet Union's Vega 2 mission in 1985[1], and fewer than 10 probes have ever touched the surface and transmitted anything back. Even then, the longest-lived Venera 13 in 1982 lasted only 127 minutes, showing the extreme difficulty of surviving in Venus's surface conditions.

However, the scientific potential of Venus is immense. Venus is Earth's closest planetary neighbor, both in proximity and in physical characteristics. Radar imaging has shown certain features that resemble tectonics and volcanic activity, but the mechanisms driving them are unclear. Most importantly, its runaway greenhouse effect could help better understand Earth's climate and potential future if no action is taken against climate change.

Thus, KYTHERA's mission was conceived: to go back to Venus with modern equipment, and to survive for more than 6 Earth months. It will investigate Venus's atmospheric and surface chemistry, measure seismological activity, optically map its landing site, and establish meteorological characteristics. All of this will be done deep inside Venus's crushing atmosphere, with 93 bar of pressure and 464 °C of temperature, making CO_2, its largest component by far, a supercritical fluid - neither gas, nor liquid. To make it worse, corrosive chemicals such as sulfuric acid in the clouds and sulfur dioxide at the surface will always be a threat to anything exposed to the Venusian air.

This report will present the preliminary design of KYTHERA. It is a unique, highly demanding mission, meant to achieve ambitious goals never attempted before: surviving on Venus's surface for 200 days. The passive cooling used on the Veneras and Vegas will not be sufficient anymore; an active cooling system will be required, and KYTHERA has been designed around it.

In order to define a goal for the design, a mission need and project objective statement have been set up in the early design stages as follows:

- **Mission Need Statement:** *To expand our understanding of Venus' evolution by collecting and returning data on its lower atmospheric, seismic, and geochemical properties over at least 200 Earth days.*
- **Project Objective Statement:** *To design a system capable of conducting long-duration in-situ measurements of the Venusian lower atmosphere and surface by 10 students in 10 weeks.*

A more technical project overview, including the top-level requirements, a market analysis, and the project's sustainability strategy, will be given in Chapter 2. By then, the reader will have an overview of KYTHERA's background, and it is time to dive into its design. Chapter 3 summarizes the previous design phases and trade-offs. This includes the selection of the lander concept and its landing site. Afterwards, the system functions, requirements, architecture, budgets, and risks are discussed in Chapter 4. Then, Chapter 5 presents the preliminary design of each of the lander's subsystems: Entry, Descent and Landing; Payload; Power and Thermal Control; Communications; Command and Data Handling; and Structures and Materials, each presents their requirements, technical background, and design choices. A system is more than the sum of its subsystems, though. Hence, Chapter 6 contains a description of the integration of the subsystems into a complete lander. The report ends with a conclusion (Chapter 7) and an acknowledgment of the invaluable people and resources without whom this project would not have been possible (Chapter 8).

[1] `https://nssdc.gsfc.nasa.gov/planetary/chronology_venus.html`, accessed on 18/Jun/2025.

2

Project Overview

This chapter will provide an overview of KYTHERA's objectives and scope. First, in Section 2.1, the user requirements and constraints are presented, followed by defining mission goals and objectives. Then, Section 2.2 goes into detail about the current scientific "market" by analyzing stakeholders, scientific opportunities, and comparable missions, and finalizes by summarizing KYTHERA's market advantage. Finally, organizational sustainability is detailed in Section 2.3.

2.1 Mission Motivation and Objectives

Venus is similar to Earth in size, composition, and distance from the Sun, but has undergone a vastly different evolution due to a strong greenhouse effect [1]. Studying Venus can offer valuable insights into planetary processes and evolution, including those on Earth. While fly-bys and orbiters have investigated its upper atmosphere, thick cloud layers prevent optical imaging and detailed surface studies from orbit. Surface missions have been limited to lifespans of only just over two hours due to extreme pressure, heat, and corrosion, leaving major gaps in our understanding of Venusian volcanism, lower atmosphere dynamics, composition, geology, and long-term variations such as rare seismic events [2], as will be discussed in Section 2.2. Consequently, a long-duration mission to the surface of Venus needs to be developed that addresses the gap in knowledge about Venus's lower atmosphere and surface properties.

The development of this mission has been driven by the needs of the users of this mission, namely the broader scientific community, represented by VEXAG (Venus Exploration Analysis Group), whose requirements are laid out in Table 2.1, labeled with ITLR (Initial Top-Level Requirement). The requirement ID also reflects that stated in the project guide [2], with UR denoting user requirements, MR mission requirements, and SR system requirements. These requirements serve as the basis for the entire design process of this mission.

Table 2.1: Initial top-level requirements.

ID	Requirement
ITLR-UR1	Lander must be deployed within the volcanic plains of Venus that compromise >80% of the surface area.
ITLR-UR2	Map the expected landing ellipse with a resolution of 1 m/pixel.
ITLR-UR3	Conduct a detailed chemical analysis (Cl-, F-, S-bearing species, CO_2, CO) of the lowest atmosphere every 12 hour throughout the lander's lifetime.
ITLR-UR4	Conduct continuous seismic investigations throughout the lander's lifetime.
ITLR-UR5	Conduct at least 20 individual chemical analyses of surface rock materials near the lander's landing sites throughout the lander's lifetime.
ITLR-UR6	Individual probability of successful analyses for each instrument suite > 80%.
ITLR-UR7	Any contamination of the atmosphere and lander landing zones by terrestrial materials should be acceptable according to what is internationally agreed upon by COSPAR's outer space treaty.
ITLR-UR8	The lander concept and target landing zone of interest must be unique; previously proposed concepts during the last 60 years or by student groups involved in earlier or competing design synthesis exercises cannot be selected.
ITLR-MR1	The mission concept should be of scientific interest to for instance ESA or NASA.
ITLR-MR2	The operational life of the lander and corresponding analytical / experimental equipment must be at least 200 days.
ITLR-MR3	Manufacturing process should be reviewed, it should be set-up such that safe working procedures are used.
ITLR-MR4	The cost of the lander, including experimental packages, is constrained to a maximum of 200 million euro for economic conditions of 2025, including operations. For clarity, this budget covers only the lander, including the science package.
ITLR-MR5	Assume that the lander can be delivered by a Venus mission that includes an orbiter that can be used as a data relay with a nominal 24 hour elliptical orbit around Venus, with an orbital insertion date of late 2035-early 2036 or 2037.
ITLR-SR1	All systems and sub-systems on the mission should have a technological readiness level (TRL) of at least 5.
ITLR-SR2	Mass of the power subsystem shall not be greater than 25% of the total system mass.
ITLR-SR3	The lander shall survive entry, descent and landing with an individual probability higher than 90 %.
ITLR-SR5	The (combined) mass of the lander including experimental packages, is constrained to a maximum of 350 kg.

In order to establish an overarching motto for the KYTHERA project, a Mission Need Statement was formulated, flowing from the user requirements shown above, such that the development team's effort can be justified in one sentence. It encapsulates not only the requirements put onto the mission, but also the team's intentions pertaining to the direction of the project.

- **Mission Need Statement:** *To expand our understanding of Venus's evolution by collecting and returning data on its lower atmospheric, seismic, and geochemical properties over at least 200 Earth days.*

The identity of KYTHERA is determined not only by its mission, but also by its team's objectives representing the project itself, giving way to the following statement.

- **Project Objective Statement:** *To design a system capable of conducting long-duration in-situ measurements of the Venusian lower atmosphere and surface by 10 students in 10 weeks.*

2.2 Market Analysis

Venus remains one of the least understood planets in the Solar System [3]. Identifying and investigating knowledge gaps would increase the scientific impact of the KYTHERA mission. To this end, a variety of sources were considered to determine the additional needs and wants of various stakeholders, primarily the scientific community.

Due to the rapid advancement in material science, manufacturing, and scientific instrumentation, there has been a renewed interest in Venus lander missions [4]. Since 1985, a number of mission concepts have been proposed exploring a long-duration lander with the intent of collecting data on seismic activities and the lower atmosphere. In this chapter, relevant parts of a number of proposals and requests were summarized, helping the team gain more insight into what the mission means to the scientific community, as well as what functions KYTHERA should perform.

A SWOT analysis is performed in Subsection 2.2.1, followed by identification of key stakeholders in Subsection 2.2.2. Next, research and insight into the scientific community's queries with respect to ground science and atmospheric science are provided in Subsection 2.2.3 and Subsection 2.2.4 respectively. Finally, an overview of similar past missions is given in Subsection 2.2.5.

2.2.1 SWOT Analysis

To begin, a market oriented SWOT analysis was performed, with the chart in Figure 2.1. It shows the analysis of the Strengths, Weaknesses, Opportunities and Threats related to the KYTHERA mission. This was done by considering what is helpful and harmful for the mission when comparing to the market, both from an internal as well as an external perspective.

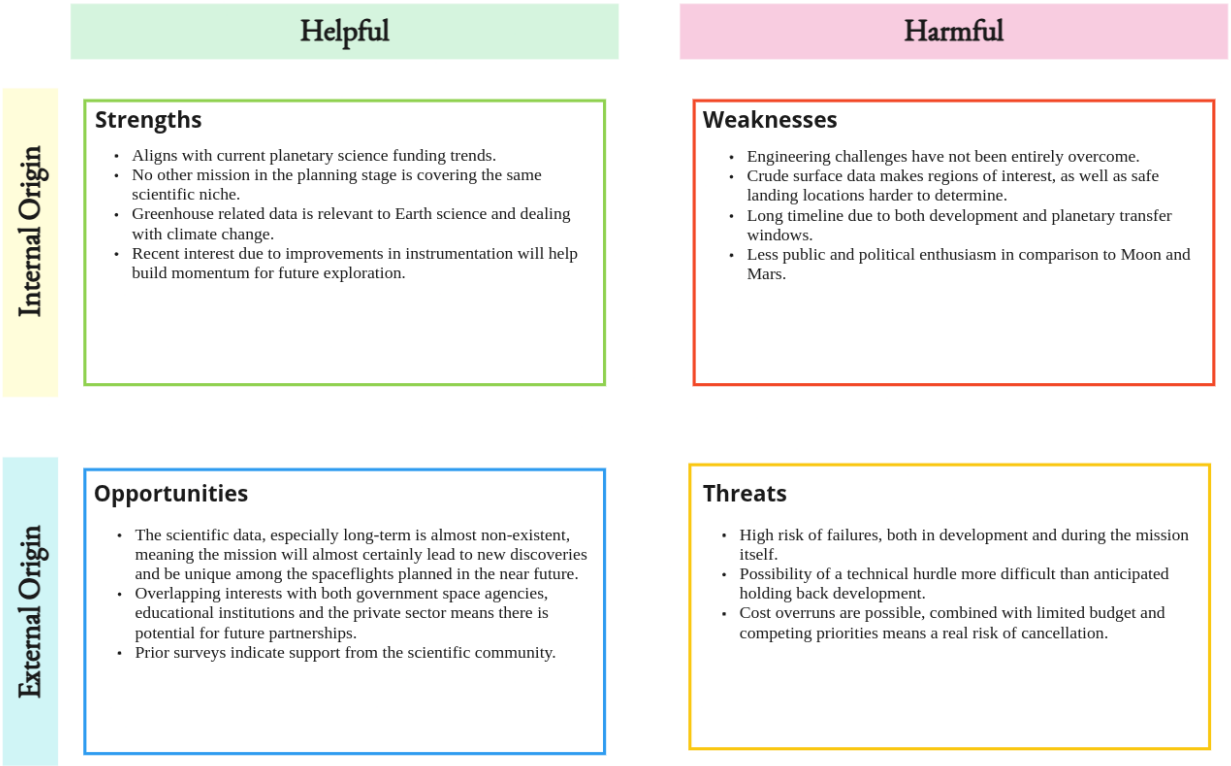

Figure 2.1: Market SWOT analysis.

2.2.2 Stakeholders

The parties involved with, benefiting from or contributing to the mission were compiled in a list of stakeholders:

- **Space agency** - contracts the mission and provides funding, resources and expertise for development and manufacturing of the lander.
- **Mission operators** - control the mission through all phases and are responsible for returning the data.
- **Venus orbiter team** - responsible for delivering the lander to the Venusian orbit.
- **Academia** - are interested in and represent the end 'users' for the data, but are not actively involved in the mission itself to a large degree.
- **Launch provider** - responsible for sending the lander, along with the Venus orbiter on a course towards Venus.
- **Governments** - are interested in good use of public funds.
- **Regulators** - will oversee the manufacturing and operations to make sure no safety, export control, contamination regulations are violated in the process.
- **Workforce** - interested in good working conditions through manufacturing and operations.
- **General public** - interested in good use of public funds, as well as major scientific breakthroughs.
- **Space advocacy groups** - interested in more funding and future commitment for space exploration, driven by this mission's success.
- **Environmental groups** - want to minimize environmental impact of the mission, as well as potential breakthroughs in climate science obtained through the research on the greenhouse effect.
- **Media** - interested in publicizing major scientific breakthroughs.

A stakeholder matrix was produced, which shows both the influence and interest of stakeholders with the purpose of determining the requirement priorities moving forward. Furthermore, the stakeholders were divided in the following groups: primary, secondary and other. It can be found in Figure 2.2.

Figure 2.2: Stakeholder matrix.

2.2.3 Geological and Seismological Opportunities

Due to the extreme conditions on the Venusian surface, no probe that reached the surface remained operational for more than a few hours. This limits the abundance of data, thus leading to larger uncertainties regarding the chemical composition of the Venusian surface.

In-situ surface measurements are invaluable for developing an understanding of Venus, especially as its thick atmosphere renders broad spectrum spectroscopy analyses from orbit impossible [5]. However, chemical analyses are available only from seven distinct landing sites of the Venera and VEGA program. Gamma-ray spectroscopy and X-ray fluorescence (XRF) were used exclusively to investigate the chemical composition of the Venusian surface. These measurements yielded data on the concentration of elements such as K, U and Th (by gamma-ray spectroscopy) and other petrogenic constituents such as Si, Mg and Al [3, 6]. However, the results have an uncertainty of 2 σ and are of low precision, especially when compared to those of other terrestrial and extraterrestrial exploration missions [6]. During the Venera and VEGA geochemical analysis, certain geological properties were not detected. This includes major elements like Na, minor elements such as Cr and Ni, and some trace elements [6]. Minerals were not directly detected, but the geochemical data obtained was used to derive the mineralogy of Venus [7].

In addition to the uncertainty in the data, the diversity in landing sites is low; all landing sites are suspected to be located in volcanic plains and rises, making up around 80% of the surface of Venus [6]. At the time of the Venera missions, the surface topography of Venus was not known, therefore the landing sites were selected based solely on interplanetary transfer and communicational considerations [3]. Note, however, that the exact locations of landing sites are uncertain to a diameter of 300 km, leaving the exact terrane analyzed uncertain [8]. Mapping of the landing sites by the Magellan mission showed that each landing site contains different types of geological terrains, which makes the measurements even more uncertain [7]. Furthermore, the Venera and VEGA landers only analyzed one sample per landing site [6]. This means that not all types of surface material (rock and regolith) were characterized and that the amount of data obtained was relatively limited. Therefore, doing multiple analysis in one mission would be valuable [6].

Since the last surface probe launched in 1984, the topography of Venus has been mapped to 98% coverage by the Magellan mission[1], enabling more precise landing site selection to investigate other terranes and improve understanding of the history of Venus. Of particular interest are volcanic rises and coronae, and highland tesserae [6]. In Venus's highlands, a "snowline" is visible in radar images as unusually high radar backscatter. This is primarily attributed to a change in surface-atmosphere interactions due to a change in atmospheric properties at higher elevations, but the exact process is unclear [9]. Therefore, analysis of the highlands' surface composition could provide valuable data for explaining this phenomenon [6, 9].

Treiman [6] suggests that more accurate data could be collected by long duration Venera-style landers. Gamma-ray spectroscopy and XRF instruments improved significantly since the cessation of the Venera program. The ability to collect and analyze multiple samples (i.e. separate samples from rocks and regolith) in a longer mission could provide serious improvements in data accuracy. Additionally, more modern techniques, specifically Laser-Induced Breakdown Spectroscopy (LIBS) could be utilized to gather more accurate data in shorter measurement time. Furthermore, current instruments can perform a more accurate analysis compared to the instruments used in the previous Venus lander missions. Seismic measurements could be conducted in-situ to obtain more accurate data on the seismology and draw conclusions on the tectonics of Venus, which are not yet fully understood.

Additionally, an improved understanding of the surface composition, movements, and topology also contributes to the continued study of the evolution and history of Venus. Especially with the increasingly mounting evidence of active or geologically recent volcanism on Venus [10, 11], investigating the crust composition and its movement is now key to gaining insights into the potential active tectonic activities on Venus. This discovery would be a major scientific breakthrough, changing current terrestrial planetary models on heat loss, mantle convection, and much more [12]. This perhaps will also explain why Venus suffered from such a different fate compared to Earth and how Venus's current inhabitable conditions developed.

The seismic activity of Venus was studied by the Russian Venera 13 and 14 missions. Both of them deployed the uniaxial Groza 2 seismometer that conducted measurements throughout the lifetime of the lander [2]. It determined the vertical displacement of the surface to micron precision [2]. The lander, however, only survived for a couple of hours, meaning that the seismological data and insights obtained are limited. Furthermore, the measurements were disturbed by violent winds throwing up small stones on the surface and by the lander itself [2]. As a result these measurements could be considered unreliable and no convincing results were obtained[2].

With all of the above in mind, the team now possesses a good range of questions to answer from the scientific community, as well as surface objectives for KYTHERA to carry out during its mission lifetime. This is best summarized by the National Research Council's Planetary Decadal Survey [13] and the VEXAG [14], with the key questions and objectives listed below.

- What is the chemical composition of the crust?
- Is the heat loss from the interior by conduction through the crust, through volcanism, or tectonics?

[1] `https://astrogeology.usgs.gov/search/map/Venus/Magellan/RadarProperties/Venus_Magellan_Topography_Global_4641m_v02`, accessed on 30/Apr/2025.

[2] `https://www.seis-insight.eu/en/public-2/planetary-seismology/venus`, accessed on 17/Jun/2025.

- Is there now, or has there ever been plate tectonics?
- What are the distribution and particle sizes at the landing sites?
- Are salts and cements present on the surface that might indicate surface-atmosphere interactions?
- Are there any structures (e.g., faults) observable in the scene that may correlate with larger-scale deformation?
- Are there landforms in the scene (e.g., dunes) that might indicate the presence and transport of sediments?
- What can be learned about the origin and diversity of the terrestrial planets?
- How could fully mapping the terrain of Venus's surface with a higher degree of precision guide future mission and deepen the planet's understanding?

2.2.4 Atmospheric Science Opportunities

Although the primary objective of the KYTHERA mission is to collect in-situ surface measurements, the EDL phase of the mission is an opportunity to collect data from different parts of the atmosphere and get a step closer to deciphering its secrets. Despite Venus being marginally smaller in both size and mass than Earth, its atmosphere is unparalleled in other rocky celestial bodies in the Solar System. The extreme pressure and temperature of the lower atmosphere, as well as the abundance of SO_2 make it both an engineering challenge to reach the surface and a place of key scientific importance, especially as the long period temporal variation of the concentration of SO_2 implies volcanic activity on the surface [15]. The main questions the scientific community is interested in answering are [3]:

- What was the original composition of the Venusian atmosphere?
- Did Venus have oceans and did life evolve?
- How has the atmosphere evolved over time?
- When and why did the runaway greenhouse effect begin?
- What are the key processes, reactions, and chemical cycles controlling the chemistry of the middle, upper, and lower atmosphere of Venus?
- How does solar energy drive atmospheric circulation, cloud formation, and chemical cycles that define the current climate on the terrestrial planets?

The primary focus on the Venusian atmosphere is the greenhouse effect aspect, the understanding of which could help gain a better understanding of its effects on Earth. This would mainly involve understanding the atmospheric composition over time, achieved through the study of isotope ratios, primarily those of carbon and nitrogen, as well as D/H measurements, which would quantify the volume of water and the process of its loss. [3]

The community is also interested in understanding the chemical cycles below the cloud layer, which would involve measuring the extent of the boundary layer, the nitrogen gradient, and trace gas species in and below the clouds. Understanding UV absorbers and aerosols would improve cloud models, while the impact of the space weather could help explain ion escape. Finally, the combined study of the ground and the atmosphere could improve understanding of the sulfur chemical cycle, as well as give insight into the possibility of volcanic activity. [3]

Seiff et al. [16] developed a model predicting atmospheric state properties at altitudes below 100 km above surface, taking into consideration the effect of geographic latitude on the state of the upper and middle atmosphere. This model is based on data collected by radio occultation by the Pioneer Venus Orbiter, and during descent by the Pioneer Venus Probes and the Venera 10, 12 and 13 lander probes. There are considerable disagreements between collected datasets, attributed to biased measurements and differences due to diurnal variability, gravity waves and other wave phenomena. Thus, analyzing the atmosphere at different longitudes at the same time taking more precise measurements could be used to improve this model by incorporating temporal variability effects.

2.2.5 Comparable Missions

To contextualize the KYTHERA mission, it is compared to past, ongoing, and future planned missions of a similar nature. This comparison highlights scientific objectives, engineering approaches, instrumentation choices as well as budgetary frameworks in an effort to identify gaps with the current exploration efforts which justifies the KYTHERA mission's focus. Through this comparison, the team will be able to analyze the scope and scale of these analogous missions and develop a better understanding of resource allocations, scientific goals, and challenges for the KYTHERA mission. Future orbiter missions to Venus, such as Envision of ESA and VERITAS of NASA, seem promising and will likely enable new scientific insights. They are however not treated in this market analysis as they are not landers and thus have different measurement methods, design, etc. which makes them hard to compare to the KYTHERA lander.

Past Venera missions

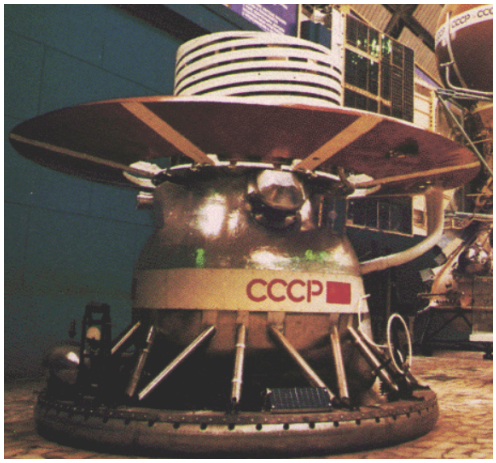

Figure 2.3: Venera 14 lander.

The Soviet Union has sent several probes to Venus from 1967 up to 1985, which provided valuable scientific insights[3]. The highlights for each Venera mission are briefly discussed below. Venera 4, 5 and 6 were atmospheric probes that returned data on the atmospheric composition, temperature and pressure of the Venus surface[3]. After collecting the data these probes were crushed by the pressure even before reaching the surface. The Venera 4 had a mass of 383 kg and the Venera 4 and 5 had a mass of 405 kg[4]. Venera 7 was the first probe that successfully landed on the Venus surface and measured the surface temperature and pressure[3]. It also collected data from the atmosphere and transmitted it after landing. Its mass was 490 kg[4]. The Venera 8 lander measured windspeeds of the atmosphere while descending and determined the surface composition using gamma-ray spectroscopy[3]. This lander had a mass of 495 kg[4]. A lander was for the first time accompanied by an orbiter in the Venera 9 & 10 missions[3]. This lander provided the first black and white panoramic images of the Venus surface and had a mass of 660 kg[4]. The Venera 11 and 12 landers investigated the Venus atmosphere. They determined the composition of the clouds and atmosphere and measured solar radiation[3]. The dynamics of the atmosphere were also studied via Doppler tracking. The first color panoramic images of the surface were taken by the Venera 13 & 14 landers[3] (shown in Figure 2.3[5]). These landers also conducted a seismic measurements an a soil analysis by taking samples and analyzing it with X-ray fluorescence spectrometer. These landers both had a mass of 760 kg[4].

Venera-17

The Venera-17, also known as Venera-D, project is a mission under development, consisting of an orbiter and a lander probe. The scientific goals of the lander include: performing a chemical analysis of the surface material, studying the interaction between the surface and the atmosphere, investigating the structure and chemical composition of the atmosphere down to the surface, performing analysis of the clouds of Venus and characterizing the geology of local landforms. [17]

The lander aims to survive for 3 hours on the Venusian surface. The mission takes a similar approach to keeping the probe operational as previous Venera landers, i.e. pre-cooling the lander module before atmospheric entry and using a heat sink to prevent the core containing scientific and radio equipment from overheating. The planned scientific objectives are: investigating the chemical composition of the atmosphere and surface, collecting meteorological data, taking radiometric and radar measurements, and optical imaging. [18]

VOICE

The Venus Volcano Imaging and Climate Explorer (VOICE) was a mission proposed by the Chinese National Space Science Center from the Chinese Academy of Sciences. This proposed mission is the first major step of Chinese exploration of Venus. It aims to answer some questions posed by VEXAG [14], namely, understanding the evolution of Venus, atmospheric chemistry and movement patterns, and understanding the surface geological history and the momentum exchange between the surface and lower atmosphere. [19]

The VOICE mission proposes an orbiter specializing in volcanic studies, tectonic movement detection, and deep atmospheric evolution. The orbiter utilizes the Synthetic Aperture Radar (SAR) to fully map the surface morphology of Venus, improving the resolution of the existing mapping data from the Magellan mission. Additionally, the combined use of the Microwave Radiation Sounder (MWRS) and Ultraviolet-Visible-Near Infrared Multispectral Imager (UVN-MSI) greatly improved understanding of the evolution and movement patterns of the Venusian atmosphere [19].

It should be noted that due to the canceled status of the VOICE mission, further detailing of the orbiter design was not performed, hence, budgeting and cost estimates are not available [20].

AREE

Overheating of electronics and communication systems is the most challenging aspect of the design of a Venus lander. As an alternative to electronics, the Automaton Rover for Extreme Environments (AREE) proposes a hybrid mechanical-electrical benchmark design, which uses a wind turbine to provide the energy for its movement on the surface and a mechanical computer controlling the rover. Multiple communications methods are still explored ranging from simple electronic transponders to mechanical retroreflectors. Additionally, mechanical measurements are proposed to collect scientific data. Utilizing high-temperature alloys would enable the rover to remain operational for extended periods of time. The mass of the rover is estimated to be of the same order of earier Venera missions, around 700 kg [21]. AREE would

[3] `https://www.esa.int/Science_Exploration/Space_Science/Envision/Past_missions_to_Venus`, accessed on 17/Jun/2025.
[4] `https://nssdc.gsfc.nasa.gov/planetary/venera.html`, accessed on 17/Jun/2025.
[5] URL: `https://pages.uoregon.edu/jschombe/ast121/lectures/surface_venus.html`, accessed on 18/Jun/2025.

focus on low-bandwidth, high-value scientific measurements that can be performed reliably with mechanical, thermal, or ruggedized sensors. These include measuring seismic activity, temperature, pressure, wind speed and surface composition.

Venus Life Finder

The Venus Life Finder is a mission under joint development by Rocket Lab and MIT, making it the first mission developed by a private company to a planet other than Earth. The main goal is the investigation of the atmosphere of Venus for the purpose of finding life, with special focus on clouds and cloud particles. The ultralight descent probe, weighting only 17 kg in total [22], will have 5 minutes to collect raw data and will continue to transmit this data to its orbiter before impacting the surface. [23]

DAVINCI

The Deep Atmosphere Venus Investigation of Noble gases, Chemistry, and Imaging (DAVINCI, formerly also known as DAVINCI+) is a planned mission by NASA, consisting of an orbiter and descent probe. The latter's scientific goal is the in-situ study the Venusian atmosphere and take optical images, mapping the surface of the planet throughout its descent[6]. Although not intended to study the surface of the planet, it could theoretically survive the surface impact and continue collecting data for up to 18 minutes[7].

SAEVe

The SAEVe mission is a long-duration Venus lander mission that will be utilizing currently developing high heat/pressure electronics and sensors in an effort to survive on the Venusian surface for more than one full diurnal cycle (116 Earth days) [4]. Its scientific objectives mainly align with those outlined by the National Research Council's Planetary Decadal Survey [13] and VEXAG [14].

This mission delves deep into seismic and geological analysis and studies the potential correlation between the surface and lower atmosphere. The main instrumentation of the SAEVe lander consists of a seismometer, heat flux, temperature, pressure, atmospheric chemistry, and wind sensors, radiometers as well as cameras. Since it is still relatively early in its development stage, most onboard scientific equipment has a relatively low TRL and is closely interlinked with another proposed mission by NASA, the Long-Lived In-Situ Solar System Explorer (LLISSE) [24]. The budgetary framework for the lander with full payload is estimated to be around $87 million, however, a more detailed breakdown of costs is not given, possibly because the mission is still in the development stages. The power storage and mass budgets are also found in the paper and are 716 Wh and 23.1 kg, respectively.

2.2.6 Market Advantage

Concluding the market analysis, KYTHERA will be an appealing opportunity in the current market. This is because KYTHERA will perform scientific measurements on the Venus surface for a considerably longer duration than has ever been done before and the landing site will be known precisely. As specified by [2], the KYTHERA mission aims to map the expected landing ellipse with a resolution of 1 m/px. The lander has various scientific instruments, which will all collect valuable scientific data. High resolution pictures will be taken, both during and after landing. Furthermore, 20 remote geological chemical analysis will be done, which will obtain data about the mineralogy and chemical composition of the Venus surface. A detailed atmospheric chemical analysis is performed, where samples are collected during descent as well as every 12 hours once landed. The lander will also contain a seismometer, which will collect seismic data and register events throughout the whole mission duration. Other instruments that the team decided to add to the lander are: pressure and temperature sensors, a wind sensor and a radiometer, which will all be collecting data throughout the whole mission. These extra instruments will provide insights in the change of temperature, pressure wind and radiation over 200 days and could lead to major breakthroughs related into the understanding of Venus, especially when combined with data from other instruments.

In order for most of the lander subsystems to remain operational on the Venus surface for the whole mission duration, the lander has to be cooled. Therefore and advanced power and thermal subsystem had to be designed. Because of mass constraints a Stirling generator was chosen, which will generate enough power for the KYTHERA mission and makes sure the lander is cooled.

KYTHERA will do all of this with a mass of 392.3 kg and a monetary budget of 286 million euros, both of these budgets exceed the requirements but it is still less than other proposed long-term landers (such as AREE), while staying for a longer time than other landers (such as SAEVe).

2.3 Sustainable Development Strategy

In the previous phases of the report, sustainable development was defined as "development that meets the needs of the

[6] `https://ssed.gsfc.nasa.gov/davinci/mission`, accessed on 01/May/2025.

[7] `https://www.nasa.gov/centers-and-facilities/goddard/nasas-davinci-mission-to-take-the-plunge-through-massive-atmosphere-of-venus/`, accessed on 01/May/2025.

present without compromising the ability of further generations to meet their own need". It was also explained that for KYTHERA, sustainability is not a dominant part of the design. Sending a system to the surface of Venus is challenging and the main focus will be on accomplishing a successful mission within the given constrains, over a sustainable one. As such, sustainability will not be a major consideration in the trade-off criteria. Still, where relevant, attention to sustainable design choices was given throughout the design process, starting with a discussion on the sustainability-related actions taken in this Final Report, and an overview of the regulations to be considered in further design stages.

2.3.1 How Sustainability is Taken into Account in the Design

The main sustainability concern for KYTHERA is not related to life on Earth, but to the Venusian environment. The one requirement related to sustainability that was given by the tutor in the project guide is "Any contamination of the atmosphere and lander(s) landing zones by terrestrial materials should be acceptable according to what is internationally agreed upon by COSPAR's outer space treaty" [2, p. 8], that is, forward contamination of Venus should be avoided.

COSPAR specifies five categories of space exploration missions and lists guidelines accordingly. A mission to Venus that does not return samples to Earth is a Category II mission, meaning there is significant interest in Venus's chemical evolution, but contamination by organic or biological materials is not considered a risk [25]. The regulations in place for Category II are documentation-related only. This documentation should include a planetary protection plan, pre-launch report, post-launch report, post-encounter report and end-of-mission report, as outlined in [25, p. 27]. A cleanroom environment, organic inventory or biological control are *not* needed for a Category II mission.

To help the implementation of COSPAR guidelines, the team will consider the report on space sustainability prepared by the European Cooperation for Space Standardization, which includes a list of requirements a system should fulfill in order to comply with COSPAR regulations. KYTHERA being a Category II mission, the relevant requirements are those in sections 5.1, 5.2, 5.5, 5.6 and 5.7 of ECSS-U-ST-20C [26, pp. 20-22, 33–35]. Again, these requirements relate to documentation only. This documentation will be constructed once the detailed design has finished, as is included in the project Gantt chart.

The main way in which sustainability was implemented in the preliminary design phases is by using it as a trade-off criteria when selecting design options. However, as the KYTHERA spacecraft is not planned to enter mass production, it is doubtful whether the use of sustainable materials is relevant beyond the scope of manufacturing safety, which can be ensured by adequate protective equipment and safety trainings. For each of the materials considered for KYTHERA's components, the safety datasheet (SDS) was consulted. The SDS contains information about hazards the material imposes on humans and the environment. Based on that information, sustainability could be given a score on the materials trade-offs. In the case that non-sustainable materials were selected because of their superior performance on other criteria, care should be taken to prevent adverse health consequences for manufacturing employees by means of protective equipment, and safety briefings about the product they are working with. Additionally, any disposal of scrap product or fumes should be done in such a way that the product does not end up in sensitive environments, such as waterways or conserved nature areas.

However, whenever two or more materials had similar performance but one of them was toxic to humans and/or the environment and the other option was not, the non-toxic material has been chosen. This was the case for the heat shield, where processing of the SIRCA tile option may cause silicosis, while Acusil specifically is not a hazard to humans or the environment.

On the other hand, the climate impact of the fuel burnt by the launch vehicle is likely to overshadow the environmental impact of the manufacturing and operation of the spacecraft (on the order of 300-500 tons of CO_2 per launch, as well as water vapor, chlorine and alumina emissions [27]). This fuel consumption is drastically influenced by the spacecraft mass, so minimizing mass is improving the sustainability of the project. Mass was indeed a high-weight criteria in all trade-offs performed during the design process - mainly to meet the tight mass requirement, but also to minimize launch vehicle fuel.

It should be noted that some of the design choices are not sustainable. If it would be the case that in the future, many Venus surface vehicles will be developed, then resources should be put towards improving sustainability. For example, a power system suitable for the Venus environment should be developed that does not depend on Plutonium isotopes.

Another consideration for future design stages, is to perform a life-cycle assessment (LCA). This should cover all KYTHERA's life stages, from production to launch and operation. The LCA is included in the post-DSE Gantt chart.

Apart from the regulations laid out above, no quantifiable metrics will be considered for KYTHERA. Adding a hard limit on e.g. a percentage recyclable materials may limit the design process to an unacceptable extend, indeed, these requirements would likely turn out to be killing. This is because design for the Venus surface requires specialized materials and technologies that can withstand high temperatures, high pressure, and a highly corrosive environment for 200 days. Additionally, the lander is not returning from Venus, so materials recycling is not possible either way. Hence, the sustainability of selected components is not a priority during the design of KYTHERA.

2.3.2 How the Design Contributes to Sustainability

Other than KYTHERA's commitment to sustainability in its design and development process, the mission is expected to make a big contribution to global sustainable development through scientific discovery and technological advancement. The mission is not only an opportunity to explore one of Earth's neighbors but also a driving force for innovation, environmental awareness, and knowledge sharing beyond the scientific community.

One of the main scientific objectives of this mission is to advance our understanding of the atmospheric and geological evolution of Venus. Venus is of particular interest for planetary science because it is an extreme example of climate transformation. Its carbon dioxide-rich atmosphere, sulfuric acid clouds, and its high surface temperatures offer insights into processes that diverged dramatically from those on Earth. The lander will help in the discovery of the Venusian climate system's past by examining the atmosphere's dynamics, composition, and structure as well as the planet's surface features and possible tectonic or volcanic activity. This aligns with Sustainable Development Goal 9[8], which promotes industry, innovation, and infrastructure. The mission will support this goal by pushing the development of new aerospace technologies, materials, and data analysis methods, while also stimulating collaborative research across institutions and different countries.

The lander's scientific analysis of Venus will give critical knowledge that improves our understanding of climate processes on Earth. Venus forms a natural laboratory for studying long-term consequences of greenhouse gas accumulation. By comparing its climate dynamics with Earth's current climate changes, scientists can refine models of atmospheric change and thus improve strategies for climate adaptation and mitigation. This also allows to better understand the possible thresholds that must be avoided to preserve Earth's habitability. This scientific knowledge is related to Sustainable Development Goal 13[8], which calls for urgent action to combat climate change and its impacts. KYTHERA aims to contributes to this goal by both generating data that informs global climate science and by inspiring awareness of planetary-scale environmental risks and the importance of sustainable practices.

[8] `https://sdgs.un.org/goals`, accessed on 01/May/2025.

3

Summary of Previous Trade-offs

This chapter will provide a review of trade-offs done in the previous design stages of KYTHERA. First, the mission architecture selection process will be explained in Section 3.1, where the choice for the single stationary lander architecture will be justified. Then, the landing site selection will be reviewed in Section 3.2.

3.1 Mission Architecture Selection

The first task in developing a system is deciding on a mission architecture. This chapter will first provide a review of finalist concept designs from the Baseline Report in Subsection 3.1.1, and will continue to perform the concept tradeoff in Subsection 3.1.2. Finally, a sensitivity analysis will be performed in Subsection 3.1.5 where the robustness of the tradeoff will be assessed.

3.1.1 Concept Design Options

During previous development of KYTHERA, numerous mission architecture concept options were considered, including ideas that were not deemed possible for the sake of completeness. A complete diagram of these, as well as their judged practicality and status can be found in the Design Option Tree (DOT) in the Appendix. In the Baseline Report, all these options were investigated and reported on, with a focus placed on the ones deemed strongest. Ultimately, by judging feasibility of every option as well as applying known limits of physics and technology, five mission architecture concept options were chosen as finalists to be considered for a preliminary design trade-off. This chapter will provide a review of the finalist concept options as presented in the Baseline Report.

Below is a list of the aforementioned finalist concepts, visualized in Figure 3.1. Later in this report, they enter a concept trade-off in Subsection 3.1.2.

(a) Lander with orbiter. **(b)** Lander with balloon. **(c)** Single lander. **(d)** Multiple landers. **(e)** Rover.

Figure 3.1: Feasible concepts (background generated using ChatGPT).

(a) **Leave all possible instruments on orbiter, only send a "bare bones" lander**: Seismic measurements can be performed from orbit. This is because Venus's dense atmosphere causes strong coupling between surface and atmosphere [28]. Hence, it might not be necessary to stay on the surface for the entire duration of the mission: some of the required data can be obtained by the orbiter, while a shorter-lived lander can collect the desired 20 rock samples. A challenge that needs to be addressed in this design concept, is the low accuracy of in-orbit lower atmospheric measurements [5, 29]. Furthermore, combining orbiter and lander data introduces analytical uncertainties due to mismatches in spatial and temporal resolution, instrument calibration, and atmospheric sampling limitations, especially for seismology and lower-atmosphere chemistry. Orbiters provide broad but indirect measurements, while landers offer precise, local data that may not scale to regional interpretations. These differences can lead to inconsistencies when comparing surface rock or atmospheric data unless carefully coordinated. In spite of these drawbacks,

this option is the simplest, lightest and cheapest option due to not having to take as many instruments to the surface of Venus.

(b) **Lander with balloon to move around**: The Venus Mobile Explorer (VME) study proposed a mobile lander/probe concept that would land in one investigation site [30]. After having done its science experiments in that first site, the VME fills its metallic bellows with helium, releases the tank the helium was initially stored in, and floats for 8-16 km to another investigation site [30]. This not only allows seismic, atmospheric, and geologic data collection from the surface; it also allows for this data to be collected from distinct locations. This could be especially useful for exploring regions with a high density of interesting features, but due to the nature of balloon transportation by wind, it is not possible to choose which direction and speed the system would fly. Furthermore, bellows for Venus have a low TRL and would require extensive development and testing, potentially increasing cost.

(c) **Single stationary Venera-like lander**: A Stationary Venus lander would be able to complete all scientific objectives, provided that the lander can operate in the harsh Venus conditions for the required mission duration. Venera 9 to 14 and Vega 1 and 2 all had similar anatomy[1], the longest lifetime of those landers being 127 minutes (Venera 13). However, these were never designed to fight against the temperature, and with active cooling it will become possible to last much longer. This option would be the second-simplest concept, behind only the ”bare bones” lander concept. However, the scientific gain from bringing more instruments to the surface of Venus would be much greater. Hence, with some adaptations, a Venera-like stationary lander could work for the KYTHERA project.

(d) **Multiple stationary landers**: Another option available as a mission architecture is to send multiple landers instead of only one. These could be sent at the same time in order to investigate different sites, or could be sent sequentially in order to shorten the necessary lifetime of each individual lander. While this option could more than double the scientific gain of the mission, it would make adhering to the cost and mass constraints substantially more difficult. The design of one lander is foreseen to be difficult within the mass budget, hence why the initial mass budget was raised from 200 kg to 350 kg in the Baseline Report. Additionally, the cost budget was also judged to be a major constraint, which will have to fit two times the construction and operations cost of a single lander instead of just one. Thus, although there is great benefit from sending multiple landers instead of one, problems already arise from budget constraints.

(e) **Semi-mechanical rover:** A rover could provide a higher scientific yield than a static lander because of its ability to seek out specific and diverse geological features to perform seismic and geological research at. Such a rover, however, has never been tested but concept studies have been done by NASA on a system using semi-analogue computers and instruments [21]. In addition, mass-wise, a rover would have to include everything that an immobile lander has, and then add a mobility system. This mobility system would have to include not only wheels, but also motors, navigation computers, navigation cameras, and others. This would make the mass budget harder to adhere to. What's more, the development, construction and testing costs of this design might be much higher than the other designs, owing to its complex nature. By comparison, NASA's Mars Exploration Rovers costed over $1 billion US dollars[2], versus NASA's Phoenix Lander mission that costed only $420 million US dollars[3], supporting the idea that a rover mission would substantially increase cost.

3.1.2 Trade-off

Given the range of design options available, a trade-off analysis was conducted to narrow down the most suitable vehicle architecture for the mission. First, a set of evaluation criteria was defined and assigned weights based on their relevance to the mission objectives. These criteria included mass, cost, technology readiness level, reliability, and performance. Each design option was assessed against these factors to determine which configuration offered the best overall balance and alignment with mission requirements. Based on this assessment, a ranking was assigned. These rankings were then multiplied by the weights of the respective categories and summed up to get an individual score for the concept. While this interim score offers insight into the viability and value of design options, the arbitrary/subjective nature of both means that a sensitivity analysis is warranted to avoid instability or a single criterion driving the design trade-off to an unacceptable degree.

[1] https://nssdc.gsfc.nasa.gov/nmc/spacecraft/display.action?id=1975-050D,
https://nssdc.gsfc.nasa.gov/nmc/spacecraft/display.action?id=1975-054D,
https://nssdc.gsfc.nasa.gov/nmc/spacecraft/display.action?id=1978-084D,
https://nssdc.gsfc.nasa.gov/nmc/spacecraft/display.action?id=1978-086C,
https://nssdc.gsfc.nasa.gov/nmc/spacecraft/display.action?id=1981-106D,
https://nssdc.gsfc.nasa.gov/nmc/spacecraft/display.action?id=1981-110D,
https://nssdc.gsfc.nasa.gov/nmc/spacecraft/display.action?id=1984-125E,
https://nssdc.gsfc.nasa.gov/nmc/spacecraft/display.action?id=1984-128E, all accessed on 30/Apr/2025.

[2] https://www.planetary.org/space-policy/cost-of-the-mars-exploration-rovers, accessed on 16/May/2025.

[3] https://www.planetary.org/space-policy/phoenix-cost, accessed on 16/May/2025.

3.1.3 Criteria Selection and Weight Assignment

One criterion initially considered was power, but it was ultimately excluded from the trade-off analysis because its impact is already reflected through the mass and reliability criteria. Power systems contribute significantly to the vehicle's mass and play a key role in ensuring system reliability. Moreover, a constraint was set to limit the power subsystem to 25% of the total mass budget, ensuring it remains within acceptable bounds. As a result, power was not assigned a separate weight but remains an implicit consideration within the existing criteria. Another criterion that was considered being added was sustainability, however, due to concerns about the technical feasibility of this project, it was not kept (see also Section 2.3). In addition, schedule is not included as a criterion at this stage, since a more thorough understanding of the subsystems would be required to gauge the timeline.

Furthermore, it is important to emphasize that the process of determining the weights and relative importance of the criteria outlined below was carried out through a group consensus. All team members were actively involved in the discussions and collectively agreed on the final decisions, ensuring all perspectives and inputs were considered and that the final outcome reflected a shared opinion, minimizing individual bias while incorporating each team member's expertise.

Throughout this subsection, weights are assigned to each criterion. These weights were first assigned qualitatively (by word) rather than quantitatively (with numbers), on a scale of Low-Medium-High. The result of these assignments was that no criteria was left on Low, and that some criteria were placed between scale increments. For this reason, and because conversion from word to number is rather imprecise, round weights were assigned to each criterion. Finally, due to the aforementioned weighing process, the weights do not add up to 100%, rather they are simply numerical weights.

Mass

Mass is one of the most critical constraints in space vehicle design, as the efficiency, performance, and feasibility of a mission are all closely tied to the vehicle's weight. Initially, a strict mass budget of 200 kg was set for the vehicle, which significantly constrained the design space. As a result, mass was given a high weight in the design evaluation process, since even small deviations could jeopardize the feasibility of the entire system.

However, after further discussions and a reassessment of the mission requirements, the allowable mass was increased to 350 kg. This adjustment introduced greater flexibility in selecting materials, subsystems, and structural configurations. With more room to accommodate design trade-offs, mass became less of a limiting factor. Consequently, its relative importance in the design criteria was reduced, and a weightage of Low-Medium (15%) was assigned to the mass parameter in the final evaluation.

Cost

Similar to mass, cost is another key constraint in the design of the vehicle. Because this mission is breaking new ground and involves objectives that have not been previously attempted, the range of available, flight-proven subsystem components is very limited. This lack of variety significantly reduces the flexibility to choose between suppliers or substitute parts based on pricing. As a result, opportunities to minimize costs through design alternatives are constrained, making cost a relatively inflexible parameter in the decision-making process.

Furthermore, with a fixed mission budget of €200 million for fiscal year 2025, managing costs becomes even more critical to ensure feasibility without compromising essential mission requirements. As such, cost has been assigned a weightage of High (30%) in the trade-off analysis to reflect its importance and impact on the overall design strategy.

Technology Readiness Level

With the mission being unprecedented, much of the technology required to enable its success is still in development. To ensure a minimum level of maturity and reduce technical risk, a Technology Readiness Level (TRL) of at least 5 is required by the time of launch. This makes TRL an important factor in evaluating design options, as it directly impacts the feasibility and timeline of the mission. Due to the inherent difficulty of quantifying TRL for Venus lander missions, a relative scoring method is employed to compare the proposed concepts.

However, despite its significance, TRL is considered to have relatively lower importance compared to other criteria such as cost, reliability, and performance. This is partly because efforts can be made in parallel to mature the necessary technologies ahead of the launch. As a result, TRL has been assigned a weightage of Low-Medium (15%) in the trade-off analysis, ensuring it is accounted for without disproportionately influencing the final decision.

Reliability

Reliability is a fundamental requirement in any space mission. Since access to the vehicle after launch is extremely limited, possible only through radio commands, all systems must function as intended throughout the mission duration without the need for intervention. This places a strong emphasis on the use of proven components, robust system integration, and thorough testing. Options that have lower TRL at the time of launch will inevitably also have lower reliability, but the reliability criterion focuses on the failure probability and complexity of the options in the trade-off, assuming they have been brought to sufficient TRL.

Reliability is a critical factor in the design trade-off, given the high consequences of potential failure ranging from mission loss to safety risks; it directly influences the success of the mission. For these reasons, reliability has been assigned a weightage of Medium-High (25%), reflecting its significant but balanced importance relative to other key criteria such as cost and performance.

Performance

The performance criterion reflects the scientific return that the mission architecture can deliver. As the primary objective of the mission is to collect valuable data for the scientific community, performance plays a central role in the design evaluation. This criterion encompasses both the quantity and quality of data that can be obtained, including the breadth of measurements possible and the precision with which they can be collected.

A design that enables greater data collection capabilities while maintaining high accuracy directly contributes to the mission's overall success and long-term impact. Therefore, to ensure that the selected architecture aligns with the mission's scientific goals, performance has been assigned a weightage of High (30%) in the trade-off analysis.

3.1.4 Trade-off Table

Each of the concept design options were first assessed qualitatively and then were assigned a ranking for easier comparability on a linear scale from 1-5, with 1 (*poor*) representing the worst and 5 (*excellent*) the best option.

Mass

1. ***Lander* + *Orbiter*: Excellent** - scientific limitations (majority of the instruments remain in orbit) and simplistic nature of the lander would reduce the mass needs significantly.
2. ***Single Lander*: Good** - the design is still comparatively simple and conservative, but still results in an increase in mass with the additional scientific requirements.
3. ***Lander* + *Balloon*: Neutral** - presents a minor increase in mass through the addition of a balloon.
4. ***Rover*: Bad** - the increase in the number of moving parts and overall system complexity over a stationary lander, even with a flotation system, is substantial.
5. ***Multiple Landers*: Poor** - since the possibility of designing even a single lander within the given budget is difficult, the requirement to duplicate all but a handful of scientific systems would be likely to make it infeasible.

Cost

1. ***Lander* + *Orbiter*: Excellent** - simplicity and established design of the system would likely contribute to low mission cost.
2. ***Single Lander*: Excellent** - the difficult environment would constitute the use of more experimental technologies.
3. ***Multiple Landers*: Neutral** - manufacturing costs are increased significantly if several landers are used.
4. ***Lander* + *Balloon*: Bad** - not only is the manufacturing budget increased, but there is also a significant amount of development and technological unknowns involved with a balloon capable of withstanding conditions on the Venusian surface.
5. ***Rover*: Poor** - the amount of development is increased significantly with not only a higher total amount of subsystems (on top of those needed for a lander), but with a number of them either completely undeveloped or in very early stages of development.

Technology Readiness Level

1. ***Lander* + *Orbiter*: Good** - while the TRL is hard to determine since there still are undeveloped technologies involved, this option maximizes the readiness level, with various aspects having been demonstrated before.
2. ***Single Lander*: Neutral** - neutral is the baseline TRL; this lander will involve numerous undeveloped technologies, but still represents a relatively conservative option.
3. ***Multiple Landers*: Neutral** - TRL similar to that of a single lander.
4. ***Lander* + *Balloon*: Neutral-Bad** - The addition of a buoyancy device and systems involved increases complexity and necessitates development of an additional unproven system (previous balloons only operated in the upper layers of the atmosphere).
5. ***Rover*: Poor** - A high number of additional undeveloped systems and mechanisms, in addition to those involved with a lander.

Table 3.1: Summary of trade-off process and results.

	Mass	Cost	TRL	Reliability	Performance	Score
Weights:	1.5	3	1.5	2.5	3	
Rover	2	1	1	1	5	25
Lander + Orbiter	5	5	4	3	1	39
Stationary Lander	4	5	3	4	3	44.5
Lander + Balloon	3	2	2.5	2	4	31.25
Multiple Landers	1	3	3	5	4	39.5

Reliability

1. ***Multiple Landers*: Excellent** - redundancy significantly improves the probability of mission success as either lander can complete all objectives individually, even if it is slightly reduced in the interest of lowering an individual vehicle's mass.
2. ***Single Lander*: Good** - with the increased mass and cost budget, this option has the least unknowns and additional critical components where a failure would critically compromise the mission.
3. ***Lander + Orbiter*: Neutral** - a simplified lander would likely not have the capability of communication with Earth without using the orbiter as a relay, meaning that failure of either would lead to either full (in the case of the orbiter) or partial (in the case of the lander) mission failure.
4. ***Lander + Balloon*: Bad** - multiple landing maneuvers and the additional complexity of a flotation system present additional points of failure.
5. ***Rover*: Poor** - the number of moving parts means an incredibly high likelihood of a component failure compromising the vehicle's capabilities.

Performance

1. ***Rover*: Excellent** - a rover would enable detailed exploration of a larger area with multiple geological features.
2. ***Lander + Balloon*: Good** - this option would enable less detailed exploration of more distant areas, but would give a lower degree of control in terms of the location to focus/aim for.
3. ***Multiple Landers*: Good** - would give less detailed data for a handful of areas, but they would not be limited in terms of distance between them.
4. ***Single Lander*: Neutral** - measurements can only be taken in one place and are limited by the range of the instruments.
5. ***Lander + Orbiter*: Poor** - all measurements except the rock analysis would have to be taken from orbit, introducing large uncertainties in the data. Measurements from the atmosphere are significantly clearer when taken in-situ, so this option would yield low scientific gain.

Table 3.1 shows a summary of the trade-off process, with green cells indicating a score of 5 (*Excellent*), and red cells indicating a score of 1 (*Poor*). It can be seen that the Stationary Venus lander concept receives the highest score indicated in blue, and it is therefore the most viable concept for further design. The Multiple Landers and Lander + Orbiter concepts receive similar scores and may still be viable. The Lander + Balloon and Rover design concepts received a low total score, indicated in red, and are assumed not to be viable. From this point onwards, KYTHERA will be developed based on the single lander concept.

3.1.5 Sensitivity Analysis

The above trade-off was performed using the weights explained in Subsection 3.1.3. However, it is also important to perform a sensitivity analysis in order to assess how the ranking changes as a function of different weights and criteria. This is done in order to determine the robustness of the trade-off methodology as well as the strength of the final choice.

The way that the sensitivity analysis will be performed is by adjusting the weights of the criteria based on different rationales as well as experimenting with the exclusion of some criteria. The results are documented and an assessment is made on how the ranking is changed.

As it stands in Table 3.1, the Stationary Lander option wins by a margin of 5 points, whereas the next two options are 0.5 points apart. However, this might be because this option was in some way given an advantage due to the somewhat arbitrary assignment of criteria weights. Thus, a reassessment of criteria was attempted, summarized in Table 3.2, where the Low-Medium, Medium-High and High weightages were reassigned to scores of 1, 2 and 3, respectively. The result stays mostly the same; the Stationary Lander remains the winner with a margin of 4 points, with the two runner-ups scoring close to each other (33 vs 35 points).

The second trial was run using identical weights for each criterion. The results can be seen in Table 3.3. Although the winner of the trade-off remains the same, the margin of victory decreased to only one 1 point, being very closely followed

Table 3.2: Trade-off table with new scores of 1, 2 and 3.

	Mass	Cost	TRL	Reliability	Performance	Score
Weights:	1	3	1	2	3	
Rover	2	1	1	1	5	23
Lander + Orbiter	5	5	4	3	1	33
Stationary Lander	4	5	3	4	3	39
Lander + Balloon	3	2	2.5	2	4	27.5
Multiple Landers	1	3	3	5	4	35

Table 3.3: Trade-off table with identical weights.

	Mass	Cost	TRL	Reliability	Performance	Score
Weights:	1	1	1	1	1	
Rover	2	1	1	1	5	10
Lander + Orbiter	5	5	4	3	1	18
Stationary Lander	4	5	3	4	3	19
Lander + Balloon	3	2	2.5	2	4	13.5
Multiple Landers	1	3	3	5	4	16

by the Lander + Orbiter option. This is not unexpected - the latter was rated as a better option in all but performance and reliability. However, the weightage in Table 3.1 provides a significant advantage to the Stationary Lander option, since it is likely to provide a much larger amount of scientific data.

Further trials were run by removing one criterion at a time. When the mass criterion was ignored, the Stationary Lander stayed a winner, but closely followed by the Multiple Landers option. When the cost criterion was ignored, the Multiple Landers won by a point versus the Stationary Lander. When the TRL was ignored, the Stationary Lander won by 5 points, followed by the Multiple Landers. When reliability was ignored, the Stationary Lander won, followed 3 points behind by the Lander + Orbiter option. Finally, when performance was ignored, the Lander + Orbiter won against the Stationary Lander by 0.5 points.

Due to the subjective nature of the weight criteria selection, bias could still be present in the final selection of the trade-off. However, as can be seen in the sensitivity analysis, the Stationary Lander option prevails over the Lander + Balloon option, which was the favored option during the team discussion stage. Thus, it is sufficient to deem the effect of team bias non-impactful in this concept trade-off.

To conclude this sensitivity analysis, it is apparent that the Stationary Lander is the most robust choice, only in the most extreme cases giving way to other options, mostly the Multiple Landers and the Lander + Orbiter options. However, these swaps in ranking are very tight in nature, with the Stationary Lander losing only by very few points. Since the ranking is only a tool to roughly gauge the best candidate, it is acceptable to elect the option that is the most robust, even if it does not always win. Therefore, the selected mission architecture will be the Stationary Lander architecture, as it has proven to be the most robust against changes of weights and criteria.

3.2 Landing Site Selection

This section will detail the process of selecting a landing site and discuss the final choice. It starts with Subsection 3.2.1, which displays the largest considerations on the problem of where to land on Venus. Next, terrain types are discussed in Subsection 3.2.2, followed by a list of landing site conditions in Subsection 3.2.3. Two candidate landing sites are detailed in Subsection 3.2.4 and Subsection 3.2.5, as well other considered sites in Subsection 3.2.6. Finally, a tradeoff is performed in Subsection 3.2.7 and a conclusion on the landing site is drawn.

3.2.1 Considerations

The question of where to land is a major concern for any mission to the surface of a celestial body. The landing site determines many aspects of the mission, ranging from the amount of potential scientific information to be gained and the environmental conditions that the spacecraft will face, to communication windows with the orbiter and overall risks of the mission. According to requirement OPS-EDL-AE-LA-1, the required landing accuracy is 100 km, meaning that landing zones have a generous 200 km-wide error margin. Nevertheless, the selection of a single landing site from an entire Earth-sized planet borders on the absurd, making a thorough selection process necessary.

The process of selecting a landing site is done through multiple criteria: terrain safety, geological terrain type, altitude, proximity to potentially active geological units, and communications windows with the orbiter. Terrain types, their geological importance and safety for landing will be discussed later in this subsection.

It was decided to only consider landing sites in the polar regions of Venus, as a relay in an eccentric polar orbit allows for significantly longer relay windows than an equatorial relay. This will be explained in more detail in Section 5.4.

Due to evidence of active volcanism on Venus [31], it would be beneficial to land close to regions of active or formerly

Table 3.4: Distribution of geological units over Venus's surface and their landing safety, taken from Ivanov and Head [36].

Unit Name	Label	Area, 10^6 km^2	% of surface	Safe?
Tessera	t	33.2	7.3	NO. Highly deformed terrain
Densely lineated plains	pdl	7.2	1.6	NO. Highly deformed terrain
Ridged plains	pr	9.6	2.1	NO. Rolling, uneven hills
Mountains	mt	1.3	0.3	NO. Dangerous slopes
Groove belts	gb	37.1	8.1	NO. Highly fractured terrain
Shield plains	psh	79.3	17.4	YES. Smooth, mostly undeformed surface
Regional plains, lower unit	**rp1**	**141.8**	**31.1**	**YES. Smooth surface with few deformities**
Regional plains, upper unit	rp2	42	9.2	YES. Smooth surface with moderate deformities
Shield clusters	sc	3.3	0.7	NO. Undeformed, but uneven terrain
Rift zones	rz	22.6	5	NO. Highly deformed terrain
Smooth plains	ps	10.3	2.3	YES. Smooth surface with no deformities
Lobate plains	pl	37.8	8.3	YES. Smooth surface with few deformities
Craters	c, cf	2.6	0.6	NO. Dangerous slopes
Gaps		28.1	6.2	NO. Unknown terrain type
Total		456.3	100	

active geological processes. The seismometer will be able to pick up potential "Venus-quakes" in case a volcanic eruption takes place, providing valuable information about Venus's interior processes. Additionally, recent research by Bledsoe and Klimczak 2025 [32] indicate that canali on Venus could be of potential scientific interest, and thus a landing location close to one would be of benefit.

Another factor that comes into play when considering landing sites is local topography. A landing site that is higher up is exposed to slightly different atmospheric conditions. For example, at 5 km altitude, the temperature and pressure decrease to 422 °C and 67 bar respectively [33–35]. Although it would be prudent to design the lander for zero-altitude surface conditions regardless of landing site, lower environmental stresses on the lander could mean a longer lifetime and thus potentially more scientific information retrieved.

3.2.2 Terrain Types

It is not possible to land everywhere on Venus; its surface consists of many terrain types, some of which are safer or more scientifically interesting than others. In addition, since this mission will perform many first analyses of the surface, it is important that the analyzed material be as representative of the entire planet as possible.

In Table 3.4 a table of all terrain types (labeled with a letter or code) and their respective distribution across the planet is shown. Information for this table is taken from Ivanov and Head [36]. A complete overview of all terrain types is beyond the scope of this report, but every geological unit is described in detail in the same paper [36]. In short, as explained also by the Project Guide [2], volcanic plains make up the largest percentage of the planet's surface, best represented by rp1 terrain, at 31.1% of the Venusian surface.

Each terrain type is assessed for its landing safety based on its morphology. That is to say, only the terrain types allowing for the safe landing of the spacecraft are considered for the landing selection. Terrains such as t or mt are not considered as landing sites because of their deformed and treacherous terrains. Instead, morphologically smooth terrain is preferred, represented best by ps, pl and psh. Less smooth but still acceptable are rp1 and rp2 terrains.

Since rp1 terrain is the most extensive terrain on Venus, it is also likely to be the most representative of its surface and geology. As such, and since it has been assessed as a safe terrain type for the lander, rp1 type terrain will be the primary target for the landing sites. This conclusion has also been drawn in the concept design study for the Venera-D mission [17] (not yet launched).

The decision is also encouraged by the few existing images from the surface of Venus, sent from Veneras 9, 10, 13 and 14: whereas 10 and 14 landed in rp1 terrain, 13 landed in rp2 and 9 landed in pr. The returned photographs showed a difficult, rocky terrain from Venera 9 (pr-terrain, see Figure 3.2[4], whereas Veneras 10 and 14 imaged fractured but relatively smooth terrain with small, sparse rocks (rp1-terrain, see Figure 3.4[4] and Figure 3.3[4]). Venera 13 returned a similarly smooth terrain with small gravel and fractured outcrops (rp2, see Figure 3.5[4]). This reinforces the conclusion that regional plains are safe landing locations, whereas the ridged plains are not.

[4] `https://www.planetary.org/articles/every-picture-from-venus-surface-ever`, accessed on 17/Jun/2025.

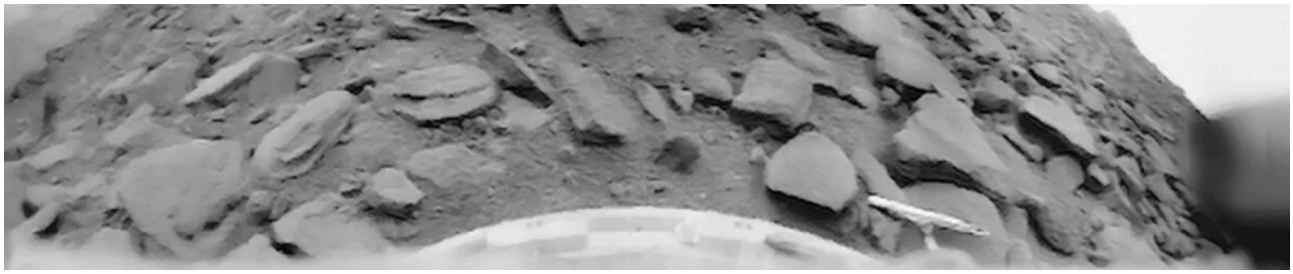

Figure 3.2: Venus surface panorama from Venera 9. Venera 9 landed in pr-type terrain. Credit: Russian Academy of Sciences/Ted Stryk.

Figure 3.3: Venus surface panorama from Venera 10. Venera 10 landed in rp1-type terrain. Credit: Russian Academy of Sciences/Ted Stryk.

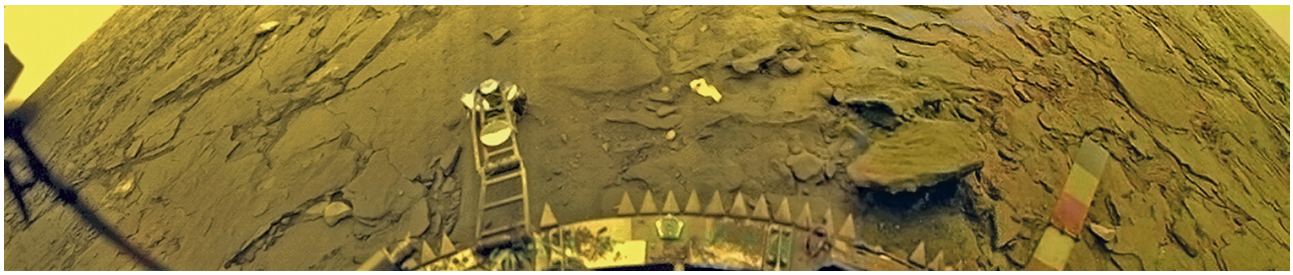

Figure 3.4: Venus surface panorama from Venera 14 front camera. Venera 14 landed in rp1-type terrain. Credit: Russian Academy of Sciences/Ted Stryk.

Figure 3.5: Venus surface panorama from Venera 13 rear camera. Venera 13 landed in rp2-type terrain. Credit: Russian Academy of Sciences/Ted Stryk.

It is important to note that, although the images returned from the Veneras seem to correlate with the previous assessment based on radar imagery, the latter cannot evaluate surface features smaller than hundreds of meters across. However, it is the decimeter-sized rocks that could pose the biggest threat to KYTHERA, as the lander may impact the ground on top of such a rock and get its outer shell pierced, leading to premature end of mission. These rocks cannot be detected with currently available data and no knowledge exists of their presence outside of the images returned by the Venera landers. As such, the radar-based evaluation of terrain safety combined with the limited imagery from previous probes represents the ”best-guess” possible, and to the authors’ knowledge, there is no further available information that could improve landing site suitability.

3.2.3 Conditions for Landing Sites

Below is a list of preferences and requirements for the selection of a landing site. These are not formulated as SMART requirements, since they were made only to help the selection of a landing site.

- Terrain type must be rp1
- Site must be near the poles, since a lower latitude would mean substantially less data transmitted (a latitude lower than ~65° would incur substantial data losses)
- A higher landing site is preferable, because it would incur less environmental stress on the lander
- Preference is given to sites closest to potentially active geologic features [31] and canali [32]
- In order to satisfy requirement OPS-EDL-AE-LA-2, the site should preferably be in daylight at the optimum times of arrival on July 28th[5]. At both these dates, the subsolar point on Venus is located at ~15° W longitude[6].

With these in mind, two main candidate landing sites have been identified. These will be presented immediately following this subsection. Other sites considered but not selected for further investigation are shown in Subsection 3.2.6.

3.2.4 Landing Site 1: Lakshmi Planum

Lakshmi Planum is a large plateau in western Ishtar Terra, bordered by Freyja Mons to the north and Akna Mons to the west. Lakshmi Planum features two large Pateras, Colette and Sacajawea, as well as extensive pl-terrain volcanic plains, the youngest of which lie in its South.

The preferred landing site of this region is located towards its north. It is a 100 km radius circle, centered at 69.6° north, 33.0° west, and lies at an elevation between 2900m and 3200m, giving a temperature of 430 °C and pressure of 77 atm [33–35]. Figure 3.6 shows a radar map of the landing site.

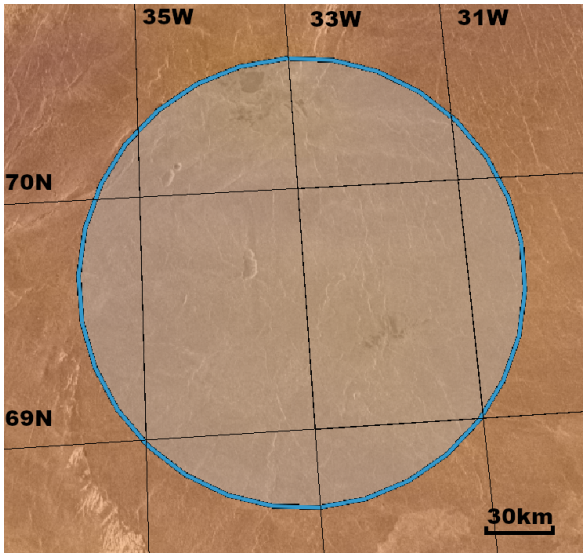

Figure 3.6: Radar image of the Lakshmi Planum landing site.

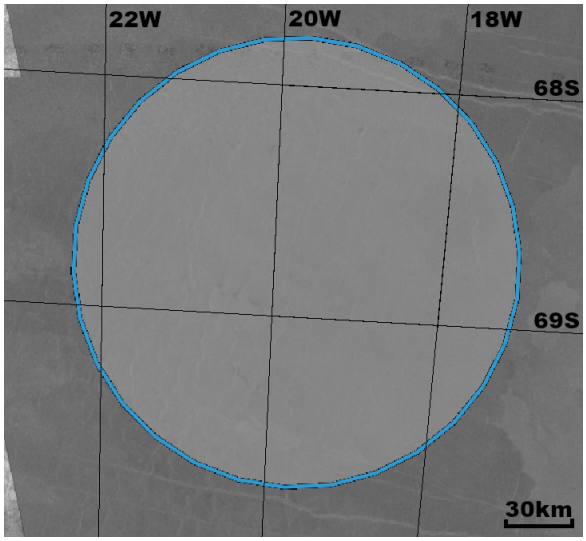

Figure 3.7: Radar image of the Lada Terra landing site.

To the South and South-West of this region lie three Coronae, of which one inactive and two of ambiguous activity: Omosi-Mama Corona, Beiwe Corona, and Xilonen Corona [31]. Although they are likely inactive, seismological research could still benefit from measuring local disruptions or otherwise global events. However, this site does lie in the vicinity of two canali, Lunang and Saga Canali, about 500 km away. Although this distance definitively prohibits any direct exploration of the canali, geological information from this area may help infer some information about their nature.

3.2.5 Landing Site 2: Lada Terra

Lada Terra is the Southernmost of the three major continental regions of Venus, and presents a large number of potentially active Coronae. The most interesting of these is Quetzalpetlatl Corona, the largest Corona on Venus. Furthermore, there are numerous nearby potentially active geological features, including Quetzalpetlatl itself [31]. These features make the Lada Terra landing site more interesting from a seismological point of view, as proximity to these features could provide more information about Venus's internal structure and mechanism. However, canali are absent from this area, the closest being Chasca Vallis, approximately 2000 km away.

The selected landing site lies completely in rp1 terrain, and is a 100 km-radius circle centered at 68.75° south, 19.7° west. Although proximity to interesting geological features make this a great landing site scientifically, its reference-level

[5] From NASA's Trajectory Browser website, for Earth-Venus transfers between 2036-2040. URL:`https://trajbrowser.arc.nasa.gov/`, accessed on 02/Jun/2025.

[6] Found using Stellarium and corroborated with manual calculations using NASA JPL's Horizons System. URL: `https://ssd.jpl.nasa.gov/horizons/app.html#/`, accessed on 03/Jun/2025.

elevation give it a temperature of 464 °C and a pressure of 93 bar, placing it at a disadvantage compared to the Lakshmi Planum site. Figure 3.7 shows a radar map of the landing site.

3.2.6 Other sites

Several other landing sites and regions have been considered but ultimately not selected as finalist options. These were dismissed due to defects such as terrain deformities, harsher conditions, poor mapping, or simply lack of proximity to scientifically interesting features. They are listed below:

- **Quetzalpetlatl Corona**: 100 km-radius circle around 67.2° South, 5.8° West, on top of Quetzalpetlatl Corona. Higher elevation and larger landing area, but terrain type is pl. Furthermore, Coronae, while very interesting scientifically, are not representative of the entire surface of Venus. Although this is a strong candidate as a landing site for future missions, it does not fit within this mission's requirements.
- **Anahit Corona**: 100 km-radius circle around 79.9° North, 76.6° West, near Anahit Corona. Chosen mostly for its proximity to the North Pole and the volcanic edifice of Laka Mons. Although terrain type is mostly rp1, a 100 km-radius circle does not fully fit within the limits of the terrain, and will include potentially hazardous terrain. Due to diminishing returns on communications-capacity with respect to latitude, this site does not offer any advantages over the nearby Lakshmi Planum site.
- **Nightingale Corona**: Extensive rp1-type terrain towards the northeast and northwest of Nightingale Corona gives an ample selection landing sites, ranging from 100 km to 200 km in radius. These are around Klenova, Monika, Selma, Dickinson, Jex-Blake, Erika Craters and Norwan Dorsa. However, these landing sites are located mostly below the Venusian reference level, some of them even going down to 2000 m below (as in the case of Norwan Dorsa), equating to 470°Cand 99 atm [33–35]. In addition, terrain in this region appears fractured, with frequent ridges and other linear features showing on the radar imagery[7]. Therefore, it was decided that this region posed too many threats and constraints when compared to the other options and was eliminated.
- **South Polar Region**: The South Polar region of Venus (90° E - 50° W) offers the widest landing site options, encompassing regions of uninterrupted rp1-type terrain up to 360 km in radius. However, it has extensive areas that are incompletely mapped. The best-mapped site in this region is a 220 km-radius circle centered at 69.9° S, 173° E, in the vicinity of Shelikhova Patera, lying between 0 and 600 m below the reference level of Venus. The terrain in this circle is smooth and mostly void of major fractures or ridges. However, it is very far away from any active or inactive volcanic or tectonic features. This, coupled with low elevation and poor mapping, render this site, and by consequence all other sites in the region, unsatisfactory.

3.2.7 Trade-off

Both Lakshmi Planum and Lada Terra sites adhere to the pre-established requirements and provide high scientific value to the mission. However, as explained before, these two sites have certain differences: whereas Lakshmi Planum lies at a higher elevation, giving a possibly longer lander liftime, the Lada Terra site lies closer to possibly active features, potentially allowing the mission to collect better science. Thus, it is difficult to decide between the two purely qualitatively, and a tradeoff is required. Three criteria are identified: Safety, Elevation and Proximity to Activity. Safety encompasses terrain deformities as well as surface features that might cause the lander to tip over or otherwise sustain damage. A smoother terrain and fewer surface features gives a higher score. A higher Elevation score indicates higher site altitude; the surface conditions become less harsh with increasing altitude, possibly giving the lander a longer life. Finally, Proximity to Activity represents the quality of scientific data that could be obtained from the seismometer. Although the seismometer can detect events from across the planet, proximity to active regions grants higher SNR which could improve later investigations.

Table 3.5 summarizes the tradeoff. Safety is assigned a weight of 50% since it is paramount to mission success; Elevation is assigned 30% since it could improve received data substantially; Proximity to Activity is given 20% because activity on Venus is not the subject of scientific consensus, but could similarly improve science returns. The scores are assigned on a scale of 1 (Worst) to 5 (Best). The Lakshmi Site receives a Neutral (3) score for Safety, since it is located on a plateau surrounded by mountains, and there are some features (most notably, a circular feature near the center of the landing site) that might be dangerous for the lander (see Figure 3.6). The Lada Site received 4 thanks to its relatively featureless radar map, but it is similarly surrounded by dangerous terrain. It receives a score of 2 in Elevation, however, as it lies at or below Venus's reference level, whereas the Lakshmi Site scores a 5 due to its very high elevation. Finally, the Laskmi Site is assigned a 3 for its Proximity to Activity because, although it is near some Canali and inactive volcanoes, it still is far away from active features. The Lada Site receives a 5 since is it placed directly adjacent to the active Quetzalpetlatl.

[7]Venus Quickmap has been extensively used to explore available imagery of Venus's surface. URL: `https://venus.quickmap.io/`, accessed 28/May/2025.

Table 3.5: Landing site tradeoff. Result is inconclusive.

Criteria:	**Safety**	**Elevation**	**P. to Activity**	**Total**
Weight:	50%	30%	20%	100%
Lakshmi	3	5	3	3.6
Lada	4	2	5	3.6

Both Lakshmi and Lada Sites receive the same total score of 3.6, making this tradeoff inconclusive. This shows the difficulty of choosing one landing site over another within an entire planet's worth of options; deeper and more thorough research should be done in order to determine more differences. As such, in the post-DSE phase of this project, a working group composed of scientists specializing in Venus science and geology will be formed in order to find the best landing sites. Until the working group determines a final list of landing sites, KYTHERA will use Lakshmi Planum as its preliminary primary landing site. In this light, since the working group might determine a different site as the best one, the lander will be designed to work at any latitude at or above 65° North and any altitude at or above the Venus reference level.

4

Systems Engineering

Systems Engineering is an interdisciplinary approach useful in managing and designing complex products. It encompasses everything from setting up the initial requirements of what the design must fulfill, to meeting stakeholder needs and managing complex interactions within the design. Furthermore, the assembly, integration and testing phase that happens after design is of critical importance, planning for this is a key tenet of systems engineering. Using this approach, risks can be managed, and designs and systems can be verified and validated.

KYTHERA is a very complex mission, which combines a myriad of novel technologies and a challenging environment. All these factors combine together and interact, leading to a clear need of the systems engineering approach. Since the Midterm Report, the design has been worked out in more detail, and more work was done on the logistical and development aspects of the mission.

This chapter will first review the functions that the system has to fulfill in Section 4.1 and then go over and recap the requirements that this mission concept started with in Section 4.2. Then, the current design is presented on a system level through block diagrams and schematics in Section 4.3, followed by Section 4.4 where key interfaces between different subsystems are identified. This is followed by an outline of the different mission phases in Section 4.5, going from pre-conceptual design, to operation of the system. Then, these phases will each be discussed in more detail along with the milestones that accompany these mission phases. Budgets are then constructed and iterated in Section 4.6. The chapter concludes with an analysis of the system level technical risks, and proposed mitigations thereof in Section 4.7.

4.1 Functions

In the development of complex space systems such as a Venus lander, one of the earliest and most crucial steps is to define the functions that the system must do. Its important that this is done independently of how it will be implemented. Functional analysis supports this goal by helping clearly structure and communicate the intended behavior of a system. As part of this baseline report, two key outputs of this process have been created: the Function Breakdown Structure (FBS) and the Function Flow Diagram (FFD). These tools are essential for informing and guiding the design and development of the lander.

Function Breakdown Structure

The FBS presents, as the name says, a hierarchical breakdown of the mission's overall objective into a set of more detailed functions. This structure begins with the lander's main purpose, which is to successfully land on Venus and conduct scientific operations. It then breaks this purpose down into major mission phases and subsystem responsibilities. Each branch of the structure defines a specific function that contributes to achieving the higher-level goals. This is done to ensure that no necessary operation is skipped and that responsibilities can be clearly assigned to specific subsystems or teams during the design process. It also provides a valuable framework for tracing technical requirements, identifying verification needs, and prioritizing development tasks. Each identified funtion is given a unique identifier of the format "F#(.#...)" where # represents an integer. The level of detail is represented by a numbering system in the identifiers and also by the different color shades, with lighter shades being lower levels. The FBS can be found in the Appendix.

Functional Flow Diagram

The functional flow diagram (FFD) complements the Functional Breakdown Structure (FBS) by showing the logical relationships between the identified functions and their order in which these should take place. While the FBS answers the question of "what" the system must do, the FFD focuses on "when" and "in what sequence" these functions must occur. It has both operations that happen in series, such as descent followed by landing, and parallel activities, such as data pro-

cessing and thermal control occurring simultaneously. This provides insight into how the system behaves dynamically throughout the mission. By showing dependencies and interactions between functions, the FFD helps making decisions related to task scheduling. It is particularly valuable for identifying bottlenecks and coordination challenges. The functions are represented by blocks and are connected by arrows, which indicate dependence and flow from one another. The arrows have a different color depending on the top-level function they are connected to. The level of precision for the functions is indicated by the ID of the function and the shade in orange/yellow. The IDs of the functions in the FBS are identical to the ones in the FFD to avoid confusion. In future design stages, the FFD and FBS will become more detailed and will be expanded to subsystem functions. The FFD can be found in the Appendix. To decrease clutter, the FFD was divided over two pages, where it should be noted that all Level 2 functions are mentioned on both pages, with functions F1-F7 expanded in Appendix B1 and functions F8-F11 expanded in Appendix B2.

4.2 Requirements Management

In this section, the management of requirements is presented. Different forms of requirements have been established in the process of designing this system. From the beginning, there have been customer requirements. There are also driving requirements, these requirements drive the design to a relatively extreme extent. Killer requirements are ones that are likely to be the most hard to fulfill, and therefore the most likely to render a design unacceptable. As the design went on, requirements got more specific, so these systems requirements were joined by subsystem requirements. Relevant subsystem requirements are discussed in their respective subsections in Chapter 5. To ensure the design fulfills these requirements, their compliance is tracked. In requirements compliance matrices it is shown whether these equirements are met. If requirements are not met, a justification must be given how the design will be changed, or why the requirement is unrealistic, and a case must be made to change it. To verify for sure that requirements are met, several methods of verification are devised. These are presented in Subsection 4.2.1. Then, a number of driving- or key requirements at the system level are presented in a compliance matrix in Subsection 4.2.2.

4.2.1 Verification Methods

To ensure that every requirement is implemented, verification must take place in different forms. A list of verification methods and their corresponding ID can be found below. These are used to tag the different requirements present throughout this report.

Table 4.1: Verification methods.

ID	Verification Method
V-DEM-TEM	Demonstrate that the component can resist the required temperature by heating it in a oven
V-DEM-PRE	Demonstrate that the component can resist the required pressure by putting it in a pressurized environment
V-DEM-COR	Demonstrate that the component can resist the Venusian corrosive environment by putting it into a chamber simulating the Venusian atmosphere
V-DEM-TSK	Demonstrate that the component can perform the mentioned task in a lab on earth
V-DEM-STR	Structural testing on a test bench on Earth
V-ANA-FEM	Perform finite element analysis
V-ANA-CFD	Perform computational fluid dynamics analysis
V-ANA-SIM	Perform mathematical simulation
V-ANA-SIM-TH	Mathematical analysis through heat transfer model
V-ANA-LIF	Reliability and lifetime modeling to calculate the probability that a system will perform its intended function without failure over a specified time and environment and to estimate how long hardware components can operate before degrading or failing
V-INS-SIZ	Measure size of component
V-INS-WEI	Measure weight of component
V-INS-SFT	Inspect software code, inputs, outputs and structure
V-INS-DAT	Inspection of data sheet or hardware label
V-INS-SMT	Ensure that all requirements are specific, measurable, achievable, relevant, and time-bound (SMART).
V-INS-COM	Ensure compliance with European and international guidelines, best practices and legal frameworks
V-TST-UNI	Perform unit tests
V-TST-GRD	Perform ground operational testing
V-TST-FUN	Verify that the component is able to perform the mentioned function by performing a test in a lab
V-CST	Cost tracking during design and budget review and cost analysis based on supplier quotes, historical data, and estimation tools

4.2.2 Requirement Compliance Matrix

Provided in Table 4.2 are system level requirements that have to be fulfilled in the design, manufacturing or operation of the vehicle. This table is a summary of the table presented in the Midterm Report. In the right entry of Table 4.2, the requirement compliance (RC) is presented. A check mark means that the requirement is met, a question mark means that

the requirement can't be verified yet and that this will be done post-DSE and a cross means that the requirement is not met.

Table 4.2: Systems engineering requirements.

Requirement ID	Requirement Description	Verification	RC
GSYS-1	Total lifetime cost, excluding the EDL system, shall not exceed 200 million EUR.	V-CST	X
GSYS-2	Total mass, excluding the EDL system, shall not exceed 350 kg.	V-INS-WEI	✓
GSYS-3	The power subsystem shall have a mass of at most 25% of the total system mass.	V-INS-WEI	✓
GSYS-8	The system shall fulfill the requirements set out by the ECSS-U-ST-20C working group regarding space sustainability.	V-TEST-FUN	✓
MFCT-ISP-1	Individual probe's EDL (Entry, Descent, Landing) probability of success shall exceed 90%.	V-ANA-LIF	✓
MFCT-AS-2	Every component of the system shall be producible with manufacturing methods of a TRL of no less than 5.	V-INS-DAT	✓
MFCT-AS-3	The integrated system functionality shall be verifiable.	V-INS$_{SMT}$	✓
MFCT-AS-4	The integrated system functionality shall be validatable.	V-INS$_{SMT}$	✓
MFCT-AS-5	The functionality of all individual components shall be verifiable.	V-INS$_{SMT}$	✓
MFCT-AS-6	The functionality of all individual components shall be validatable.	V-INS$_{SMT}$	✓
MFCT-HC-1	No part of the manufacturing process shall violate EU work standard regulations.	V-INS-COM	✓
MFCT-2	No parts used in the system shall violate European export and dual use regulations.	V-INS-COM	✓
OPS-LND-T-2	All non-cooled components of the system shall retain their function up to 800 K ambient temperature for the duration of the mission.	V-DEM-TEM	✓
GSYS-5	The system shall have an operational lifetime of at least 200 Earth days.	V-ANA-LIF	✓

The description of verification method IDs are found in Table Table 4.1.

4.3 System Architecture

All subsystems on the lander have to function together to accomplish the mission goals. To make sure that all subsystems work together, it is imperative to map all the ways in which subsystems interact and to document any interfaces - parts of a system that are used for interaction with other systems. These can be mechanical, electrical or software based. For a first effort to map these dependencies, an N-squared diagram was created, shown in Table 4.3.

This table puts the different subsystems on the diagonal, with outputs of this subsystem on the horizontal, and inputs to this subsystem on the vertical. This means that every item is an output of one subsystem and an input for another. In this way, it can be easily seen what a design change in one subsystem has for effect on other subsystem. This way, the systems engineer and the relevant subsystem engineers can keep track of the effect of changes, and how they cascade throughout the entire system. To give an example from the N-squared diagram: The payload generates data, this data then needs to be processed by the CDH subsystem, if it does not have enough storage, the communications subsystem must transmit all of this data quickly, this may require more electrical power, leaving less power for the payloads, which reduces the generated data, etc.

Furthermore, block diagrams are made of the mechanical, electrical and software design of the vehicle. These block diagrams illustrate how different subsystems operate in the spacecraft and how they are connected physically, electrically or by software to each other. This is another way of identifying interfaces between these subsystems or components and make sure that care is taken that the spacecraft will work as a whole.

Table 4.3: N-squared diagram.

Power	Provides electrical power for C&DH subsystem	General Purpose Heat sources generate heat which can create noise for comms amplifier.	Generates heat that needs to be dissipated, especially during EDL. Generates shaft power that powers cooling system.	The power subsystem may stick out of the lander, so aeroshell must be designed around this.	Provides electrical power for payload functioning.	Generators on top of drag plate require reinforcements.	
C&DH requires electrical power	**C&DH**	Stored data must be able to be sent to orbiter when it's overhead.	Some electronics will require cooling from the thermal subsystem.		Send commands to instruments.		
Comms require electrical power	The comms system receives commands that have to be processed by the C&DH subsystem.	**Comms**	Required Cooling.	EDL has to be timed such that comms are overhead.		Comms system must be mounted and protected from corrosive venusian atmosphere.	Range of antennae influence desired apoapsis of orbiter.
Cooling system requires mechanical shaft Power.	Cooling from power reduces the amount of heat resistant electronics needed.	Better cooling of amplifiers reduces required antenna size or gain.	**Thermal**		Provides cooling to instruments.	Heatshield mounting, cooling systems.	
Attitude control power requirement, battery sizing		Entry plasma creates temporary comms blackout.	Heat generated during EDL must be dissipated, aid from thermal subsystem may be required	**EDL**		EDL causes acceleration and shock loads that the lander structure must survive.	Slowing & Steering
Payloads require electrical power.	Payload data generation needs to be stored and processed before transmitting.	Landing site influences communication windows	Payloads may require cooling, and also generate their own heat	Required landing site accuracy & Atmospheric measurements during Entry.	**Payload**	Payload needs to be mounted and may need to be protected from atmosphere. Also mechanisms may be required for deployment.	
		Structure can block radio signals if in the wrong place or of the wrong material.	A heavier structure is harder to heat up but also harder to cool down, more surface area means more heat entry or rejection.	Must have secure but separable mountings to EDL subsystems, Aeroshell and heatshield must be sized around structure.	Structure must allow for measurements to be made through openings or windows.	**Structure**	
		Orbiter astrodynamics influence the possible communication windows.		Entry trajectory and velocity influence required heatshield design.			**Navigation / Astrodynamics**

4.3.1 Mechanical Block Diagram

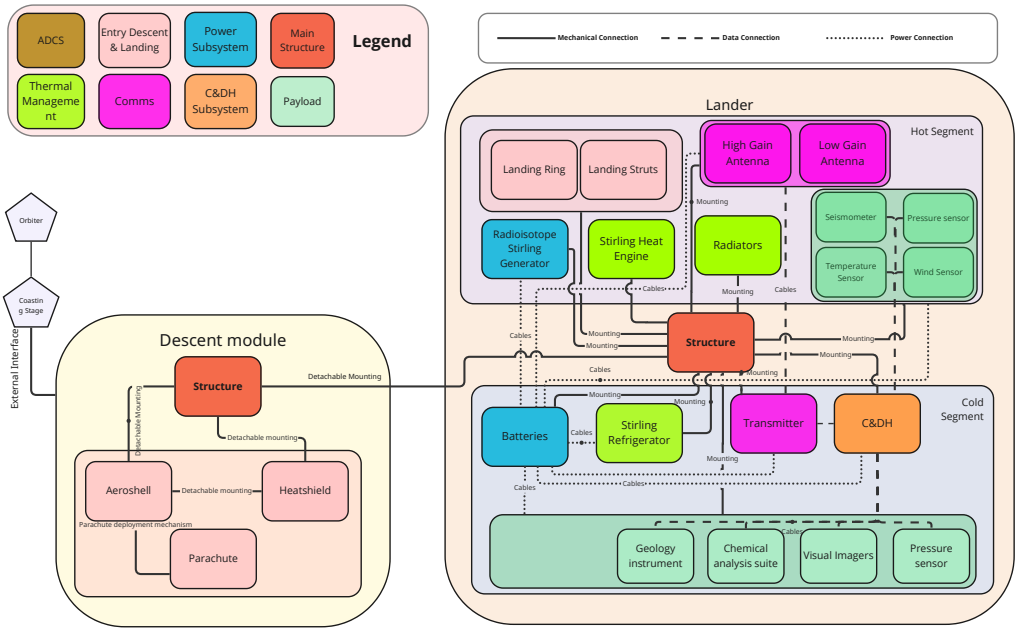

Figure 4.1: Mechanical block diagram for lander and EDL system.

In Figure 4.1 it can be seen that the overall system can be divided into a descent module and a lander part. The potential design of the descent module is described in Section 5.1. This part of the system is used to safely land on the Venusian surface but will be discarded before beginning the nominal science phase. The lander on the block diagram again divided

into two parts, namely a cold and a hot part. The lander will incorporate a cooled section for some components as discussed in Section 5.3. In the block diagram there is also a distinction made between permanent and detachable mountings, e.g. the heatshield, followed by the lander itself, must separate from the EDL stage onward. In a design change since the midterm report, a coasting stage has been added. It will provide the lander system with cooling and attitude control during the time between orbiter separation and atmospheric entry. In the previous design iteration, this was done by the lander itself, with the required components added to the lander's aeroshell. This was deemed too complex and infeasible, so a simple disposable stage is preferred. The whole lander system is attached to this coasting stage during transit to Venus, which in turn is attached to an accompanying Venus orbiter. These are all connections that, over the course of the mission, are to be mechanically severed. Cables for the transfer of power and data are vaguely shown in the block diagram. These connections are further detailed in the electrical and software block diagrams, with some of these interfaces explained in more detail in Section 4.4.

4.3.2 Electrical Block Diagram

The electrical block diagram in Figure 4.2 shows that the main subsystems of the lander (ADCS, Instruments, Power, CDH, Comms) share all of the primary components of the power system electronics, whereas the EDL subsystem has some dedicated components. This is primarily due to the fact that the EDL subsystem should be largely separated from the rest of the lander prior to landing, and some critical components such as batteries and dedicated interface electronics are necessary to ensure a successful separation. The voltage represents the standard bus voltage chosen for the power system.

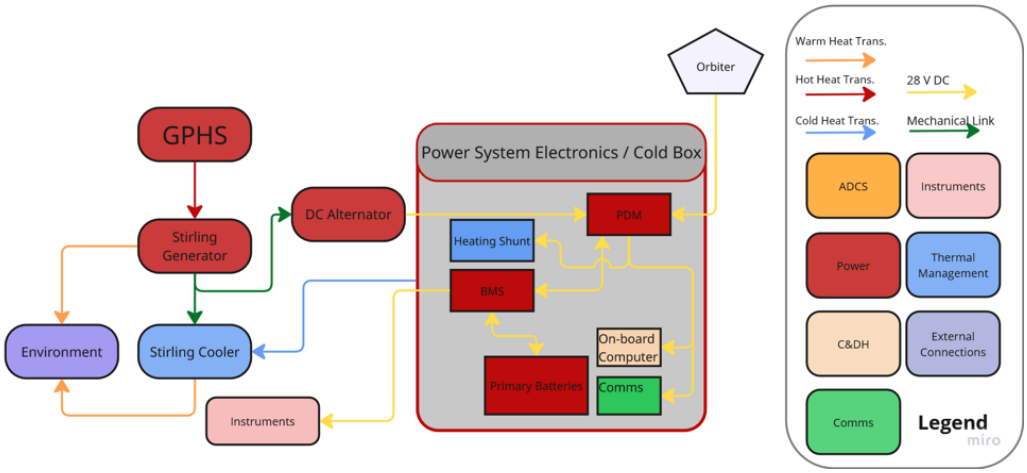

Figure 4.2: Electrical block diagram for lander and EDL system.

4.3.3 Software Block Diagram

The software block diagram is given in Figure 4.3 and it can be seen that the main computational tasks are each give a big blue block. The precise functions that each task must perform are given in smaller blocks within the main task block. When the arrow points into the function, this represents an input and when it points out, it represents an output. For example, the output of the function "turn generator on and off" would affect the power generator, which in turn the task "distribute loads" function would take these as an input to perform its calculations.

Lines of Code

The software used by the lander is estimated to be between 300,000 and 500,000 lines of code. This estimate is based on the complexity required to manage the different systems of board present in this design. The code covers functions such as instrument control, data handling, thermal control, power distribution and other operations. While the lander does not require any mobility related software, it must be able to operate independently for long periods and manage the operation of extremely advanced systems such as the chemical analyzers. Finally, it includes multiple algorithms related to data compression, communication protocols and real-time decision making to ensure it can perform its mission with minimal intervention from Earth.

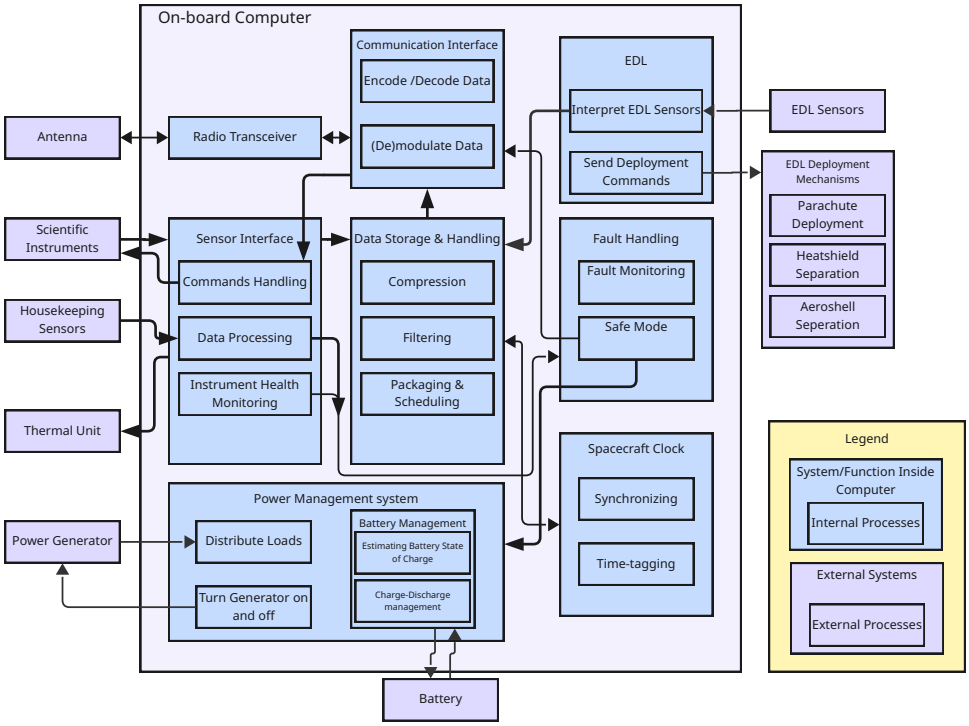

Figure 4.3: Software block diagram for lander and EDL system.

4.4 Key Interfaces

In this section, a summary of key interfaces are detailed. These are grouped in internal and external interfaces, representing those within and outside the spacecraft.

4.4.1 Internal Interfaces

- **Power from RSG to cooling.**: In the previous report, a design choice was yet to be made for the method of transferring power from the radioisotope Stirling generator. The choice was between using electrical power, and using a shaft to transfer mechanical power. It was found that the energy losses from converting the mechanical output of the RSG to electrical power, and using that to power the Stirling heat engine are very significant. The mechanical losses and increased mass of using a shaft to transfer mechanical power are less severe, making it the more appropriate option. Because the two systems are mechanically linked, they are now situated quite closely together. More information about the power and thermal control subsystem can be found in Section 5.3.
- **Heatshield detachment mechanism**: As mentioned in the midterm design report, the heatshield is a critical part of the EDL system, but it must be detachable. Then, there was not a decision yet made on how it interfaces directly with the lander, notably to support the lander through the intense entry decelerations. Instead of rigidly connecting them, a non-rigid support is chosen. This means that there is a structure that supports the lander from the bottom, without being rigidly connected. This removes the need for a separation mechanism between them, with the heatshield only connected to the aeroshell. This connection will be made with pyrotechnic bolts that are used as fasteners, but can be cut when a specific voltage is applied through them. These devices have a rich flight heritage as they are used in launch vehicle and satellite staging mechanisms.
- **Aeroshell detachment mechanism**: The lander is rigidly connected to the aeroshell. For both these interfaces, more information can be found in Section 5.1.
- **Seismometer (and sampler) actuation mechanism**: The payload comprises among other things a seismometer and a geological science experiment. As the seismometer likely has to be deployed outside the lander for optimal science gain, depending on the geological science suite chosen, this experiment also has to use deployment mechanisms. This is an interface between the payload and the structures subsystem. Further details are written in Section 5.2.
- **Data distribution throughout the lander**: In the lander there will be scientific data generated by the various instruments and sensors on the lander, and this it has to be returned to Earth. The CDH subsystem handles this interface between the payload and communications subsystems by means of cables, computing and filters. This is seen in more detail in the data handling block diagram, Figure 5.46.
- **Parachute deployment**: The parachutes are mounted on the top of the aeroshell, however a method is needed to deploy them. First a drogue chute is deployed via a mortar, and then acts as a pilot chute to pull out the main.

4.4.2 External Interfaces

- **Wake-up from hibernation**: During cruise flight the lander will be in hibernation, and its antenna will not be pointed at Earth. The orbiter will therefore be responsible for receiving the signal to wake up the lander, which should subsequently end the lander's hibernation mode. This reduces wear and tear on the onboard systems and extends their lifetime.
- **Lander + EDL module detachment mechanism from Orbiter**: The entire lander and EDL module assembly will be attached via a coasting stage to the orbiter from the start of the mission until arrival near Venus. This connection has to be strong enough to survive the forces of launch and all the necessary maneuvers. Upon separation, the connection has to be severed in a way that does not impose high shock loads. For the separation between the Orbiter and the coasting stage this will be achieved through the use of pyrotechnic bolts, which, as mentioned earlier, are very reliable. These bolts do potentially impart a bit of tumble if their charges do not fire at the exact same time, but, because the coasting stage has it's own ADCS system, this is not considered an issue. Just before Venus entry, the coasting stage orients the lander correctly before separating itself. Because the lander at this point is unguided, this separation has to happen with little to no tumbling. Therefore a simple latching mechanism with synchronous springs is preferred. While this has the disadvantage of requiring moving parts, it has the required separation accuracy. Besides severing the structural connection, feed lines and cables have to be severed. This will be done using quick disconnects and pogo connectors with magnets respectively.
- **Fueling and handling ports and interfaces for ground ops**: The entire vehicle needs to be serviced while still on the ground. This includes fueling, pressurizing any systems as needed and charging batteries. This necessitates the presence of interfaces and ports that allow for these interactions. All these operations have to happen before encapsulating the payload in the launch vehicle's fairing. Furthermore, the GPHS is installed on the vehicle after it has been mounted inside the entry descent and landing module, necessitating an access hatch in the aeroshell.

4.5 Design Phases

The design of a spacecraft is divided in different phases, according to ESA, there are six distinct ones[1], ranging from phase 0 to phase F.

- **Phase 0, Mission Definition**: In the mission definition phase, the mission needs and science performance goals are identified. This results in a initial set of technical requirements on a system level.
- **Phase A, Mission Feasibility Study**: The actual design phase starts with a mission feasibility study. From the previous phase, a set of technical requirements has been identified. In the Mission Feasibility phase initial design concepts are produced, and their feasibility is assessed against these imposed requirements. The non viable concepts are discarded and the a trade study is done on the remaining concepts. From this, one mission concept is selected to work out further. Then a large number of new, concept-specific, requirements are generated both for the spacecraft as a whole and for the subsystems. Initial budgets are created and risks are assessed. An overall system architecture is designed and required subsystems and their functions are identified.
- **Phase B, Preliminary Definition**: In the preliminary definition phase, the focus switches from concept design, to subsystem design. This is where trade-off studies are done for these subsystems to find the preferred solutions to meet the requirements that have been generated in the previous phase. The end of this phase is usually marked by a preliminary design review (PDR).
- **Phase C, Detailed Definition**: In the detailed definition phase the general design is done, and what remains is the sizing of the actual components. Furthermore, a detailed definition is made of all the interfaces and work starts on building engineering models. While the subsystem designs are being finished in detail, a final plan is made for the assembly, integration and testing of the vehicle. The required milestone before the next phase can start is a critical design review (CDR). If this CDR is successful, the design if frozen. If it is not, iterations have to be made.
- **Phase D, Qualification and Production**: In this phase the Design is frozen and work can start on assembling and integrating the hardware. This is accompanied by extensive verification and testing. This testing is done at multiple levels of detail. As the spacecraft becomes more and more integrated, the testing is done at a lower and lower level of detail, peaking with qualification tests of the entire spacecraft. This phase ends with a successful launch readiness review. This phase is explained in more detail in Subsection 4.5.1.
- **Phase E, Operation and Utilization**: After passing the launch readiness review, the operation and utilization phase begins. This is marked by the launch of the vehicle, after which it will be commissioned. There is always some time between launch and beginning of actual operations, depending on the vehicle and mission profile. The operation phase also includes the actual scientific phase of the vehicle, and the accompanying operations of the ground segment in support of the mission. After the primary mission phase has passed, there is a chance of a mission extension. Whether this happens depends on the health of the vehicle at that point, and on budgetary constraints. If a mission

[1] `https://www.esa.int/Science_Exploration/Space_Science/Building_and_testing_spacecraft`, accessed on 10/Jun/2025.

extension does not happen, phase F begins. This phase is discussed in further detail in a concept of operations (ConOps) in Subsection 4.5.2.

- **Phase F, Disposal**: After the end of the operational phase of the mission, the remaining data is stored and recorded and the vehicle is decommissioned. Depending on the state of the vehicle this can be done in several ways. The Disposal phase end is marked by a Mission Close-out Review (MCR). When the vehicle is decommissioned, reporting is finished and the data is publicized for the wider scientific community.

The Design Synthesis Exercise roughly coincides with the end of phase B, preliminary definition. The post DSE-activities then are the Phases C until F. The post-DSE activities are laid out in more detail in the following project development and design logic (PD&D).

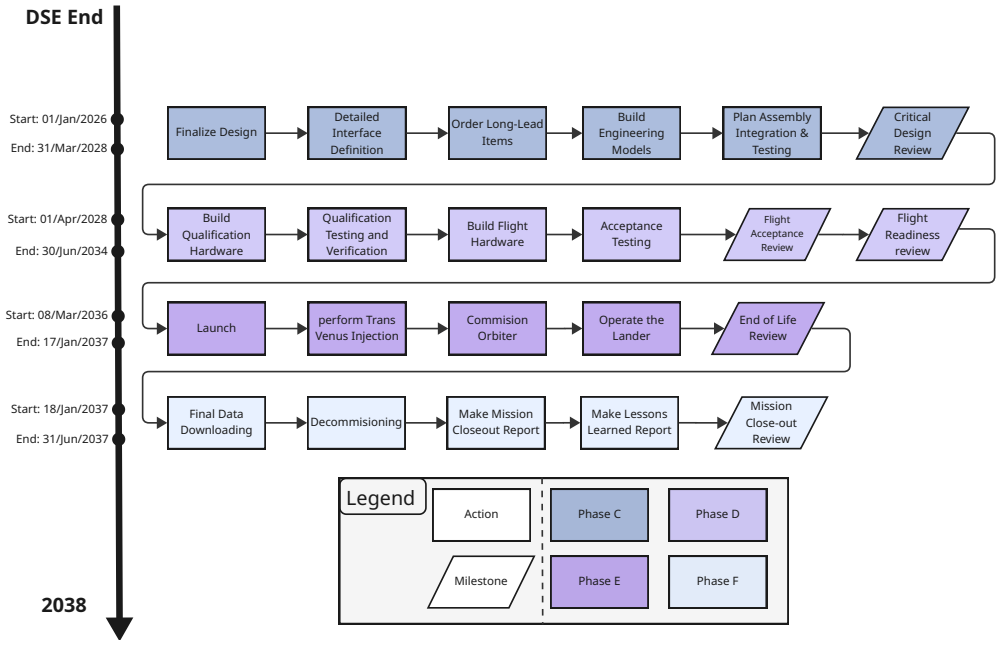

Figure 4.4: Project development & design logic.

4.5.1 Qualification and Production

With the design frozen, the first long-lead components are ordered and the primary contractors work on assembling all parts of the spacecraft. These are then also tested. Different parts of the vehicle are produced by different contractors or institutions. These components are then also verified to work according to requirements. At some point, all these components have to be integrated into the final spacecraft. As these parts have to come from different contractors at very different locations, this is a real logistical challenge. This is why this process is thoroughly planned out.

Typically, more than one model is manufactured. There is the test model, which is used for qualification testing, and will not be kept after the testing has ended. Then, a backup model can be constructed to use for additional validation, but its main use is after the flight model, the one that will be the actual spacecraft, is launched into space. The backup model is used by engineers on the ground for possible troubleshooting before sending commands to the flight model in space.

Components that are produced in different places include the heat shield, aeroshell, parachute, power subsystem, main lander structure, the scientific instruments, etc. When these complete their own tests they need to be transported to a location for integration where the full stack will again be subject to further testing. The diagram below outlines the schedule for integration of these components.

As can be seen in Figure 4.5, the different vehicle subsystems go through their own tests, while the main vehicle structure goes through its test. When subsystems finish testing, they are added to the structure in sequence such that gradually the vehicle becomes more and more complete. It is of note that the general purpose heat source (GPHS) is mounted to the vehicle late in the integration flow, this is because it degrades and loses too much power if integrated early. At some steps in the process, the vehicle as a whole is tested, to see if not only the subsystems themselves work as intended, but also that they work together to let the spacecraft function as a whole. After final acceptance testing, the lander in its EDL stage is mounted to the accompanying orbiter. Since the design of this orbiter is beyond the scope of this report, its own integration and testing flow, while needed, is not discussed.

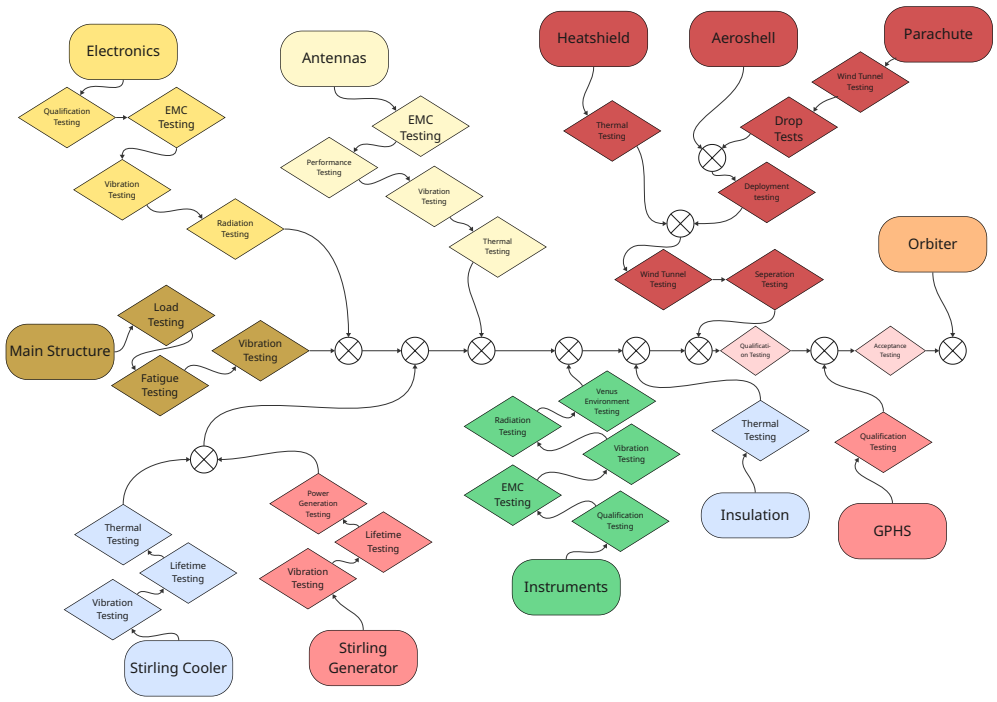

Figure 4.5: Integration and testing flow diagram.

With the schedule known, it is important to shed some light on some of these tests and where they could be done. It is not uncommon for a spacecraft to visit multiple locations throughout its testing campaign.

Testing components for a Venus lander requires simulating the planet's extreme surface environment. Because no single facility can fully recreate all Venusian conditions simultaneously at scale, the testing process for projects like this is typically divided into stages, each focusing on a specific environmental factor.

Thermal testing, which involves exposing parts to the surface temperature of Venus, can be conducted at facilities such as NASA Glenn Research Center in the United States. Their Glenn Extreme Environments Rig (GEER) can performed extended high-temperature tests and is especially useful for evaluating electronics and materials intended for the Venusian surface[2]. Here in our country, ESA's ESTEC facility in Noordwijk also offers thermal vacuum chambers that can be adapted for high-temperature endurance testing of subsystems[3] .

It is essential to perform high-temperature testing to ensure that enclosures and mechanisms can withstand Venus' surface pressure of 92 atm. This can both be performed at NASA Glenn as well as specialized high-pressure test chambers within institutions like DLR (German Aerospace Center). These chambers are capable of reaching pressures equivalent to deep-sea environments and can be modified to include temperature and atmospheric composition control[4].

To simulate the chemical environment, particularly the presence of sulfuric acid, corrosion testing facilities must be used. These are found in materials science departments of universities or national laboratories. For example, certain CNRS laboratories in France and industrial testing centers across Europe can expose materials to concentrated acidic vapors to test long-term durability[5].

Each type of test plays a critical role in advancing technologies to the level required for this mission. While a full-system test under all the Venusian conditions together remains difficult due to technical and cost limitations, distributed tests offer a practical approach to qualifying individual components and subsystems. For the testing of the whole system, scaled down models and advanced simulations are needed.

Estimating the costs of conducting Venus environmental tests depends on several factors: type of test, duration, complexity of the setup. Whether custom infrastructure or instrumentation is required. High-temperature and high-pressure testing in specialized facilities ranges from tens to hundreds of thousands of euros per campaign, especially if extended test durations or multiple iterations are needed. Corrosion testing is generally less expensive but still requires careful handling and long-term exposure periods. Finally, additional costs that need to be taken account by the team include personnel,

[2] `https://www1.grc.nasa.gov/space/geer/`, accessed on 18/Jun/2025.
[3] `https://www.esa.int/About_Us/ESTEC`, accessed on 18/Jun/2025.
[4] `https://www.dlr.de/en`, accessed on 18/Jun/2025.
[5] `https://lhfa.cnrs.fr/index.php/en/facilities/common-services/chemical-analysis`, accessed on 18/Jun/2025

travel, equipment transport, and post-test analysis. Engagement with facilities such as NASA Glenn, ESA ESTEC, or DLR can provide tailored cost estimates based on test objectives and readiness level.

4.5.2 Concept of Operations

This section outlines the Concept of Operations (ConOps) for the KYTHERA mission. This is a high level description of how the proposed system will function and how it will fulfill it's operational goals. A ConOps is written with the perspective of all stakeholders in mind and serves as a bridge between the mission objectives and the technical implementation. First, the proposed mission timeline will be presented. Then some light will be shed on what stakeholders are involved in the successful completion of the KYTHERA mission. Then, the different mission phases are described in more detail, namely the launch, cruise and science phases. Finally, a concept will be proposed on the possibility of mission extension programs, and the final wrap up of the mission. First, a general overview of the operational concept is presented in a ConOps diagram:

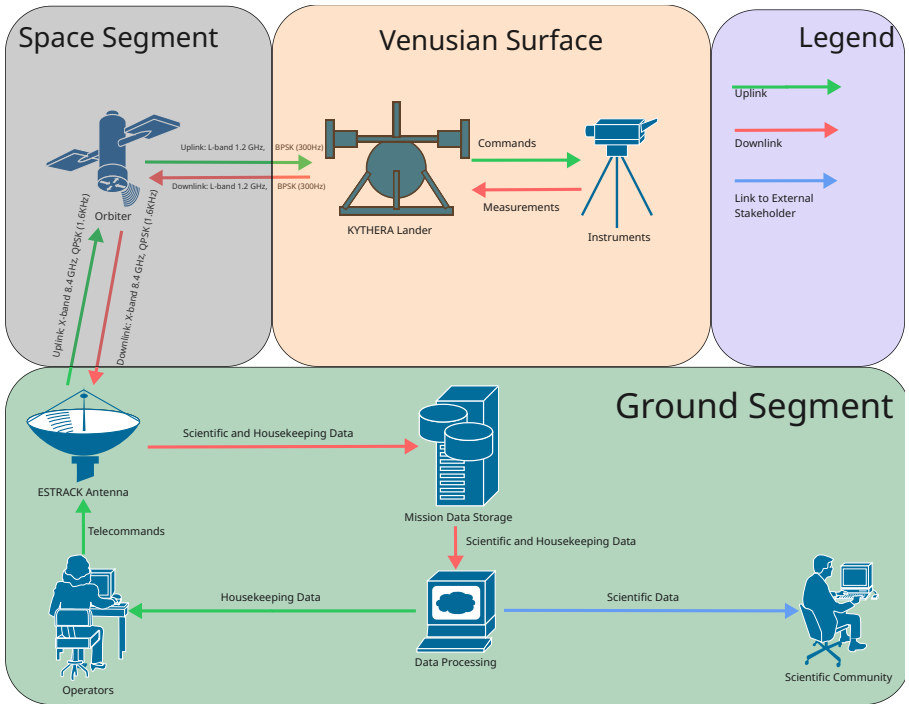

Figure 4.6: KYTHERA Mission Concept of Operations Diagram

Mission Timeline

The mission timeline spans from launch to the end of the mission. Several launch opportunities exist, constrained by optimal transfer windows based on the relative positions of Earth and Venus. This is explained in more detail in Section 5.1. Figure 4.7 depicts the mission timeline for the earliest available launch window.

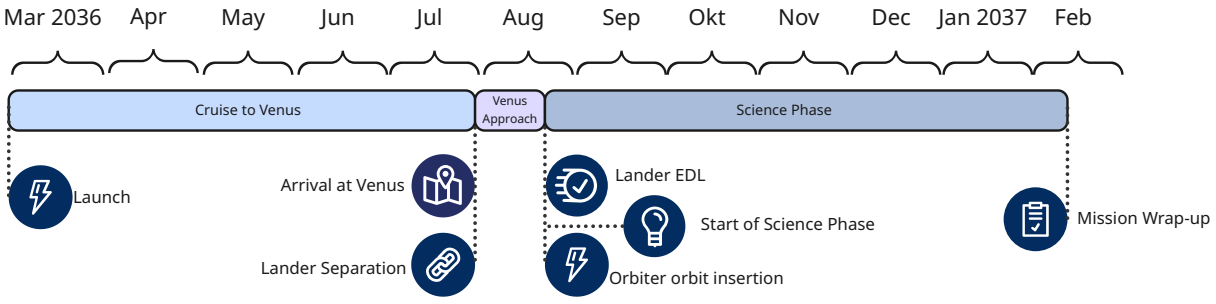

Figure 4.7: Mission timeline.

The mission begins at launch, where the orbiter with the EDL module attached is launched from Earth, followed by a five-month cruise stage towards Venus. During the Venus approach phase, the lander encapsulated in the EDL module is separated from the orbiter, after which the orbiter will begin orbit insertion to enter the target elliptical polar orbit. After successfully landing, the lander will then activate and deploy scientific instruments and antennas, starting the science phase. The orbiter will act as a relay for data transmission from the lander to mission control on Earth. This phase will

be active for the entire duration of the mission, for around 200 days. In the event of exceeding expected lifetime, the mission can get an extension, where the instruments continue to gather data for analysis until the lander loses contact. The decommissioning of the lander will then ensue, as operational systems are shut down and communication with the orbiter stops.

The sections below elaborate on the major events and phases in the timeline, from launch to decommission. The science phase will be discussed in detail, mainly on science data processing once it's been received by the Deep Space Network (DSN) antennas.

Stakeholders

This project will be influenced by several stakeholders, both internal and external. The design is being made by the authors of this report. Manufacturing of the spacecraft, lander, and related components is contracted as much as possible to European industry. The operation of the spacecraft after launch is handled by the European Space Agency (ESA) Science Directorate. Scientific instruments are provided by institutions and academia. After completion of a mission, per ESA standards, all scientific data is released freely to the scientific community. The study of Venusian geology and atmospheric composition may also spark interest in environmental organizations to understand the evolution of the Venusian atmosphere in an effort to stop Earth from suffering the same fate.

Launch Phase

The launch phase is critical for the mission, as many considerations go into configuring the launch. After confirming the launch date based on launch window calculations, the next step is to choose a launch vehicle and launch sites for the KYTHERA mission. The launch vehicle selection is dependent on many factors, such as orbital parameters, orbit insertion techniques, and the structural and mechanical parameters of the orbiter. Example launchers used for this mission include the Ariane 6[6], or the Falcon Heavy. The licensing and permits required for both the launch vehicle and launch site will also be obtained. An ESA launch site will most likely be chosen, such as the equatorial Kourou Space Center in French Guiana[7].

Next begins the pre-launch testing phase, which tests the integration of all mechanical, electrical, and software components. The final milestone before approving for launch is the 'flight readiness test'[8]. Upon confirmation from ESA, Government agencies, and other relevant parties, the launch phase will begin. The injection stage begins with main stage and booster ignition, followed by the upper stages propelling the orbiter into a transfer orbit. The orbiter will perform correction maneuvers and fine-tune its trajectory before continuing onto the cruise phase towards Venus.

Cruise Phase

After leaving the transfer orbit, the cruise phase begins, lasting roughly five months before approaching Venus. The orbiter during this phase employs a few key mechanisms: Firstly, the Cruise Heat Rejection System (CHRS) ensures that from cruise until before atmospheric entry, the ambient temperature inside the EDL module is kept at 333 K. This system is discussed in more detail in Section 5.1, and the corresponding requirement is OPS-EDL-TC-1.

There will most likely also be telemetry tracking from the Estrack ground stations during the cruise phase. The orbiter will gather and store housekeeping and other orbital parameters onboard before transmitting them to the Estrack deep space antennas. This keeps Mission Control updated on the conditions of all subsystems, including the attached EDL module. This will also be the communication method between the orbiter and Earth during the following science phase when the lander is successfully deployed. All uplink and downlink operations between the orbiter and Estrack antennas will utilize X-Band frequencies at 8.4 GHz throughout the entire mission duration.

Science Phase

Immediately after starting the approach to Venus, the lander is separated, and the orbiter performs maneuvers and adjusts its orbit. The lander will then enter its coasting phase before engaging in EDL and landing on the Venusian surface at the expected landing zone. This procedure and the technical details will be discussed in Section 5.1. Entering EDL marks the start of the science phase that will last for an expected duration of 200 Earth days, where numerous geological and atmospheric data are collected and sent from the lander to the orbiter via the onboard L-Band antennas and relayed back to the deep space tracking antennas on Earth.

The KYTHERA lander is equipped with a multitude of advanced scientific instruments that measure a wide range of highly valuable data from Venus's surface. The lander is capable of not only measuring ambient temperature, pressure, wind direction and speeds, radiative flux, and seismic vibrations, but also making measurements never previously conducted, such as surface geological and lower atmospheric composition analysis.

There are a total of three temperature and pressure sensors on the lander, placed in the coldbox, hotbox, and outside environment, respectively. These sensors generate not only data for the ambient environment, but also provide housekeeping

[6] `https://centrespatialguyanais.cnes.fr/en/ariane-6`, accessed on 11/Jun/2025.
[7] `https://centrespatialguyanais.cnes.fr/en`, accessed on 11/Jun/2025.
[8] `https://www.esa.int/Science_Exploration/Space_Science/Getting_ready_for_launch`, accessed on 11/Jun/2025.

data about the ambient conditions of different sections of the lander. The CPU onboard in the CDH module passively logs and stores voltage data from subsystems, which can infer power usage, operational status, and general health of all instruments. These housekeeping data are transmitted to the orbiter and relayed back to Earth, which are then monitored by the mission operations team at ground stations to ensure lander functions. These data will also be used by the engineering team to find faults in subsystems and provide insight in the event of subsystem failure. Housekeeping data, while not prioritized or primary science data, is essential to everyone involved in running, supporting, or learning from the mission.

The main scientific equipment onboard the lander is the geological chemical analyzer (GCA) and atmospheric chemical analyzer (ACA). These instruments collect and analyze samples from the surface and lower atmosphere of Venus and use spectroscopy to calculate the chemical composition of the atmosphere and surface geological materials. This is extremely valuable information to the science team at ESA, as it improves the understanding of multiple major questions and objectives posed by the scientific community: Seismological events, active/recent volcanism or tectonics, surface-atmosphere exchange, planetary geological and atmospheric evolution. The data collected with these instruments is also of interest to environmental groups, as understanding Venus's climate provides insight into the greenhouse effect and surface-atmospheric chemical exchanges.

The wind sensor, radiometer are supporting instruments that provide information in addition to the chemical analyses. In the event of a seismological event, these instruments can provide insights and help develop a deeper understanding of the nature of these events.

The science operations center[9] (SOC) will first process and handle the raw telemetry data received, which is then relayed to the European Space Operations Center[10] (ESOC) and other specialized instrument teams for thorough analysis. All data are then used to contribute to scientific papers and reports, published in major journals and conferences, which will also be accessible to the public. Finally, some of the data will be stored at the ESA archives.

Mission End Phase

After the designated 200 day duration, the mission is deemed to have completed its primary objectives. If the lander is still functional and providing valuable information, the relevant stakeholders can potentially approve a mission extension if proven to be technically and financially feasible. There will be additional scientific objectives such as additional measurements observations of terrain and other interesting events. This would then continue until either the information provided by the lander is no longer scientifically valuable, or if the lander is no longer operational.

Finally, the mission will enter the final wrap-up phase, where the lander will be safely decommissioned, where all operational instruments are shut down and resources such as batteries are fully depleted to ensure safety and sustainability. Then relevant teams at mission control may conduct a final calibration and validation of the instruments. The collected data will then be used to construct scientific papers and reports to be published or archived.

4.6 Budgets

Requirements GSYS-1, GSYS-2 place direct limits on aspects of the system. This creates a ceiling for the cost- and mass budgets respectively. Furthermore, requirement GSYS-3 presents an indirect requirement on the power draw of the system. As the total allowable mass of the power subsystem is given, a maximum available power for the system is calculated is taken from Section 5.3 to be 350 W. These maximum values are then divided up and allocated to the different subsystems. These budgets can not be changed without the system engineer's approval, and because changes in budget allocation influence other subsystems, these changes happen in discussions with other subsystem engineers. On the other hand it can happen that when allocating a budget, a subsystem is allocated more of this budget than what is envisioned to be used. These discussions are then where a reallocation is made. This leads to iterations in the design and allows budgets to flexibly change as the design becomes more mature, while still providing incentive to subsystem engineers to keep power, mass, cost etc low and provides the system engineer with control and oversight. In the following sections, these divided budgets envisioned usages of these budgets and any iterations are shown.

4.6.1 Cost Budget

Cost budgets were allocated to the different subsystems. In Figure 4.8 below, the allocated and the used budgets can be seen.

[9] `https://www.esa.int/About_Us/ESAC/Science_Operation_Centres`, accessed on 11/Jun/2025.
[10] `https://www.esa.int/About_Us/ESOC/Where_missions_come_alive`, accessed on 11/Jun/2025.

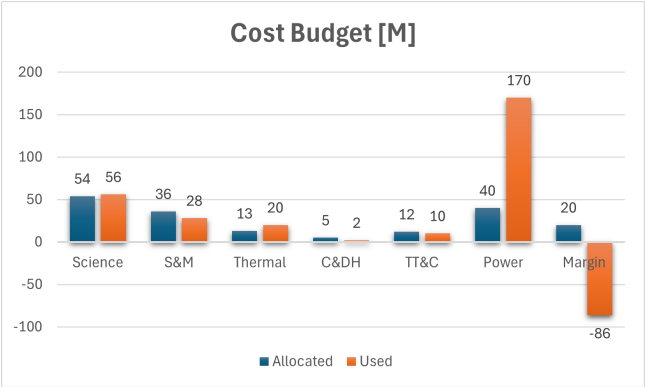

Figure 4.8: Cost budget.

The allocated budgets were devised by looking at other space missions and statistical data. Extensive use was made of the Space Missions Analysis and Design (SMAD) book for this [37]. However, due to the uniqueness of the KYTHERA mission it was particularly difficult to compare to relevant missions, since there are none that match this project's scope. For the used cost, use was made of the NASA Cost Estimation Handbook [38]. Furthermore, prices were looked up for off the shelf components, and statistical relations from SMAD were used for structural components and manufacturing costs. It is immediately apparent that the cost budget has a negative margin, meaning that the design is over budget. This is mainly caused by a much higher than estimated cost for the power system, as well as a Thermal subsystem that is 50% more expensive than budgeted for. This makes a degree of sense, as this subsystems are very unique to this mission, and were therefore the hardest to predict. The Scientific, CDH and TT&C subsystems were accurately predicted, because these components are widespread and not unique to the KYTHERA mission. Because the price of Radioisotope Stirling Generators are not foreseen to go down in the design time of this mission, and because there is no viable alternative for this solution it is concluded that this cost overrun can not be adequately fixed. For this reason, a requirement deviation request is put forward. It can be found in appendix E.

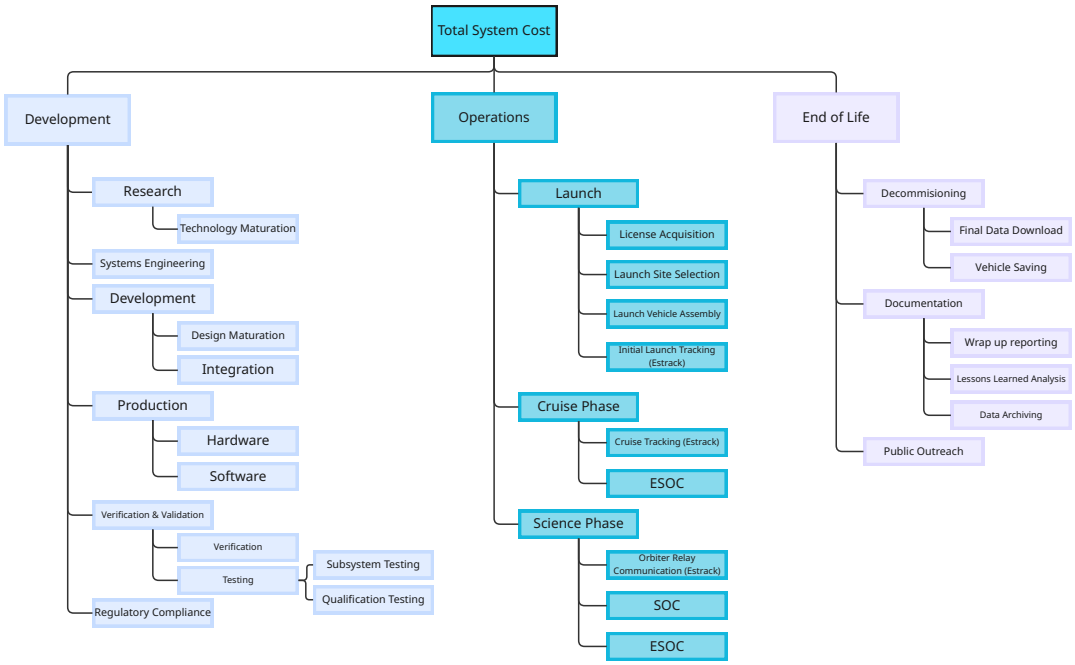

Figure 4.9: Cost breakdown structure.

Because there is still a uncertainty in the cost budget regarding the development, testing and operation of the mission, a cost breakdown structure is also made. This breakdown structure aids in finding all possible cost items of the project and helps to start estimating detailed costs, lowering the risk of unforeseen costs being identified too late in the development. A final, accurate cost prediction is then made in the detailed design definition phase. As can be seen in Figure 4.9, these cost items are divided into three distinct mission phases. Development costs entail the costs that are associated with the production, verification and testing of the final system, as well as compliance to any relevant regulations. Operational costs are those that are associated with the day to day running of the mission, so staffing mission control, communications

via the deep space network, and potential costs due to having to respond to anomalies in-flight. Finally, there are some costs associated with ending the mission properly, these mostly have to do with wrapping up and documenting the mission.

4.6.2 Mass Budget

The mass budget serves to distribute the maximum allowed total mass over the different subsystems. This creates a limit for how heavy each subsystem can be. This is then compared to the estimation of how heavy subsystems will be. It is important to try to stay below the set mass limit for each subsystem, but as designing went on, iterations were needed. It was obvious that the original 200 kg maximum mass was unrealistic, and this was negotiated to 350 kg. The way that this budget is divided over the subsystems also changed. Some subsystems ended up requiring a larger part of the budget while some were estimated to use less than the allocated mass budget. These iterations were kept track of, and four iterative mass budgets are presented below.

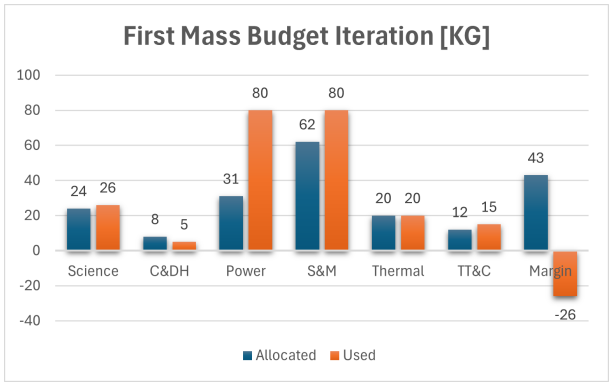

(a)

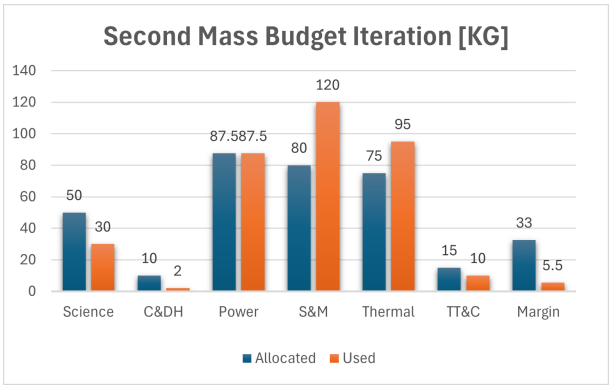

(b)

Figure 4.10: First and second mass budget iterations.

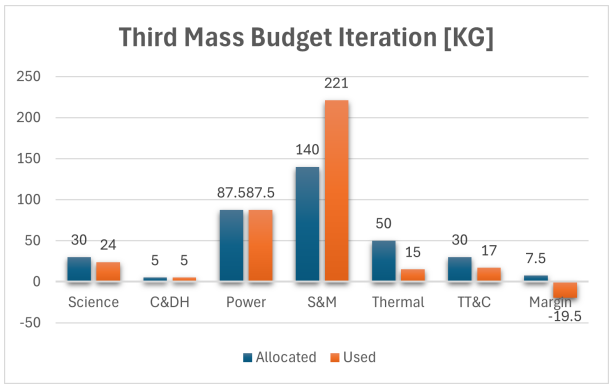

(a)

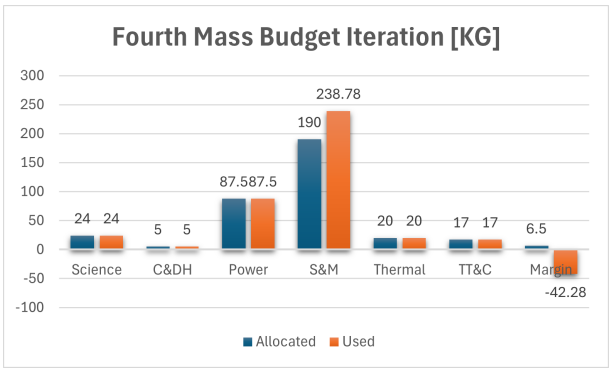

(b)

Figure 4.11: Third and fourth mass budget iterations.

As seen above, the mass budget is divided into different subsystems. Science entails all payloads used for scientific research and their casings, electronics, and other accompanying components. C&DH is the command and data handling system. This encompasses the brains of the spacecraft, and the accompanying cables and devices. Power entails the power source, power distribution system and power storage. The thermal part comprises the active cooling system and the passive insulation of the vehicle. TT&C handles the communication of the vehicle. Antennas, receivers, amplifiers and cables are all part of this subsystem. Finally, there is a margin category. This margin is unallocated or unused mass budget which can be used if components go over budget. Negative mass margin means the design is overweight, while a too high mass margin means that the mass budget is underutilized. It can be seen in Figure 4.10a that the mass margin is negative. This means that the design mass is over budget. This was still the original 200 kg maximum mass. The second mass budget iteration, seen in Figure 4.10b reflects the budget increase to 350 kg. The subsystems are heavier, but the mass margin is now positive. It was then found that some subsystems were overestimated in mass and some were underestimated. Efforts were made to decrease mass where possible, and a new allocation of the mass budget was made. This leads to the mass budget seen in Figure 4.11a. This is where a calculation of the systems and mechanisms mass resulted in a mass budget violation. An attempt was made to reduce this mass. While some mass reduction was achieved, going over this mass again also revealed, resulting in a net mass increase again. The resulting fourth budget iteration is seen inFigure 4.11b. The mass estimate is still preliminary, and because of design uncertainties, all mass estimates are made with very high margins built

in, so it is expected that with more design optimization this mass will come down. This is explained in more detail in the section describing this subsection; Section 5.6.

4.6.3 Power Budget

The power budget has been updated by giving the power requirement for each subsystem in terms of Watts instead of percentages of total power required, as displayed in Figure 4.12. The power budgets differ depending on whether the lander is in science mode (i.e. conducting scientific measurements) and in transmission mode (i.e. communicating scientific or housekeeping data).

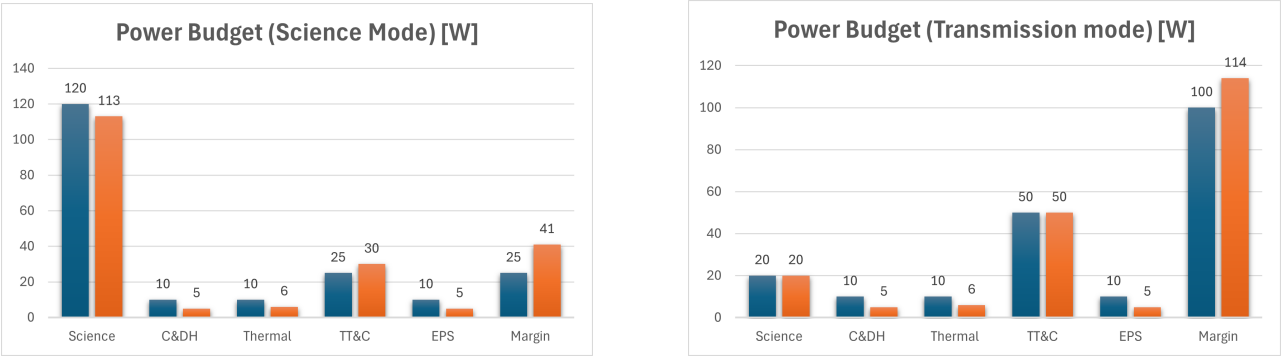

Figure 4.12: Power budgets in science and transmission operation modes.

4.7 Risk Analysis and Management

A mission of this scope inherently carries a lot of risks. Risks are the combination of the probability of an event happening combined with the impact that this even happening has on the functioning on the vehicle, or on the completion of the mission. In short, the risk is a statistical estimate of the expectation of vehicle loss. Risk can manifest itself in different ways, there can be technical failures, cost overruns, schedule impact or even safety incidents. Managing these risks is therefore critical to ensure safe success of the mission objectives. However, it is never possible to eliminate all risk of a complex project like this, this is why a certain amount of risk must be accepted. This is called a risk appetite. For manned systems like crew rated launch vehicles, capsules or space station components, this risk appetite is very low. For unmanned and more experimental missions, this appetite can be higher. Risk management is the process by which all this risks are identified, mitigated if possible, and accepted. It is important to start identifying these risks and mitigating them from early on in development, because risks become exponentially more expensive in terms of schedule and cost to mitigate the later they happen in design. This is because the further along the design is, the more will have to be redesigned and retested. Because of this, so far a detailed risk assessment was performed at each stage of the project up to and including the final design by considering both system level and sub-system level risks. Additionally, the team considered in which design phase risks could occur (based on the design phases in the Post-DSE Gantt Chart, Appendix D). Each one of the risks was assigned a likelihood score from 1 (very low) to 5 (very high) and a consequence score from 1 (benign) to 5 (catastrophic), explained in Table 4.5. The scores are given following European Co-operation for Space Standardization (ECSS) guidelines [39]. The quantitative overview of what the different likelihood and consequence scores mean is given below:

Table 4.4: Risk Severity and Likelihood scores

Score	Impact on Performance	Impact on Schedule	Likelihood
5	Maximum: Unacceptable performance degradation, no workarounds exist	Maximum: Can't achieve major project milestone	Maximum: Certain or almost certain to occur, will occur at least once, the chance is 1 to 1
4	High: Major reduction in performance, but workarounds available	High: Project milestone slip $\geq$ 1 month or critical path impacted	High: Will occur frequently, the chance is between 1 to 1 and 1 to 10
3	Medium: Moderate reduction in performance, but workarounds available	Medium: Project milestone slip $\leq$ 1 month	Medium: Will occur sometimes, the chance is between 1 to 10 and 1 to 100
2	Low: Moderate reduction in performance, some approach retained	Low: Additional activities required to meet end dates	Low: Will seldom occur, the chance is between 1 to 100 and 1 to 1000
1	Minimum: Minimal or no performance impact	Minimum: No impact	Minimum: Will almost never occur, the chance is less than 1 to 1000

Multiplying the likelihood with the consequence score resulted in individual risk factors. The risk table also included a

description of the impact of each risk, as well as a mitigation strategy and post-mitigation likelihood, consequence, risk factor and impact. Finally, a technical lead was assigned to manage each risk.

Table 4.5: Risk table IDs.

Technical Roles ID	TEC - Technical Risk	Likelihood ID	Consequence ID
Structures & Mechanisms (incl. Materials) - SMS	BG - Budget Risk	1-Very Low	1-Benign
Sustainability - SUS	SB - Sustainability Risk	2-Low	2-Marginal
Thermal Control - TC	PF - Performance Risk	3-Moderate	3-Harsh
Entry, Descent & Landing - EDL	MK - Market Risk	4-High	4-Critical
Power - POW	DS - Design Risk	5-Very High	5-Catastrophic
Communications - COM	SYS - Systems Risk		
Payload - PAY			
Systems Engineering & Integration - SE&I			
Command & Data Handling - CDH			

During different design phases, the risk table was reevaluated and updated. Updates included new subsystem and system level risks and the re-assigned technical roles. This yielded a long list of risks. The ones that are most critical, i.e. the risks with the highest pre-mitigation risk factor (of value 14 and higher) have been selected to receive elevated attention. These critical risks and their mitigation strategies are given in Table 4.6 and 4.9 along with some lower scoring risks that were identified as crucial in driving the design.

Table 4.6: Most critical subsystem level risks table.

ID	Risk	Likelihood	Consequence	Risk Factor	Impact	Mission Phase
TEC-DS-5	Safety factor taken in structural design not sufficient	3	5	15	Structural integrity failure, could compromise the mission	Preliminary Design
TEC-PF-1	TPS failure	3	5	15	Catastrophic failure during EDL	Lander EDL
TEC-PF-33	Radiation-induced faults	4	4	16	Errors in the CDH system	Science Phase
TEC-PF-34	Lander transmitting antenna malfunction	3	5	15	Antenna degredation due to high temperature, or corrosive atmosphere, eventual failure	Science Phase
TEC-PF-47	Corrosion of structural components	4	4	16	Materials' mechanical properties drop and cause structural failure	Science Phase
TEC-PF-48	Vacuum cannot be maintained due to leaks	3	5	15	Passive cooling fails, and structural failure may occur.	Science Phase
TEC-PF-54	Tangling of parachute ropes	4	4	16	Reduced parachute drag, which may render TPS separation impossible	Lander EDL
TEC-MK-2	Optimal instruments scarcity or unavailablilty	3.5	4	14	Limits or hinders design	Production
TEC-PF-63	Link budget failure for receiving mode	3	5	15	Causes the orbiter to be unable to downlink commands to the lander, possible due to the high thermal noise at the receiving antenna. Would not be catastrophic but very significant negative impact	Science Phase
TEC-PF-66	Heat released from the Stirling generator, the cooler, and the GPHS modules interfere with the communication instruments	4	4	16	Communication antenna unable to receive command due to increase in antenna noise temperature	Science Phase
TEC-PF-61	Dust or particles getting caught up in the chain sprocket system in the Stirling power generator and cooling	3	5	15	This may jam the chain sprockets and/or damage it, causing the piston movement to stop leading to failure of active cooler and power generation system, which would lead to the failure of the lander.	Science Phase
TEC-PF-32	Connector/cabling failure due to thermal cycling or corrosive atmosphere	2	5	10	Instrument not able to deliver measurements to CDH	Science Phase
TEC-PF-38	Seismometer gets deployed on a rock	3	4	12	Seismometer won't be able to take optimal readings	Lander Commissioning
TEC-PF-39	CCD and laser cannot be cooled to required temperature	3	4.5	13.5	Damage of CCD and laser, resulting in complete failure of geological instrument	Lander Commissioning
TEC-PF-40	H_2SO_4 condensates inside VMS sampling array	5	4	20	VMS inlet clogged, instrument performance affected or inhibited	Science Phase

Table 4.7: Most critical technical risks post mitigation.

ID	Mitigation Strategy	Post-Mitigation Risk	Likelihood	Consequence	Risk Factor	Responsible Technical Lead(s)
TEC-DS-5	Using a higher safety factor where seen required	Lander may be overengineered	3	2	6	SMS
TEC-PF-1	Overdesign TPS	Catastrophic failure during EDL	1	5	5	EDL
TEC-PF-33	Radiation-Hardened Components	Even with radiation-hardened components a high-energy particle event (e.g., solar flare) could still cause simultaneous or cumulative upsets	1	5	5	CDH
TEC-PF-34	Temperature, corrosion resistant outer shell, redundancy design by adding more	Degradation still occurs but over longer period of time	2	4	8	COMM
TEC-PF-47	Use corrosion-resistant materials for components in contact with Venus atmosphere, and/or use corrosion-resistant coatings	Materials choices might be limited, causing heavier or more expensive options to be chosen	2	4	8	SMS
TEC-PF-48	Test the lander thoroughly in Venus-like conditions (e.g. GEER), and add redundant getters.	High cost for testing and added cost for getter redundancy.	2	4	8	POW-TC
TEC-PF-54	Careful packing and use of parachute deployment bag	Reduced parachute drag, which may render TPS separation impossible	1	4	4	EDL
TEC-MK-2	Discuss alternatives	Delayed selection or compromise	2	2	4	PAY
TEC-PF-63	Have ample link margin to account for additional losses, include housing or partial cooling to decrease the thermal noise temperature of the antenna	The link margin is not enough and the link still fails	1	5	5	COM
TEC-PF-66	Place the communication equipment and the Stirling generator and cooling system as far out as possible.	May still interfere with the communication equipment.	3	3	9	POW-TC
TEC-PF-61	Place housings or coverings over the chains and sprockets and not have them be exposed to the ambient	Particles or dust may still form somewhere within the housing	1	5	5	POW-TC
TEC-PF-32	Corrosion-Resistent Cables	Thermal degradation or mechanical failure of cable insulation	1	4	4	CDH
TEC-PF-38	Incorporate mechanism that allows for the seismometer to be deployed elsewhere	New location also falls on a rock	1	4	4	PAY
TEC-PF-39	Substitute the CCD and laser with ones that have higher operating temperature	New components still have low operating temperatures	1.5	4.5	6.75	PAY
TEC-PF-40	Add heater to inlet to evaporate H_2SO_4; include multiple inlets for redundancy	Heater failure after some time	1	3	3	PAY

In order to better visualize the distribution of the risks and the effects of mitigation procedures, a risk map was constructed and can be seen in Figure 4.13. The risk heat map is consists of a 5×5 grid based on the 1-5 rating system

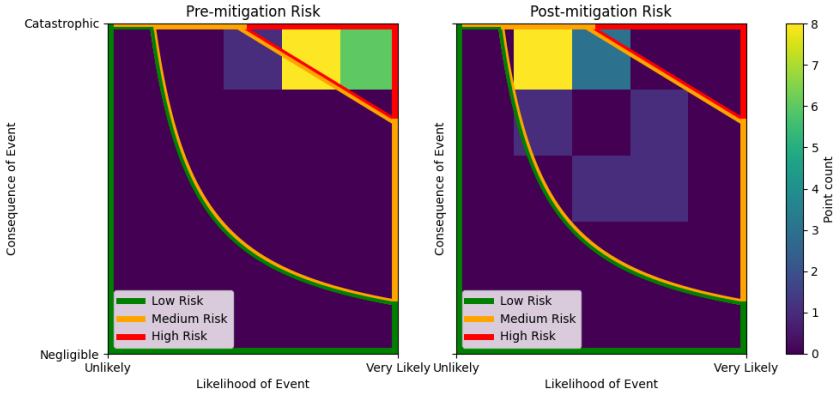

Figure 4.13: Critical technical risks heatmaps.

for both likelihood and consequence. All of the critical risks are plotted and categorized into a square section on the grid. Furthermore, the classification for low, medium, and high risk regions is plotted as curves and overlaid on top of the heatmap, enforced with outlines to still show the overall zonal distribution of all technical risks. As seen from the map, all of the critical risks are situated in the high risk area initially, and move towards medium risk after mitigation. They are still considerable, but at least they can be managed.

Furthermore, system level risks have also been identified and are included below. These are risks that are not dependent on single subsystems, but rather risks that stem from the actual development of the system, or because of interplays between different subsystems. For these risks, the same process is applied. Tabulated below are the risks pre- and post mitigation.

Table 4.8: System-level risks table.

ID	Risk	Likelihood	Consequence	Risk Factor	Impact
SYS-1	Launch Vehicle Failure	2	5	10	Loss of Mission, potential loss of project or massive schedule and cost impact.
SYS-2	Integration Failure	2	4	8	Interface redesign needed, considerable cost and schedule impact.
SYS-3	Mishandling During Testing	1	4	4	Repairs needed, cost and schedule impact.
SYS-4	Failure to Wakeup from Hibernation	2	5	10	Loss of mission due to non-responsive vehicle.
SYS-5	Failure of Spacecraft Stages to Separate	2	5	10	Failure of spacecraft stages to separate, resulting in loss of mission.
SYS-6	Faulty Software Upload	3	4	12	Could introduce bugs into the spacecraft, leading to unintended behaviour or loss of mission.
SYS-7	Unwarranted Safemode Activation	1	4	4	Could lead to temporary loss of scientific data, and loss of mission in the worst case.
SYS-8	Faulty Commands Sent	3	2	6	Unintended behaviour.

Table 4.9: Most critical technical risks post mitigation.

ID	Mitigation Strategy	Post-Mitigation Risk	Likelihood	Consequence	Risk Factor	Responsible Engineer
SYS-1	Select reliable launcher with rich flight heritage. Purchase launch insurance.	Loss of mission, big schedule impact with lower cost impact.	1	4	4	SE&I
SYS-2	Follow ECSS standards, apply proper interface management	Redesigns would be needed but discovered at an earlier stage.	1	3	3	SE&I
SYS-3	Following of proper procedures. Use 4 eyes principle.	Repairs needed, cost and schedule impact.	1	3	3	SE&I
SYS-4	Build in software redundancy	Loss of mission due to non-responsive vehicle.	1	5	5	CDH
SYS-5	Redundancy in pyrotechnic bolts, use flight proven separation mechanisms.	Failure of spacecraft stages to separate.	1	5	5	SE&I
SYS-6	Use 4 eyes principle. Live backups to rollback to previous software versions.	Could introduce bugs into the spacecraft, leading to unintended behaviour or loss of mission.	2	3	6	CDH
SYS-7	Design safemode in a way such that it can always be removed from safe mode quickly.	Temporary loss of scientific data.	1	2	2	CDH
SYS-8	4 eyes principle. Live backups to rollback to previous software versions.	Unintended behaviour.	2	2	4	CDH

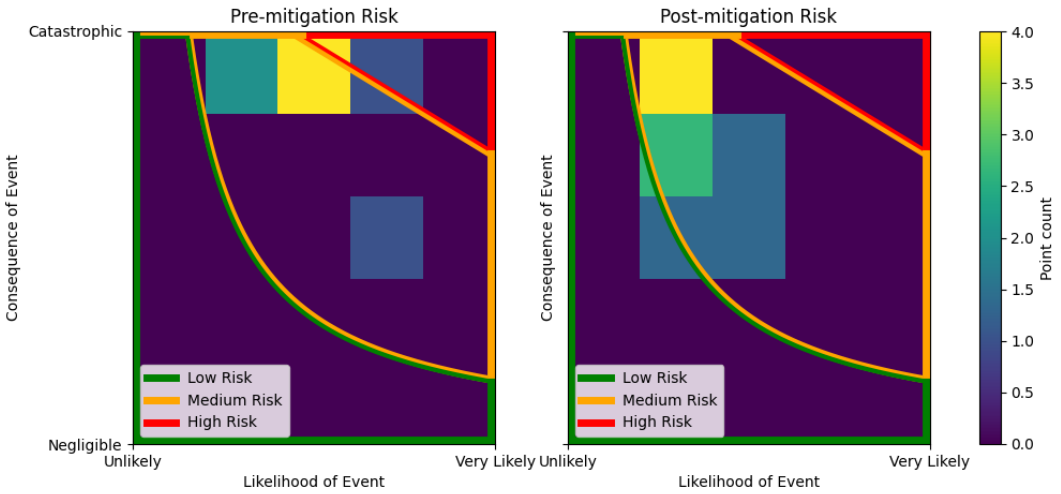

Figure 4.14: System-level technical risks.

4.7.1 Impact on Design

As can be observed in the previous tables, identifying relevant risks has had a lot of impact on the design. For instance, the risk of deploying the seismometer on a rock or some other suboptimal spot lead to the implementation of a mechanism to allow for a second deployment spot as can be read in Section 5.2. The risk of the heat shield burning up during EDL similarly lead to an increase in size to allow for redundancy. Similarly, the need for safe instrument data acquisition required the use of corrosion-resistant cables. The impact of such risks could also have an impact on the overall architecture of the lander itself, as presented by TEC-DS-5. Given the gaps in information on the Venusian atmosphere and the lack of heritage missions, a factor of safety can be implemented in designing the structure of the lander to account for extreme unforeseen circumstances. As well intentioned as that may be, though, including a higher factor of safety could result in the over design of the structure, leading to unnecessary mass and power usage which in the end could limit the mission duration and consequently the scientific return.

Risks TEC-PF-49 and -46 indicate that the use of a parachute could be problematic for the final phase of descent and after landing. The simplest answer is to not use a parachute, and replace it with a drag plate, which can be made of highly resistant materials and has no chance of covering the instruments, short of structural failure. However, that would only be possible given extreme loading, at which point there are bigger issues for the lander.

The geological analyzer was found to have CCD's with a negative operating temperature. This introduces a high risk of the instrument to become nonoperational as cooling it that much would challenging given the conditions. Therefore, the team decided to replace the CCD's of the instrument by ones that have an maximum operating temperature of 30 °C and a maximum surviving temperature of 50 °C. This way the risk of the geological analyzer becoming nonoperational is significantly reduced because the coldbox will be cooled to 30 °C. Furthermore, it was decided to have a vacuum inside the coldbox. This results in more efficient cooling as the amount of heat generated by certain instruments and heating up others is limited.

5 Subsystems

The next step in designing KYTHERA requires deep knowledge of possible options for each subsystem. For this reason, this chapter describes in detail the research done for each part of KYTHERA, and design options were explained. The overview of the EDL procedure, capsule geometry definition and TPS sizing are explained in Section 5.1. Section 5.2 will investigate all the instruments that must and can be taken onboard. Next, Section 5.3 details the power and thermal control system. Section 5.5 then details the CDH subsystem. Section 5.4 then determines possible communication subsystem architectures, and finally the structures and mechanisms subsystem is detailed in Section 5.6. In these sections, an elementary sensitivity analysis is performed where relevant. While this suffices for the current design stage, a Monte-Carlo simulation will be performed in later stages for a more accurate and detailed analysis.

5.1 Entry, Descent and Landing

Atmospheric entry is possibly the most critical phase of the mission due to the high loads encountered in this phase. The Entry, Descent and Landing (EDL) Subsystem is responsible for the safe delivery of the lander from orbit to the preferred landing site on the Venusian surface. It must protect the lander from the immense heat and aerodynamic forces that are imposed on the vehicle as it gradually slows down. When the vehicle has slowed down to safe speeds, a parachute system is deployed so that the thermal protection system (TPS) can be separated safely. A drag plate is attached to the lander body to stabilize and slow it down in the final stage of the descent. Finally, the system must also make sure that the ground impact shock is dissipated to prevent damage to the lander.

The requirements the EDL subsystem needs to fulfil are found in Subsection 5.1.1. Subsection 5.1.2 presents an overview of the EDL sequence. Pre-EDL operations are outlined in Subsection 5.1.3. EDL on-board thermal management is sized in Subsection 5.1.4, and the geometry as well as the aerodynamics of the selected entry capsule are presented in Subsection 5.1.5. Alongside the sizing of the TPS, Subsection 5.1.6 explains the method for sizing the TPS, the models and assumptions used by the solver developed, as well as the verification and validation of said solver. The parachute design is presented in Subsection 5.1.7, and an uncertainty analysis of the landing site is made in Subsection 5.1.8. The reliability of the EDL subsystem is assessed in Subsection 5.1.9. Recommendations and future work that needs to be carried out in the following stages of the design are given in Subsection 5.1.10.

5.1.1 Requirements

The requirements of the EDL subsystem and their proposed verification methods are listed in Table 5.1. There have been minor changes and additions since the Midterm Report. The maximum deceleration was reduced from the initial 132 g to 120 g. The thermal and TPS requirements, which previously used TBD values, have been quantified. An entry corridor between entry flight path angles of -11° and -12.8° has been identified and added to the requirements. Requirement OPS-EDL-ACD-3 cannot be verified without performing a detailed aerodynamic stability analysis with high-fidelity software such as NASA's Langley Aerothermodynaoc Upwind Relaxation Algorithm code for the continuum flow regime and Direct-Simulation Monte Carlo analyses for the rarefied flow regime, with additional verification by wind-tunnel tests. Therefore, this requirement is marked with a "?".

Table 5.1: Requirements of the EDL system, their verification methods and requirement compliance (RC) with the current design.

ID	Requirement Description	Verification	RC
OPS-EDL-AE-S-1	The system in entry configuration shall be capable of withstanding a peak deceleration of 120 g.	V-DEM-STR	✓
OPS-EDL-AE-C-1	The system in entry and final descent configuration shall be capable of withstanding 90 ppm of H_2SO_4 for 2h.	V-DEM-COR	✓
OPS-EDL-AE-LA-1	The system shall be capable of landing within a 100 km radius circle from the planned landing site.	V-ANA-SIM	✓
OPS-EDL-AE-EI-1	The system shall enter the atmosphere at a flight path angle between $-11°$ and $-12.8°$.	V-ANA-SIM	✓
OPS-EDL-AE-EI-2	The system shall enter the atmosphere at a relative-to-ground speed of no more than 12 $\mathrm{km\,s^{-1}}$.	V-ANA-SIM	✓
OPS-EDL-AE-LA-2	The system shall land on the day side of Venus.	V-ANA-SIM	✓
OPS-EDL-GI-I-1	The system in landing configuration shall be capable of surviving a ground impact at 8.5 m/s.	V-TST-GRD	✓
OPS-EDL-GI-A-1	The system in landing configuration shall be capable of landing on slopes up to 10° without tipping over.	V-TST-GRD	✓
OPS-EDL-FD-T-1	The system in final descent configuration shall be capable of withstanding temperatures up to 464 °C for for 60 minutes.	V-DEM-TEM	✓
OPS-EDL-TC-1	The EDL system shall keep the internal temperature below 333 K (60 °C) between separation from the orbiter and aeroshell detachment.	V-ANA-SIM-TH	✓
OPS-EDL-SCI-3	Atmospheric measurements shall be conducted from the middle atmosphere during descent.	V-DEM-FUN	✓
OPS-EDL-DO-1	The system shall safely separate from the orbiter.	V-DEM-TSK	✓
OPS-EDL-DO-2	The system shall have an initial relative velocity away from coasting stage after separation between 0.1 m/s and 1 m/s.	V-TST-GRD	✓
OPS-EDL-DO-3	The deployment system shall not induce relative angular velocities between the coasting stage and the lander larger in magnitude than 0.01 rad/s.	V-TST-GRD	✓
OPS-EDL-ACD-1	The system shall hit the atmospheric interface with a total angle of attack of less than 0.5°.	V-ANA-SIM	✓
OPS-EDL-ACD-2	The system shall determine its orientation during entry with 0.1 degrees of precision.	V-DEM-FUN	✓
OPS-EDL-ACD-3	The absolute angle of attack of the system shall not exceed 3° during entry.	V-ANA-SIM	?
OPS-EDL-TPS-1	The main heat shield shall withstand maximum of 2884 $\mathrm{W/cm^2}$ heat flux at peak entry heating.	V-TST-GRD	✓
OPS-EDL-TPS-2	The aftbody heat shield shall withstand maximum of 65.9 $\mathrm{W/cm^2}$ heat flux at peak entry heating.	V-TST-GRD	✓
OPS-EDL-TPS-3	The main heat shield shall be capable of absorbing a total of at least 42938 $\mathrm{J/cm^2}$ of heat during entry.	V-ANA-SIM	✓
OPS-EDL-TPS-4	The aftbody heat shield shall be capable of absorbing a total of at least 1526 $\mathrm{J/cm^2}$ of heat during entry.	V-ANA-SIM	✓
OPS-EDL-FD-V-1	The EDL system shall slow down the craft to at most 8.5 m/s just above the surface.	V-ANA-CFD	✓
OPS-EDL-FD-H-1	The main heat shield shall be safely separated from the rest of the craft.	V-TST-GRD	✓
OPS-EDL-FD-H-2	The aeroshell shall be safely separated from the lander.	V-TST-GRD	✓
OPS-EDL-ST-1	The lander shall be secured inside the EDL system until the separation of the latter.	V-TST-GRD	✓

The description of verification method IDs are found in Table 4.1.

5.1.2 Overview of the EDL Sequence

The preliminary timeline for the EDL operations is shown in Figure 5.1. The time between the atmospheric entry and landing is 57 minutes.

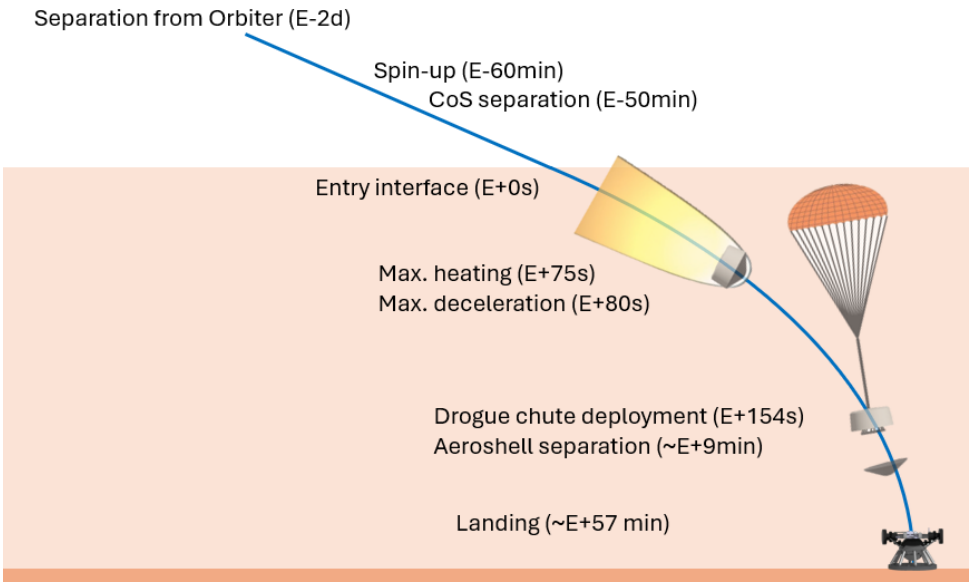

Figure 5.1: Overview of the EDL timeline for an entry trajectory at -12.8°entry flight path angle and 12 km/s entry velocity.

5.1.3 Pre-EDL Operations (Transfer and Coast)

A primary and a backup Venus transfer window was selected. Table 5.2 shows the departure and arrival time, as well as the time spent in transfer and the flyby velocity[1]. For both of these transfers, the local solar time at the landing site is between 11:00 and 13:00, thus the site is on the day side of Venus and requirement OPS-EDL-AE-LA-2 is fulfilled.

Table 5.2: Time of departure, time of arrival, duration, and flyby velocity for the selected primary and backup transfer windows[2]..

Transfer window	Date of departure	Date of arrival	Transfer duration	Flyby speed
Primary	08/Mar/2036	28/Jun/2036	112 d	11.65 km/s
Backup	21/Oct/2037	25/Jan/2038	96 d	11.97 km/s

It was decided in the Midterm Report that the transfer stage delivering the KYTHERA spacecraft to Venus will also act as a relay satellite. As a direct entry procedure will be used, the EDL subsystem with the lander encased in it needs to separate from the orbiter (the orbiter will perform a propulsive capture separately). To support the EDL subsystem before it enters the atmosphere, a Coasting Stage (CoS) will be used. A render of the CoS can be found in Figure 6.7b in Chapter 6.

As discussed in Section 5.3, the GPHS modules produce 3.5 kW of heat when idle. Although the Stirling generator is locked in place until the lander reaches the surface, the GPHS blocks cannot be turned off. To prevent overheating between launch and entry, a radiative Cruise Heat Rejection System (CHRS) is used to radiate heat into space and keep the internal temperature of the lander at 60 °C (333 K).

The EDL system needs to orient the spacecraft so that the main heat shield faces the flight direction. Additionally, the spacecraft will be spun up to 13.5 RPM before the entry interface, designated to be at 250 km altitude. This is done to provide the vehicle with gyroscopic stability during entry. To facilitate these needs, an Attitude Determination and Control System (ADCS), using star trackers and gyros for determination and thrusters for control, is to be integrated into the CoS, along with the CHRS. The thrusters of the ADCS will also be used to perform necessary course corrections during coast.

The CoS is not equipped with thermal protection, therefore it is detached 50 minutes before entering the atmosphere and will subsequently disintegrate. The remaining fuel will be used to build up additional separation from the entry capsule. Before separation, the thermal connection' valves are closed and the lander's EDL mode is armed. The electrical and thermal interfaces are cut using pyrocharges. The CoS is mechanically separated by a spring system, as these are better for applications, where low tip-off rates are required, than explosive solutions [40].

5.1.4 Thermal Management

The internally generated heat, as well as the received solar radiation power needs to be distributed during cruise and entry. To take the heat away from the GPHS blocks in cruise, a looped heat pipe (LHP) system is used. An LHP is a passive, two-phase heat transfer system which transfers heat by circulating a fluid in a closed loop. The heat evaporates the fluid, which then travels to the cool side (the CHRS in this case). As heat is rejected, the fluid condenses and the liquid loops back to the heat source, where the cycle is repeated. LHPs can provide transport powers up to 24 kW and start up on their own as soon as a threshold temperature gradient is built up [41], making them ideal for this application. Mishkinis et al. [42] tested an LHP setup intended for European Mars rovers, weighing 254 g and a maximum power transfer of 80 W. The mass of the LHP aboard the KYTHERA EDL subsystem is linearly extrapolated from this design, giving an LHP mass estimate of 17 kg, including a 50% margin. The LHP system is mechanically attached to the aeroshell and is located above the heat exchangers on the drag plate, so that the pipe loop can be connected to the CHRS through the backshell interface plate.

While the spacecraft flies in the upper atmosphere, the CHRS is not available anymore and the aeroshell of the TPS hinders heat dissipation. To absorb the heating power of the GPHS blocks, a phase-change material (PCM) is used. Paraffin waxes are often used for this purpose because of their noncorrosive nature and high heat of fusion. In the EDL system of KYTHERA, n-Triacontane ($C_{30}H_{62}$) will be used as a PCM. Table 5.3 shows the properties of this material [43].

Table 5.3: Properties of n-Triacontane [43].

Melting point [°C]	Heat of fusion [kJ/kg]	Density (liquid 78 °C) [kg/m^3][3]
65.4	251.1	775

It is assumed that CoS separation and aeroshell separation happen within 1 h of each other. Assuming all generated heat is absorbed by the PCM, the required mass for the PCM, including 10% margin, is 56 kg, taking up a maximum volume of 0.0723 m^3, equivalent to a 41.7 cm side cube. Note that the density of paraffins decrease as they melt [43],

[1]Transfers taken from `https://trajbrowser.arc.nasa.gov/`, accessed on 21/Jun/2025.
[2]`Transfers taken from https://trajbrowser.arc.nasa.gov/, accessed on 21/Jun/2025.`
[3]`https://cameochemicals.noaa.gov/chemical/21137, accessed on 12/Jun/2025.`

therefore the solid phase is not limiting the sizing of the container. As the PCM needs to absorb heat during entry, where decelerations are expected to be in the order of ~100 g. This inhibits the use of traditional heat pipes, which operate using capillary action, several orders of magnitude weaker than the inertial forces. Although they are less sensitive to gravity and orientation [41], their performance is reduced with increasing gravity [42]. A paraffin heat-switch will be used instead. Its operating principle is conduction, so the heat switch is not affected by high loads. The heat switch is toggled passively by a paraffin inset that expands and contracts with temperature. After the CHRS is decoupled, the temperature starts rising. Ideally, the paraffin mixture's melting point is tuned just below the melting point of Triacontane, i.e. 65.4 °C. Then the heat switch activates shortly before the melting point is reached, and the heat exchanger of the GPHS blocks becomes thermally connected to the PCM container. The phase-change nature of the heat sink ensures that the inside is kept at a constant temperature as long as the phase change is ongoing. The mass of the heat switch system is estimated to be 7 kg, including a 10% margin, from data presented in [41, p. 366]. A heat pipe system will be integrated into the aeroshell support structure to help distribute the heat evenly in cruise and coast. The aeroshell support structure is allocated 108 kg of mass, which includes the aeroshell and heat shield support structures with the heat pipe system, the support struts and cup connecting the drag plate to the aeroshell and the outer shell to the heat shield, respectively and the containers of the PCM.

5.1.5 Description of the Capsule

There were three capsule-styles considered: the Apollo-, the Mars Exploration Rover-, and the Stardust Sample Return Capsule (SRC). Out of these, the Stardust SRC design was selected due to the similarity of the Stardust Sample Return mission to the KYTHERA spacecraft's entry phase. The Stardust SRC returned to Earth from an interplanetary trajectory and performed the fastest re-entry (12.9 km/s) by a man-made object, while only relying on spin-stabilization [44]. The KYTHERA EDL subsystem is also not planned to have an active control system after CoS separation.

The geometry is scaled up by a factor of 2.7 from the original Stardust SRC design. The main heat shield is a cone frustum with a half-cone angle of 60° with a spherical cap of radius 617.2 mm on the nose. The maximum radius of the KYTHERA capsule is then 1097.3 mm. The backshell is also a cone frustum. To accommodate the lander, the backshell's half cone angle is decreased from the original 30° to 5°. The height of the backshell is set to be 900 mm. Figure 5.2 shows the capsule geometry. The capsule is axissymmetric.

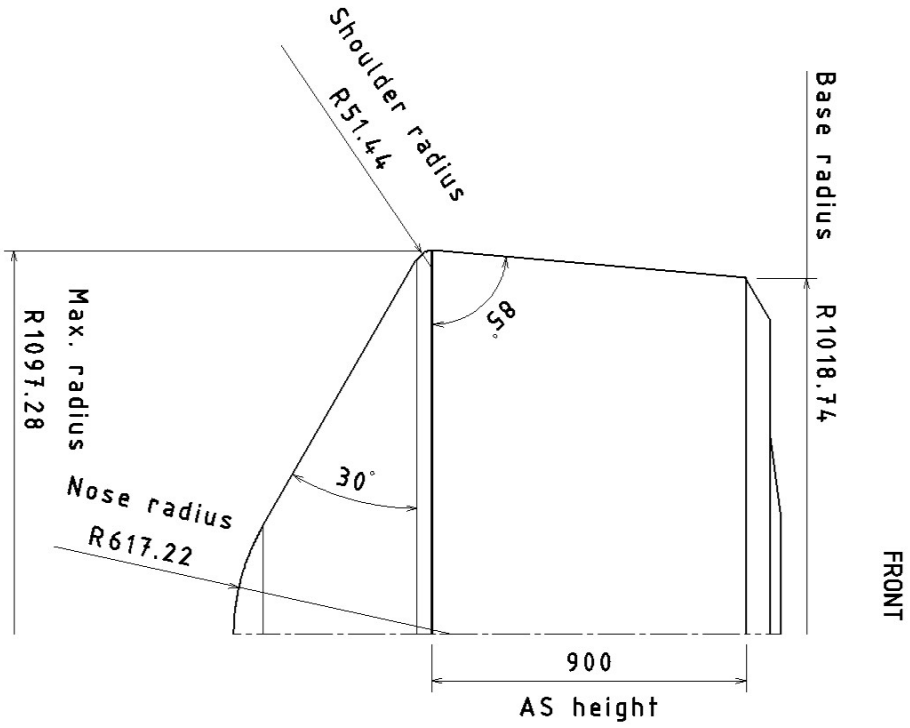

Figure 5.2: Dimensions of the KYTHERA entry capsule. All dimensions in mm.

During entry, the flow can be divided into five flow regimes, characterized by the Mach (M) and Knudsen numbers (Kn) [44–46]:

1. Free-molecular flow: If the Kn is high, there is very little interaction between the gas molecules. The aerodynamic coefficients are a function of Kn and angle of attack.
2. Transitional flow: As Kn decreases, the interaction between particles becomes more significant.

3. Hypersonic continuum flow: If $Kn < 10^{-3}$, the flow can be modelled as a continuum flow. The flow is dominated by a strong bow shock and the contribution of the aeroshell's pressure distribution is insignificant compared to that of the forebody (main heat shield).
4. Supersonic flow: For $M < 7$, the contribution of the aeroshell is not negligible anymore.
5. Transsonic flow: At M~1, the flow transitions from subsonic to supersonic and shocks form, drastically increasing the drag coefficient.
6. Subsonic flow: as M decreases, the flow becomes less compressible and the drag coefficient decreases.

The axial force coefficient model used for the entry simulation is shown in Figure 5.3.

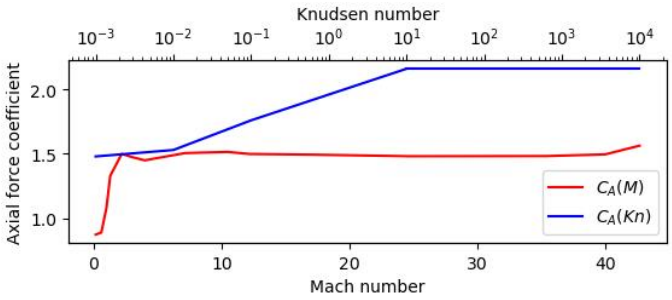

Figure 5.3: Axial force coefficients of the Stardust SRC. The data for free-molecular flow is adapted from [45]. Hypersonic ($M > 7$) and subsonic data was taken from [46]. Transsonic ($M < 1.3$) data is taken from [47] and supersonic data is from [48]. Note that [47] and [48] measured aerodynamic coefficients of blunt nosed cones without an aftbody, therefore the results are only indicative. For $M > 42.7$ and $Kn < 10^{-3}$, the axial force coefficient is taken to be the limit value.

It is important to address the stability of the capsule during entry, as the capsule will need to rely on its aerodynamic stability to maintain the correct attitude. Mitchelltree et al. [46] found that the Stardust SRC has a dynamic instability in the free-molecular and early transitional flow regime. The initially planned 5 RPM was increased to 13.5 RPM, so that gyroscopic stability prevented capsizing. However, because of Stardust SRC's smaller size, it reaches transition at higher densities than KYTHERA would, and KYTHERA will have significantly higher mass moment of inertia as well, making spin-stabilization more effective. However, the change in backshell geometry likely influences the dynamic behavior. Therefore, the pitching moment characteristics need to be evaluated in a later stage of the design, when more is known about the mass distribution of the spacecraft. This can be done, for example, by three-dimensional Direct Simulation Monte Carlo (DSMC) analysis and the Langley Aerothermodynamic Upwind Relaxation Algorithm (LAURA) program [46]. It should be then evaluated if spin-stabilization is feasible and whether reconfiguration of mass distribution or other forms of stabilization are needed.

5.1.6 Thermal Protection System

The TPS is responsible for protecting the payload from the intense heating that occurs during entry. Due to Venus's thick atmosphere and the selected direct entry procedure, the thermal loads are expected to exceed 1000 $\mathrm{W\,cm^{-2}}$. As described in the Midterm Report, an ablative TPS will be used. The heat shield's ablator degrades, absorbing heat. In addition, hot vapors created in the process are released, removing more heat from the shield.

TPS Sizing Methodology

The TPS sizing will be performed as follows. An initial mass for the heat shield (HS) of 200 kg and aeroshell (AS) of 100 kg is assumed. The "dry" mass (i.e. the mass that does not change with iterations) budget of 565 kg is broken down in Table 5.4. Then, the entry trajectory and heating is simulated for different entry flight path angles (γ_E). The entry velocity (V_E) is assumed to be not more than 12 km/s (the minimum entry velocity at the atmospheric interface at 250 km altitude is 10.51 km/s for a perfect Hohmann-transfer from Earth to Venus). The heating rate is integrated to get the total heat load (per unit area). The Mass Estimation Relationships (MERs) developed by Sepka and Samareh [49] are used to get an estimate for the TPS thickness. The new TPS mass is calculated and the total mass of the spacecraft is updated. The simulation is iterated until mass convergence is reached.

Table 5.4: "Dry" mass budget breakdown of the EDL.

Component	Mass [kg]
Triacontane PCM	56
Parachute System	22
Structures	108
LHP	17
Heat Switches	7
Cabling and Sensors	5
Lander	350
Total	565

Models and Assumptions

A 2D solver, named Parametric Entry Trajectory Simulator for Venus (PETS4V) was developed. It uses the explicit Runge-Kutta 4 method to calculate the entry trajectory for given initial position and velocity. PETS4V makes use of the following

assumptions:

- The spacecraft is a perfect axissymmetric body, thus the angle of attack and the sideslip angle can be combined into the total angle of attack, and the roll angle does not have any effect on the aerodynamic properties.
- The spacecraft remains at 0 degrees angle of attack throughout the flight, thus the drag equals the axial force.
- The surface and atmosphere of Venus are nonrotating.
- The effect of wind is negligible on the heating and deceleration characteristics. The atmosphere is assumed to be stationary.
- It is assumed that the density above the the atmospheric interface is 0, therefore there is no drag.
- There is no side force, i.e. the motion of the vehicle can be simplified to a 2D motion.
- Buoyancy is neglected.
- The only gravitating body is Venus. The effect of the Sun, Jupiter and other planets, as well as the spacecraft's gravitational pull on Venus, are neglected.
- Venus' gravitational field is perfectly spherical. Higher order harmonic coefficients are neglected when the gravitational acceleration is computed.
- To give a conservative estimate for the total heat load, it is assumed that the stagnation point heat flux is applied to the entire HS.
- The incident heat flux on the AS is 5% of the convective heat flux on the HS [49].
- The shape of the HS does not change as it undergoes ablation. In reality, Stardust SRC's axial force coefficient reduced by approx. 8% due to reduction in cross-sectional area and change in nose radius [46].

To get the atmospheric properties used in the simulation (density and the speed of sound), PETS4V uses NASA's Venus Global Reference Atmospheric Model (Venus-GRAM), acquired as a part of the GRAM-Suite package, version 2.1.0[4]. Figure 5.4 shows the density and speed of sound plotted against altitude. In the lower atmosphere (0-100 km), the model uses data for 70° latitude. In the middle (100-150 km) and upper (150-250 km) atmosphere, the mean values are used. For the middle atmosphere, this is taken as the average of the values for local solar noon and midnight, i.e. the average of the diurnal cycle. For the upper atmosphere, the mean values are taken to be those for a solar zenith angle of 90° [50].

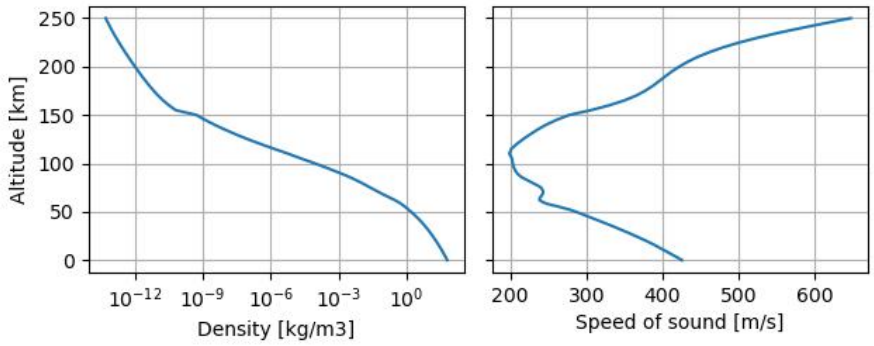

Figure 5.4: Atmospheric properties vs. altitude plotted up to the atmospheric interface at 250 km.

The entry heating model consists of two components: convective and radiative heating. The Sutton-Graves relation [51, 52], shown in Equation 5.1 is used to model convective heating.

$$\dot{q}_{\text{conv}} = K\sqrt{\frac{\rho_\infty}{R_N}}V_\infty^3 \tag{5.1}$$

where $\dot{q}_{\text{conv}}$ is the convective heat flux in $\mathrm{W\,cm^{-2}}$, $K = 1.8960 \cdot 10^{-8}$ $\mathrm{W\ cm^{-2}\ s^3\ m^{-1}\ kg^{-0.5}}$ is a constant that is only dependent on the atmospheric constituents [52, 53], ρ_∞ is the free-stream density in $\mathrm{kg\,m^{-3}}$, R_N is the nose radius in m and V_∞ is the free-stream velocity in $\mathrm{m\,s^{-1}}$.

Radiative heating is modeled by a modified version of the Tauber-Sutton relations, presented in Equation 5.2, developed specifically for Venus entries by Tauber et al. [54]:

$$\dot{q}_{\text{rad}} = \begin{cases} 8.497 \cdot 10^{-67}\ \rho_\infty^{1.2}\ R_N^{0.49}\ V_\infty^{18} & \text{for } 10028 < V_\infty < 12000\ \mathrm{m\,s^{-1}} \\ 2.195 \cdot 10^{-26}\ \rho_\infty^{1.2}\ R_N^{0.49}\ V_\infty^{13.4} & \text{for } V_\infty < 10028\ \mathrm{m\,s^{-1}} \end{cases} \tag{5.2}$$

[4]The software can be requested from `https://software.nasa.gov/software/MFS-33888-1`. accessed on 13/Jun/2025.

where the variables are in the same units as for Equation 5.1. For $V_\infty > 12000\,\mathrm{m\,s^{-1}}$, the heat flux is approximated as the limit value at $V_\infty = 12000\,\mathrm{m\,s^{-1}}$ [55]. To reduce computational time, heating is neglected below 300 and 2000 $\mathrm{m\,s^{-1}}$ for convective and radiative heating, respectively. Equation 5.2 was found to underpredict heating rates at lower stagnation pressures by up to 25%, but is very accurate at peak heating [54]. To ensure the conservativeness of the heat flux figures, a thermal safety factor of 1.5 is applied.

The heat flux $\dot{q} = \dot{q}_{\text{conv}} + \dot{q}_{\text{rad}}$ (for aftbodies, only $\dot{q}_{\text{conv}}$) is integrated with respect to time to get the total heat load per unit area, q. The MERs were developed for two forebody ablators, PICA and CP/ACC, as well as five aftbody ablators. MERs for the two forebody ablators, as well as SIRCA and Acusil-II for backbody applications, are implemented in PETS4V. The MERs for the materials are shown in Table 5.5.

Table 5.5: Mass estimation relationships for PICA, CP/ACC, SIRCA and Acusil-II [49].

	PICA	**CP/ACC**	**SIRCA**	**Acusil-II**
Max. allowable heat flux [$\mathrm{W\,cm^{-2}}$]	1200	30000	100	100
Ablator thickness [cm] q in $\mathrm{W\,cm^{-2}}$ V_E^2 in $\mathrm{km^2\,s^{-2}}$	$1.8696 \cdot \left(\frac{q}{V_E^2}\right)^{0.1873}$	$1.1959 \cdot \left(\frac{q}{V_E^2}\right)^{0.2102}$	$0.5281 \cdot \left(\frac{q}{V_E^2}\right)^{0.5416}$	$0.623 \cdot \left(\frac{q}{V_E^2}\right)^{0.5697}$
Ablator density [$\mathrm{kg\,m^{-3}}$]	274	1430	259	250

The relationships in Table 5.5 was found to under-predict TPS thicknesses for the considered ablators by up to 16.6% compared to results obtained by a higher fidelity tool, NASA's Fully Implicit Ablation and Thermal Analysis program (FIAT), which was used to develop the MERs [49]. Therefore, PETS4V uses a thickness safety factor of 2 to obtain a conservative estimate of the size of the TPS.

For the purpose of calculating surface area, the HS is assumed to be a cone with half cone angle α_{HS} of 60°. The AS is modelled as a cone frustrum with half cone angle α_{AS} of 10° and base radius r_{base} of 1018.74 mm. The geometry is displayed in Figure 5.2. Then the area of the HS and the AS are approximated as

$$A_{HS} = \frac{r_{\text{max}}^2 \pi}{\sin \alpha_{HS}} \qquad (5.3) \qquad A_{AS} = \pi \left(\frac{r_{\text{max}}^2 - r_{\text{base}}^2}{\sin \alpha_{AS}} + r_{\text{base}}^2 \right) \qquad (5.4)$$

Equation 5.3 over-predicts the HS area, because it ignores the reduction in area due to the tip of the HS being a spherical cap instead of a perfect cone. The volume of the TPS is then calculated assuming that the TPS thin-walled, i.e. $v = A_{HS}\, t_{HS} + A_{AS}\, t_{AS}$ where t_{HS} and t_{AS} are the thicknesses of the HS and the AS calculated earlier. Thus the iterated mass of the TPS is $m_{TPS} = A_{HS} t_{HS} \cdot \rho_{HS} + A_{AS} t_{AS} \cdot \rho_{AS}$.

Program Description, Verification and Validation

The main program loop, the trajectory simulation loop, and the RK4 solver loop are shown in Figures 5.5, 5.6 and 5.7, respectively.

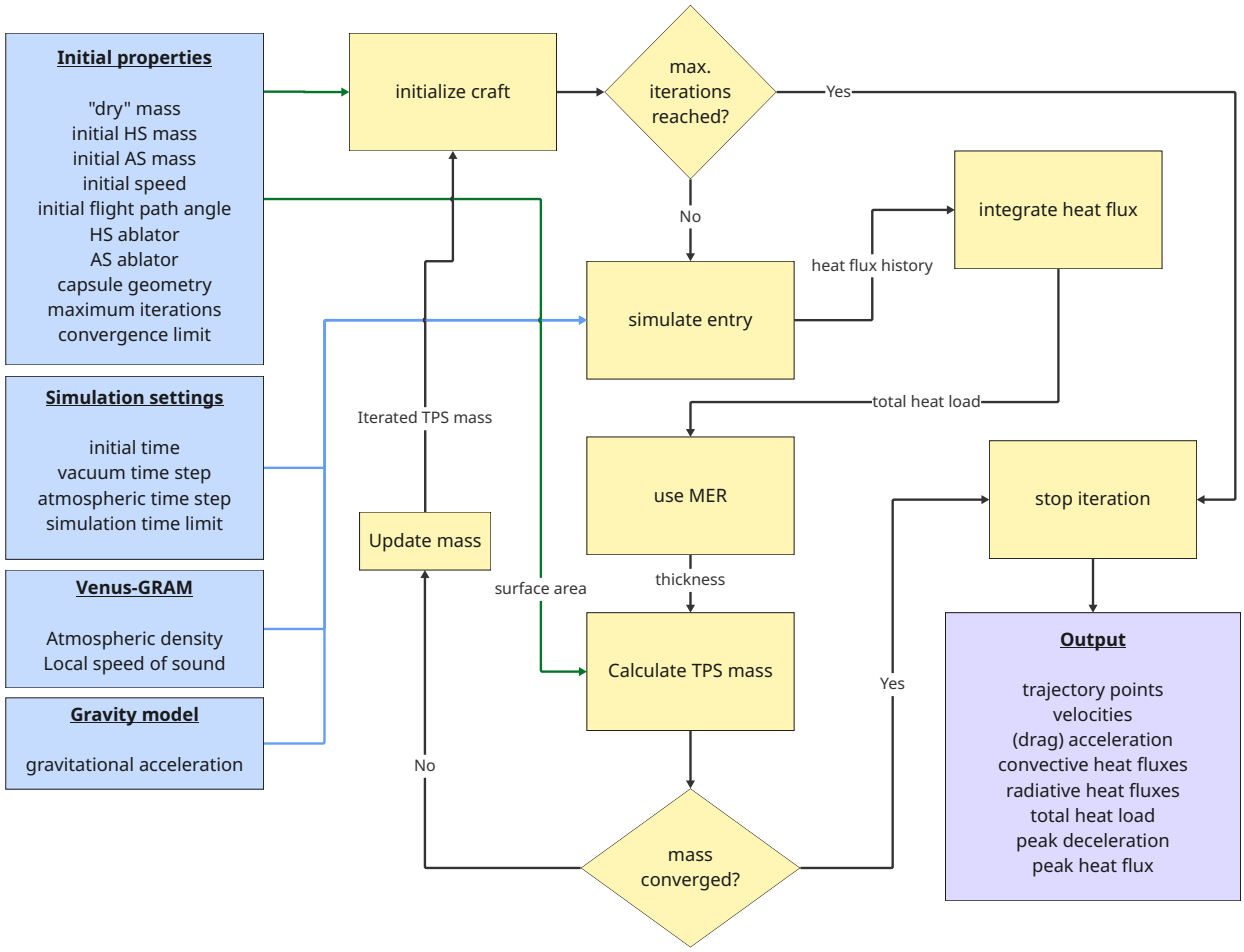

Figure 5.5: Main program loop of PETS4V.

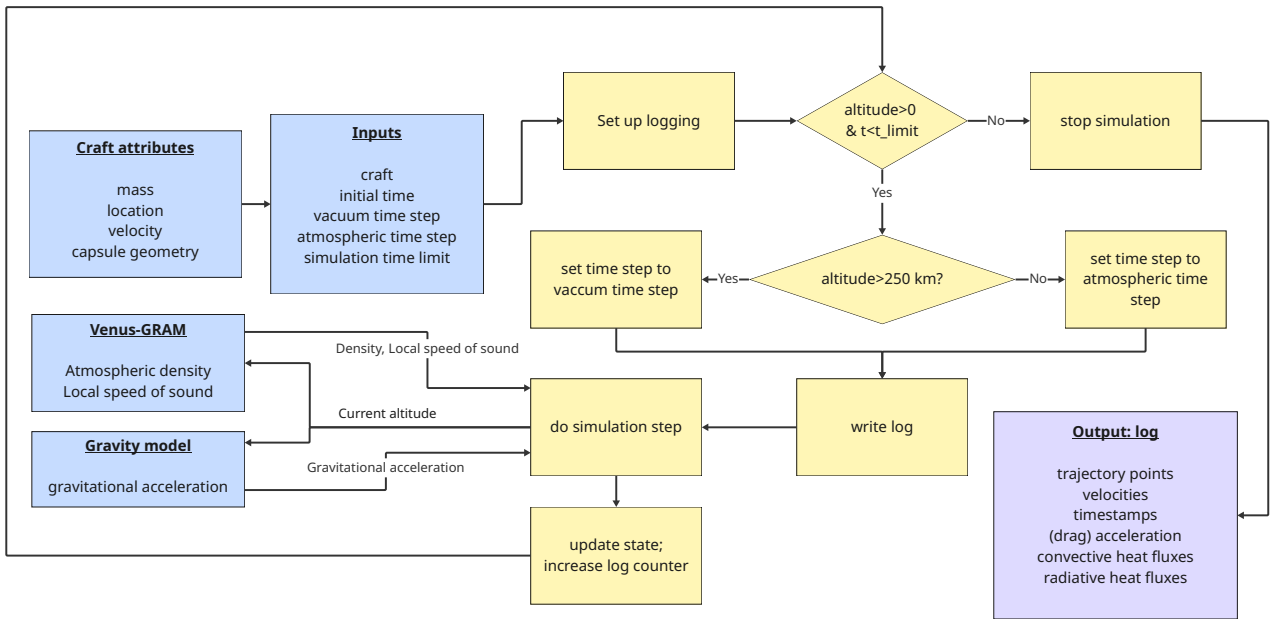

Figure 5.6: Simulation loop of PETS4V. This corresponds to the ”simulate entry” block in Figure 5.5.

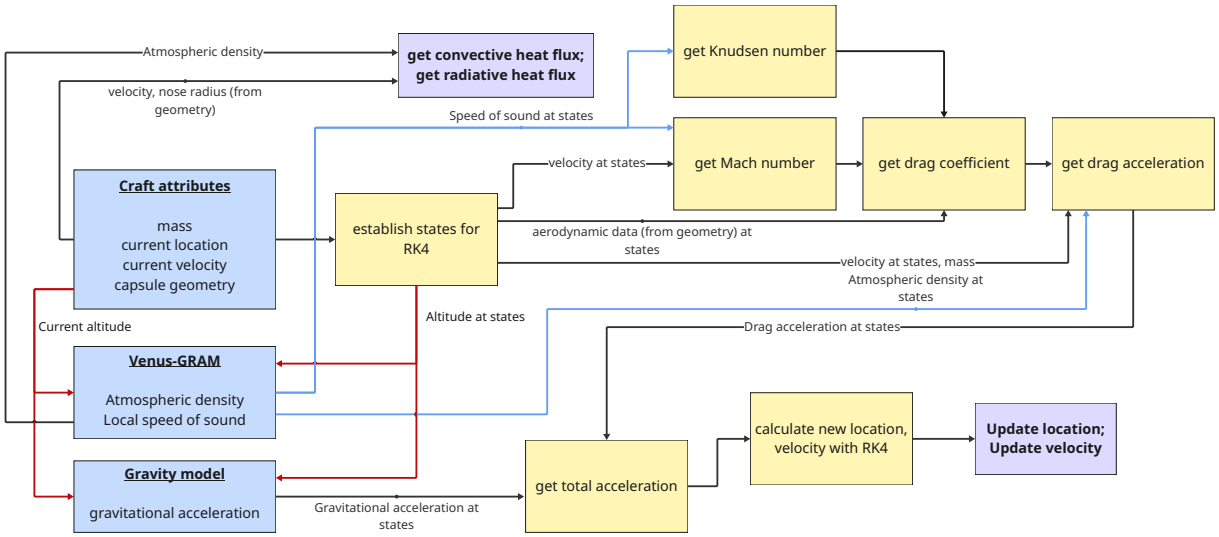

Figure 5.7: Numerical method diagram of PETS4V. This corresponds to the ”do simulation step” block in Figure 5.6.

The program was verified by an extensive set of unit and system tests. An example of a system test, `ST_simulate`, verifying that the gravity model and the RK4 method is implemented correctly, is explained below.

To check that the simulation loop is working as intended, a test craft is given the inital conditions for a circular orbit. The simulation loop is run until the theoretical orbital period, predicted by Kepler’s third law, is elapsed. Then the position at the end of the simulation is compared to the position predicted by the analytical model at the corresponding timestamp. The input and output data are collected in Table 5.6. The data is visualized in Figure 5.8.

Input parameter	Value	Time step	Distance error
Orbital radius	10591.46963268082 km	$dt = 100$ s	14.81 m
Expected period	12016.170622265263 s	$dt = 50$ s	0.83 m
Initial position (x, y)	(7489.3, -7489.3) km	$dt = 10$ s	0.0137 m
Initial velocity (x, y)	(3.916111147, 3.916111147) $\mathrm{km\,s^{-1}}$	$dt = 1$ s	0.0125 m

Table 5.6: Input and output values for `ST_simulate`.

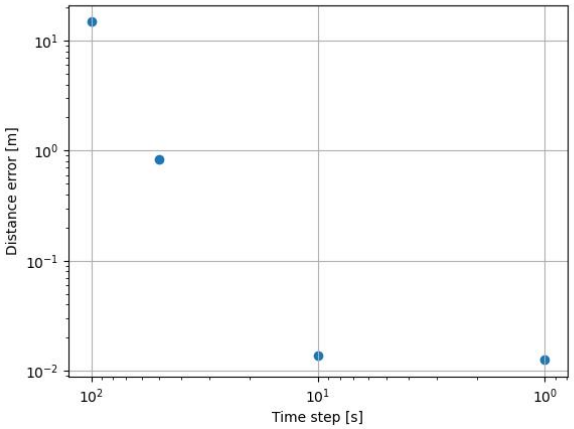

Figure 5.8: Error of the predicted position of the simulation loop as a function of time step over a ~200 min long interval.

From Figure 5.8 and Table 5.6, it is clear that the solution converges. However, the error does not converge to zero, but fluctuates around 0.01 m. This is due to floating-point error due to the limitations of the binary representation of numbers (64 bit floats were used in the program), which is not reduced by decreasing the step size but by increasing the number of bits. Nevertheless, the simulation loop was successfully verified.

To validate the code, its output was compared to reference data from the Pioneer-Venus large probe, presented by Tauber et al. [54]. The initial conditions, as well as the aerodynamic properties of the simulated craft were changed to those used

in the reference. The initial altitude was 137.78 km, the initial speed 11584 m/s, with a flight path angle of -31.829°. The test craft in the simulation had a constant ballistic coefficient of 190 $\mathrm{kg\,m^{-2}}$. These reference values and those computed by PETS4V are shown in Figure 5.9.

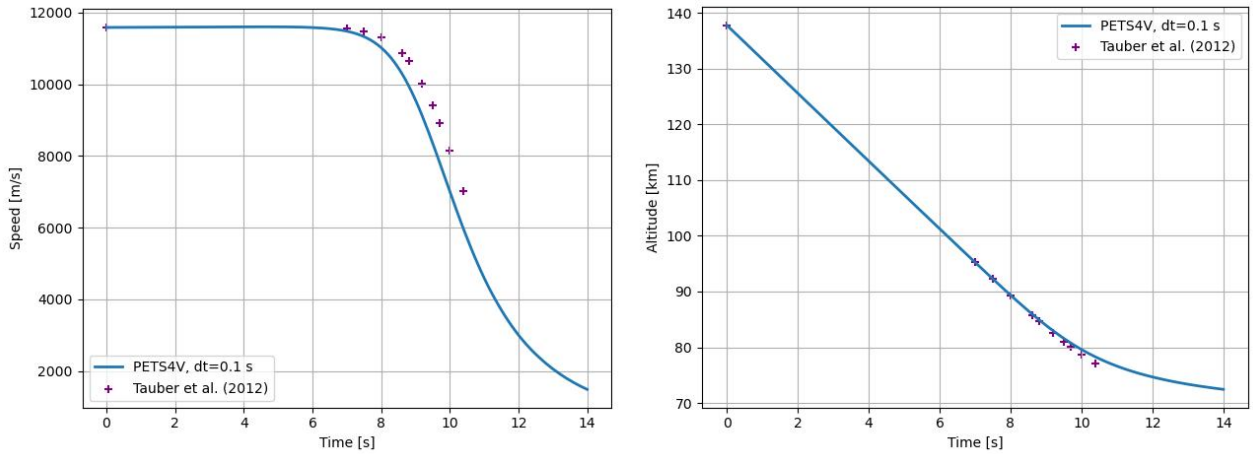

(a) Airspeed vs. time.

(b) Altitude vs. time .

Figure 5.9: Comparison of reference values form [54] and those predicted by PETS4V. Further reducing the simulation time step had no effect on the predictions..

As seen from Figure 5.9a, PETS4V predicts the deceleration to start around 0.4 seconds earlier than the reference data. Figure 5.9b plots altitude against time. The difference between the simulation output and the reference values increases with time. For the last data point, PETS4V predicts an altitude 1.13 higher than the reference altitude. The following are identified as potential causes of this discrepancy:

- The effect of high velocity winds in the upper layers of the lower atmosphere [16] is not included in the simulation.
- The ballistic coefficient of the reference spacecraft was assumed to be constant, i.e. the effects of Mach and Knudsen number on the axial force are not reflected in the simulation results. Additionally, deviations from the ballistic trajectory, i.e. the presence of normal forces due to deviations of the angle of attack from the nominal 0° are not modelled.
- In the lower atmosphere, PETS4V uses the Venus-GRAM data for 70° latitude, without perturbations. However, the large Pioneer Venus Probe landed in the equatorial regions[5]. Figure 5.10 shows the disagreement between the Venus-GRAM model implemented, and the values reported in [54], where data from [56] is used.

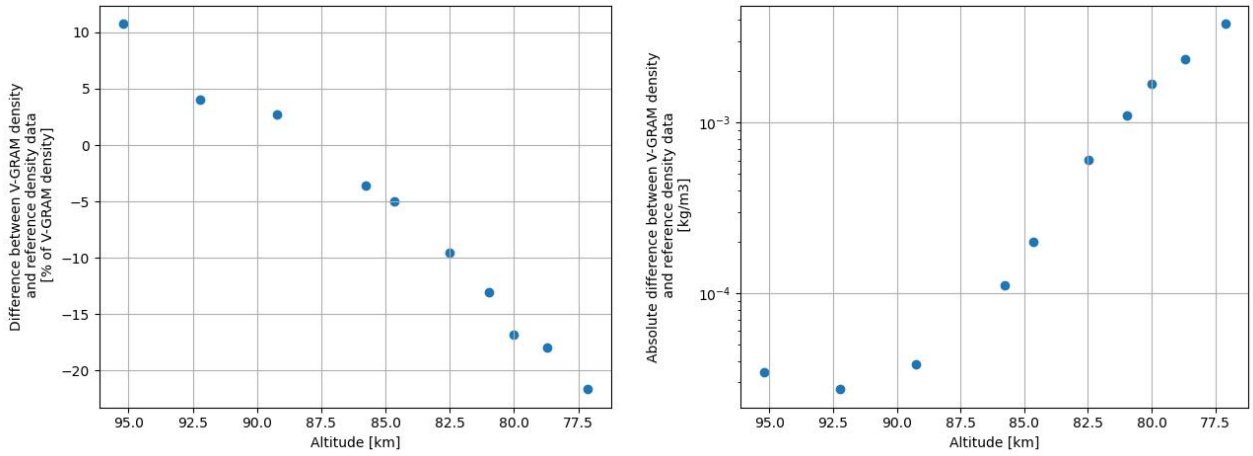

(a) Relative difference.

(b) Absolute difference.

Figure 5.10: Disagreement between the Venus-GRAM and the reference density model.

It can be seen from Figure 5.10a that for altitudes higher than ~87.5 km, Venus-GRAM predicts more than 10% higher density than the reference data. For lower altitudes, the reference assumes a denser atmosphere, and the disagreement

[5] `https://nssdc.gsfc.nasa.gov/planetary/pvprobes.html`, accessed on 15/Jun/2025.

can be even higher than 20%. However, the value of the atmospheric density increases by two orders of magnitude as the altitude decreases from 95 to 77 km. This explains the delayed onset of the deceleration. Overall, PETS4V gives reasonable predictions and therefore will be used as a tool for parametric analysis.

Results and Discussion

PETS4V was used to simulate entry trajectories and estimate the resultant mass of the TPS for each HS-AS ablator combination for entry speeds ranging from 10800 $\mathrm{m\,s^{-1}}$ to 12000 $\mathrm{m\,s^{-1}}$ and entry flight path angles from -10.2° to -15°. For comparison, the Pioneer-Venus large probe entered the atmosphere at ~11.5 $\mathrm{km\,s^{-1}}$. The trajectory simulation was stopped when 500 s elapsed or 60000 m of altitude was reached. The mass convergence limit was set at 1 kg. Most of the runs converged within 3-4 iterations. For deceleration, a safety factor of 1.5 was used.

Figure 5.11 shows the resulting total system masses for different entry angles and ablator configurations. The datapoints where the maximum allowable heat flux (see Table 5.5) including the previously discussed 50% safety margin for the given ablators was exceeded are marked with an additional red cross.

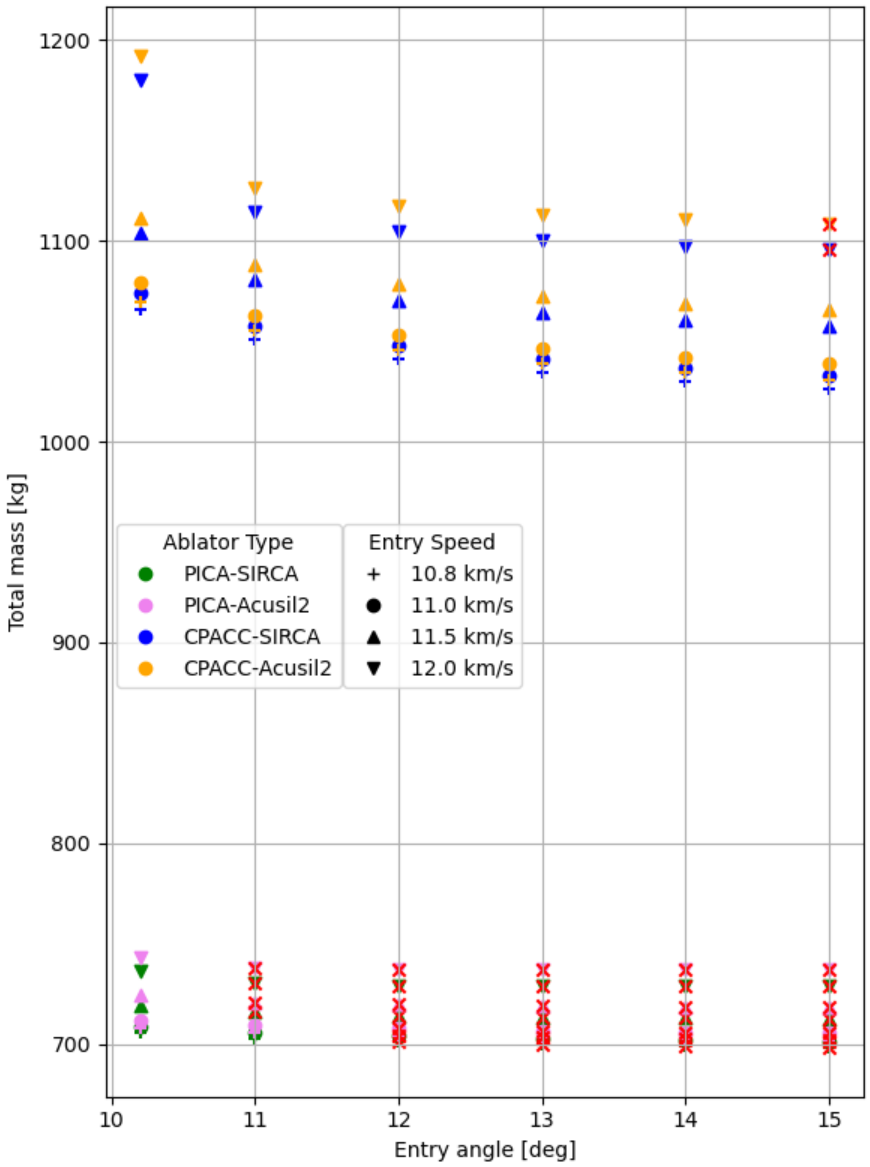

Figure 5.11: Mass output of PETS4V different ablator combinations and entry speeds as a function of entry flight path angle. The runs where the maximum allowable heat flux is exceeded are crossed out with red..

Counterintuitively, the required mass increases with decreasing entry angle. This is because the thickness of the TPS scales with the total absorbed heat, which is higher for shallower angles due to the longer time of flight and weaker shockwave formation in front of the HS [57]. The lower heat for steeper trajectories comes at the cost of higher peak heating. The PICA-based main heat shield configurations yield a significantly lower total system mass than those with CP/ACC. Unfortunately, they are not feasible, as the maximum allowable heat flux for PICA is considerable smaller than

that of CP/ACC (1200 $\mathrm{W\,cm^{-2}}$ vs. 30000 $\mathrm{W\,cm^{-2}}$), therefore overheating occurs for almost all entry angle and speed configurations. Of the remaining two options, the CP/ACC-SIRCA combination is marginally better in terms of mass. SIRCA can be easily machined to custom shapes [49, 58]. However, the machining of SIRCA tiles releases silica particles into the air, which can be a cause of silicosis, lung cancer and other lung diseases, although the risk of developing these can be mitigated with appropriate protective equipment [59]. On the other hand, Acusil can be simply molded onto the aeroshell surface, therefore there is no machining required, potentially reducing manufacturing costs. There are no toxicity or environmental risks associated with Acusil [60]. Because of this, the CP/ACC-Acusil II ablator configuration will be used. As it will be seen later, the heat and deceleration intensive part of entry does not last longer than a few minutes. Therefore, corrosion was not a significant factor for the design of the TPS.

For shallow entries, especially for those with high initial velocity, quasi-skipping can occur. Normal skipping occurs in lifting entries, when the lift generated is enough to increase the altitude of the spacecraft and make it ”skip” out of the atmosphere. If the entry trajectory is shallow and the entry velocity is high enough, the curvature of Venus becomes significant and the spacecraft will actually gain altitude, even though technically the lift is zero. This phenomenon is shown in Figure 5.12.

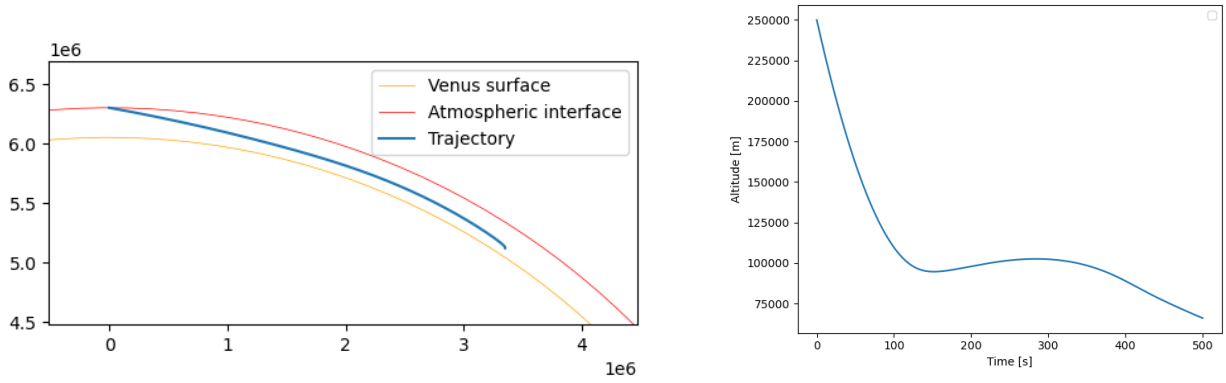

(a) Entry trajectory.

(b) Altitude vs. time.

Figure 5.12: Quasi-skipping behavior for $V_E = 12\ \mathrm{km\,s^{-1}}$, $\gamma_E = -10.2°$, CP/ACC-Acusil II configuration.

As can also be seen in Figure 5.11, quasi-skipping greatly increases the required mass of the TPS system due to the increased heat load discussed earlier. In addition, shallow entry angles are also not desirable because the longer ground track reduces the landing accuracy. For these reasons, the maximum entry flight path angle is limited to -11°.

Figure 5.11 also shows that overheating occurs already at $\gamma_E = -15°$ for $V_E = 12\ \mathrm{km\,s^{-1}}$, due to the thermal limitations of the aeroshell. For safety, the γ_E should not be lower than $-14°$.

The maximum entry speed simulated was 12 $\mathrm{km\,s^{-1}}$. For entry speeds higher than this, it is not possible to verify whether the TPS can survive. It is also unlikely that the spacecraft would enter the atmosphere with higher speeds from an efficient Earth-Venus transfer orbit.

The most limiting trajectory for TPS performance is the one at $\gamma_E = -11°$. As can be read off Table 5.7, the TPS should be sized to withstand a total stagnation point cold wall load of 43 $\mathrm{kJ\,cm^{-2}}$ and a total convection load of 1.53 $\mathrm{kJ\,cm^{-2}}$ on the aeroshell. The required TPS thickness and mass properties are compiled in Table 5.8 Note that The heat fluxes and thus the heat loads are cold-wall values. In reality, the wall of the TPS heats up and radiates away heat. The ablation and the associated mass efflux also removes considerable heat from the TPS.

Table 5.7: Critical heating and deceleration figures for γ_E between -11°and -13°for optimal TPS sizing.

	Entry flight path angle		
Quantity	**-11°**	**-12°**	**-13°**
HS max. heat flux [$\mathrm{W\,cm^{-2}}$]	2204	3043	3717
AS max. heat flux [$\mathrm{W\,cm^{-2}}$]	65.8	80.6	90.2
HS total heat [$\mathrm{J\,cm^{-2}}$]	42938	38324	36183
AS total heat [$\mathrm{J\,cm^{-2}}$]	1526	1252	1117
Max. deceleration [g_0]	63.1	96.9	122.9

The entry trajectories for $\gamma_E = -11°, -12°, -13°$ are plotted in Figure 5.13. The distance between the extreme trajectories’ final points is 380 km. Therefore, it is important to note that the limitations on γ_E come only from a TPS survivability consideration and that the entry point must be adjusted by trajectory corrections so that the desired landing site is reached within the required 100 km radius.

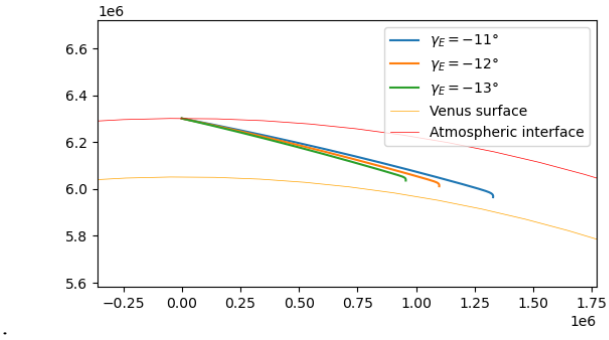

Figure 5.13: Plots of entry trajectories.

Table 5.8: Thicknesses and masses of the heat shield and the aeroshell..

Property	Heat shield	Aeroshell
Thickness [cm]	8	3
Mass [kg]	495	66
Total system mass: 1126 kg		

The maximum deceleration occurs at $\gamma_E = -14°$. Because the values in Table 5.7 were reported for optimal TPS sizing, i.e. the minimum TPS mass required to prevent burning up, the maximum deceleration at the limit angle was evaluated and found to be 144 g with margin. This is not within the maximum allowable deceleration of 120 g. The minimum entry flight path angle for which the maximum deceleration is below 120 g was found by trial and error to be 12.8° at 118 g. Therefore, the entry flight path angle should be between -11°and -12.8°. The maximum cold-wall stagnation heat flux is 2420 $\mathrm{W\,cm^{-2}}$ and the maximum aeroshell heat flux is 59.2 $\mathrm{W\,cm^{-2}}$. For landing accuracy, the steepest possible trajectory, so $\gamma_E = -12.8°$ is preferred. Figures 5.14 to 5.18 show the entry data of these two limiting trajectories.

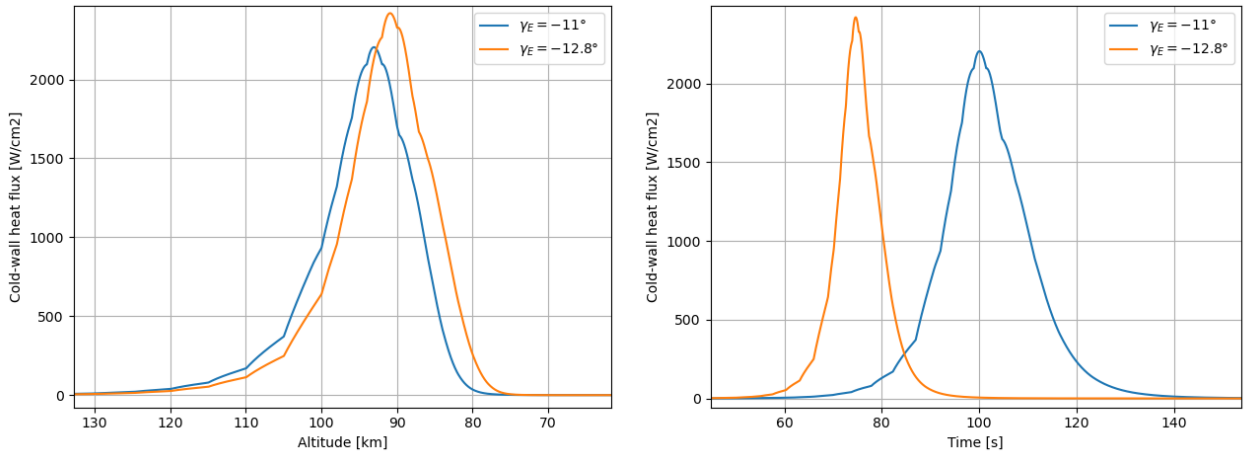

(a) Vs. altitude.

(b) Vs. time.

Figure 5.14: Cold-wall heat flux data.

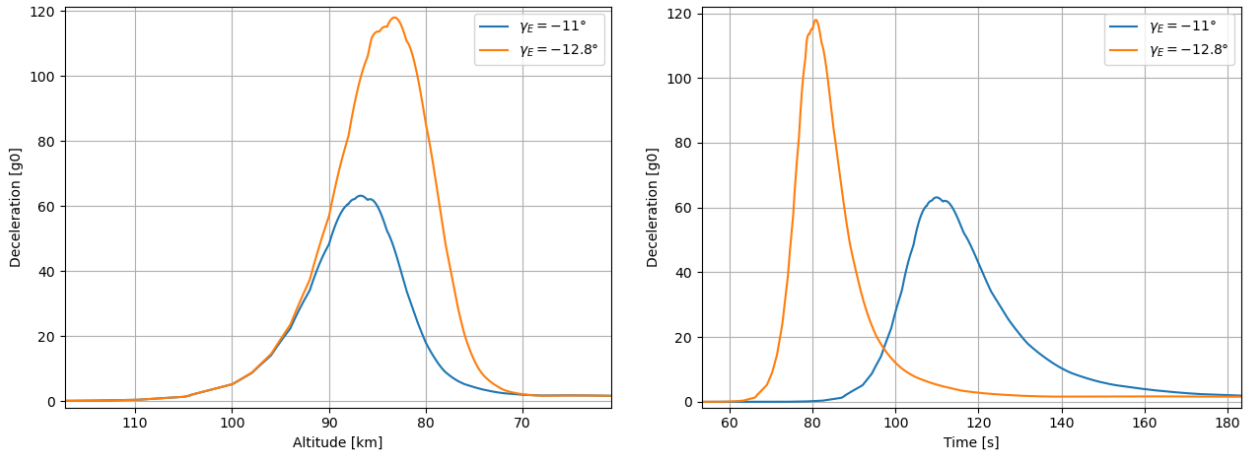

(a) Vs. altitude.

(b) Vs. time.

Figure 5.15: Deceleration data.

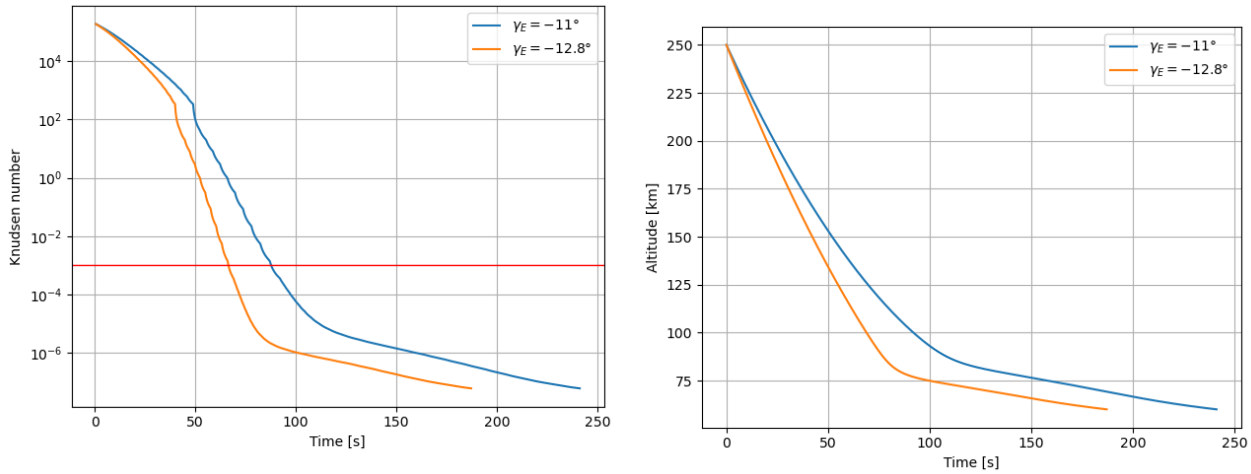

(a) Knudsen number vs. time. The red line marks the assumed cutoff for continuum flow, $Kn = 10^{-3}$..

(b) Altitude profile vs. time.

Figure 5.16: Knudsen number and altitude trends against time.

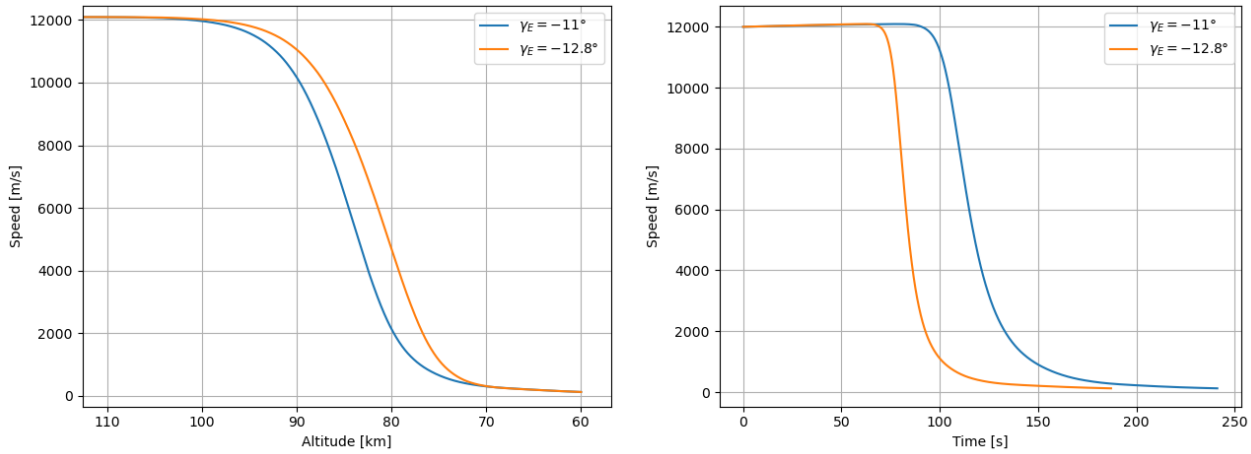

(a) Vs. altitude.

(b) Vs. time.

Figure 5.17: Design limiting parameter trends vs. time.

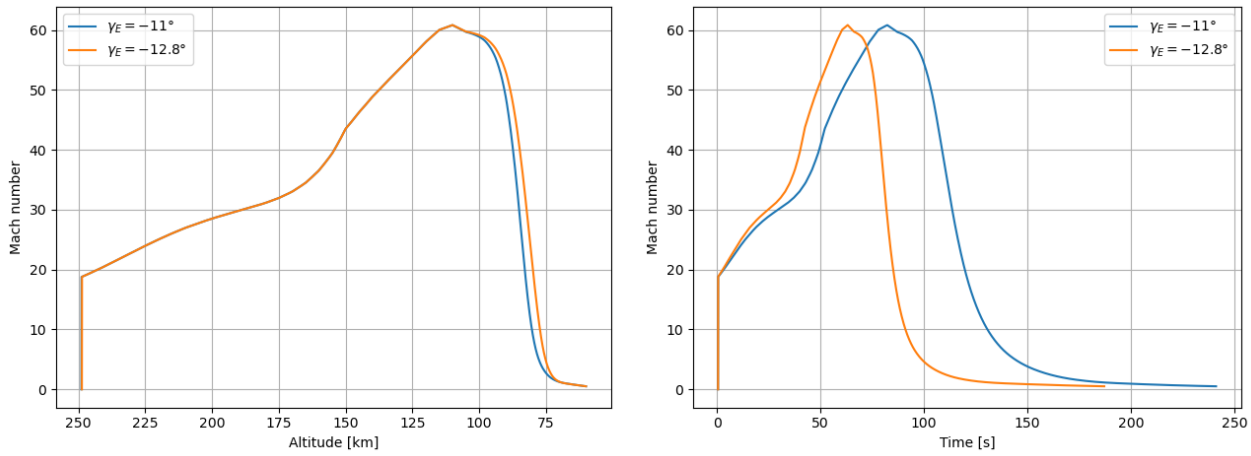

(a) Vs. altitude.

(b) Vs. time.

Figure 5.18: Mach number trends.

It can be seen from Figure 5.14a and 5.14b that maximum heating will occur between altitudes 94 km and 91 km or E+100s and E+75s, respectively. Heating is significant until ~75 km altitude is reached at E+140s. Figure 5.15a and 5.15b show that the spacecraft undergoes the peak deceleration between 86 and 84 km, or E+110s and E+80s. As expected, peak heating always occurs before peak deceleration. These plots are used to determine the timescale of the parachute deployment procedure, outlined in the following subsection.

5.1.7 Parachute System

After the entry heating and decelerations have subsided, the TPS must be separated as soon as possible to minimize the chance of TPS debris falling under/onto the lander. For this purpose, a mortar-deployed high-subsonic Disk-Band-Gap (DBG) parachute will be used with a drogue, so that the drag acceleration of the aeroshell+lander+parachute assembly is greater than that of the HS alone. The drogue will be deployed at 65 km altitude, between E+154s and E+209s (Mach 0.8) The DBG will deploy at an altitude of 61.5 km (between E+176s and E+230s, Mach 0.6). Initially, it will be reefed and then gradually unreefed over 10 s to minimize shock loads on the lander, parachute lining and mount. 20 s after the initial parachute deployment, the parachute state stabilizes and the HS is separated with pyrobolts. After 5 minutes of HS separation, the aeroshell is jettisoned as well, along with the parachute, leaving the lander in free fall.

The time of parachute deployment varies greatly with the trajectory chosen. Because of this, a g-switch, a timer and a pressure sensor will be used in combination to initiate the parachute deployment.

The mass of the parachute system is estimated to be 22 kg. This is reached by taking an estimate for the parachute mass for a similar system of 13 kg [61]. Assuming the other components weigh 11% of this value [62], and an uncertainty margin of 50%, the final parachute mass is 22 kg.

5.1.8 The Effect of Wind on Landing Accuracy

The main source of uncertainty in the landing site is assumed to be wind in the atmosphere. Venus-GRAM was used to predict the mean wind data at a latitude of 70° N and a local solar time of 12 h. The mean wind magnitude profile is shown in Figure 5.19a. The altitude history of the lander after aeroshell separation is shown in Figure 5.19b. It can be seen that the lander touches down approximately 57 minutes after the entry interface.

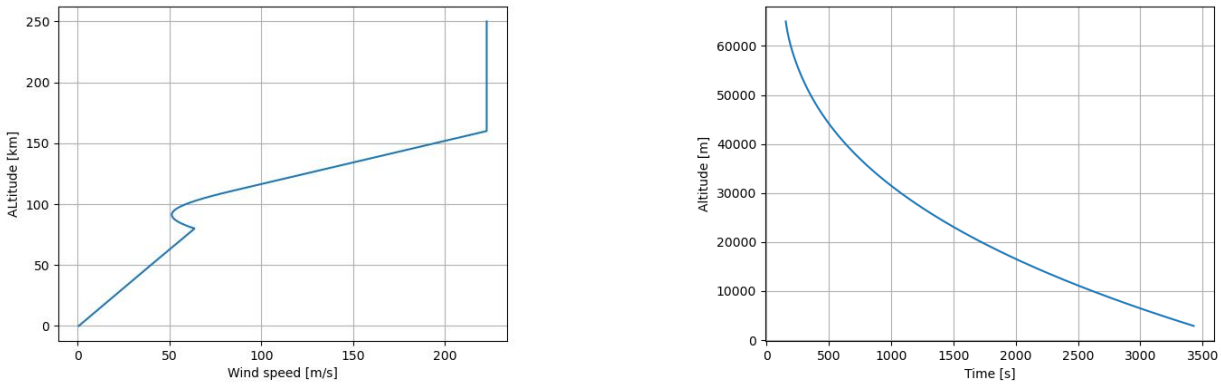

(a) Mean wind speed profile at latitude 70° N and solar time 12 h.

(b) Altitude vs. time of the lander after aeroshell separation.

Figure 5.19: Wind speed profile at the landing site and altitude of the lander after aeroshell separation.

The upper bound of the offset caused by wind is estimated as the displacement that would be caused if the lander had the same velocity as the wind after aeroshell separation. The effect of wind before this point is ignored.

$$\Delta x_{\text{wind}} = \int_{\tau_{\text{aeroshell}}}^{\tau_{\text{touchdown}}} V_{\text{wind}}\, d\tau \tag{5.5}$$

The worst-case displacement due to wind is found to be approximately 45 km, but this assumes that the wind is unidirectional throughout the descent, which is not the case, therefore the real value is considerably smaller and the 100 km landing radius can be easily fulfilled (especially if wind is fully modelled during the entry simulation).

5.1.9 Reliability

The failure of the EDL system almost always results in catastrophic failure. ”Although the application of standard reliability statistics to mechanical systems is often inappropriate, redundancy can be used to increase the numerical value” [40, p. 17]. Unfortunately, there is inherently limited room for redundancy for most components of the EDL system, therefore the components must undergo rigorous testing and validation to ensure reliability before they are qualified to fly.

At any stage of the design, it is important to keep the stakeholders updated about the probability of success of the system. The reliability of the system will be quantified as the product of the component reliabilities, because it is expected for the EDL system that a single component failure is enough to pose a serious threat to the mission. The most critical points of failure and a conservative lower bound on their reliability from literature is summarized in Table 5.9. The EDL system is estimated to have a reliability of at least 91%.

Table 5.9: Reliability of critical components of the EDL system.

Point of failure	Reliability	Source
LHP system	>0.95	[63]
Separation devices	>0.99	[64]
Parachute deployment	>0.9975	[65]
ADCS	>0.97	[66]
Total	>0.91	

5.1.10 Future Work and Recommendations

The CoS has not been sized in this report. Therefore, the integrated CHRS and ADCS systems need to be still developed in the following stages of the design.

The aerodynamics of the entry capsule are affected by the increase in the backshell angle (especially below hypersonic speeds). The stability of the entry capsule cannot be verified in the current stage of the design due to the modified geometry of the entry capsule. Therefore, higher fidelity tools will be used to perform an extensive stability analysis, such as 3d LAURA and DSMC analysis to estimate the axial, normal force and pitching moment coefficients for different flight regimes and determine whether

- spin-stabilization is truly feasible;
- the capsule is stable throughout all flight regimes;
- additional stability-enhancers, e.g. fins or propulsive attitude control are needed.

Adding active control systems will likely increase the costs and reduce the reliability of the EDL system.

A Monte Carlo analysis will be performed by varying the atmospheric properties and wind profile to give a more accurate estimation on the landing accuracy. This can be done with Venus-GRAM, which has built-in Monte Carlo capability, however, this was not implemented in PETS4V due to time constraints.

Detailed structural and thermal analysis and sizing needs to be performed. The mass of e.g. the heat shields and support structures can be potentially reduced by topology optimization. With higher fidelity results, the factors of safety can also be reduced in the later stages of design.

In the next stage of the design, a transfer orbit analysis should be performed to assess the time of arrival and the approach direction. This can be used to assess the entry trajectory in greater detail, especially if the recommendations for the augmentation of PETS4V are realized. The wind effects should also be accounted for in greater detail to increase the landing accuracy.

The parachute system will need to be sized in detail and the parachute deployment procedure accurately determined when the entry path is known to a higher precision.

Recommendations.
The results presented for the TPS system were based on semi-empirical mass estimation relationships, which were developed by simulating Earth entries with FIAT, a higher fidelity code. Therefore it is recommended to develop separate specific MERs for Venus entries, to improve the accuracy of the PETS4V tool and reduce the necessary safety factors for preliminary sizing. PETS4V only considered 2D planar trajectories, but it could be augmented into a 3D tool with relatively little work. PETS4V is mainly implemented in Python 3.12, but a large performance boost and easier integration of the Venus-GRAM can be achieved if the program is rewritten in C/C++. The current version also does not support the full Venus-GRAM functionality, as the density and speed of sound profiles are calculated only for 70° latitude and solar time of 12 h. In the next version of the program, these functionalities could be implemented. In the current analysis, PICA was only considered as a forebody TPS ablator, however, its low density and high maximum tolerable heat flux could make it a promising aftbody material as well. Therefore, it is recommended to investigate the behavior and feasibility of PICA when used on a less heat-intensive surface such as the backshell of entry vehicles.

5.2 Payload

Designing a payload for a Venus lander requires careful evaluation of each instrument's scientific value, technical feasibility, and ability to operate under extreme surface conditions. Based on the scientific ambitions of this mission, a set of candidate instruments were selected. These include a seismometer, cameras, atmospheric chemical analyzer, geologic chemical analyzer, radiometer, pressure sensors, thermometers and a wind sensor. Each instrument supports specific mission goals such as investigating Venus's internal structure, analyzing the surface and atmospheric composition, and monitoring the environmental conditions. During the design trade-off process for each instrument the scientific return was weighted against constraints such as mass, power consumption, data handling, and environmental durability. In Subsection 5.2.1, a list of the most important requirements for the payload is presented. Subsequently, the different instruments present are presented along with their purpose and implementation, followed by a section about the layout of the different instruments and their operating timeline in Subsection 5.2.11. Finally, some recommendations are given in Subsection 5.2.13.

5.2.1 Requirements

A list of key and driving requirements related to the payload along with their verification method can be found in Table 5.10. These include some of the user requirements the team received as well as some requirements that were generated after careful analysis of the functions the lander should perform. Finally, the last column indicates whether the requirement has been met or not.

Table 5.10: Science instrument requirements.

ID	Requirement Description	Verification	RC
SCS-1	All individual experiments shall have successful analysis probability of no less than 80%.	V-TST-FUN	✓
SCS-SEI-1	The seismometer shall characterize background seismic noise within 2 Earth days.	V-TST-FUN	✓
SCS-SEI-2	The seismometer shall be able to perform continuous seismic measurements throughout the mission lifetime.	V-ANA-LIF	✓
SCS-SEI-11	The seismometer shall measure motions within a frequency range of 0.1–10 Hz.	V-TST-FUN	✓
SCS-SEI-7	The seismometer shall be able to be operational until a maximum temperature of 464 °C.	V-DEM-TEM	✓
SCS-SEI-8	The seismometer shall be able to be operational until a maximum pressure of 93 bar.	V-DEM-PRE	✓
SCS-SEI-9	The seismometer shall be able to be operational in the corrosive environment of Venus for the entire mission.	V-DEM-COR	✓
SCS-GEO-1	The geological analysis system shall conduct at least 20 individual chemical analyses of surface rock materials.	V-TST-FUN	✓
SCS-GEO-10	The geological analysis system shall have a pointing accuracy of 0.5 degrees.	V-TST-FUN	✓
SCS-GEO-11	The geological analysis system shall be able to take measurements of rocks from a distance of at least 3 m.	V-TST-FUN	✓
SCS-CHA-1	The atmospheric chemistry sensor(s) shall conduct analyses of Cl^-, F^-, S-bearing species, CO_2 and CO every 12 hours.	V-ANA-LIF, V-TST-FUN	✓
SCS-SM-10	The camera shall have a minimum resolution of 1 MP.	V-INS-DAT	✓
SCS-SM-1	The lander shall have cameras capable of imaging with a field of view of 90 degrees.	V-INS-DAT	✓
SCS-SM-2	The camera(s) shall take image(s) of local morphology and horizon.	V-DEM-TSK	✓
SCS-SM-11	The camera(s) shall document the landing site during descent with an accuracy of 1 m/pixel at 1000 m altitude.	V-INS-DAT	✓
SCS-MET-RAD-1	The radiometer(s) shall measure the radiation over a diurnal cycle.	V-ANA-LIF	✓
SCS-MET-WND-2	The wind sensing system shall measure the wind direction variations over at least a diurnal cycle.	V-ANA-LIF	✓
SCS-MET-WND-4	The wind sensing system shall measure the wind speed variations over at least a diurnal cycle.	V-ANA-LIF	✓

The description of verification method IDs are found in Table 4.1.

5.2.2 EDL Instruments

While most of the payload instruments are needed to perform the scientific measurements once the lander has reached the surface, some of them are exclusively used during the EDL phase. These include accelometers and gyroscopes for attitude determination as well as a camera for mapping of the landing surface.

Camera

As it is wished to take good quality pictures of the terrain during landing, a camera was placed on the bottom of the lander to take pictures from the moment that the heat shield is detached. It documents the soil through a sapphire window during landing and is enclosed within a paraffin wax phase change material to ensure it survives throughout the landing but dies off due to the high temperatures after. The exact camera model used is the same as the one inside the cool box and is documented in more detail in Subsection 5.2.4.

Gyroscopes and Accelerometers

During Entry, Descent and Landing it is important to keep track of the attitude and acceleration of the lander. To do this, gyroscopes and accelerometers are needed. Gyroscopes are used to measure the rotational motion of the lander and accelerometers are used to measure the (linear) acceleration of the lander, as the name already suggests. An Internal Measurement Unit (IMU) has been selected that contains 3 gyroscopes and 3 accelerometers such that all degrees of freedom are covered. The LN-200S developed by Northrop Grumman was chosen because it is lightweight, small, radiation hardened and has a high reliability[6]. Furthermore, it was used in multiple NASA missions such as: Mars rovers (Spirit, Opportunity, Curiosity, and Perseverance), Deep Space 1, etc[6]. It is visualized in Figure 5.20. The engineering budgets can be found in Table 5.11. The IMU is operational until 71° C and survives up to 85° C. It will be placed inside the coldbox of the lander because of its size. It is however allowed to die off after the EDL phase as it is not needed anymore afterwards.

Figure 5.20: LN-200S IMU[6].

Table 5.11: Budget breakdown and dimensions of the EDL instruments[6][7].

Instrument	Power [W]	Mass [kg]	Cost (M€ FY2025)	Dimensions
EDL Camera	2[8]	0.0025[9]	0.00043	14.5 x 18.1 x 19.5 mm[10]
LN-200S IMU	12	0.748	0.087	Diameter: 8.89 cm Height: 8.51 cm

[6] https://www.northropgrumman.com/what-we-do/ln-200s-inertial-measurement-unit, accessed on 12/Jun/2025.
[7] https://www.ebay.com/itm/326002607418, accessed on 12/June/2025.
[8] https://www.e-consystems.com/usb-cameras/4k-sony-imx317-8mp-usb-camera.asp, accessed on 6/Jun/2025.
[9] https://www.kailaptech.com/Product.aspx?id=3039&l1=2971&utm_s, accessed on 6/Jun/2025.
[10] https://www.kailaptech.com/Product.aspx?id=3039&l1=2971&utm_s, accessed on 6/Jun/2025.

Table 5.12: Budget breakdown and dimensions of the seismometer.

	Power (W)	Mass (kg)	Cost (M€ FY2025)	Dimensions
NASA Glenn Seismometer	0.1[12]	0.3[13]	1.03	20cm x 20cm[14]

5.2.3 Seismometer

Due to the short duration of previous lander missions to Venus, little accurate data about seismology on Venus is available. Understanding this topic better remains therefore one of the main focuses of this mission. As such, a seismometer is one of the required instruments for this mission. Due to the high amount of vibrations caused by the lander itself, it is preferred to have the seismometer separate from the lander itself. This means that the seismometer cannot be cooled and thus will have to survive the harsh Venusian conditions on its own. Furthermore, seismometers tend to be significantly more fragile than other instruments and their calibration is very sensitive to the high loads during entry.

Types of Seismometer

Different types of seismometers exist: mechanical, electromagnetic, piezoelectric, optical, micro electromechanical system (MEMS), broadband, strong motion and ceramic. MEMS and Piezoelectric Seismometers were identified as the most promising options for a Venus lander because they are compact, energy-efficient, and have the potential to withstand the extreme conditions on the planet's surface. MEMS, in particular, offers the added benefit of small size and low power consumption, which are critical for long-term operations on Venus.

Selected Option

Due to the critical surface condition, none of the commonly known seismometers used on Earth would work for this mission. However, NASA Glenn has developed a seismometer for the HOTTech program that incorporates a combination of highly durable materials, shock-resistant structures, and high temperature resistant silicon carbide electronics to ensure it survives both the high loads during entry and the extreme environmental conditions [67]. More specifically, the seismometer is a miniaturized MEMS-based device designed to detect ground motion through capacitive sensing.

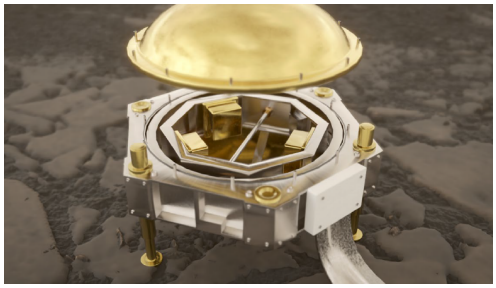

Figure 5.21: Venus compatible tri-axial, self leveling seismometer suite [67].

This seismometer works by measuring tiny changes in the distance between a fixed electrode and a small mass that's suspended inside the sensor. When the ground shakes, the mass shifts just a little, which changes the capacitance. That change is then measured and turned into seismic data. Unlike more traditional seismometers that use magnets, this one avoids magnetic parts altogether, which makes it much better suited for very high-temperature environments. It relies on capacitive sensing, which works better under extreme heat and is more reliable overall.

The system uses custom-built electronics made from silicon carbide, a material that can handle temperatures well above 460 °C without failing. These electronics are responsible for gathering data, processing the signals, and communicating the information. The instrument was designed with Venus in mind and has passed rigorous testing that simulates the planet's harsh conditions, including long stretches of intense heat and pressure. These tests have shown that the seismometer can keep working reliably for the entire mission duration. Its sturdy build, use of heat-resistant materials, and simple mechanical design all contribute to a success rate above 80 percent, making it a strong candidate to meet the mission's scientific goals.

The mass, power and dimensions were found and documented in Table 5.12. The cost was estimated to be approximately 1.2 million dollars, based on the cost of similar high-temperature space instruments, factoring in specialized materials, development, and environmental testing for Venus-like conditions. Furthermore, the seismometer is projected to have a technology readiness level of 5 by 2026[11], which is required for all the components of the lander.

Deployment

Placing the seismometer directly on the Venusian surface, separately from the lander, is essential to ensure accurate and sensitive seismic measurements. When a seismometer is mounted on the lander structure, it is subject to various sources of artificial noise. These include mechanical vibrations produced by internal systems such as pumps, cooling equipment, or motors, as well as structural expansion and contraction due to temperature fluctuations. Additionally, in Venus's dense

[11] https://ntrs.nasa.gov/api/citations/20230011587/downloads/HOTTech2%20F2F%20MEMS%20Final.pdf, accessed on 02/Jun/2025.
[12] https://ntrs.nasa.gov/api/citations/20240013230/downloads/HOTTech%20QUAD%20-%20MEMSseismometer%20-10-17.pdf, accessed on 6/Jun/2025.
[13] https://www.academia.edu/111337508/SAEVe_Seismic_and_Atmospheric_Exploration_of_Venus_A_Long_Lived_Lander_Concept_for_Venus accessed on 6/Jun/2025.
[14] https://ntrs.nasa.gov/api/citations/20240013230/downloads/HOTTech%20QUAD%20-%20MEMSseismometer%20-10-17.pdf, accessed on 6/Jun/2025.

atmosphere, acoustic and vibrational noise is more effectively transmitted through both the air and the structure, further contaminating the seismic signal. By deploying the seismometer directly on the ground, the instrument achieves better coupling with the surface and is shielded from lander-induced noise allowing it to detect authentic seismic activity more reliably.

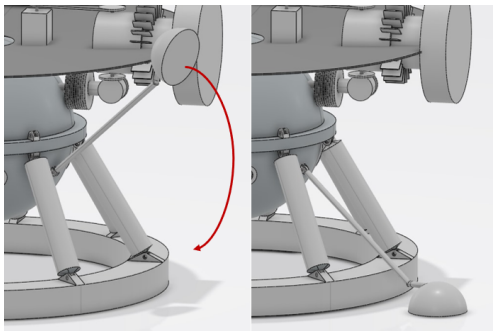

Figure 5.22: Seismometer deployment mechanism.

The seismometer deployment mechanism was chosen to be based on a spring-loaded passive mechanical arm. Before launch, the spring mechanism is preloaded and securely latched in place. Upon landing, the lander first takes images of its immediate surroundings to assess the terrain. These images are analyzed to determine whether the location where the seismometer is intended to be deployed is suitable. If the terrain is found to be unsuitable, for example, if it is too uneven or obstructed by a rock being present, a secondary mechanism is activated to rotate the arm by approximately 30 degrees, aiming the seismometer toward a more favorable placement site. Only after this adjustment, if needed, is the deployment initiated using a small explosion in a frangible nut to release the latch. Once activated, the mechanical energy stored in the spring drives the arm into motion, deploying the seismometer to the surface. To prevent sudden or damaging movement during deployment, a mechanical damper is integrated into the system. This works with the spring to moderate the speed and force of the arm's motion. The result is a smooth and controlled placement of the seismometer, reducing the risk of impact damage or misalignment. All components are constructed from high-temperature-tolerant metals and ceramics that maintain structural integrity. By eliminating the need for motors or electronic actuators, this system provides a mechanically simple, and reliant solution optimized for the harsh environment. The deploying arm can be visualized in Figure 5.22.

5.2.4 Cameras

Due to the fact that the last lander to visit Venus did so in the 1980s, and because of its thick cloud cover obscuring the surface, recent mapping has relied primarily on radio waves, thermal imaging, and spectrometry. As a result, high-quality images of Venus taken during both descent and after landing are invaluable to the scientific community. Not only is there an interest in mapping the landing site, but having a camera on board is crucial for visualizing the terrain that the lander will be chemically analyzing to better interpret measurements.

Sensor Type

The choice for a camera sensor type that is suitable for this mission comes down to either using a complementary metal oxide semiconductor (CMOS) or a charge-coupled device (CCD). Although CCDs generally have a higher image quality in low light, it was chosen to use a CMOS sensor due to their lower power consumption, faster readout, higher resistance to radiance and smaller size.

Image Resolution

The team was given the requirement to capture images during descent with a spatial resolution of one pixel per square meter. Since no specific altitude was defined for this requirement, preliminary evaluations were performed to evaluate the available uplink data rate and then base the picture quality on that parameter. It was initially estimated that it would be approximately 2 MB per day, limited by a requirement imposing a maximum transmission rate of 300 bits per second. Given this constraint, a resolution of approximately 1000 by 1000 pixels with 24-bit color depth was initially selected, resulting in an uncompressed image size of about 3 MB. More advanced research and calculations later revealed that higher transmission rates could be achieved by the communications subsystem, leading the team to engage in negotiations which resulted in the requirement on data transmission to be removed. With a new budget of approximately 6 MB per day, it was chosen to increase the resolution of the pictures to 3840 by 2160 pixels, which results in raw files the size of 23.7 MB. This image resolution would fulfill the previously mentioned requirement at an altitude of roughly 500 meters. Due to the high-risk nature of the mission, the team plans to initially transmit heavily compressed images to maximize the likelihood of receiving visual data in the event of early mission failure. Once critical measurements have been successfully acquired and relayed, the transmission of raw, high-quality images will follow. More about the compression of the image can be found later in Section 5.5.

Internal Cameras

To maximize scientific gain, it is wished for the lander to capture a 360 degree panoramic view of the soil and horizon. For this reason, four small windows with 100-degree sapphire fisheye lenses were installed in the hotbox. Inside the cooled section, four cameras connected to the lenses through fiber-optic cables were used to capture images from all four sides of the lander. These would allow the lander to send a panoramic view of its surroundings, subsequently allowing scientists on Earth to select where exactly they want to point the geologic analyzer at. As previously mentioned, it also allows the scientists to check if there are obstacles where the seismometer would be deployed.

Selected Option

Table 5.13: Budget breakdown and dimensions of the camera.

	Power (W)	Mass (kg)	Cost (M€ FY2025)	Dimensions
Single Camera	2[15]	0.0025[16]	0.00043	14.5mm x 18.1mm x 19.5mm[17]

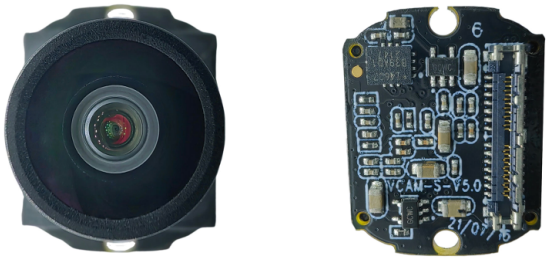

Figure 5.23: Front and back view of the IMX317.

The selected imaging system for deployment within the cooled compartment of the lander is the KLT-CMFL143004-IMX317 V1.0 equipped with the Sony IMX317 CMOS sensor. This camera was chosen based on its ability to meet the required high imaging resolution having a resolution of 3840 by 2160 pixels, and thus ensuring that high-quality scientific images of the Venusian surface can be acquired. The Sony IMX317 sensor is known for its excellent image quality and low-light performance, both critical for operation in the limited lighting conditions expected in the landers environment. Additionally, the camera offers a compact form factor being the smallest implementation of the IMX317 sensor minimizing volume and mass impact. Its compliance with the UVC standard ensures broad software compatibility, facilitating rapid implementation and testing. The combination of high resolution, robust sensor performance, and practical integration features makes this camera an ideal candidate. It's properties can be found in Table 5.13.

5.2.5 Atmospheric Chemical Analysis

Performing long-term atmospheric chemical analyses on the surface of Venus represents one of the most difficult technological and engineering challenges KYTHERA will face. The planet's environment, as extensively described previously in the report, imposes strict constraints on instrument design, reliability, and longevity. Most existing planetary chemical analysis instruments have only been designed to operate under drastically milder conditions or for comparatively short durations.

Selected Option

The most advanced concept that approximates the performance needed for this mission is the recently developed NASA DAVINCI Venus Mass Spectrometer (VMS), which was designed for use during atmospheric descent. The VMS is tailored for rapid chemical analysis as it falls through the atmosphere, where it encounters moderate temperatures and pressures compared to the conditions at the surface. It is not designed to survive prolonged exposure to the surface environment, nor to repeatedly conduct sampling cycles over an extended period [69].

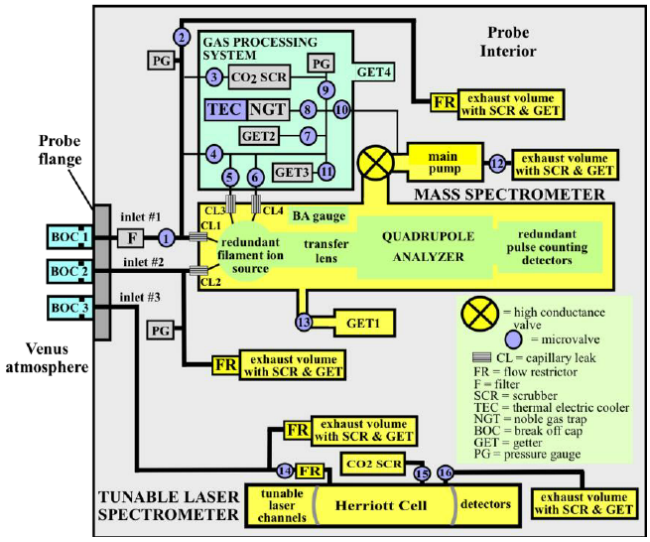

Figure 5.24: Schematic block diagram of the Neutral Mass Spectrometer (upper section) and Tunable Laser Spectrometer (lower section) showing gas flow connections. For illustrative purposes only [68].

The VMS consists of several major components: the Quadrupole Mass Spectrometer (QMS), a Noble Gas Trap (NGT), pumps, detectors, an electronics box, inlets, and outlets. The QMS is identical to the one installed and currently operating on the Curiosity rover [70]. Alongside the VMS, the DAVINCI probe also carries the Venus Tunable Laser Spectrometer (VTLS), which will be used on KYTHERA too. The VTLS was similarly based on the Curiosity rover's TLS instrument aboard the Sampling at Mars (SAM) instrument suite [70]. Figure 5.24, from a concept study on a similar instrument called the Neutral Mass Spectrometer [68], shows a potential connection diagram of the VMS's components. Note that the actual block diagram of the VMS will be different as it does not contain the same components as the NMS.

The selected instruments are capable of running a wide range of analyses on atmospheric chemistry. The NGT is able to measure the concentration of He, Ne, Ar, Kr and Xe [70]. VTLS can measure isotope ratios of D/H, O_{18}/O_{16}, C_{13}/C_{12} in CO_2, $S_{34}/S_{33}/S_{32}$ in SO_2 and OCS with a 0.2% precision [71]. The QMS is able to measure mixing ratios of CO_2, Ar, N_2, O_2, CO, Ar_{40}/Ar_{36}, and isotopes of C in CO_2 as well as detect any molecule between 1.5 and 535.5 Da [71]. These

[15] https://www.e-consystems.com/usb-cameras/4k-sony-imx317-8mp-usb-camera.asp, accessed on 06/Jun/2025.
[16] https://www.kailaptech.com/Product.aspx?id=3039&l1=2971&utm_s, accessed on 06/Jun/2025.
[17] https://www.kailaptech.com/Product.aspx?id=3039&l1=2971&utm_s, accessed on 06/Jun/2025.

Table 5.14: Budget breakdown and dimensions of the main VMS components.

Instrument	Power (W)	Mass (kg)	Cost (M€ FY2025)	Dimensions
QMS	14.5 [72]	1.3 [72]	12.06[19]	46cm x ø9.1cm [70]
VTLS	27.1 [71]	3.7 [73]	8.62 [74]	35cm x ø12cm[20]

specifications fulfill part of requirement SCS-CHA-1 on conduction of analyses on Cl-, F- and S- bearing species, CO_2 and CO and thus satisfy the goals of KYTHERA's mission.

Instrument Adaptation

The VMS was only designed for short-term operations. As such, in order for KYTHERA to use the VMS on its long-duration surface mission, it will need to be modified. This begins by enclosing the entire instrument in a thermally insulated, actively cooled, and pressure-resistant compartment located within the lander. From this enclosure, the instrument will have access to a small port hole linking to its sampling inlets through a high-temperature valve. The valve's role is to sever flow connection from the outside and to minimize heat leaks into the cooled compartment. The existing capillaries that connect to these inlets will be slightly lengthened to increase pressure drop and allow the instrument to work in higher ambient pressures than originally designed. In the same vein, the VMS's existing outlets will be connected to another port hole through another high-temperature valve with the same function. Evacuating exhaust from the instrument in the higher-than-designed ambient pressure can be done with minimal modifications to the existing Wide Range Pump.

Next, the NGT will be modified to operate continuously across the entire mission lifetime. In the original VMS instrument, the NGT had to be kept at a very low temperature, which was executed using a phase change material. However, this method is single-use only and will not work for KYTHERA. As such, before and during use, the NGT will have to be actively cooled down to its operating temperature using heat exchangers connected to the same system that the entire compartment is cooled with. Further redesign could be done to raise its operating temperature in order to reduce power requirement, but this might lead to budget and schedule issues and would have to be carefully considered. The NGT is not the only component of the VMS that requires a specific temperature, different from others; certain components within the QMS go up to 1100°C [71]. This warrants the use of a vacuum inside the compartment in order to minimize power consumption by limiting heat conduction and convection.

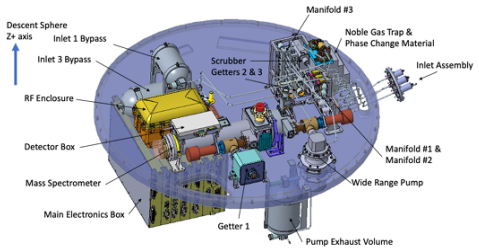

Figure 5.25: The Venus Mass Spectrometer (VMS) laid out on the DAVINCI Descent Sphere Instrument Deck [69].

The VMS will be further modified by merging it with the VTLS. These are complementary instruments that share the same gas inputs and outputs, and the inclusion of two different inlet and outlet arrays would introduce increased heat leaks into the payload compartment that could otherwise be avoided. Another factor for merging the two instruments is space constraints, as the size of the cooled compartment must be minimized for optimal heat rejection.

Table 5.14 displays the required power, masses, costs and dimensions of the two main components of the VMS. Whereas the VTLS requires up to 6 hours to run its analysis, the QMS can run for short periods of time, taking approximately 0.02 seconds per mass-to-charge ratio measurement[18]. The masses are the instruments themselves, but not cabling or afferent electronics. Costs are rough estimations based on similar systems or extrapolations from higher-order system costs. Finally, the dimensions include only the components themselves, excluding wiring or afferent electronics.

By cycling the instrument every 12 hours, the lander could create a time series of atmospheric composition over an extended time period. This would enable the detection of dynamic processes such as chemical gradients, diurnal variations, and transient phenomena, such as surface gas emissions. Such an extended observational capability would represent a major scientific advance over earlier Venus missions. Successfully adapting the VMS architecture for this role would demonstrate the feasibility of conducting advanced chemical analyses in one of the harshest environments in the solar system, opening new possibilities for future planetary exploration. The architecture of the VMS can be seen in Figure 5.29.

Risk Management and Reliability

The instrument's reliability depends on its constituent components. Thus, exploration of failure modes begins with assessment of the risks afferent to each component. The sampling inlet array poses a risk that previously materialized on Pioneer Venus [70], namely the condensation of H_2SO_4 and subsequent clogging of the sampling inlets. This risk can be terminated by the use of a separate sampling inlet below the sulfuric acid clouds, as well as using heaters to evaporate

[18] https://www.planetary.org/articles/curiosity-instrument-sam, accessed on 6/Jun/2025.
[19] NASA Fiscal Year 2010 Full Budget Request. URL:https://www.nasa.gov/fiscal-year-2010-budget-request/, accessed on 06/Jun/2025.
[20] URL: https://www.nasa.gov/image-article/tunable-laser-spectrometer-nasas-curiosity-mars-rover/, accessed on 04/Jun/2025.

any liquid material clogging the inlets. The sampling valve could malfunction due to high temperatures, but the risk of instrument failure can be avoided with the use of multiple sampling inlets as well as extensive testing before and during integrated tests on the ground. The extremely high pressure difference between the 92 atm Venusian atmosphere and the vacuum inside the spacecraft could lead to leaks, particularly through capillaries, potentially enough to overwhelm the getters and introduce a CO_2 atmosphere inside the lander. This could precipitate into increased conduction and convection and would ultimately lead to catastrophic failure through system overheating. This scenario can be avoided by thorough leak-testing to sufficient safety margins as well as prolonged exposure tests to Venus atmosphere simulants. The failure of individual instruments is most likely to be due to shock loads during landing. This risk can be treated by re-evaluating the current shock load tolerance of the instruments via analysis and testing and hardening them when needed. Finally, the pump evacuating exhaust gasses from the individual instrument could fail for any reason. This risk cannot be fully avoided, but can be minimized by using proven hardware with flight heritage.

The quantification of individual instrument cycle reliability is very difficult without a detailed model of hardware and software, both of which are outside the scope of this report. However, the measures described in the paragraph above are likely to be sufficient to minimize the risk of instrument failure to below 20%, satisfying requirement SCS-1.

5.2.6 Geologic Chemical Analysis

The surface of Venus is not well understood yet because of the limited amount of data obtained by previous landers and the extent of possible analysis from orbit because of the thick Venusian clouds. During the KYTHERA mission twenty individual chemical analyses of surface rock materials will be conducted on a volcanic plain of Venus. This new data will enable scientists to obtain more insight into the evolution of Venus, rock composition and how these rocks were formed.

Types of Methods

There are several options for instruments to choose from for the geological analysis. The instruments often detect different elements and work in different ways and thus have different requirements on how the analysis needs to be performed. For some, a sample needs to be brought inside the lander, while other instruments would have to be in direct contact with the surface, and some can operate remotely. This results in three design options for integration in the lander. The first one is to collect twenty samples of surface material, bring these inside a chamber of the lander and do the chemical analysis. The second one is to add a robotic arm to the lander. The instrument would be mounted on the tip of this arm, such that it can touch the surface and perform the analysis. The last option is to have the instrument fully inside the lander and doing the measurements remotely. This can be either done by aiming a laser beam to the wanted area and analyze the received beam or by measuring naturally emitted radiation. The advantage of this method is that it is the least complex to implement and the potential area that can be researched is larger. In Table 5.15 below, all the geological analysis methods can be found with the method they require in order to do a geochemical analysis, and the elements that they can detect.

Due to the unforgiving external conditions at the surface, an instrument that can operate remotely is preferred. Although sample collection and analysis inside the lander was done by the Venera landers[21], collecting twenty samples and bringing them inside the lander for chemical analysis brings extra risks and complications. A robotic arm with a spectrometer mounted on the tip of it has been done for rock analysis on Mars, for example on the Mars Pathfinder mission [75], but not on Venus. Finding a spectrometer that can operate at the high surface temperatures of Venus is practically impossible since these spectrometers usually require active cooling [75, 76]. Furthermore, designing a robotic arm that can operate in the corrosive environment is challenging due to the moving parts. One of the limitations of remote sensing is that taking measurements from a distance decreases the quality of the analysis compared to analyzing a sample inside or with direct contact. Furthermore, certain minor and major elements will likely not be detected by remote sensing methods as can be seen in Table 5.15.

Table 5.15: Geological chemical analysis instruments with their operating mode and detectable elements.

Method	Operating mode	Detectable elements
Mass spectrometry[22] [77, 78]	Sample	Major, minor and trace elements and isotopes
Gamma-ray spectroscopy[23] [79]	Remotely	Radioactive trace and major elements
X-ray fluorescence spectrometer[24] [80]	Surface contact or sample	Major and minor elements
X-ray diffractometry	Sample	Crystal structure
Laser Induced Breakdown Spectroscopy (LIBS) [81, 82]	Remotely (up to 7-20 m)	Low atomic number elements
Raman spectroscopy[25] [83]	Remotely (up to 7 m)	(An)hydrous minerals
Alpha proton X-ray spectrometry[26] [75]	Surface contact	Major elements
Alpha particle X-ray spectrometry [84]	Surface contact	Major and trace elements
Mossbauer[27]	Sample or surface contact	Fe-bearing minerals/oxidation states
Infrared (IR); Near-Infrared (NIR) spectroscopy[28]	Sample or remotely	Minerals

[21] `https://nssdc.gsfc.nasa.gov/nmc/experiment/display.action?id=1981-106D-09`, accessed on 08/May/2025.

Viable Options

The options for the rock analysis methods that are left over now are all the remote sensing ones: gamma-ray spectroscopy, Laser Induced Breakdown Spectroscopy (LIBS), Raman spectroscopy and remote IR/NIR spectroscopy. Gamma-ray spectroscopy is a method that detects gamma-rays that are naturally emitted by radioactive decay of chemical elements in the surface or atoms from the surface struck by cosmic rays. The energy of the gamma-ray is absorbed by the spectroscope and converted into a voltage signal[22]. The LIBS spectroscope focuses a laser onto the wanted location of analysis [81]. This leads to plasma formation of which the emission spectrum can be measured by the spectroscope to determine the chemical elements [81]. In Raman spectroscopy minerals are exposed to a laser beam, which stimulates atomic vibrations[22]. Because of these vibrations the light from the laser is scattered. This light is then collected and analyzed by the spectrometer[22]. A promising type of IR spectroscopy is thermal infrared remote sensing. This method of IR spectroscopy is passive, which means that it will simply detect IR radiation that is naturally emitted by the surface [85].

Selected Option

Now that all the viable options for the geochemical analysis have been selected a trade-off between them can be performed. The team would like to select two instruments in order to maximize the scientific yield and the types of elements that can be detected. The criteria on which the remote methods will be judged are: the scientific yield, the operating temperature, the operational time and the operating simplicity. The scientific yield was given the highest weight, 5, since the selection is done for a scientific instrument and therefore this is the main goal of the instrument. The instruments were mostly judged on the detectable elements and the variety of data obtained. The operating temperature of the instrument (or components) was also found to be an important criteria and therefore given a weight 4. For all of the instruments there were some components (detector and laser) that needed to be at a negative temperature [6, 86]. Maintaining this in the coldbox, that is still relatively hot, would be challenging so a higher operating temperature that matches more with the coldbox temperature is preferred. Therefore, there was looked into substitution components for each instrument that operate at higher temperatures. When judging the performance of the instrument with respect to the operating temperature the substitution component has been taken into account. Operational time is good to be limited, as more time is available for the operation of other subsystems, but it is not a major concern. It was given a weight of 3. Lastly, the operating simplicity is about which instrument is less complex to operate and how easily it can be integrated in the lander. This is also important to take into account as the lander itself is already complex and adding another subsystem for an instrument might add complexity that is not necessarily needed, therefore given weight 2. The power, mass and cost were not taken into account in this trade-off as the values were either similar or it was not possible to find information about it. The trade-off can be found in Table 5.16:

Table 5.16: Trade-off remote geological chemical analysis methods.

	Scientific Yield	**Operating Temperature**	**Operational Time**	**Operating Simplicity**	
Weights	5	4	3	2	**Score**
Gamma-ray Spectroscopy	4	4	3	5	55
LIBS	5	3	5	4	60
Raman Spectroscopy	4	3	5	4	55
Thermal IR Spectroscopy	3	3	3	5	46

As can be seen in Table 5.16 the score given for each instrument on each criteria varies between 3 and 5. 3 corresponds to ”sufficient”, 4 to ”good” and 5 to ”excellent”.

For the scientific yield LIBS scored the highest as it can detect minor, major and trace (low atomic number) elements, which can’t be detected by other methods. The detectable elements for all methods can be found in Table 5.15. Thermal IR spectroscopy was given a low score because observing IR might be hard as the atmosphere scatters IR radiation a lot, which impacts the quality of the data [87]. The maximum surviving temperature for all the methods, using the substitution components, was found to be 50 °C and the maximum operational temperature 30 °C, except for gamma-ray spectroscopy which operates at temperatures up to 100 °C[29] [88, 89]. The operational time is dependent on whether the technique

[22] https://space-science.llnl.gov/research/gamma-ray-spectrometers, accessed on 14/May/2025.
[23] https://science.nasa.gov/ems/12_gammarays/, accessed on 15/May/2025.
[24] https://www.horiba.com/int/scientific/technologies/energy-dispersive-x-ray-fluorescence-ed-xrf/xrf-analysis-theory/#:~:text=XRF%20(and%20particularly%20EDXRF)%20is,spectra%20obtained%20in%20seconds%2Fminutes, accessed on 14/May/2025.
[25] https://www.irocks.com/identifying-minerals-using-raman-spectroscopy#:~:text=Raman%20spectroscopy%20is%20a%20technique,via%20use%20of%20a%20spectrometer, accessed on 15/May/2025.
[26] https://pds.nasa.gov/data/mpfr-m-apxs-2-edr-v1.0/mprv_0001/document/apxsinst.htm?utm_, accessed on 09/May/2025.
[27] https://serc.carleton.edu/research_education/geochemsheets/techniques/mossbauer.html, accessed on 15/May/2025.
[28] https://chem.libretexts.org/Bookshelves/Physical_and_Theoretical_Chemistry_Textbook_Maps/Supplemental_Modules_(Physical_and_Theoretical_Chemistry)/Spectroscopy/Vibrational_Spectroscopy/Infrared_Spectroscopy, accessed on 16/May/2025.
[29] https://www.msl-chemcam.com/chemcam/how-does-chemcam-work/how-does-chemcam-work-step-3/, accessed on 03/Jun/2025.

used for analysis is passive or active. Passive techniques don't use a laser and simply observe naturally emitted radiation. But they take more time to collect enough data to be valuable, resulting in score 3. Gamma-ray spectroscopy and LIBS are both very quick methods and are therefore given a score 5 [90]. For the operating simplicity it is again dependent on whether the technique is passive or not. LIBS and Raman spectroscopy both require a laser, therefore increasing the complexity and having a lower score compared to the passive methods.

It can be observed from Table 5.16 that the highest score is obtained by LIBS, followed by gamma-ray and Raman spectroscopy on a shared second place and thermal IR spectroscopy on the third place. It was decided to select Raman spectroscopy over gamma-ray spectroscopy based on the type of elements it can detect. Raman spectroscopy detects minerals while both LIBS and gamma-ray spectroscopy focus on the elemental composition, which might result in an overlap. Therefore, it seems more interesting for this mission to have one instrument detecting the elemental composition of the rocks and one detecting the minerals. Furthermore, minerals have not been directly detected by the Venera landers, while radioactive elements were [6]. This also makes Raman spectroscopy scientifically more interesting. Another advantage is that Raman spectroscopy can be integrated in LIBS, which for example reduces the weight of the system [90]. It should be noted that Raman spectroscopy is usually done in the dark to reduce the amount of background noise, while the rock analysis for this mission will be done in daylight [91]. During the day the detector would become oversaturated from the high amount of background light. Furthermore, the high surface temperature of Venus results in interference between the thermal blackbody radiation from the samples and the Raman spectra of minerals [91]. A solution for this is using time-resolved Raman spectroscopy, which can work during the day and at high temperatures. It has a pulsed laser that contains a large number of photons and the detector is only activated when the Raman signal is expected to have traveled back [91]. It's important that this is timed well as the Raman signal is weak and the signal only lasts for a few nanoseconds [91]. With the above method the amount of Raman photons are maximized while minimizing the background light, increasing the signal-to-noise ratio.

Since the team has a limited amount of time and limited knowledge about space instrumentation, a set of instruments were selected where LIBS and time-resolved Raman spectroscopy are already integrated into each other. This resulted in the choice for NASA SuperCam from the Perseverance Mars rover. SuperCam however contains some instruments that are not required for our purposes so they will be removed. This includes a Remote Micro Imager, a microphone and an IR spectrometer [90]. The instruments that are kept, together with their respective layout, can be found in Figure 5.29.
As can be seen the geochemical instrument consists of three main components: a laser, a telescope and a spectrometer unit (SU). The laser oscillator produces a pulsed green beam at 532 nm in case of Raman analysis or a pulsed red beam at 1064 nm in case of LIBS analysis [90]. It is sent to the telescope where the laser is directed and focused through the window on the target outside. After that the emitted radiation is received through the telescope and is sent via optical cables to the spectrometer unit. This contains the demultipexer, which distributes the light over the spectrometers. The ultraviolet and the violet spectrometers will be used for LIBS and the transmission spectrometer for both LIBS and Raman spectroscopy. The spectrometer CCD's of SuperCam operate at negative temperatures , so these components were substituted by the ChemCam CCD's which are operational until $30\ ^\circ$C and survive until $50\ ^\circ$C[29].

In order to reach the target rock material with the laser and telescope and receive the emitted radiation, they need to be able to point to it. This is done with the use of stepper motors inside the coldbox. The instruments are mounted downwards with an angle of 20 degrees with respect to the horizon by default. This corresponds to a distance of 3 meters between the lander and the target. The motors allow the instruments to observe targets between one and seven meters distance, which corresponds to an angle of 40 degrees and 8 degrees below the horizon respectively. A view over the majority of the landing site is provided by letting the instruments move left or right with a maximum of 45 degrees. This is done by another axis on the stepper motor.
When performing a geochemical analysis, first LIBS analysis will be done and after that Raman. This order is advantageous because the LIBS laser will remove the dust, increasing the scientific return [90]. The LIBS laser is expected to likely have no effects on the Raman spectra [90].

As already mentioned, Raman spectroscopy will be used to detect minerals of Venus surface rocks. Figure 5.26 provides an overview of the minerals that were measured by the SuperCam with their respective spectra.

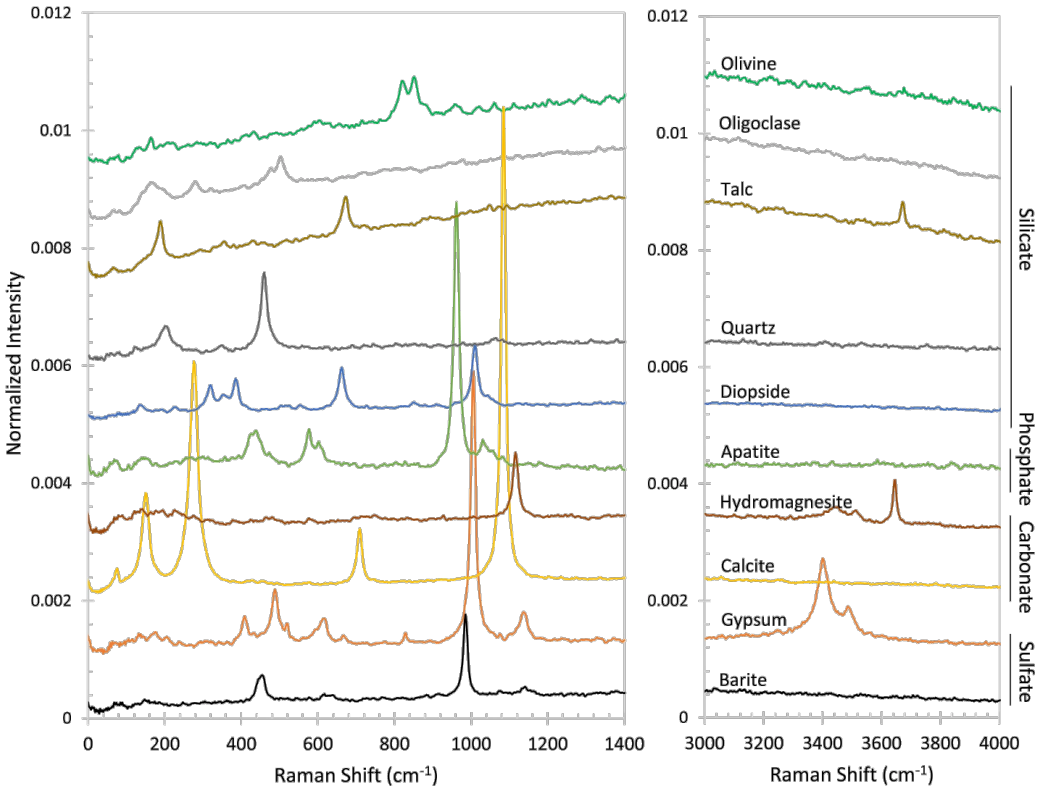

Figure 5.26: Raman spectra of pure minerals taken by SuperCam [86].

Laser Induced Breakdown Spectroscopy will detect major, minor and trace elements with a low atomic number. Examples of spectra obtained by LIBS can be found in Figure 5.27. In the figure an example is shown for each of the spectrometers. It should be noted that the examples are meant to represent the variety of materials of the Mars Jezero crater, which is likely not representative for the Venus geology.

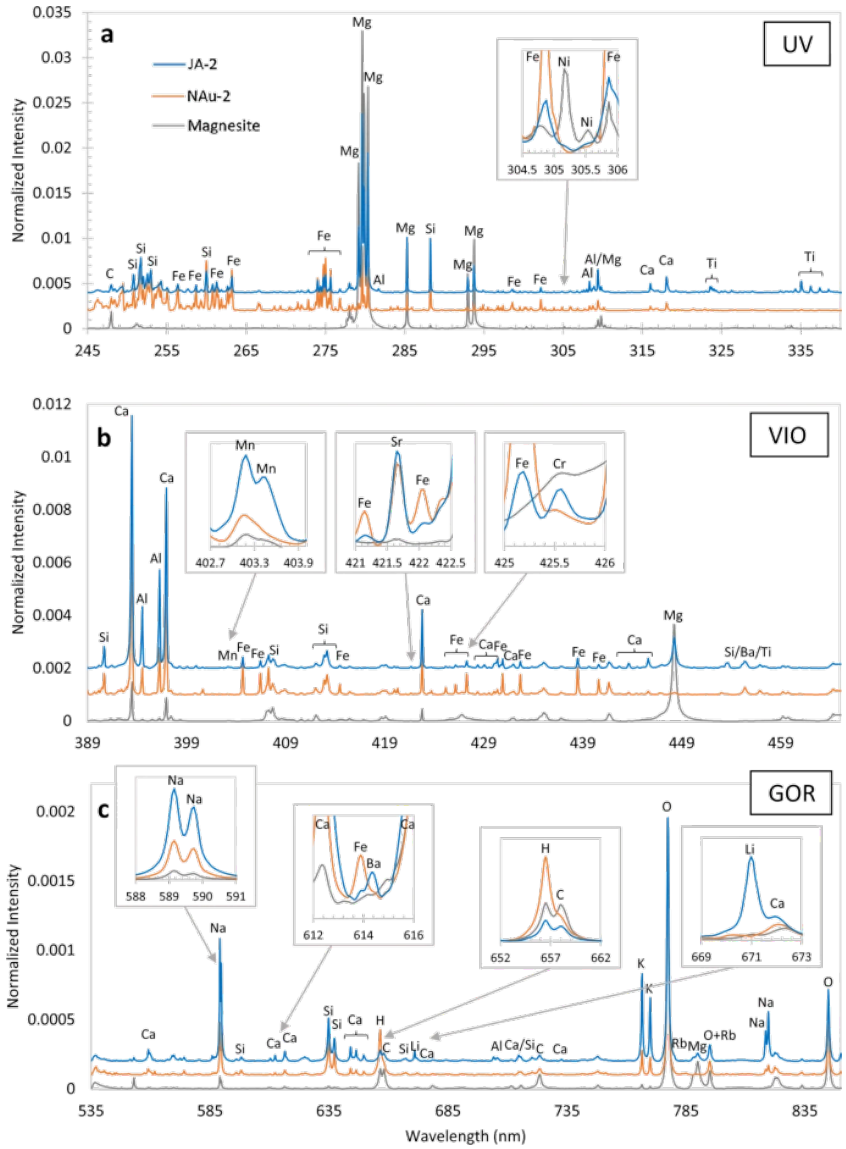

Figure 5.27: Example spectra for LIBS, based on Mars Jezero crater [86].

Engineering Budgets

From Figure 5.29 it can be seen that there are 4 windows each having their own telescope and laser. This means that 4 lasers, 4 telescopes and one spectrometer unit need to be produced. This is taken into account in Table 5.17.

Table 5.17: Budget breakdown and dimensions of the geological analyzer.

Instrument	Power [W]	Mass [kg]	Cost (M€ FY2025)	Dimensions
First Instrument (SU + 1 laser + 1 telescope)	40-70	6.98	19.5	Laser: length 16.1 cm , diameter 3.5 cm Telescope: length 10 cm, diameter 5.5 cm Spectrometer Unit (SU): 22 x 16 x 21 cm
Total amount of Instruments (SU + 4 lasers + 4 telescopes)	40-70	14.72	25.35	Same as above values

The power consumed when only the spectrometer unit is operating was found to be about 40 W [86]. When the spectrometer unit is operated together with LIBS the total power consumed is 60 W and when the spectrometer unit is combined with Raman it is 70 W [86]. The power consumed with 4 lasers and telescopes is the same as the first instrument power because geological analysis will be done at only one window at a time.

The mass of the laser is 0.58 kg and from the spectrometer unit 4.4 kg [90]. The mass of the SuperCam telescope could not be found, so it was assumed that it was 1/3 of the SuperCam mast mass (6.1 kg [90]) resulting in a mass of 2 kg.

The cost for the SuperCam could not be found, so an estimation was made for this. The only cost that was found was M$130

for 7 instrument packages, not including the SuperCam mast that contains the laser and the telescope[30]. This value was divided by 7 to obtain an estimate of the cost for one instrument package and converted to Euros resulting in M€16.25 per package. This estimation seems a bit high on one end when knowing that other instrument packages collected samples, but it compensates for the fact that the laser and telescope were initially not included in this cost. Because of a high uncertainty in this estimation the cost was multiplied by two. Considering that NASA developed these instruments already and that only minor changes will happen, the cost can be reduced to M€19.5 using a multiplication factor of 0.6 [92] for the first instrument. The other three lasers and telescopes only need to be manufactured, so they don't have a development cost. For those a multiplication factor of 0.1 can be used [92]. This results in the final cost of M€25.35 total. All costs are for FY2025.
For the volume of the instruments several estimations had to be made because not all the information could be found. The laser length was found to be 230 mm but the laser diameter was not available. Therefore, by visual inspection, it was assumed to be 1/4 of the depth (20 cm) of the SuperCam mast [90]. When placing all the payload instruments into the coldbox it was found that the laser was too long to make everything fit. Therefore the team decided to reduce the laser size by 30%. This means that the laser will have to be redesigned in the post-DSE design phase. For the telescope a similar approach had to be used. This time the diameter was found to be 110 mm and the length was assumed to be equal to the mast depth of 20 cm by visual inspection [90]. It was decided to reduce the size of the telescope by 50% since the telescope in the Perseverance mission was mostly used for the camera to look far [90]. Since the Remote Micro Imager has been removed for this mission the telescope is not needed to be as powerful as it is now, therefore the size could be reduced more. The telescope will also be redesigned in the post-DSE design phase. Lastly, the spectrometer unit dimensions were not changed as it was not needed and no components were removed. This results in dimensions of 22 x 16 x 21 centimeters[31].

5.2.7 Radiometer

Another measurement the mission would like to record is the amount of radiation present and possible fluctuations of it through time or during seismic events. For this reason, a radiometer should be implemented in the design. The different types of radiation present on Venus include thermal infrared radiation from the surface, down-welling solar and infrared radiation from the atmosphere, and possibly reflected solar radiation. Because radiometers have an operating temperature range which is significantly lower than the Venusian conditions, taking one on board either requires for it to be housed in the cooled part of the lander or for it to be able to withstand the surface conditions. The team initially planned on having radiance measurements be taken through a sapphire window in the lander with appropriate anti-reflective coatings to maximize transmission in the desired spectral range. However, upon further research, it was found that placing the Hukseflux NR01 radiometer (the radiometer model that won the trade-off) inside the cooled electronics box and having it measure through a sapphire window would introduce several limitations. Sapphire can transmit some parts of the shortwave and longwave spectrum well, but it does not offer full coverage of the range needed for precise net radiation readings. Adding a window between the sensor and the outside world would also affect how the radiometer is calibrated, introducing issues like light reflection, absorption, or heating of the window itself. These side effects would make the system more complex and could interfere with the reliability of the data. Because of this, the team opted for the LLISSE radiometer, which was built specifically to operate in direct contact with the surrounding environment. This instrument avoids the need for extra protective layers or optical components, helping it keep accurate readings over time. Developed under NASA Glenn's Long-Lived In-situ Solar System Explorer effort, the LLISSE radiometer uses durable materials and electronics that can withstand Venus-like temperatures. It uses thermopile sensors and silicon carbide parts to record solar input and surface heat loss without losing performance. Its straightforward build helps avoid distortion and keeps the thermal layout of the lander simple. The instrument has also gone through environmental tests meant to simulate conditions on Venus, showing that it can deliver consistent and accurate data for extended missions.

Engineering Budgets

While detailed subsystem specifications are not publicly available, a grounded estimate based on LLISSE's total mass and volume constraints, as well as on analogous radiometer systems developed for other planetary missions was performed. The complete LLISSE platform is limited to approximately ten kilograms in total mass, with multiple instruments, power systems, and communication hardware onboard. Given these constraints and the necessity to minimize thermal and structural loads, the radiometer likely occupies a small fraction of the total system volume. A reasonable estimate places its size at ten centimeters in length, five centimeters in width, and five centimeters in height. This dimension is comparable to heritage radiometers used on Mars missions, but adapted for a more compact, rugged form factor.

The weight was estimated to be around 350 grams, based on the estimated size and the use of lightweight ceramic substrates, refractory metal shielding, and a simple optical or thermopile sensor assembly. This mass accounts for the structural enclosure, optical window, sensor head, and necessary silicon carbide electronics for signal processing and data transmission. The power consumption is estimated at one watt, which is consistent with low-duty-cycle radiometers designed for continuous or periodic sampling using low-voltage digital electronics. This power level fits within LLISSE's anticipated power

[30] `https://www.jpl.nasa.gov/news/nasa-announces-mars-2020-rover-payload-to-explore-the-red-planet-as-never-before/`, accessed on 06/Jun/2025.
[31] `https://science.nasa.gov/mission/mars-2020-perseverance/science-instruments/`, accessed on 06/Jun/2025.

budget, which is designed to support extended duration operation.

Finally, the cost of the LLISSE radiometer was estimated to be around one million US dollars. This figure reflects the cost of custom engineering for extreme planetary environments, including sensor miniaturization, high-temperature electronics packaging, and extensive environmental qualification. The estimate is informed by historical cost data for similarly specialized planetary science instruments, scaled down in complexity and size for LLISSE's tightly constrained platform. The final estimated values can be found in Table 5.18.

Table 5.18: Estimated budget breakdown and dimensions of the radiometer.

	Power (W)	Mass (kg)	Cost (M€ FY2025)	Dimensions
Radiometer	1	0.350	0.86	5cm x 5cm x 10cm

5.2.8 Pressure Sensor

To survive and operate on the surface of Venus, where the environment is extremely hostile, a pressure sensor must be highly specialized. For this reason, the team will opt for the use of a High-Temperature Silicon Carbide (SiC) Pressure Sensor developed by NASA Glenn, which has been proved to work in the Venusian surface conditions[32]. To measure pressure on the inside of the cooled box, where conditions will be more Earth-like, a Keller PAA-33X will be used. This is a piezoresistive pressure transducer with digital output, high precision (0.05%), and an operating temperature between –40°C to +125°C. This model fits perfectly as it is small enough to be easily integrated, has an excellent long-term stability and has been proven in aerospace applications. Due to the simple nature of a pressure meter, no advanced trade-off was required for this instrument. Its specifications were sourced online and are shown in Table 5.19

The NASA Glenn capacitive pressure sensor system, lacks detailed public specifications and was therefore reasonably estimated based on its intended use in extreme environments and its integration through borescope ports. The device likely measures approximately 50 millimeters in length and 20 millimeters in width, resulting in a volume op approximately 30 cubic centimeters. As it is constructed with high-temperature materials such as silicon carbide and alumina, the estimated mass is around 30 grams, although this is not of great importance to the design. Power consumption is expected to be very low, between 5 and 25 milliwatts, which is typical for capacitive sensors using oscillator-based readout circuits. Due to the specialized materials, high-temperature packaging, and limited production volume, the cost was estimated to be around 20,000 euros per unit.

Table 5.19: Budget breakdown and dimensions of the pressure sensor.

Instrument	Power (W)	Mass (kg)	Cost (M€ FY2025)	Dimensions
NASA Glenn	0.005	0.03	0.017	50mm x ø20mm
Keller PAA-33X	0.28[33]	0.250[34]	0.00043[35]	120mm x ø27mm[36]

5.2.9 Thermometer

Even though the scientific community has established that the surface temperature on Venus is not subject to significant changes throughout time [30], it is still important for the lander to measure both surface and interior temperatures to put the rest of the collected data in a more complete scientific context and to monitor the health of internal subsystems. The temperature inside the cooled box will already be measured by the previously mentioned pressure meter, but the choice for an external one is far more limited due to the extreme conditions. Thermocouples stand out as a great option due to their service temperatures ranging up to 1600 °C [93]. at which they still maintain high accuracy and stability. They are excellent at resisting the harsh chemical conditions of Venus and were therefore used during previous Venera missions. Their only disadvantage is that they require careful calibration and compensation electronics. A different option would be the use of Resistance Temperature Detectors (RTD), which have a temperature range of up to around 800 °C. These also have high accuracy but would require thermal shielding for optimal performance and are more sensitive to chemical and mechanical degradation than thermocouples. A third option would be the use of an infrared pyrometer, which would perform contactless measurements from inside the actively cooled part. In this case the disadvantage would be that the instrument would be affected by optical window contamination, atmospheric absorption and emissivity variations. Finally it requires a line of sight, which may not be reliable on Venus's dusty or chemically reactive surface. For these reasons, using a thermocouple thermometer stands out as the most robust choice for the mission.

[32] `https://technology.nasa.gov/patent/LEW-TOPS-119`, accessed on 21/May/2025.
[33] `https://download.keller-pressure.com/api/download/LhMuKZcKtfdfWhUvqus9cd/en/latest.pdf`, accessed on 15/Jun/2025.
[34] `https://download.keller-pressure.com/api/download/LhMuKZcKtfdfWhUvqus9cd/en/latest.pdf`, accessed on 15/Jun/2025.
[35] `https://www.omniinstruments.co.uk/p/keller-series-33x-pressure-transmitters/`, accessed on 15/Jun/2025.
[36] `https://download.keller-pressure.com/api/download/LhMuKZcKtfdfWhUvqus9cd/en/latest.pdf`, accessed on 15/Jun/2025.

Detailed Design

The detailed design of the external thermocouple begins with careful selection of materials, focusing on type B, which offer excellent high-temperature performance and chemical resistance. The thermocouple will be housed in a protective sheath made from refractory metal alloys such as Inconel or platinum-rhodium, chosen for their ability to withstand prolonged exposure to high temperatures and reactive atmospheric compounds. This will then be attached to the lander's outer shell using high-temperature ceramic insulators. These are essential for both electrical isolation and thermal stability.

Integration into the lander requires routing the thermocouple leads through the lander's thermal insulation layers into the cooled electronics compartment. This interface will include compensation wiring made of matching thermocouple alloys to minimize error, and the connection will be thermally and electrically shielded to prevent signal drift or interference. The leads will be connected to a signal conditioning circuit that includes cold-junction compensation and analog filtering, followed by an analog-to-digital converter for data integration into the CDH system.

Special attention will be given to calibration, with the thermocouple being tested against traceable temperature standards in thermal vacuum environments prior to installation. Once installed, software algorithms in the CDH will apply correction factors to account for any known nonlinearities or environmental offsets. The final assembly ensures a robust and accurate temperature monitoring system that will support both the scientific goals of the mission and the thermal management of critical systems.

Specifications

The cost, power consumption, weight, and dimensions of the external thermocouple were estimated based on heritage data from previous space missions, using technical datasheets of high-temperature sensors, and with integration constraints specific to Venus landers. The total cost was estimated to be around 5000 euros. This figures comes from accounting for space-rated Type B thermocouple, high-temperature shielding, wiring, calibration, and signal conditioning electronics. Because it is a passive sensor, the thermocouple itself consumes basically no power. The signal conditioning electronics involved draw less than 100 milliwatts, making it highly efficient. The total weight, including the sensor, protective housing, mounting brackets, and wiring, is then finally expected to be in the range of 200 grams. Its physical dimensions were estimated to be approximately 20 centimeters in length and 2 centimeters in diameter, based on standard thermocouple probe sizes and the addition of high-temperature insulation.

Table 5.20: Budget breakdown and dimensions of the thermometer.

	Power (W)	Mass (kg)	Cost (M€ FY2025)	Dimensions
Thermometer	None	0.2	0.0043	20cm x ø2cm

5.2.10 Wind Sensor

Even though having a wind sensor is not a requirement, it is still considered by the team as an additional instrument because of the valuable data it could provide scientists [94]. This data will enable them to get a better insight into the atmospheric dynamics and structure.

Designing an anemometer that can withstand the high temperature and corrosive environment on Venus is challenging. Mechanical or spinning wind sensors are affected by dust and corrosion, therefore they will not be an option for a long duration Venus mission [94]. Furthermore, the team wants the anemometer to be lightweight and to have a low power consumption such that it does not affect the power and mass budgets from other subsystems [94, 95].

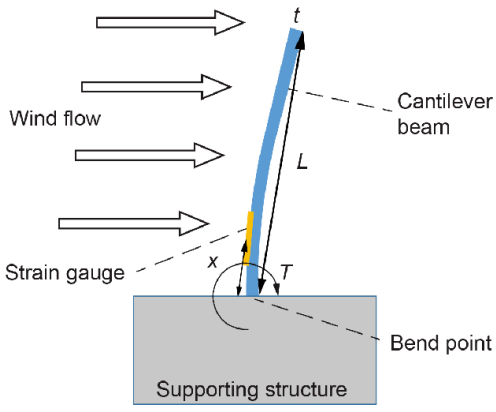

Figure 5.28: Wind on NASA miniature drag-force anemometer [94].

Currently, NASA is developing a 3-axis miniature drag-force anemometer that measures wind velocity and direction. It is lightweight and has a low power consumption as can be seen in Table 5.21. It consists of a cantilever beam which bends due to the flow of the wind as can be seen in Figure 5.28. The deformation of the beam is measured by strain gauges [94]. A prototype of this wind sensor has already been made and tested for 60 days in the Glenn Extreme Environment Rig (GEER) that simulates the Venus environment [95]. The goal of the NASA team is to make the anemometer survive the Venus conditions for 125 days, which is close to the KYTHERA mission duration. This NASA anemometer is the most suitable one for the KYTHERA mission, therefore it has been selected for the mission. The wind sensor budgets can be found in Table 5.21. The cost could not be found, so this was estimated in the following way. The Beagle 2 lander, that is part of the Mars Express mission had a wind sensor onboard as well. The working principle of this anemometer is a bit different as it is a thermal one, but the cost of the Beagle 2 payload for this lander is available so with this a good estimate for the KYTHERA wind sensor can be

made. The Beagle 2 instrument cost was found to be 9.0815 million dollars[37]. The lander consists of several instrument packages. An estimate of the cost for the Environmental Sensor Suit, which contains the wind sensor, was made based on its relative mass [96]. Then this cost was multiplied by two to account for the uncertainty of the estimation.

Table 5.21: Budget breakdown and dimensions of the wind sensor [94, 95].

	Power [W]	Mass [kg]	Cost (M€ FY2025)	Dimensions
NASA Miniature Drag-Force Anemometer	0.001	1	0.28	40 x 8.4 mm

5.2.11 Payload Layout and Operating Timeline

In Figure 5.29 all the payload instruments are represented, together with their location on the lander: the coldbox, the hotbox or the outside of the lander. Furthermore, there are some instruments specifically for the EDL phase of the mission. For some of the payload instruments the diagram is further expanded into its instruments to illustrate the working principle of the instrument.

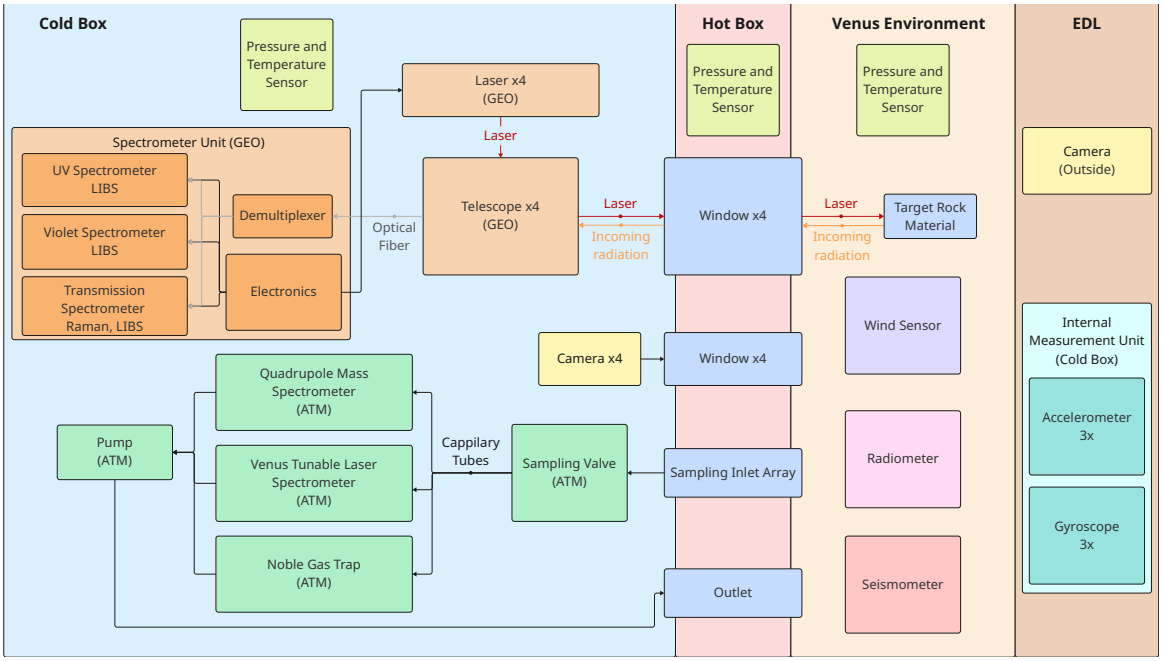

Figure 5.29: Payload instruments block diagram [86].

As can be seen in Figure 5.29 there are several connections between the coldbox and the outside. There are 4 windows for the geological analysis and 4 windows for the camera. A more in-depth explanation and the design choices for this can be found in Chapter 6. Furthermore, there is an inlet to collect the atmospheric samples through and an outlet to push the sample back to the environment after analysis. The geological chemical analysis instruments (dark orange), the camera and the atmospheric analysis instruments (dark green) are located inside the coldbox. The geological and atmospheric analyzer working principles are explained in more depth in their respective subsections. There will be placed pressure and temperature sensors in the coldbox, hotbox and on the outside. The wind sensor, radiometer and seismometer will all be on the outside of the lander as is shown in the diagram. Lastly, an Internal Measurement Unit and the EDL camera are added to take measurements during Entry, Descent and Landing. The camera will be on the bottom of the lander, exposed to the Venus environment, and the IMU will be inside the coldbox. After EDL these instruments are allowed to die off.

In Figure 5.30 a suggestion for a timeline of instrument operations is shown. It should be noted that this timeline is not to scale. This means that the size of the blocks doesn't represent the operating duration of the instrument. There are three phases in the mission: the EDL phase, the first mission phase and the second mission phase. The difference between the first phase and the second phase is that during the first phase pictures will be taken and the geology is analyzed, while during the second phase these things don't happen anymore. It is expected that the first phase will have a shorter duration than the second phase. It can also be observed that there are instruments operating continuously and discontinuously in time, for the latter one an operating duration is indicated. All the continuous instruments will take measurements in parallel, sometimes together with a discontinuous instrument as well. For the continuously operating instruments all the data will be stored, but a selection will be made and only part of it will be transmitted to Earth. The gaps between the

[37] `https://publications.parliament.uk/pa/cm200304/cmselect/cmsctech/711/711we05.htm`, accessed on 17/Jun/2025.

blocks of the discontinuously operating instruments represent the moments communication or data transfer to the orbiting satellite happens. This is needed because there is not enough power available for the simultaneous operation of high power-consuming payload and the communications subsystem.

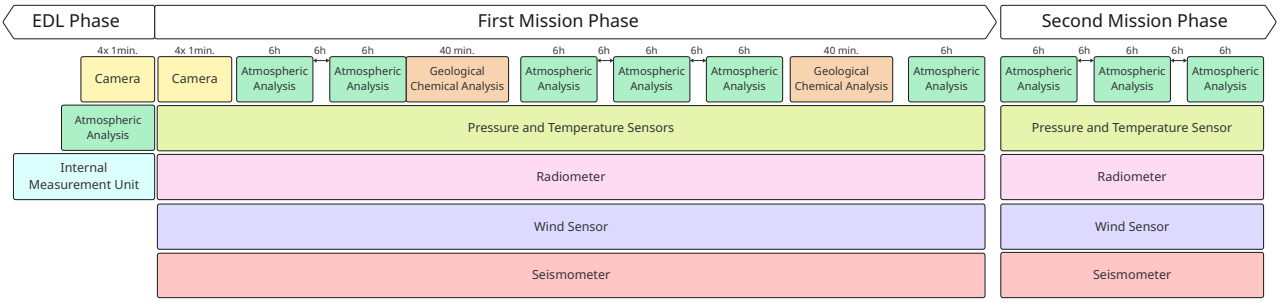

Figure 5.30: Payload operating timeline.

During EDL the attitude and acceleration are continuously measured by the IMU. During descent the atmospheric chemical analyzer will conduct measurements every 200 meters in the same manner as the DAVINCI probe. When approaching the landing site and the heatshield is detached, the EDL camera will map it and will take a total of four pictures. It is estimated that each picture is taken in one minute. At the beginning of the first mission phase the camera will take one picture through every window. This way a 360 degree panoramic view of the surface and horizon is obtained. It is possible to take more pictures on a later stage of the mission, but for now that is not planned. Furthermore, an atmospheric analysis is done every 12 hours, as required. For each measurement the VTLS is estimated to take six hours and the QMS to take one hour to complete the analysis. Throughout the first mission phase, 20 geological analysis are performed. It is estimated to take about 40 minutes per analysis [90]. This includes collecting the data and fully characterizing the chemical composition and mineralogy of the target rock material. Lastly, the pressure and temperature sensors, radiometer, wind sensor and the seismometer are operating continuously on both the first and second mission phases.

5.2.12 Sensitivity

In this section the performance of the different instruments is analyzed based on several events that could happen. Examples of these are a power shortage, the coldbox that is not sufficiently cooled due to a defect, etc.
In case of a long-term power shortage the team will have to prioritize certain instruments over others or plan the operational times of the instruments differently. What instruments will be prioritized over others will depend on the stage of the mission and how much scientific data for each instrument has already been collected. In case the available power is below the required instrument power, the instrument will simply have reached its end-of-life if the problem can't be resolved. The power required for an instrument can be found in the budget breakdown table of the respective instrument.
If the coldbox is not sufficiently cooled, the geological analyzer is the first instrument that would fail as it has the lowest operating temperature of all the instruments. In Figure 5.31 an overview of the operating and surviving temperatures of all instruments can be found. As can be observed, the Keller-PAA-33X pressure and temperature sensor and the command and data handling components are the most temperature resistant. It is important that these instruments are the most temperature resistant as the Keller-PAA-33X pressure and temperature sensor is used for housekeeping and the C&DH components are used to give commands and store data.
The instruments that are mounted on the outside of the lander are continuously exposed to the Venus environment. This means that the risk of failure is increased due to the high temperature and pressure, corrosive environment and strong winds that can occur as discussed in Section 2.2. All the instruments (wind sensor, radiometer, seismometer and pressure sensor) that the team selected were designed by NASA specially for Venus conditions. In this way the risk of failure due to the Venus environment is significantly reduced. The only instrument that was not designed for the Venus environment is the type B thermocouple. This thermometer is a good choice for the KYTHERA lander as it can operate at very high temperatures and it is chemically resistant. To guarantee the operation of this instrument throughout the whole mission, it is placed inside a protective sheath.

5.2.13 Recommendations

All the payload instruments have been carefully selected, but there is still room for improvements. In this project the resources such as people, time, knowledge, etc. are limited. Because of this the instruments had to be selected instead of being designed specifically for the KYTHERA mission as what is usually done for scientific instruments of space missions. It is suggested by the KYTHERA team that a team of space instrumentation specialists and scientists handles the post-DSE design phases and takes into account the following recommendations. First of all, a recommendation for all the instruments is to make a better cost estimation, since the current values for most of the instruments are based on rough estimations.

For the seismometer it is advised to develop the deployment mechanism in more detail. Furthermore, it is recommended to do additional tests because this is a product that is currently still in development.
A recommendation for the camera is to increase its resolution. This was a limiting factor during the selection because it would take too long for the communication subsystem to transfer this amount of data.
The atmospheric chemical analyzer was suggested to be redesigned to fit the needs for the KYTHERA mission. These design suggestions should be revised and implemented by a team of space instrumentation specialists and scientists to assure the reliability and compatibility of the instrument.
For the geological chemical analysis it is advised to revise the choice for the ChemCam CCD for the spectrometers and to make sure that it is integrated well into the SuperCam. It is recommended to even consider selecting another CCD and laser as they limit the operating temperature to 30 °C of the whole geological chemical analysis instrument. This way the coldbox would not need to be cooled to 30 °C. Another problem that was identified during the design was the heat leaking into the coldbox through the window of the telescope. One way to solve this, could be by redesigning the geological analyzer, especially the laser and telescope, to be operational even in the hotbox such that the window in the coldbox can be removed. Another way is to redesign the telescope such that its diameter can be reduced even more and the diameter of the window can be reduced accordingly. Since there has been made several assumptions for the reduction of the dimensions of the telescope and laser, it should be further verified by the post-DSE design team. This is similar for the cost of the geological analyzer. The last recommendation is to reevaluate the addition of the gamma-ray spectroscope to the set of geochemical analyzers, only in case the budgets allow it. This would enable the detection of radioactive elements as well, expanding the types of elements that can be detected, which is scientifically valuable.
For the type B thermocouple it is advised to develop a detailed design of the protective sheath in which it will be housed.
For the wind sensor the main recommendation is doing additional testing for high pressure, high temperature and the Venus environment such as in GEER, as this is only been done for 60 days so far.

5.3 Power and Thermal Control

The power and thermal control subsystem is responsible for providing, distributing, and controlling electrical power as well as providing cooling for the lander to ensure its survivability at the harsh Venus surface temperature of 464 °C.

Thermal control of spacecraft can be achieved either actively or passively. Active cooling refers to cooling techniques that are achieved through the use of mechanical or electrical energy, or by movements of fluids. In spacecraft design, it is typically preferred to only employ passive cooling methods as active cooling methods are typically significantly more heavy, complex, and power hungry. It was however concluded early on that it would be impossible to have a long-duration mission on the Venus surface if KYTHERA only used passive cooling methods. For reference, the VENERA missions done by the Soviet Union between the 1960s and 1980s did not employ any significant active cooling methods and the longest surviving mission at the Venus surface lasted just over 2 hours.

Although power and thermal control are typically separate subsystems in a spacecraft, in the case of KYTHERA, the two are closely related and will thus be treated as a single subsystem. The power and thermal control subsystem primarily consist of the following [92]:

- **Primary power** - Produces electrical and mechanical power.
- **Secondary power** - Stores electricity in periods of surplus to be used when the power of the primary system is insufficient.
- **Distribution system** - Distributes and regulates power provision to individual subsystems.
- **Passive Cooling** - Using materials and surface coatings to maintain a desirable temperature range [97]. Passive cooling does not use any electric or mechanical power for it to function.
- **Active Cooling** - Uses powered and/or mechanical devices to maintain a desirable temperature range [97].

5.3.1 Requirements

The subsystem requirements of the power and thermal control subsystem is given in Table 5.22 below. Note that the labeling convention of the IDs of the following requirements are based on when power and thermal control were still treated as separate subsystems before the detailed design phase.

Table 5.22: Power and thermal control subsystem requirements. For the verification identification codes refer to Table 4.1.

ID	Requirement Description	Verification	RC
MFCT-FB-4	The power system shall cost no more than 40 million EUR, FY2025.	V-CST	X
MFCT-MB-4	The power system shall weigh no more than 87.5 kg (25% of total mass budget).	V-INS-WEI	✓
OPS-POW-1	The power system shall be capable of providing at least 100 W of constant electrical power for the mission duration.	V-TST-GRD	✓
OPS-POW-2	The power system shall be capable of providing at least 180 W of mechanical power for the mission duration.	V-TST-GRD	✓
OPS-POW-3	The power generation system shall be capable of operation with a cold side of no less than 464 °C.	V-TST-GRD	✓
OPS-POW-4	Cooled parts of the system shall be capable of operation at no less than 303 K.	V-TST-GRD	✓
OPS-POW-6	The exposed part of the system shall be capable of operation at 93 bar of ambient pressure.	V-TST-GRD	✓
OPS-POW-7	Cooled part of the system shall be capable of operation in vacuum.	V-TST-UNI	?
MFCT-MB-6	The thermal control subsystem shall weigh no more than 20 kg.	V-INS-WEI	?
MFCT-PB-3	The thermal control subsystem shall use no more than 180 W of total power in both science mode and transmission mode.	V-TST-GRD	✓
MFCT-FB-3	The thermal subsystem shall cost no more than 14M in 2025 EUR.	V-CST	X
OPS-TH-1	The thermal control subsystem shall keep the cooled payload box within a temperature range of 273 to 303 K for the duration of the mission.	V-ANA-SIM-TH	✓
OPS-TH-ACT-1	The thermal control subsystem shall remove 100 W of internally generated heat.	V-ANA-SIM-TH	✓
OPS-TH-ACT-2	The thermal control subsystem shall remove 180 W of heat leaking in from the Venus atmosphere.	V-ANA-SIM-TH	✓
OPS-TH-PAS-1	The thermal control subsystem shall limit the heat leak into the coldbox to 200 W.	V-ANA-SIM-TH	✓

The description of verification method IDs are found in Table 4.1.

As can be seen in Table 5.22, all of the requirements with the exception of cost are met, which is expected to be approximately 170 million EUR, nearly three times the budget. However, as this solution is the only possible option enabling the mission, a budget increase is required.

In order to determine at which temperature the coldbox should be kept, an overview of each of the instruments inside the box and their operating temperature ranges was made. This overview can be seen in Figure 5.31. Instruments that are inside the coldbox, are shown in blue, while instruments that are on the outside of the lander are colored green. The temperature starts from 0°C at the left side and goes until 500°C on the right, with 50°C steps indicated with a yellow-to-red-to-purple temperature gradient. Two coldbox instruments have an operating temperature that is lower than their survival temperature. In those cases, the survival temperature range is indicated in purple while the operational temperature range is indicated in blue.

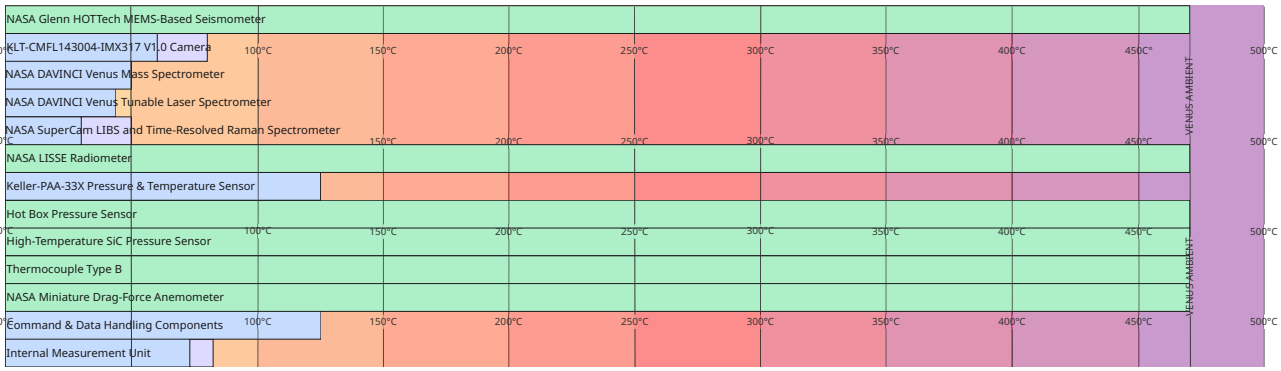

Figure 5.31: Graphical overview of operating temperature ranges of components.

From the figure, it can be seen that the lowest maximum operating temperature of any of the coldbox instruments is 30°C. At first, it was chosen to keep the temperature at 80°C, but as will be discussed in Figure 5.3.6, a switch to 30°C allows for all instruments to survive without further adaptations and can still be achieved with the power system.

5.3.2 Summary of Trade-off

In this section, a summary of the trade-off phase of each aspect of the power and thermal control subsystem is given.

Primary Power

When considering the power production, various parameters, including technical readiness and reliability were considered. However, when combining the expected extremely low-end power requirement of 100 W, and accounting for the blackout periods requiring batteries (e.g. Venusian night with solar power), it was discovered that Radioisotope Stirling Generator is the only viable option, with all others exceeding the mass budget significantly, as can be seen in Table 5.23, with the

gap increasing significantly once the power requirement is increased. Note that 100 W was viewed as the minimum conceivable power (e.g. for cooling a small coldbox producing no internal heat) and was found to be significantly lower than the actual requirement. However, since all other options have higher specific masses, meaning the gap increases with the power needed, they do not represent feasible solutions to power production.

Table 5.23: Comparison of possible power sources for the lower end of possible power needs (approximately 100 W).

Source	Technical readiness	Failure probability	Source+battery mass [kg]	% of m_{max}
RTG	High	Low	93 + 0	128
RSG	Low	Medium	33 + 3	50
H2 Cell	High	Low	181 + 0	249
CH4 Cell	High	Low	258 + 0	355
Wind	High	High	98 + 3	140
Solar	Medium	Low	79 + 464	746
Battery	High	Low	0 + 1600	2194

Secondary Power

Various battery options were considered, if power storage turned out to be needed to a large degree. These were divided into two options: ambient operating and cooled, with the sodium-based liquid metals being chosen for the ambient temperature operation, and off-the-shelf Li-ion batteries for the use within the coldbox.

- **EDL operation (crucial, 40%)** - The main purpose of the batteries is to power the spacecraft between the separation from the EDL module and Stirling generator activation, which is why optimal performance in this phase of flight is key. In this case, Li-ion is advantegeous as high minimum operating temperature of the sodium-based batteries [98] would require active heating during descent.
- **TRL (significant, 30%)** - With a number of experimental technologies already involved, it is desired to use proven technology wherever possible to minimize the total development cost. While the liquid sodium batteries have been flown [99], they are significantly less ready and would require additional development [98], while Li-ion is available off-the-shelf [100].
- **Thermal load (medium, 20%)** - If the batteries are housed within the coldbox, any heat produced has to be rejected to the environment, significantly reducing the system power efficiency. This, however, is only a major issue on the surface after the active cooling system is engaged and it affects the Li-ion batteries. Liquid metal batteries, being located on the outside, would present a minimal thermal load to the system.
- **Surface capacity (minor, 10%)** - While the power use on the surface is not expected, it may be advantageous as it could allow flexibility with the instrument usage profiles if the electrical power produced is ever momentarily exceeded. In this case, allowed capacity of ambient temperature batteries would be significantly higher with higher power density [98, 100] and without sizing constraints of the coldbox.

Table 5.24: Result of trade-off process for battery options.

Criterion / Option	EDL Operation	TRL	Thermal Load	Surface Capacity	
Weights	0.4	0.3	0.2	0.1	**Score**
Sodium-based (ambient)	2	2	5	4	2.8
Li-ion (cooled)	5	5	2	3	4.2

After performing simulations it was found that electrical power requirements are lower than originally expected (with none being necessary through the surface operation), hence the technologically less risky option of smaller, off-the-shelf batteries was selected.

Distribution System

The only major decision in regards to the distribution taken already was the bus voltage and current type - 28V direct current. Based on a combination of literature recommendations, and the fact that at typically around 10% of total weight it represents a less significant part, and more technically mature since off-the-shelf components can be used, a more detailed tradeoff was not performed.

Passive Cooling

Passive thermal control encompasses materials and surface finishes designed to keep the temperature of a spacecraft within a desired range [97]. In previous phases of the design, it was established that the only viable option for passive thermal control on KYTHERA would be insulation. A trade-off between different off-the-shelf thermal insulation materials was then performed, where Aerogel Pyrogel HPS was deemed the best candidate. However, using solid insulation caused a considerable problem: large holes would have to be made to allow a field-of-view for the chemistry analysis instruments

and cameras. Hence, it was considered to use a gas as an insulator. This gave rise to other problems. First of all, most gases are supercritical in Venus conditions, causing their thermal conductivity to rise significantly [101]. Four gases were found that are not above their critical temperature and pressure in 464 °C, 92 atm: ammonia, bromine, water vapor, and iodine[38] [102]. Water vapor was selected because of its non-toxicity, low thermal conductivity and low density, even in Venus conditions [103]. Corrosion also was not a problem with the considered materials [104]. It seemed like a very good candidate. That is, until a convection calculation revealed several megawatts of heat would be transferred into the coldbox when using water vapor, dismissing the concept. Finally, it was found that the structural requirements of sustaining a vacuum with respect to ambient pressure are still lower in terms of mass, compared to thick insulation. Combined with lower thermal leakage, with only radiation and limited convection through coldbox supports, this option was pursued in the end.

Active Cooling

In the Midterm Report two design options for active cooling systems were left open for further investigation at the detailed design phase, one being a Stirling-cycle based cooling system and the other being a cascaded multistage vapor-compression refrigeration system. The original trade-off criteria consisted of the following. Inside the parentheses indicates the level of importance for each criteria (categorized as crucial, high, medium, and low) and their respective weights in percentages.

- **Power (crucial, 22.5%)** The overall power budget is rather tight, and it will be of high importance to choose a system where overall power requirement is lower.
- **Sensitivity of power requirement with respect to changes in inputs (crucial, 22.5%)** One should also consider how sensitive the power requirements for each design option are to changes to the heat input or temperature requirements.
- **Mass (high, 16.25%)** The mass of the active cooling system may depend on several factors such as the power requirement and/or number of stages for the cooler. Although mass is an important consideration for any spacecraft design, it is not as crucial as the power criteria for the active cooler and is thus given the high level of importance for now.
- **Sensitivity of mass requirement with respect to changes in inputs (high, 16.25%)** It is also important to consider how sensitive the mass of the active coolers are to changes in inputs such as power requirements or level of complexity.
- **Complexity (medium, 10%)** A complex design may entail greater challenges in the manufacturing process or increase of risk of failures and is thus worth giving a consideration.
- **Cost (medium, 10%)** Information regarding the cost of material to be used for components of active coolers are not readily available, but they must be considered in order to meet KYTHERA's financial budget.
- **Sustainability (low, 2.5%)** Sustainability of active cooler design options should be studied in order to collect information regarding potential health hazards or environmental impact of the manufacturing process or gathering materials for the components of the active coolers.

It was however concluded in the start of the detailed design phase that performing a trade-off as described in the midterm was not feasible under the limited amount of resources, time, and level of expertise that was not available to the team. In order to accurately determine the power and mass, for example, one needed to account for all the non-idealized effects that may be present at a harsh environment like in Venus through the use of computer simulations. However, software such as SAGE or COMSOL which are typically used for designing active cooling systems were either expensive or involved a very steep learning gradient and it was concluded that the team cannot reasonably expect one to obtain a formal simulation of the active cooling system within the given time frame. In light of this, a simpler modified trade-off was performed, with the criteria being as follows:

- **Electric power consumption (crucial, 35%)** The overall power budget is rather tight, and it will be of high importance to choose a design option where the overall electrical power consumption is lower.
- **Design simplicity (high, 30%)** A complex design affects reliability, and would require more time (and hence cost) to realize the design option. As such, a simpler design is favorable.
- **TRL (medium, 20%)** A higher TRL offers a higher chance for the success of the active cooling system during operation. For the vapor-compression refrigeration system, literature gives an estimated TRL of at least 5 [105]. No explicit information is given regarding the expected TRL of the Stirling coolers, however, given the fact that many of the literature consulted on Venus Stirling coolers dates back to early 2000s, it can be expected that they will reach the required TRL level by the launch date [98, 106–108]. Thus, either option would likely satisfy the top-level customer requirements of the TRL needing to be at least 5, so they are given a lower level of importance here compared to other trade-off criteria.

[38] `https://periodictable.com/Elements/035/data.html` and `https://periodictable.com/Elements/053/data.html`, both accessed on 06/Jun/2025.

- **Sustainability (low, 15%)** Sustainability of active cooler design options should be studied in order to collect information regarding potential health hazards or environmental impact of the manufacturing process or gathering materials for the components of the active coolers. They are, however, of low importance compared to other trade-off criteria.

The result of the trade-off process is presented in Table 5.25 below. A score of 1 (bad) to 5 (excellent) is given for each trade-off criterion of both design options. Note that MVCRS stands for multistaged vapor-compression refrigeration systems.

Table 5.25: Result of trade-off process for active cooling system.

Criterion / Option	Electric Power Consumption	Design simplicity	TRL	Sustainability	
Weights	0.35	0.3	0.2	0.15	**Score**
Stirling cooler	5	5	4	2	4.35
MVCRS	3	2.5	4	3	3.05

An explanation for each individual score is given below.
Electric power consumption

- ***Stirling cooler*: 5** - As will be explained in later sections, a GPHS (general-purpose heat source) module and Stirling heat engine setup can effectively power the pistons and displacers of a Stirling refrigerator mechanically without needing any electrical power [98, 108].
- ***MVCRS*: 3** - Electricity power is most likely needed to power certain components such as compressors, so is given a neutral score.

Design simplicity

- ***Stirling cooler*: 5** - Numerous sources for Stirling cycle based cooling systems developed for long-duration Venus landers exist including detailed drawings with dimensions [106, 107]. In addition, as will be explained later, the GPHS module + Stirling heat engine could be used to also power an alternator to generate electricity, effectively taking care of both power generation and active cooling at once. If the coldbox temperature and the amount of heat it needs to lift from it is low enough, a single stage design may also be viable, further reducing complexity [98].
- ***MVCRS*: 2.5** - A multistage design is likely necessary for this design as a single stage design may be too impractical when the temperature differential is too large [109]. As there are no detailed drawings showing the set up and the dimensions of each of the components for this option, the team would also have to invest a considerable amount of time figuring these out.

TRL

- ***Stirling cooler*: 4** - Although no sources give the exact TRL for a Stirling coolers developed for Venus lander missions, several sources such as [108] also outline the procedure of which the cooler can be tested and simulated in a Venus-like environment. It can thus be reasonably assumed that the Stirling cooler system will reach a sufficient level by the mid 2030s.
- ***MVCRS*: 4** - Sources estimated that the multistage vapor compression refrigeration system can be developed with hardware that have a TRL of 5 or higher [105].

Sustainability

- **Stirling cooler: 2** - Plutonium-238 is used in the GPHS modules to provide the Stirling cooling system thermal energy. Plutonium isotopes emit alpha radiations, which can be highly hazardous to the human health, and great care must be taken during manufacturing [110]. In the event of a mission accident, there is a potential that the plutonium may be released into the atmosphere and then exposed to humans, which has been addressed by the design of the GPHS modules which have several layers of protective materials to prevent any plutonium release even in the event of a catastrophic accident such as a launch vehicle failure[39].
- **MVCRS: 3** - For the most part, the multistage vapor compression refrigeration cooling uses standard components, materials, and working fluids and is thus given a neutral score for sustainability.

From the trade-off analyses, it was concluded that the Stirling cycle based cooling system was suitable for KYTHERA.

5.3.3 Background

Stirling Cycles In KYTHERA, the power generation and active cooling of the coldbox is generated through the principles of a Stirling cycle.

[39] `https://science.nasa.gov/planetary-science/programs/radioisotope-power-systems/safety/`, accessed on 10/Jun/2025.

The rest of this section explains the working principles of a Stirling cycle, which was first given in the Midterm Report. The explanation remains roughly the same in content but was adjusted slightly based on the outcome of the detailed design of the power and active thermal control subsystem.

A Stirling cooler works by causing a working gas (typically Helium) to undergo a Stirling cycle, which in the ideal model consists of two isothermal processes, (i.e. changing volume of gas at constant temperature) and two isochoric (changing temperature of gas at constant volume) processes [111]. A typical idealized Stirling cycle setup and their pressure vs volume diagram is shown in Figure 5.32b, Figure 5.32a, and Figure 5.32c.

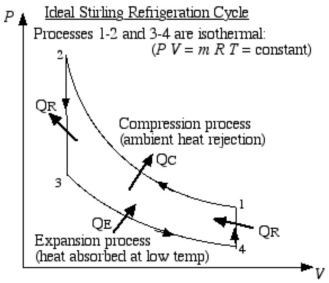

(a) Pressure-volume diagram of an Ideal Stirling Refrigeration Cycle [40].

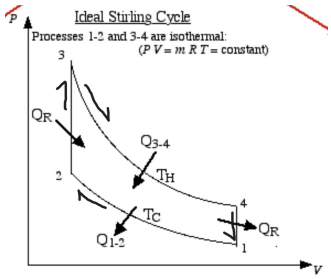

(b) Pressure-volume diagram of an Ideal Stirling Heat Engine Cycle. Original diagram taken from Urieli's work, modified by adding arrows for clarity [40].

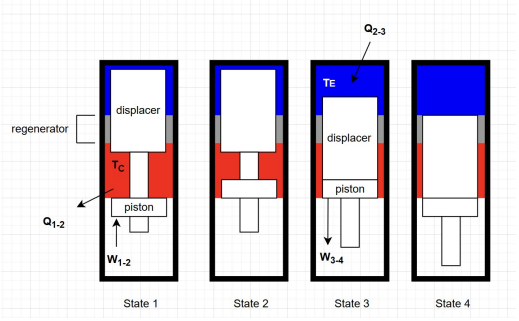

(c) Schematic of a Stirling Cooler System (Own work, developed based on Urieli's work [40].

Figure 5.32: Diagrams of a Stirling cycle.

The process of an idealized Stirling heat engine as shown in Figure 5.32b is explained below.

- **State 1 to 2 (Isothermal compression)** - The piston moves up, compressing the gas. Under the ideal gas law, a gas undergoing compression would experience an increase in temperature. However, since this process needs to be isothermal, heat is rejected to the ambient to keep the temperature of the gas constant[40].
- **State 2 to 3 (Isochoric process)** - The displacer moves down, forcing the gas to relocate to the space colored in blue through the regenerator which supplies heat to the gas causing an increase in the temperature[40].
- **State 3 to 4 (Isothermal expansion)** - Both the piston and the displacer move down causing the gas to expand. Under the ideal gas law, a gas undergoing expansion would usually experience a decrease in temperature. However, since the process needs to be isothermal, heat is absorbed to keep the temperature of the gas constant[40]. In the context of a Stirling cooling and power generation system for KYTHERA, the heat from the GPHS modules will be absorbed.
- **State 4 to 1 (Isochoric process)** - The displacer moves back up to the original position, forcing the gas to the red-colored zone. As it does so, the regenerator absorbs heat from the gas, lowering the temperature of the gas[40].

In the case of Stirling refrigerators the process shown above flows in the opposite direction (i.e. in counterclockwise direction) as shown in figure, to lift the heat from the cooled compartment and reject it to the ambient.

In real Stirling heat engines or Stirling refrigerators, numerous assumptions used in the ideal model do not hold. The effects of voids in the regenerative matrix and any aerodynamic- and mechanical-friction effects are some of many factors that must be taken into account when designing real Stirling refrigeration systems [112].

5.3.4 Detailed Design

In this subsection, the detailed design process for the power and thermal control subsystem is documented. It is important to note that the bulk of the design work focused on the unknown parts - the external power production system, with the established components only sized and given possible components to be used as a mass and cost estimate, with the final selection to be performed at a later point.

Passive Cooling

The current design of KYTHERA uses vacuum as an insulator. Initially, only the cold payload box would be in vacuum, but since no convection and conduction take place in vacuum, it was decided to also create a vacuum in the hotbox [113]. This means that the coldbox shell did not need to be a structural component anymore, too, since there is no pressure differential between the hotbox and coldbox.

Although the joints and seals of the spacecraft are intended to keep a vacuum inside the hotbox until the end of the mission, leaks will inevitably occur due to manufacturing errors, outgassing from instruments, or from any other source.

[40]URL:`https://people.ohio.edu/urieli/thermo/Intro/Chapt.1_6/Chapter3b.html`, accessed on 16/Jun/2025.

For simplicity, a vacuum pump is not implemented, as it would require a large amount of moving parts and would imply a single point of failure. Instead, getters will be used. Getters are devices which maintain an existing vacuum by reacting with gasses and turning them into solid materials or by adsorbing them to their surface. Inside KYTHERA, such devices will be employed to maintain a vacuum inside the hotbox throughout the entire mission, a vacuum which will be created before launch using ground support equipment. Getters are usually lightweight, can be used to "get" gasses inside the hotbox with a performance of 0.7 Pa-l/mg for CO_2[41].

The relevant heat transfer modes in the new configuration are the following:

- Radiation from the hotbox shell to the coldbox shell.
- Radiation from the hotbox shell and hotbox windows to the coldbox windows.
- Radiation from the hotbox shell to the rods connecting the hotbox to the coldbox.
- Conduction from the hotbox shell to the coldbox shell through the rods connecting the hotbox to the coldbox.

These different heat transfer modes were preliminary calculated in Excel, using Equation 5.6 and Equation 5.7, where $\sigma_* = 5.67 \cdot 10^{-8}$ is the Stefan-Boltzmann constant, A_{rad} is the radiative surface area (of the coldbox or the windows, in this case) and A_{cond} is the conductive surface area (the cross-section of the connection rods), F is a factor that incorporates the geometry of the radiative surfaces and their emissivity, T_{in} is the coldbox temperature and T_{out} is the outside temperature, κ is the material thermal conductivity, and Δx is the length over which heat is conducted (i.e. the length of the connection rods). Note that heat transfer is defined positive from inside to outside, indeed, these equations are expected to yield negative results.

$$Q_{rad} = \sigma_* A_{rad} F (T_{in}^4 - T_{out}^4) \tag{5.6}$$

$$Q_{cond} = \kappa A_{cond} \frac{T_{in} - T_{out}}{\Delta x} \tag{5.7}$$

In Equation 5.6, the factor F is calculated with Equation 5.8 for the case of two concentric spheres (i.e. radiation from hotbox shell to coldbox shell), and with Equation 5.9 for two parallel planes (i.e. radiation from outside to inside windows, and from hotbox shell to connection rods) [114, p. 16]. In these equations, ϵ_1 is the emissivity of the innermost surface, ϵ_2 is the emissivity of the outermost surface, and r_1 and r_2 are the radii of the corresponding spheres.

$$F = \left(\frac{1}{\epsilon_1} + \left(\frac{r_1}{r_2} \right)^2 \left(\frac{1}{\epsilon_2} - 1 \right) \right)^{-1} \tag{5.8}$$

$$F = \left(\frac{1}{\epsilon_1} + \frac{1}{\epsilon_2} - 1 \right)^{-1} \tag{5.9}$$

The emissivity of engineering metals lies around 0.9. To minimize radiative heat transfer, some low-emissivity coating needs to be used. Literature mentions several types of coatings, going to an emissivity as low as 0.02 [113]. This literature is more than 20 years old, though. It is assumed that by the time KYTHERA goes into production, a coating with an emissivity of 0.015 will exist. This coating will be used to line the inside of the hotbox shell and the outside of the coldbox shell, ensuring low radiation from one to the other. The emissivity of the sapphire windows is 0.48, which is also lower than other optically transparent materials such as silica glass or quartz.

It became clear that the difference in radius between the hot and the coldbox had a large influence on the total heat transfer. As can be deduced from Equation 5.7, a large hotbox was beneficial for conduction, since the connecting rods (Δx) would be longer. It would negatively impact radiation, though. The most optimal value would hence be a compromise. Python was used to find this optimum, plotting how conduction and radiation varied with hotbox radius. In the end, conduction turned out to be very small compared to radiation. Hence, the hotbox needed to be as small as possible, while of course allowing mounting between the two spheres, with a radius 3 cm larger than the coldbox radius. This is also discussed in Section 6.3.

Once a hotbox radius was established, the values for the heat flow into the coldbox could be calculated for each of the heat leak sources. Adding them all up gave the total heat leak that needs to be pumped out by the active cooling system. The values are shown in Table 5.26. Note that all values are shown as positive, as the description of the heat leak source is given from the outside to the inside in the table.

[41] `https://vacaero.com/information-resources/vac-aero-training/1166-getter-materials.html`, accessed on 17/Jun/2025.

Table 5.26: Values for heat leak into coldbox.

Heat Leak Source	Heat Transferred [W]
Radiation hotbox shell - coldbox shell	142.407
Radiation hotbox shell - connection rods (8 rods)	0.392
Radiation hotbox - coldbox spectrometer windows (4 windows)	30.140
Radiation hotbox - coldbox camera windows (4 windows)	1.260
Total radiation	*174.199*
Conduction through connection rods	0.138
Total conduction	*0.138*
Total Heat Transfer	**174.3**

Active Cooling and Power Generation System

Stirling Generator

The Stirling cooling and power generation system was developed based upon the works of [98, 106–108] with minimal modifications required to meet the specific needs of KYTHERA (primarily related to the mounting position, where the cooler and generator had to be placed somewhat closer together). Helium gas is used as a working fluid in the Stirling heat engine and the Stirling refrigerator. While the dimensions of the module itself stayed identical as to allow the team to rely on the established SAGE simulation, the power and cooling requirements necessitated the use of two externally mounted units.

Each of the units is approximately cylindrical, measuring 28.8 cm in diameter at the widest parts (hot side interface and radiators), and 35.4 cm in length. The mechanism itself weighs 21.6 kg [98] for a unit, with the addition of 7 GPHS modules and a 1.6 kg cooler [98] totaling up to 33 kg per unit. The unit is a β type converter, which means that it includes a single cylinder to house the piston and displacer. It uses helium as a working fluid and is designed for use with hot and cold sides of 1200 and 500 °C respectively. It is designed for operation at 10 Hz [107].

The technology is estimated to be at TRL 5-6 in the form of the advanced Stirling Radioisotope generator (ASRG) [115]. While this does not apply to the design adapted for use on Venus, it also lays out a development timeline, estimating approximately 5 years from the start of design phase to flight-ready units [115]. While this did not happen due to budgetary constraints it shows that the technology could be brought up to a required technical readiness level within the mission time frame.

In terms of cost, estimates vary widely. For the NASA's Discovery missions, the estimate for flight units set at 27M USD, not including development [115]. It is important to note that this design only uses 2 GPHS units instead of 7 [115]. Further considering the Multi-Mission RTG used aboard Curiosity and Perseverance rovers is estimated to cost approximately 110M USD, it can be inferred that in both cases cost is proportional to the number of GPHS units used at approximately 13-14M USD per unit. Extrapolating this to the system to be developed, which utilizes 7 units, and 2 generators, the total cost can be set at approximately 190M USD, which is significantly above the set budget.

Alternatively, a per-unit estimate could be used, which is not inconceivable since the design given is comparable in size and weight to the ASRG, which weighs approximately 25 kg when including reserve [115] (the higher output of the system proposed is a consequence of more heating units, and possibility of direct mechanical power transfer which is not used on the ASRG. Each unit costs approximately 27M USD [115], which would bring the total to just under 60M USD. This, however is considered less likely and per-GPHS estimate will be used for budgeting purposes.

Heat Source

Heat is provided by a set of 7 GPHS modules per generator (total 14 for the missions), which are mounted in a housing that is conductive on the side contacting the hot end of the generator, and insulated on all others, directing as much heat as possible into power extraction. The modules themselves are flight proven and have been used on missions since the 70s, having first flown on the Voyager missions [116]. Each of them includes two pellets of Pu-238, surrounded by Iridium cladding and a graphite aeroshell [117]. The total heat produced by a unit is approximately 250 Watts [107], decreasing with a half life of 87.7 years [118], meaning that any notable reduction will be well out of the scope of this mission.

Since these modules have been flown before the certification process is not expected to differ significantly in comparison to traditional radioisotope thermoelectric generators (RTGs), and aeroshell cladding is proven to address any contamination concerns in case of a launch or pre-departure failure that would result in the return of the spacecraft to Earth, including an unshielded reentry from orbit [117].

Alternator

To convert a part of the mechanical power generated into electricity, an alternator is used. To satisfy the ambient temperature requirements, a motor designed for used in jet engines was employed [119]. While the design has been tested up to TRL 5 at 250 °C, it was verified that components are designed to withstand temperatures up to 550 °C by the design team[42], necessitating a test campaign to bring it up to TRL 5 for our use case. Individual units are designed for operation at 28 V, up to 300 W, meaning that a single unit is sufficient to satisfy the power requirements. However, as it does

represent a critical component and since its weight, while not specified exactly, is, inferring from a photo, on the order of less than a kilogram [119], two units shall be used, with each generator having one.

Reliability
The paper used as a main source for operation on Venus focused on the purely technical aspect and did not discuss cost or reliability of such a system. A similar system, however, NASA's Advanced Stirling Radioisotope Generator has been designed with a 90% reliability over a lifetime of 17 years [120], indicating that similar level of reliability could be expected. Using the reliability formula[43] $R(t) = e^{-\lambda t}$ to obtain λ if $R(17 \text{ years}) = 0.9$, we obtain that $R(200 \text{ days}) = 0.996$ (only the 200 days on the surface are considered since the mechanism will be stationary during cruise). This value, while highly preliminary and offering very little insight into the system itself, does signify that the technology is applicable when considering the expected mission lifetime.

Since the value above includes its own alternator, and no information in this regard was provided for the alternator picked, a comparable reliability value, and therefore comparable total reliability is assumed.

Materials
A list of components and their materials used is given in Table 5.27. The precise properties of each material is given in Table 5.47.

Table 5.27: Materials for each component in Stirling power generation and cooling system.

Component	Material	Comments
Stirling generator hot end	Molybdenum P/M (powdered metallurgy) TZM alloy 364	This material is a good candidate for ultra high-temperature use, with a yield stress of about 360 MPa at 1200 °C. Oxidation issues in the rich CO2 and high temperature environment of Venus must be addressed however with additional protective coating [107].
Stirling refrigerator components and Stirling generator cold end	Inconel X-750	High-temperature Nickel alloys are a good candidate for the refrigerator components [106]. Inconel X-750 is used as the material for the refrigerator components and the generator cold end in [106, 107]
Generator and cooler rejection radiator	Pure nickel	Pure nickel is assumed to be the material for the generator and cooler rejection radiators in the papers [106, 107]. No explanation is given as to why pure nickels were used, however, as per conversation with a generative AI tool (DeepSeek), it may be due to the high thermal conductivity of pure nickel which is important for radiators. The screenshots of the full AI conversation prompted on 13/Jun/2025 can be found through [44]
Generator and cooler regenerator matrix	50 μ dia, random nickel alloy fiber 80% porosity (Exact wording from the papers [106, 107]	Generative AI tool DeepSeek was consulted for clarification. The full AI conversation prompted on 13 June 2025 can be found through [45]. The regenerative matrices are made of nickel-based alloy fibers with 50 μm diameter each wih 80% porosity (i.e. 80% of the regenerator matrix volume is void space, and 20 % is occupied by he nickel alloy fibers)
Bearings/bushings	Graphalloy®	The papers by Mellot mention that Graphalloy® can be used for the bearings/bushings [106, 107]. Precise information regarding material properties has been requested from the manufacturer. The team received a reply from the manufacturer on 23 June 2025 with a document containing technical specifications and design information of Graphalloy® products. According to this, Graphalloy® bushings are a family of bushings made of graphite/metal alloy that can operate in high temperatures of up to 535°C with a low coefficient of friction. In many applications, they can be used from ten to twenty years without replacement [121]. The degree of corrosive resistance, however, at Venus surface environment will need to be investigated on in future research.

Assembly and diagram of Stirling Generator and Cooler
An drawing of the Stirling generator is shown in Figure 5.33.

[42] https://www.helioselectricmotors.com/, accessed on 18/Jun/2025.
[43] https://www.studysmarter.co.uk/explanations/engineering/engineering-mathematics/reliability-engineering, accessed 18/Jun/2025.
[44] https://drive.google.com/file/d/1ct_Y3BrrVnQswDiViT5u6XGsYlsftT-W/view?usp=drive_link and https://drive.google.com/file/d/1ct_Y3BrrVnQswDiViT5u6XGsYlsftT-W/view?usp=drive_link, both prompted on 13/Jun/2025.
[45] https://drive.google.com/file/d/1rbYx-mX8Bt7x08xTHT1ZOs-YEgapOqmU/view?usp=drive_link and https://drive.google.com/file/d/1rbYx-mX8Bt7x08xTHT1ZOs-YEgapOqmU/view?usp=drive_link, both prompted on 13/Jun/2025.

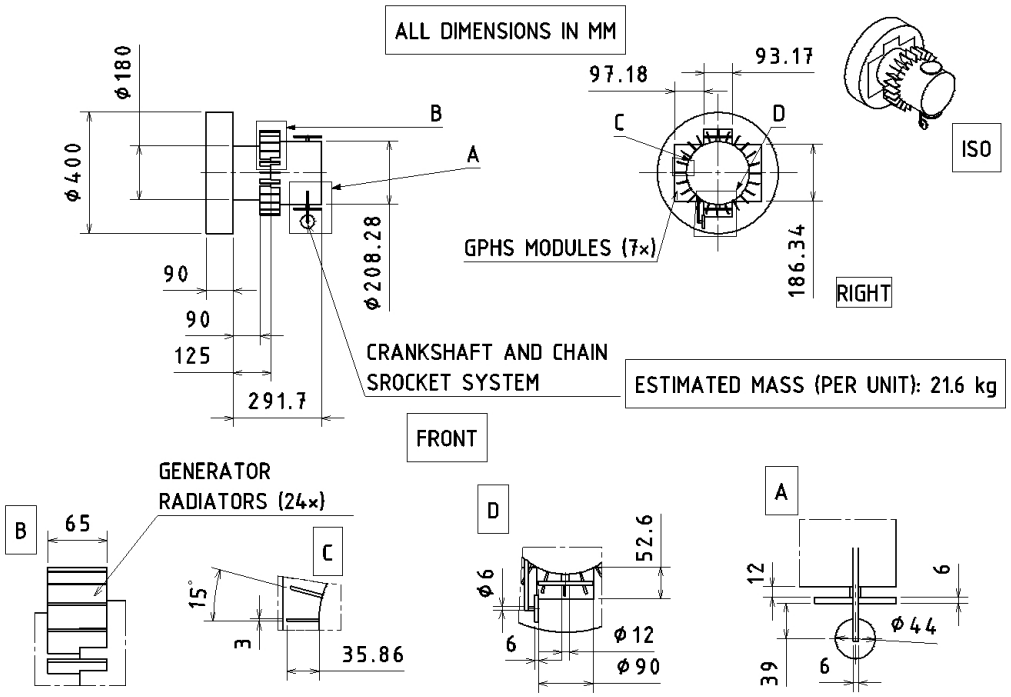

Figure 5.33: Engineering sketch of Stirling Generator. Own work created based on Mellot's work [107].

The piston and displacer of the Stirling generator are located horizontally in the cylinder with diameter 180 mm in the front view of Figure 5.33. The piston and displacer cause rotational motion of a crankshaft (located vertically in the cylinder section with diameter 208.28 mm in the front view of Figure 5.33), which is connected to a chain sprocket and this will serve as a connection between the generator and cooler. The engineering sketch of the Stirling cooler is shown in Figure 5.34.

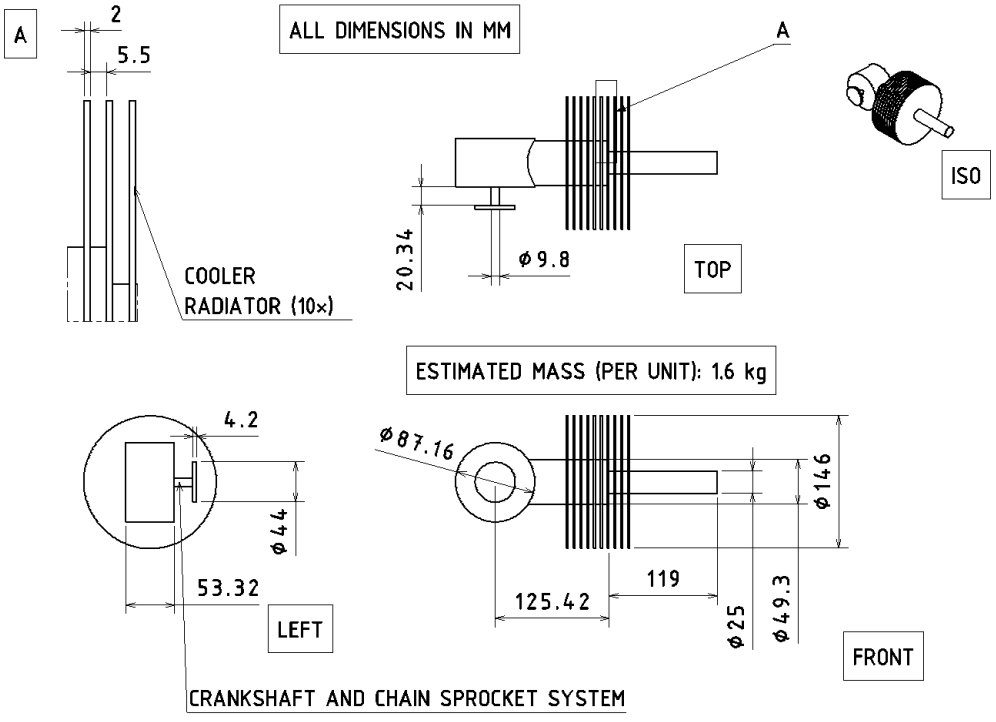

Figure 5.34: Engineering sketch of Stirling Cooler. Own work, created based on Mellot's work [106].

The crankshaft and chain sprocket system shown in Figure 5.33 and Figure 5.34 serves as the connection between the generator and the cooler. The chain sprocket is made up of two teeth wheels of different sizes. The larger tooth wheel is

the a thin cylinder with diameter 90 mm in the D-view on Figure 5.33 and the smaller tooth wheel is thin cylinder with diameter 44 mm in A-view of Figure 5.33 and the left view of Figure 5.34 (Note that although the latter appears both in the generator and cooler sketches, they are the same component). Although not visible in the sketches, they are connected together through a chain. The smaller tooth wheel is then connected to another crankshaft in the Stirling cooler, which will cause the movements of pistons and the displacer which are located in the cylindrical sections with diameter 25 mm and 49.3 mm in the front view of Figure 5.34.

It is beneficial to design the tooth wheel that is connected to the cooler to be smaller than the one connected to the generator. Consider Figure 5.35 on the right. Two teeth wheels are shown, connected together with a chain. The radius of tooth wheel B is twice of that of tooth wheel A. Suppose that tooth wheel B rotates with an angular velocity ω_B. The velocity of the chain is the same everywhere at v_t. The angular velocities of the two teeth wheels can be related as follows.

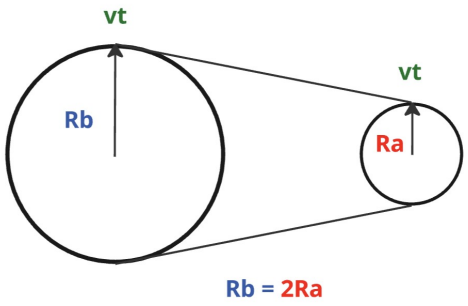

Figure 5.35: Chain sprocket connecting two teeth wheels (own work).

$$V_t = \omega_b r_b = 2\omega_b r_a = \omega_a r_a \tag{5.10}$$

$$\omega_a = \frac{2\omega_b r_a}{r_a} = 2\omega_b \tag{5.11}$$

As was shown in Equation 5.10 and Equation 5.11, the angular velocity of the smaller tooth wheel B is twice of that of tooth wheel A. In the context of the Stirling generator and cooler for KYTHERA, a higher angular velocity for the cooler tooth wheel (the smaller wheel) would allow the cooler to achieve higher frequency of the pistons and displacer of the cooler, allowing the cooler to remove more heat from the coldbox.

A similar crankshaft and chain sprocket system is used to connect the Stirling generator to an alternator to produce the electricity, as indicated in Figure 5.33. Although not visible in the sketches, a chain will connect this tooth wheel, to the tooth wheel of the alternator (again, the radius of the latter is smaller than the former).

Power Storage and Distribution System

As established in the previous section, the power provided by the generator is sufficient for all surface operations, including peak power provision. However, as the power requirements decreased, the role was reduced to powering the spacecraft before its startup, with the power required as follows:

Table 5.28: Power consumption during descent and surface phases.

Phase of Flight	Duration	Power Consumption
EDL separation – entry	60 min (+60 min reserve)	5 W
Entry – parachute release	15 min (+15 min reserve)	5 W
Parachute release – touchdown	50 min (+50 min reserve)	60 W
Surface reserve	120 min	60 W
	Total Energy Consumption	233 Wh

Since the battery is housed within the coldbox, standard off-the-shelf components can be used. The 232 Wh requirement even places it on the low end of the commercial satellite batteries. A viable solution is an Ibeos 28 Volt 275 Wh Li-ion battery, which weighs less than 2 kg, has a proven use in space (TRL 9) is capable of discharge operation at temperatures up to 55 °C [100], above the target coldbox temperature and components involved.

While the price is not provided directly, comparable models for use in spaceflight show values on the order 50,000 EUR [122], meaning that the price is not significant in comparison to the expected cost (and cost variability) of the generators and is to be finally decided at a later point depending on the market availability, and could be split into multiple cells if the volume availability within the coldbox changes. The same applies for system reliability - the long heritage of use in both orbital and deep space applications means that direct reliability largely depends on the final system chosen,

5.3.5 Subsystem Mass Breakdown

The masses of individual components, along with their quantities were added up to obtain the expected system mass, as can be seen in Table 5.29. Finally, additional 15% was added on top of this to account for wiring, 50% margin over the suggested literature value of around 10% [92]

Table 5.29: Mass breakdown of power subsystem components..

Component	Weight [kg]
Generator mechanism (×2) [98]	$21.6 \times 2 = 43.2$
Cooler mechanism (×2) [98]	$1.6 \times 2 = 3.2$
GPHS Modules (×14) [123]	$1.44 \times 14 = 20.2$
Battery [100]	2.0
Wiring and distribution (+15%) [92]	10.0
Total	76.6

5.3.6 Operational Model

As a part of detailed design, a model of the full system was produced, detailing the interaction between thermal-power system components, the environment and other subsystems. It consists of 5 main parts:

1. Hot side
2. Cold side
3. EDL Cooling system
4. Electrical/power system

General Overview

The heat is produced by the GPHS modules, directed through the Stirling generator, which produces mechanical energy. From it the power demand of the electrical system is subtracted, with the remainder used for cooling. The general overview in Simulink can be seen in Figure 5.36.

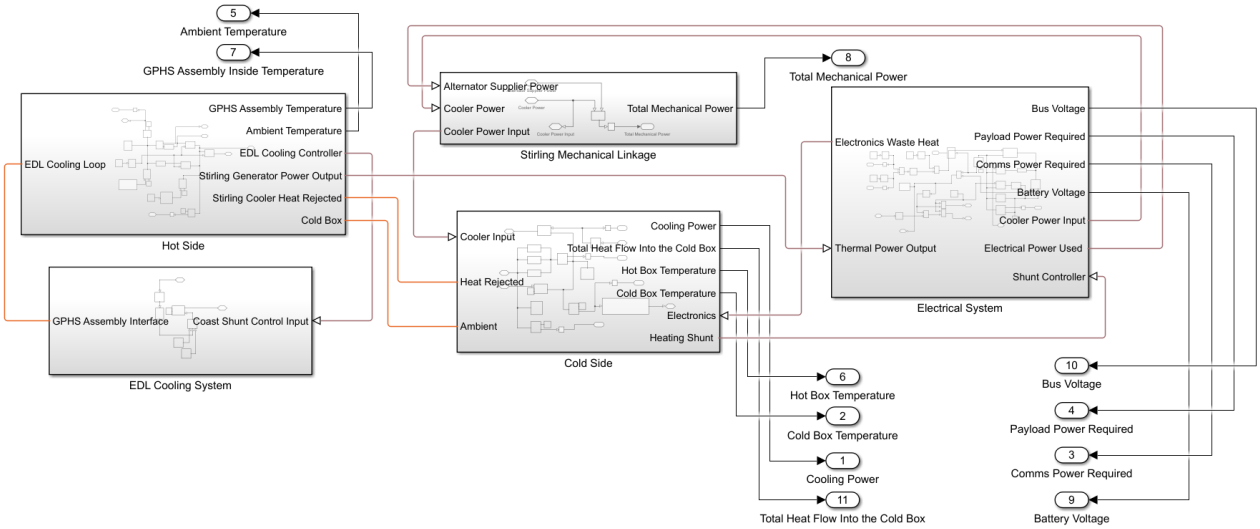

Figure 5.36: General overview and interfaces between parts of the model.

Hot Side

Starting at the GPHS modules, the heat is, as it is flowing to the outside radiators/convectors distributed between the transfer through insulation, and through the heat engine. The heat engine then converts it to mechanical energy, which is considered the initial power output. The thermal resistance within the model was adjusted such as to receive the expected temperature gradient of approximately 700 K.

Assumptions:

1. Conversion efficiency from heat transfer to mechanical power constant.
2. Heat flow through the generator is infinitely higher than flow through the insulation (and any heat loss is encompassed within the generator conversion efficiency itself).
3. Reduction in heat produced by the modules reduces exponentially with half life of Pu-238.
4. The maximum torque of the generator is not considered. This might require changing the gear ratio.

Relevant parameters:

1. Thermal resistance of the Stirling engine: 0.015 K/W - calculated from the expected temperature gradient and power output [98].
2. Stirling engine thermal efficiency: 27% [98].
3. GPHS initial power: 250 W [98].
4. Pu-238 half-life: 87.7 years [118].

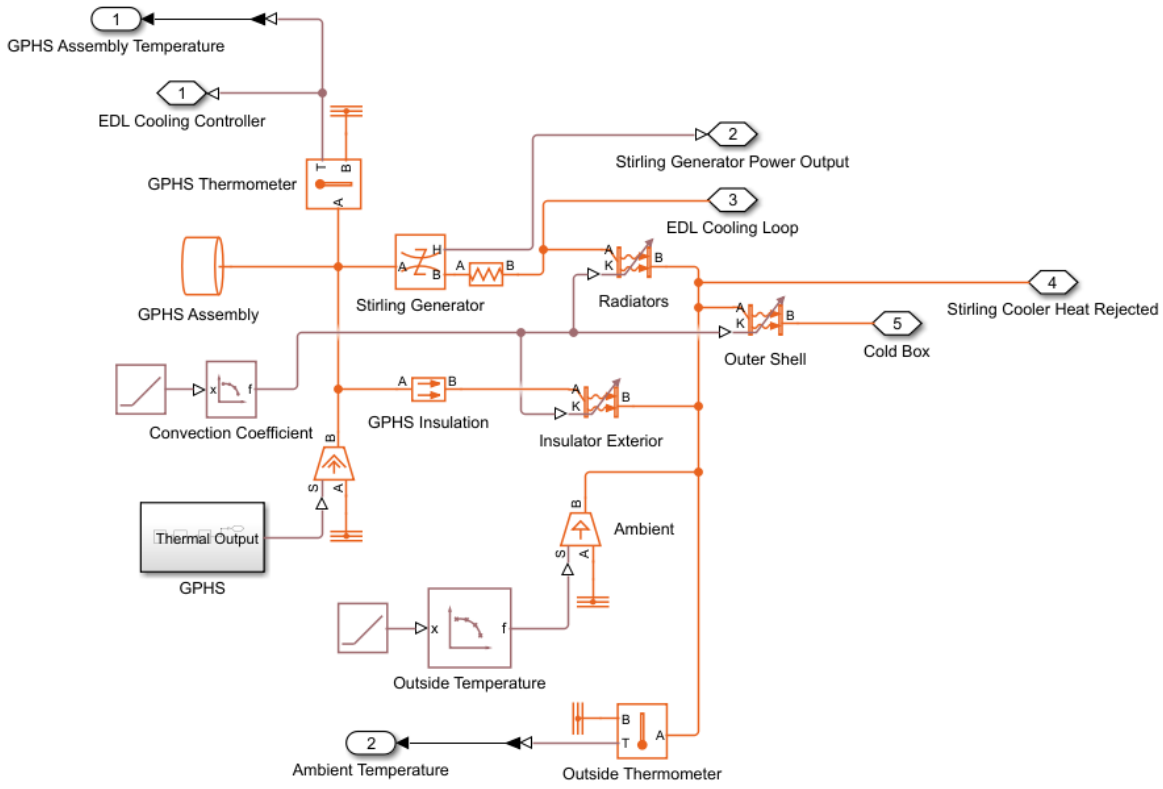

Figure 5.37: Schematic of the thermal control of the hot side of the system produced in Simulink.

Power Control

Payload and communication power consumptions are based on a combination of relay windows, frequency of use, and duration of use of individual experiments over the course of the mission. Their involvement in the power system was simulated as a single resistor when using the set bus voltage - power consumptions were added and converted to resistance using Ohm's law: $R = U^2/P$, where U is the voltage across and P is the power draw from the resistor. In addition, another resistor was added as a power shunt - when additional cooling is not desired (e.g. when reaching the lower end of operational temperatures), the resistance on the alternator will increase, decreasing the amount of cooling, while also increasing the amount of heat produced within the coldbox. The resistance set - 4 Ω - was found as an optimum through trial and error, in a final system such a component could be much more advanced and be capable of varying resistance (rather than just shutting on and off), however, this proved to be sufficient for the purpose of the model.

Finally, a battery is included, however, simulations have shown that it is not needed during surface operation and is only to be used during descent and landing.

Assumptions:

1. Idealized conversion from mechanical power to direct current.
2. Constant voltage output on the alternator.
3. Generator inactive during EDL.

Relevant parameters:

1. Battery capacity: 8.3 Ah (based on 233 Wh and 28V).
2. Alternator efficiency: 80% [124].

3. Bus voltage: 28 V.
4. Communication power consumption: variable with time (Figure 5.40).
5. Payload power consumption: variable with time (Figure 5.40).
6. Power/heating shunt resistance: 4 Ω

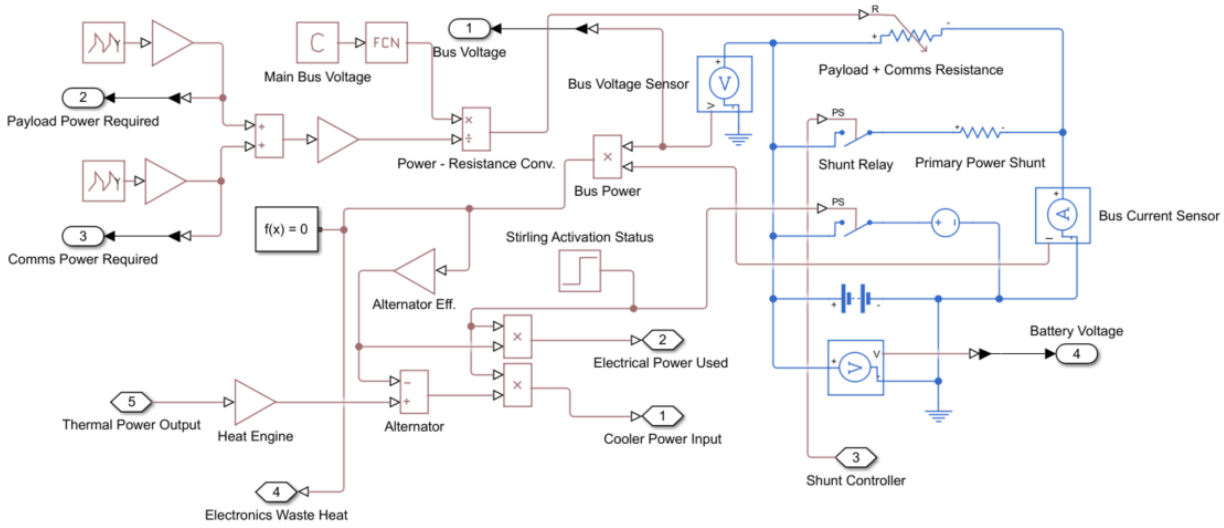

Figure 5.38: Schematic of the electrical system model produced in Simulink.

Cold Side

The cold side receives heat from a combination of radiation between the cold and hotbox, through the support structure, and from electronics located within. This heat is then pumped out using a Stirling heat pump with a literature efficiency. Finally, if the temperature is too low, a heating shunt is activated as described in section 5.3.6.

Assumptions:

1. There is no convection between the hot and coldbox (approximately perfect vacuum).
2. Radiation behaves in accordance with the black body radiation model.
3. All of the power used by the electronics is converted into heat.
4. The heat introduced is distributed uniformly through all of the components within the box.

Relevant parameters:

1. Inner wall combined emissivity: 0.0893.
2. Power/heating shunt resistance: 4 Ω.

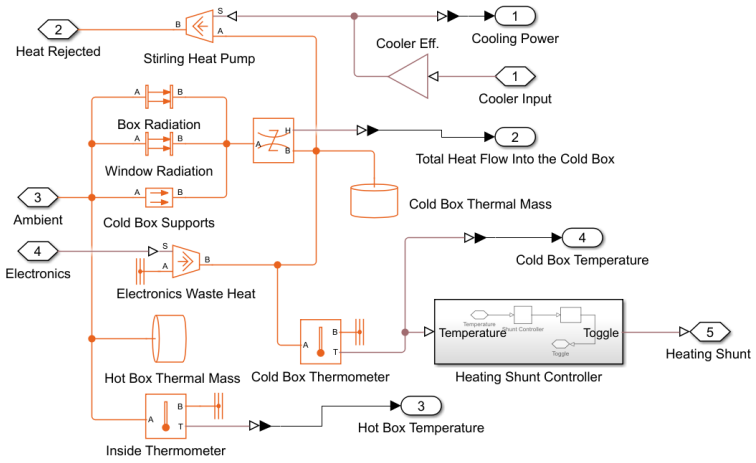

Figure 5.39: Schematic of the thermal control of the cold side of the system produced in Simulink.

EDL Operation

Since the Stirling generator is not designed to operate at extreme G-forces due to the presence of moving parts, alternate systems have to be used for the time between orbiter separation and landing, when the generator is mechanically locked at the shaft linkage. From separation to entry interface, a radiator is used to reject heat from the GPHS modules, a function that is delegated to a paraffin wax container once that is separated prior to the entry interface. Once the aeroshell is separated, the system relies on heat being transferred through the working fluid into the convectors, which are increasing in operational capability as the atmosphere thickens. Finally, following a touchdown, the mechanism is unlocked and is started up with the help of the alternator that is used as a motor powered by the battery. Finally, the thermal masses were order-of-magnitude estimates based on the materials used and weight of the components. since these do not matter for the transient state, and there is a form of cooling provided through the descent, more accurate estimate was not performed.

Assumptions:

1. Perfect connection between the paraffin wax container and the GPHS modules.
2. Only static convection considered (a conservative estimate).

Relevant parameters:

1. Coast time (after separation from EDL cruise stage): 60 min.
2. Entry time: 15 min.
3. Descent time: 50 min.
4. Hotbox thermal mass: 50 kJ/K.
5. Coldbox thermal mass: 40 kJ/K.
6. Convective capacity of the atmosphere: 0-62.5 W/(m^2K) [107], increasing linearly through the descent phase.

Power and Temperature Plots

The model was used to model the power usage and expected temperature within both the cooled and non-cooled parts of the spacecraft. The power inputs were based on payload and communication requirements and can be seen in Figure 5.40.

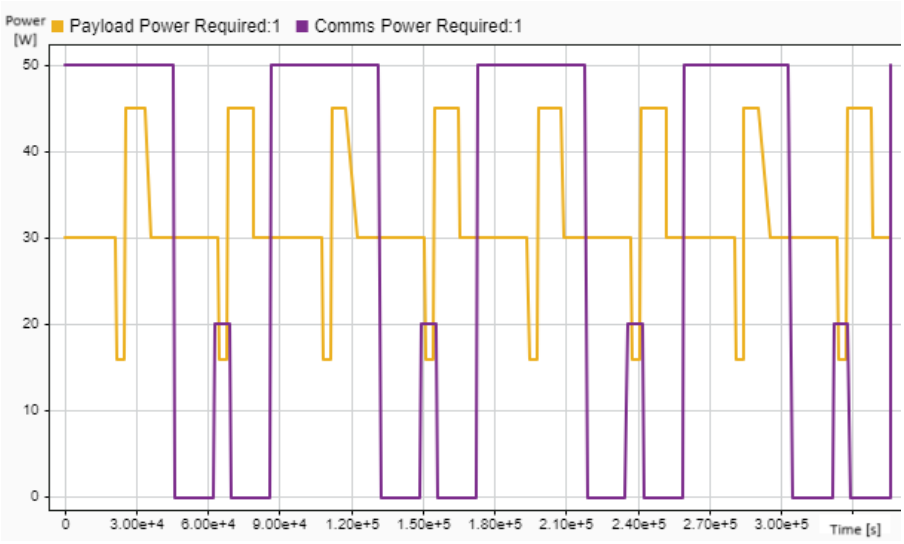

Figure 5.40: Power use over time for communication and payload subsystems over the course of approximately 4 Earth days, with this pattern repeating through the surface phase of the mission..

With this, the power available for cooling was obtained and combined with power required. Figure 5.41a shows the cooling power used and heat flux through the coldbox insulation in the first 12 hours after separation (after which the values stabilize and remain constant within a narrow range. It is low through the initial EDL phase, increasing through the descent, as the convective coefficient increases. Finally, the hotbox starts heating up first, followed by the coldbox, hence why the flux rises slower than the ambient temperature and convection. More cooling is required as in addition to the heat leakage, the waste heat produced by the electronics also has to be removed. Finally, the oscillation in cooling power is due to the toggling of the heating shunt, which lowers the power available to the cooling system.

These heat fluxes were then combined with the thermal masses of the hot and coldbox to obtain the actual temperature and verify that it meets the operating requirements of the electronics contained. These plots can be seen in Figure 5.41b. The initial temperature is assumed to be the minimum operating temperature of electronics - 270 K, with the inside increasing

as the heater is powered on and it starts targeting 300 K, while the unheated outside remains constant. As the convection and ambient temperature increase, the hotbox temperature increases rapidly, while this increase is gradual for the coldbox as active cooling is powered on upon touchdown and remains mostly stationary at the operating temperature of 300 K for the remainder of the mission.

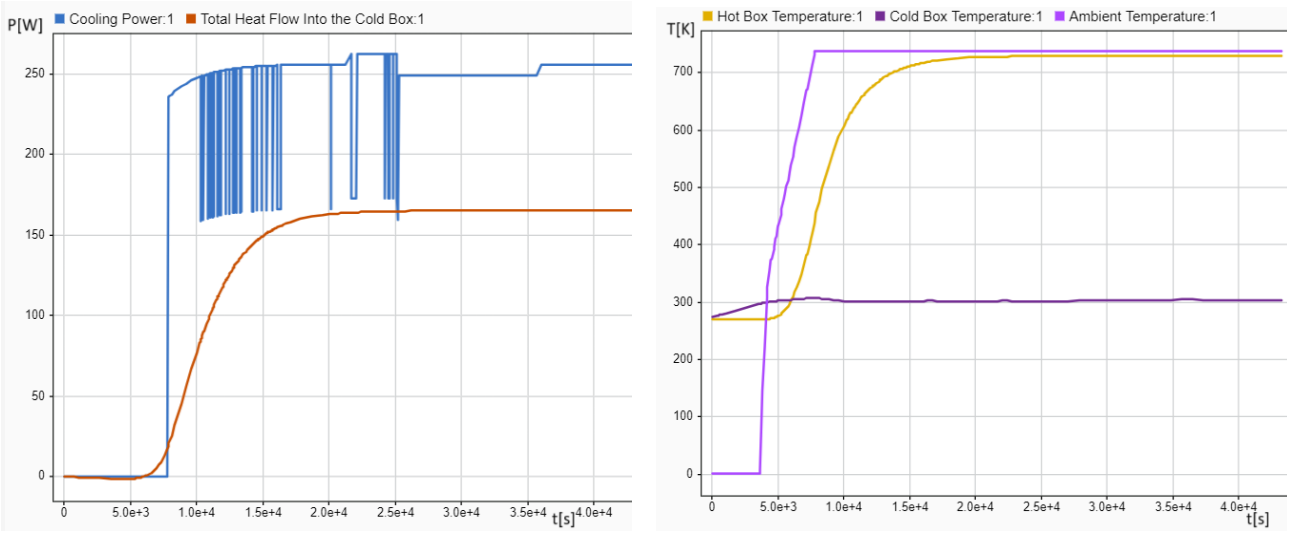

(a) Heat flux and cooling power required.

(b) Hot-, coldbox and ambient temperature.

Figure 5.41: Thermal trends in the first 12 hours after coasting stage separation.

Verification and Validation

For verification, the thermal, electrical and physical system functionalities were assumed to be correct on the unit level due to the established nature of the model - only standard blocks were used. The values that needed to be calculated - e.g. heat flows through individual elements - were compared with manual calculations performed for initial sizing.

Sensitivity Analysis

In the very early design phases, the coldbox temperature was assumed at 100 °C. Later on, this evolved to 80 °C to accommodate a wider range of instruments and electronic components. This is the value that was designed for. However, the overview of operating temperature ranges showed that some of the instruments cannot operate above 30 °C. This caused the Power and Thermal team to try and run a simulation with a 30 °C coldbox temperature. As it turned out, the power system can handle this lower cooled box temperature, and it only caused an increase in heat leak of 5 W (from approximately 161 to 166 W). Hence, it was decided to cool the cooled box down to 30 °C, to allow for all instruments to comfortably operate without a need for adjustments.

Future Work

With the amount of simplifications involved it is clear that this is only an initial version of the model. Following the work done in this paper, individual components could be expanded: the Stirling generator's cycles could be implemented for both cooling and energy production, more realistic voltage output on the alternator, and rectifiers if necessary, could be added, and there is a good deal of expansion that could be done in regards to power profiles of individual instruments once they're better understood.

In addition, research and modeling of Variable Conductance Heat Pipes (VCHPs) may be beneficial for KYTHERA as well. VCHPs may be used to attached to locally control the temperature of each component housed in the coldbox. Furthermore, according to works by Dyson et al. [108] and Anderson et al. [125], VCHPs may be used in the context of long-duration Venus lander to provide temporary cooling as a backup in the event of an unexpected shutdown of the Stirling coolers or to restart it.

5.4 Communications

The communication subsystem is vital for any spacecraft to transmit and relay data observed or measured back to Earth for analysis. This is especially true for the KYTHERA lander. During its mission operation, various measurements must be taken to contribute to a better understanding of the Venusian surface and lower atmosphere, which are discussed in detail in Section 5.2. Next, the data are stored onboard the lander, as described in Section 5.5. Finally, the data are relayed and transmitted to the orbiter. This section will detail all aspects of the chosen communication system, including background research, requirements, detailed design, budgets, and recommendations for future design phases.

5.4.1 Background Research

Before any communication architecture can be chosen, the overall structure and variability of the equipment of the KYTHERA lander must be estimated. It is concluded that the communication system can be broken down into the following sequential subsections: antenna type selection, communication band selection, communication architecture selection, and relay window calculation.

To begin the process, research was conducted into the basics of the spacecraft telecommunication systems, antenna theory [127–129], past and proposed future missions with their telecommunication systems[46] [130] as well as link budget calculations[47]. It was found that due to the extreme and harsh conditions of the Venusian surface and lower atmosphere, many commonly used telecommunication apparatuses will not be as viable on the surface of Venus, especially for the entire duration of the mission.

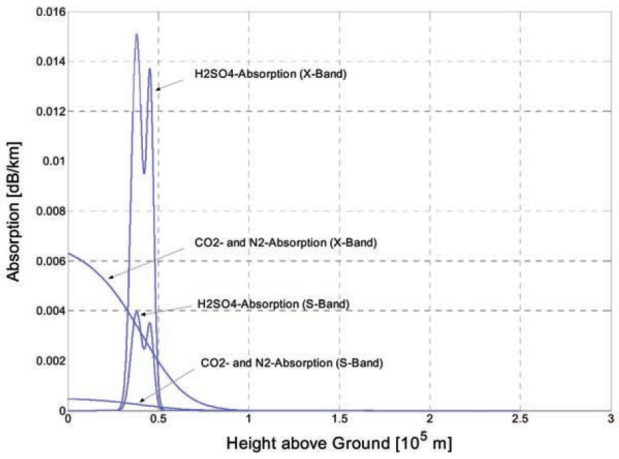

Figure 5.42: Absorption of communication bandwidths in the Venusian atmosphere [126].

It was found that common higher-gain communication frequencies, such as the X, Ku, K, Ka bands (frequency of 8-40 GHz), encounter strong atmospheric absorption from the high concentration of sulfuric acid in the cloud layers and carbon dioxide throughout the atmosphere. An absorption graph can be seen in Figure 5.42. Estimates for the thickness of the sulfuric haze and cloud layer are predominant for around 30 km of Venus's middle-lower atmosphere[48][49]. This brings the atmospheric attenuation loss of X-band signals to around 0.5 dB from the H_2SO_4 and approximately 0.3 dB from CO_2. These values, however, drastically decrease for S-band, where the longer wavelength of the signal is more resistant to atmospheric losses. In addition to the absorption, the atmosphere also scatters signals with short wavelengths, mainly in the form of Raleigh scattering, where the suspended particles in the Venusian atmosphere reflect the electromagnetic waves, causing them to lose strength and integrity.

High temperature is another major challenge for successful telemetry. The surface temperature of Venus is estimated to be around 464 °C [50]. This greatly increases the difficulty, especially because the Low Noise Amplifier (LNA) housed in the receiver/transceiver onboard the lander will suffer from large thermal noises, common electronics do not survive, and the coaxial cable connecting the transmitter with the ground plane and helix will suffer from significant loss and decreased efficiency. Therefore, the communication architecture will need to be carefully designed with very little margin for error. An alternative and novel approach will be to use active cooling systems to maintain the transceiver at a preset temperature so that all components at risk of thermal degradation can operate normally.

Additionally, the surface of Venus has extremely high concentrations of CO_2 at high pressure, which means that supercritical CO_2 exists on the surface[51]. A lot of properties and behavior of matter at supercritical states still remain a mystery; however, it is found that it can potentially possess very strong corrosive properties if in the presence of other compounds. This is yet another potentially catastrophic risk, where the cable, ground plane, or helical wire is corroded and no longer conductive. Trace amounts of SO_2 in the atmosphere also pose the same threat. Potential mitigation strategies using coatings with high temperature and corrosion tolerance. Another approach is to encase the antennas in a radome filled with either an inert gas or in vacuum.

Finally, a fully digital communication system has not yet been deployed on a Venus lander mission. The high temperatures and corrosive nature of Venus's atmosphere degrade many of the commonly used communication antennas; hence, active cooling will be necessary for certain configurations.

5.4.2 Requirements and Verification

The key and driving requirements for the communication subsystem are outlined in Table 5.30. The table consists of requirement ID, requirement description, verification code, for which the corresponding method can be found in Table 4.1, and their verification status. The list of requirements is broken down into subcategories, including general requirements, transmitter (uplink) requirements, receiver (downlink) requirements, and operational requirements. The value for requirements COMM-GEN-1 to COMM-GEN-4 is based on the most recent budget iterations during systems engineering, seen in Section 4.6.

[46] `https://ipnpr.jpl.nasa.gov/progress_report/42-236/42-236A.pdf`, accessed on 09/May/2025.
[47] `https://www.recw.ac.in/v1.8/wp-content/uploads/2021/10/OFC-UNIT-V.pdf`, accessed on 12/May/2025.
[48] `https://www.esa.int/Science_Exploration/Space_Science/Venus_Express/Acid_clouds_and_lightning`, accessed on 9/Jun/2025.
[49] `https://www.math.cmu.edu/~amanita/math122/handouts/m122_f08_handout8.pdf`, accessed on 9/Jun/2025.
[50] `https://nssdc.gsfc.nasa.gov/planetary/factsheet/venusfact.html`, accessed on 9/Jun/2025.
[51] `https://www.scientificamerican.com/article/did-venus-have-carbon-dioxide-oceans/`, accessed on 9/June/2025.

Table 5.30: Communication subsystem requirements.

ID	Requirement Description	Verification	RC
COMM-GEN-1	The communication system shall have a mass of no more than 17 kg, 20% margin.	V-INS-WEI	✓
COMM-GEN-2	The communication system shall cost no more than €14M in FY25, 30% margin.	V-CST	✓
COMM-GEN-3	The main antenna shall receive no less than 50W of power during transmission mode, 50% margin.	V-ANA-SIM	✓
COMM-GEN-4	The secondary antenna shall receiver no less than 30W of power during science mode, 50% margin.	V-ANA-SIM	✓
COMM-SIG-TX-1	The lander antenna shall be able to transmit signals in L-band at 1.2 GHz.	V-TST-FUN	✓
COMM-SIG-TX-2	The lander LGA shall have a gain of at least 2 dBi, 20% margin.	V-TST-FUN	✓
COMM-SIG-TX-3	The lander HGA shall have a gain of at least 10 dBi, 20% margin.	V-TST-FUN	✓
COMM-SIG-TX-4	The uplink communication system shall possess a minimum transmitted power of 42.27 dBm for the primary antenna, 20% margin.	V-ANA-SIM	✓
COMM-SIG-TX-5	The uplink communication system shall possess a minimum transmitted power of 40.05 dBm for the secondary antenna, 20% margin.	V-ANA-SIM	✓
COMM-SIG-TX-5	The orbiter shall be capable of receivibg a signal with power of at least -115dBm sent from the lander, 20% margin.	V-ANA-SIM	✓
COMM-SIG-RX-1	The communication system shall be capable of receiving commands at all times given line-of-sight is maintained.	V-TST-FUN	✓
COMM-SIG-RX-2	The downlink communcation system shall be capable of receiving a signal with power of at least -110 dBm, 20% margin.	V-ANA-SIM	✓
COMM-SIG-RX-3	The lander antenna shall be able to receive signals in L-band at 1.2 GHz.	V-TST-FUN	✓
COMM-OP-1	The communication system shall be capable of operating within 50 and 500 degrees celcius, upper limit with 10% margin.	V-DEM-TEM	✓
COMM-OP-2	The communication system shall be capable of operating in conditions up to 100 bars, 10% margin.	V-DEM-PRE	✓
COMM-OP-3	The communication system components shall withstand contamination by sulfuric acid.	V-DEM-COR	✓
COMM-OP-8	The communication system shall maintain line-of-sight with the orbiter for at least 15 hours per day, 20% margin.	V-INS-SFT	✓

The description of verification method IDs are found in Table 4.1.

5.4.3 Detailed Design

In this section, the detailed design of the communications subsystem is discussed and broken down in subsequent subsections: antenna and communication band selection, communication architecture trade-off, link budget analysis, system budget, pointing mechanism, material selection, and relay window calculation.

Signal Selection

For space missions, a wide range of communication configurations is typically available, dependent on the requirements and constraints of each mission. However, no lander has ever been successfully operated on the Venusian surface for more than a few hours, making the design of the communication subsystem particularly challenging due to the harsh and largely untested surface conditions.

Firstly, research was conducted into analog signals and their feasibility in this mission. Analog signals use continuous-time carrier waves typically modulated in amplitude, frequency, or phase to convey information. While generally unfeasible for large volume data transfers due to susceptibility to noise, lack of error correction, and requiring a custom demodulation system[52], analog systems have some strengths as well, such as simplicity of hardware, ease of integration, high thermal and pressure tolerances, and continuous data transmission. Potential candidates for analog systems include radar detection systems, advanced AM/FM/PM systems, vacuum tube radios, and the proposed record and balloon communication system. A recent study demonstrated the possibility of utilizing such systems in a Venus mission [131]; however, there are still concerns and potential flaws not addressed by the study, such as narrow data bandwidth, possible signal distortion from densely packed AM tones, vulnerability to amplitude noise and atmospheric attenuation, and reliance on Phase-Locked Loop (PLL) carrier tracking, which has not yet been validated under these conditions. Therefore, although promising, this system requires further research and development before consideration for implementation into the KYTHERA mission.

For this reason, a digital signal was chosen to be the final communication method. Digital signals encode data as discrete binary values modulated onto a carrier wave [132]. These systems offer error detection and correction, noise tolerance, and significantly higher data rates compared to analog systems, making them standard in modern wireless and space communications [133, 134]. However, operating in Venus's extreme environment presents major challenges. Extreme surface temperature limits the use of conventional electronics, requiring either advanced materials such as Silicon Carbide (SiC) or strong thermal regulation, such as active cooling [135]. Digital systems also have more complexity, increasing the power consumption and costs. To mitigate this, the KYTHERA lander plans to use an active cooling system capable of maintaining an internal temperature of 30 ° C, where the sensitive components will be housed.

[52] `https://ieeexplore.ieee.org/stamp/stamp.jsp?tp=&arnumber=4323127`, accessed on 14/May/2025.

Antenna Selection

Next, the antenna type was chosen, where options were split into two major categories: Link via Orbiter (LVO) and Direct to Earth link (DTE). LVO provides a more stable connection due to shorter distance, resulting in lower free-space losses and reduced link sensitivity to pointing errors. Active pointing antennas also require a smaller antenna size compared to that for a direct Earth link[53]. However, relying on the orbiter introduces additional layers of technical risk. In contrast, a DTE allows for tunable and easily maintainable ground stations and near-continuous connectivity with at least one European Space Tracking network (ESTRACK) antenna, assuming sufficient coverage. Its drawbacks include greater free space loss, high power requirements, and the need for significantly lower data transmission capacity. Additionally, the operating costs of using ground antennas from the ESTRACK/DSN network for primary communication lead to significant operational costs [136, 137], which could exceed the allocated operations cost budget. On the other hand, the orbiter can store information from the lander onboard and schedule data transmission with Earth during optimal time windows. Ultimately, LVO was chosen to be the main form of transmission, as the orbiter's highly eccentric polar orbit enables long relay windows per pass, and a more efficient and reliable link can be established.

The antenna selection is critical for establishing a stable link between the lander and orbiter, ensuring sufficient coverage, minimal losses, and high transmission capacity so all important science data are relayed. The primary design decision is whether to use a directional or omnidirectional antenna. Table 5.31 summarizes key characteristics of the considered antenna types, along with their respective advantages and disadvantages. Directional antennas are denoted with 'D' and omnidirectional antennas are denoted with 'O'. For simplicity, efficiency, and to meet constraints on mass and volume, the same antenna will be used for both uplink and downlink operations.

As shown in Table 5.31, many antennas possess strengths that prove beneficial for the mission, though some present integration challenges. Link budget calculations are thus performed for a few representative antennas with minimal drawbacks. Among directional options, the parabolic dish antenna is selected for its simplicity and effectiveness. The Cassegrain and phased array antennas are excluded due to their complexity, high cost, and demanding mass, volume, and thermal requirements. For omnidirectional antennas, more research and calculations were done, as simplifying the lander by avoiding moving parts is preferred. Given the low initial data rate requirement of 300 bps, the use of high-gain antennas (HGAs) can potentially be avoided, sacrificing data signal strength and thus effective communication window duration. The helical antenna is of particular interest for its flexibility to switch between normal and axial modes. Patch antennas are also viable due to their low weight, moderate gain, and wide coverage. Monopole and dipole antennas are omitted due to limited bandwidth, low efficiency, and size constraints.

Table 5.31: Antenna type overview.

Antenna Name	Type	Description	Advantages	Disadvantages
Parabolic Dish	D	Uses a parabolic reflector to focus radio waves into a narrow beam	High directivity, high data transmission rate, supports high-frequency bands	Precise pointing, mechanically complex, mass constraints
Cassegrain	D	Now includes a second reflector, the feed horn is behind the focal point	High directivity, high data transmission rate, compact feed system, better noise performance, mechanically stable	Precise pointing, narrow beam width, volume, mass, cost constraints
Phased Array	D	Multi-element antenna which steers without physical movement by manipulating phase in each element	No moving parts, agility and ability to host multiple beams, fault tolerance, compact	High complexity, requires heat management, power, cost constraints
Helix (Axial/Normal Mode)	D/O	Specialized antenna consisting of coiled wire and ground plane, produces circular polarized waves	Resistant to signal degradation, flexible mode changes, robust structure	Precise sizing requirement
Quadrifilar Helix	O	Advanced helical structure, four helical structures wound in a cylindrical or conical shape to achieve a more stable radiation pattern	Resistant to signal degradation, omnidirectional coverage, wide bandwidth, phase stability	Complex feed, sensitive to manufacturing imperfections, technological limitations
Monopole	O	Single element antenna which consists of a rod or wire mounted perpendicular to a conductive ground plane, very common	Simple, low cost, omnidirectional, compact, easy integration	Limited bandwidth, low efficiency
Dipole	O	Fundamental antenna that uses two conductive rods or wires aligned end to end with a feed point at the center	Simple, low cost, omnidirectional in horizontal plane, no ground plane, moderate bandwidth	Inefficient at long distances, sizing constraints, sensitive to surrounding structure
Patch	O	Printed circuit antenna consisting of flat rectangular patch mounted over ground plane, separated by a dielectric substrate	Low profile, lightweight, easy to manufacture, wide coverage while still maintaining some directionality	Narrow bandwidth, sensitive to surroundings, lower efficiency

Preliminary link budgets are calculated with different communication bands for the chosen antenna types. Calculations

[53] `https://mars.nasa.gov/internal_resources/828/`, accessed on 14/May/2025.

use empirical formulas[54] and are informed by similar mission studies [126, 138–141]. The link budget equation used to calculate received power is described in Equation 5.12. The pointing loss factor L_p is only accounted for in directional antenna designs where active steering is required.

$$P_{RX} = G_{RX} + G_{TX} + P_{TX} - L_{FS} - L_{atm} - L_{pol} - L_p \tag{5.12}$$

where P_{RX} is the received power, G_{RX} and G_{TX} are the receiver and transmitter gains, respectively, P_{TX} is the transmitted power, L_{FS}, L_{atm}, L_{pol} and L_p are the free-space, atmospheric (consisting of attenuation and scattering), polarization and pointing losses, respectively. All terms are understood to be in dB.

From the preliminary link budget calculations, it was found that the received power from the orbiter is around -110 dBm, which is weak but achievable through implementing high-sensitivity receivers onboard the Venus orbiter. It can also be observed that the link margin estimates are positive, allowing room for additional or unexpected signal losses. It was suspected that the high link margin is the result of underestimating the value of the Noise Power Spectral Density (N_0). The link budget is refined and recalculated in detail once the final configuration for the communication architecture is chosen, which will be discussed in the following sections.

Digital Communication Bands

After confirming the selection of antenna type and communication method, a trade-off is conducted to select the optimal band frequency for the communication subsystem of the KYTHERA lander. The design options used are Ultra High Frequency (UHF) at $\sim$ 0.92 GHz, L-Band at $\sim$ 1.2 GHz, S-Band operating at $\sim$ 2.4 GHz, and X-Band at 8.4 GHz. These entries are then assessed in numerous factors such as losses, power requirements, sizing, data rates, and environmental tolerances. Bands with frequencies higher than X-band are excluded from this trade-off table and the link budget calculations, as they are considered impractical for this mission. Higher frequency bands have shorter wavelengths, leading to greater free space path loss, significantly increased atmospheric attenuation, and pose greater integration challenges for lander missions [142]. It is more likely that higher frequency bands like the Ku band are more suited for communication between the orbiter and Earth ground stations.

It was determined that X-band scored the lowest in the trade-off because of poor efficiency and high losses. Longer wavelengths like UHF and L-Band perform best, offering strong atmospheric penetration and moderate losses. While UHF has been used in past missions such as the early Venera missions, the size of the antenna required is a significant constraint; for conservative estimates, the main parameter of the antenna is not to exceed 1.5 meters. Due to these considerations, L-band communication is selected for digital communication, providing a balance between robustness against signal losses, moderate data rates, good power efficiency, and thermal toleration. It was also determined that the coldbox housing will accommodate the transceiver, where the same antenna and L-Band communication would be used for orbiter uplink and downlink. The transceiver will employ a time-division duplexing scheme (TDD) [143] to switch between transmission and receiving mode at different scheduled time slots. This way, the communication subsystem can be more mass and cost efficient, and suffer from fewer potential losses or degradation risks from the increased complexity.

Communication Architecture

With the communication band selected, the final communication architecture will be determined. This process begins with a design trade-off to identify the most suitable general configuration, as outlined in Table 5.32. Following this, the appropriate antenna type for the chosen configuration will be selected. Five proposed configurations for the communication subsystem are presented in the first list, while the second list shows the evaluation criteria used in the trade-off, along with their respective weights.

Configuration options:

- **Disposable HGA + LGA**: The core concept behind this approach is to deploy a pre-cooled, steerable high-gain antenna that remains operational during the initial few days of the mission. This enables the lander to transmit a large volume of data shortly after arrival, prioritizing bandwidth-intensive tasks such as high-resolution imaging and geological sample data transmission. Once the HGA is decommissioned, long-term, robust low-gain antennas (LGA) take over to handle the reduced communication demands for the remainder of the lander's operational lifetime.
- **Part. Cooled HGA + LGA**: This concept centers on the use of active cooling systems onboard the KYTHERA lander. The communication dome will incorporate a closed-loop cooling architecture, designed to lower its internal temperature by around 100 °C. This significantly expands the range of viable antenna materials and enables more efficient and optimized designs. The configuration includes a single HGA, supported by LGAs used for location triangulation and redundancy. The use of active steering systems such as gimbals and motors was initially considered; however, due to the low survivability of motors and lubricants under Venusian surface conditions, even with partial cooling, these systems were not suitable for long-term operations. Instead, a passive counterweight mechanism will be deployed to orient the HGA towards the zenith at landing.

[54] `https://www.recw.ac.in/v1.8/wp-content/uploads/2021/10/OFC-UNIT-V.pdf`, accessed on 12/May/2025.

- **Partially Cooled LGA**: This design is similar to the previous configuration as it integrates partial cooling. This configuration replaces the higher-gain antenna with more omnidirectional, relatively low-gain antennas.
- **Uncooled HGA + LGA**: In this configuration, the communication dome is not actively cooled and is exposed to ambient surface temperatures of approximately 464 °C. A movable HGA is used alongside fixed-position omnidirectional LGAs. At such extreme temperatures, material selection for antenna components becomes highly constrained, particularly for the HGA's steering gimbal system if active steering is used, as there exists almost no lubricant that can provide long-term survivability. The same conditions can be observed with the antenna materials, as the dielectric materials used will most likely thermally degrade for long-duration operations.
- **Uncooled LGA**: This is the simplest and most robust option, and it has been the most commonly used in similar missions. In this configuration, LGAs with very low data rates are mounted directly onto the main body of the lander. These antennas are designed to be highly temperature-resistant, offering excellent reliability; however, this comes at the cost of significantly reduced data quality and transmission capacity.

Trade-off criteria:

- **Performance (Weight 4)**: This criterion evaluates the overall effectiveness of the communication configuration, including achievable data rates, effective range, and the system's ability to meet the mission's communication requirements. This factor is critical as it determines whether all necessary scientific data can be successfully transmitted to the orbiter without significant degradation or power draw. It should be noted that data transmission demands are front-loaded, with significantly higher rates needed during the initial days of the mission.
- **Reliability (Weight 3)**: Reliability refers to the likelihood of avoiding unexpected part failures throughout the mission. It is closely tied to system complexity, as systems with more intricate or moving parts have higher chances of failure. This parameter is important as it necessitates balancing performance and system complexity against robustness and operational simplicity..
- **Power Requirement (Weight 3)**: This criterion assesses the power requirements of the communication architecture needed to reach the orbiter at apoapsis. Low-gain omnidirectional antennas are incapable of covering the estimated distance of ca. 66,000 km without excessive power consumption and significant signal degradation. While this factor is not currently critical since the lander can generate sufficient power for all proposed configurations, it remains important in any future event that changes the power budget.
- **Size (Weight 1)**: The physical size of the antenna varies across different configurations. However, this criterion is given lower priority, as the aeroshell is sufficiently large to house all proposed antenna designs.
- **Mass (Weight 1)**: This criterion assesses the total mass of the communication configuration. In general, LGAs and passively or partially cooled antenna systems tend to have lower mass compared to steerable or non-actively cooled high-gain systems. This factor is assigned a low weight, as the mass budget of the lander is sufficiently large for all configurations.
- **Longevity (Weight 4)**: Longevity defines the expected operational lifespan of the communication architecture. It is how long the system will remain functional if no unexpected failures were to occur. It is a critical factor, as a long design life will ensure the lander can transmit the maximum possible volume of data to the orbiter.

Table 5.32: Communication architecture trade-off.

	Performance	Reliability	Power Req.	Size	Mass	Longevity	
Weights	4	3	3	1	1	4	**Score**
Disposable HGA + LGA	4	4	3	3	2	3	54
Part. Cooled HGA + LGA	5	2	5	4	3	5	68
Part. Cooled LGA	2	3	3	5	4	5	55
Not Cooled HGA + LGA	3	3	4	2	1	2	44
Not Cooled LGA	1	5	2	3	5	4	49

From Table 5.32, it can be seen that the partially cooled high-gain antenna configuration achieved the highest overall score. This option effectively balances simplicity and reliability with thermal performance. By incorporating a partial active cooling system, the configuration enables the use of more efficient high-gain antennas with a more compact size and better transmission performance. The included low-gain antennas provide redundancy and additional coverage for maximized data transmission. Overall, this architecture is the best option for extended planetary missions in extreme environments such as the Venusian surface, where elemental resistance and robustness are key.

In addition to the primary tradeoff, a sensitivity analysis is conducted to investigate further how changes in criteria weights affect the outcome of the design trade-off. For this trade-off, a total of three separate sensitivity analyses were performed,

with each instance altering the weight of one or more key criteria. Table 5.33a shows a scenario where the size and mass of the communication subsystem are heavily constrained and their weight increases from one to three. In this case, the partially cooled HGA + LGA configuration still achieves the highest score, due to its compact size while still maintaining efficiency and good performance. Table 5.33b shows a power-constrained scenario where the power requirement becomes a critical element with weight increasing from three to five. In this case, the part-cooled HGA + LGA configuration emerges as the most optimal again, due to their relative and long design life and low power requirement to communicate with the orbiter. The final scenario is shown in Table 5.33c where focus is put on robustness. In this scenario, the non-cooled LGA configuration is the best option due to its extreme simplicity and resistance to the harsh Venusian environment. Notably, the partially-cooled HGA + LGA configuration also scored very high in this tradeoff, only trailing by 2 points.

Table 5.33: Sensitivity analysis for communication architecture trade-off.

(a) Size and mass constrained trade-off outcome.

Communication Architecture	Score
Disposable HGA + LGA	64
Part. Cooled HGA + LGA	82
Part. Cooled LGA	73
Uncooled HGA + LGA	50
Uncooled LGA	65

(b) Power constrained trade-off outcome.

Communication Architecture	Score
Disposable HGA + LGA	70
Part. Cooled HGA + LGA	92
Part. Cooled LGA	79
Uncooled HGA + LGA	58
Uncooled LGA	69

(c) Robustness focused trade-off outcome.

Communication Architecture	Score
Disposable HGA + LGA	65
Part. Cooled HGA + LGA	70
Part. Cooled LGA	79
Uncooled HGA + LGA	39
Uncooled LGA	81

Thus, it can be concluded that the option involving a partially cooled efficient high-gain antenna, along with low-gain antenna(s) for greater coverage and data redundancy, is the most optimal system for the KYTHERA mission and will be selected as the final communication architecture. Due to the inability to integrate an active pointing system onboard the lander, the HGA will still need to have a relatively large half-power beam-width (HPBW), ensuring line-of-sight (LOS) and communication with the orbiter for as long as possible during its orbital period. However, the antennas are designed for no partial cooling as the current stage, ensuring that in the event of cooling system failure, the antenna will still have a sufficient link margin to accommodate the increase in thermal noise temperature and decreased efficiencies. The material selection will also need to be able to withstand ambient Venusian conditions.

A monofilar right-hand circular polarized (RHCP) axial mode helical antenna is hence chosen for its compact size, simplicity, strong signal integrity due to circular polarization, and good environmental tolerances, especially in a partially cooled environment. In this final configuration, a quadrifilar RHCP helical antenna (QHA) will also be included for a full omnidirectional coverage for additional data transmission when the orbiter is away from the apoapsis. The receiver antenna onboard the Venus orbiter will also be RHCP to minimize polarization loss. The comprehensive overview, including lists regarding sizing values, link parameters, and material selection, is discussed in the next section.

5.4.4 Communication Subsystem Overview

In this section, the final values and budgets for various parameters for the communications subsystem will be shown. Accommodating the large ground planes of the antennas while keeping the two antennas at least 25 cm apart led to the design decision to use a coating directly on the antennas rather than constructing radomes. The dimensions for the antenna structure and their preliminary material selections are discussed in the sections below.

Link Budgets Overview

With the communication bands and the antenna types chosen, the link budget is revised and values are refined with multiple estimation methods [128, 129, 140]. Below in Table 5.34, the final calculated uplink link budgets can be seen for both the axial monofilar helical high-gain antenna and the low-gain helical quadrifilar antenna, respectively.

Table 5.34: KYTHERA communication uplink link budgets.

(a) Primary high gain helical antenna uplink link budget.

General Parameters		
Frequency	1.2	GHz
Wavelength	0.250	m
Distance between antennas	65800	km
Lander Transceiver (Transmission Mode)		
Transmitter Power	44.77 (30)	dBm (W)
Transmitter Efficiency	0.6	—
Transmitter Cable Loss	-1	dB
Transmitted Power	43.77 (23.82)	dBm (W)
DC Power Supply	50	W
Modulation Scheme (BPSK) Measurement Bandwidth	300	Hz
FEC Performance Ideal (Convolutional + RS)	-1.5	dB
FEC Performance Real	-1	dB
Channel Maximum Capacity (60%)	915.9	bps
Lander Transmitting Antenna		
Circumference	0.250	m
Diameter	0.080	m
Coil Spacing	0.062	m
Number of Turns	6	—
Antenna Efficiency	0.6	—
Gain (Linear)	13.5	—
Gain (Log)	11.30	dBi
-3dB Beam Width	42.46	deg
EIRP	53.07	dBm
Losses		
Free-Space Path Loss	190.39	dB
System Loss	2	dB
Atmospheric Loss	1	dB
Polarization Loss	0.2	dB
Orbiter Receiving Antenna		
Receiver Gain	30	dBi
Received Power	-108.52	dBm
Receiver Noise Temperature	100	K
Orbiter Noise Power	-153.83	dBm
Signal-to-Noise Ratio	45.31	dB
Target Bit Error Rate	1.00E-06	—
Eb/N_0 (AWGN)	9.50	dB
Eb/N_0 (Actual)	15.70	dBm
Link Margin	6.20	dB

(b) Secondary low gain quadrifilar helix antenna uplink link budget.

General Parameters		
Frequency	1.2	GHz
Wavelength	0.250	m
Distance between antennas	26600	km
Lander Transceiver (Transmission Mode)		
Transmitter Power	42.55 (18)	dBm (W)
Transmitter Efficiency	0.6	—
Transmitter Cable Loss	-1	dB
Transmitted Power	41.55 (14.29)	dBm (W)
DC Power Supply	30	W
Modulation Scheme (BPSK) Measurement Bandwidth	300	Hz
FEC Performance Ideal (Convolutional + RS)	-1.5	dB
FEC Performance Real	-1	dB
Channel Maximum Capacity (60%)	870.6	bps
Lander Transmitting Antenna		
Circumference	0.333	m
Diameter	0.106	m
Coil Spacing	0.067	m
Number of Turns	2	—
Antenna Efficiency	0.600	—
Gain (Linear)	1.765	—
Gain (Log)	2.467	dBi
-3dB Beam Width	360.00	deg
EIRP	42.02	dBm
Losses		
Free-Space Path Loss	182.52	dB
System Loss	2	dB
Atmospheric Loss	1	dB
Polarization Loss	0.1	dB
Orbiter Receiving Antenna		
Receiver Gain	30	dBi
Received Power	-111.60	dBm
Receiver Noise Temperature	100	K
Noise Power	-153.83	dBm
Signal-to-Noise Ratio	42.23	dB
Target Bit Error Rate	1.00E-06	—
Eb/N_0 (AWGN)	9.50	dB
Eb/N_0 (Actual)	12.83	dB
Link Margin	3.33	dB

Values regarding orbiter communication architecture are estimated and taken from industy as the complete design of the orbiter's communication system is outside the scope of the current design phase. The receiver noise temperature value is given as an estimate for the temperature at the receiver antenna, assumed to be 100 K, taken from industry [144]. Another value is the receiver antenna gain of 30 dBi, estimated based on different communication band frequencies, taken from industry[55]. It can be seen that the uplink link margin from the primary antenna is around 6.2 dB, and the secondary antenna has a link margin of around 3.3 dB, indicating the receiver antenna onboard the orbiter can pick up the transmitted signal and has a moderate margin to accommodate any unexpected losses. The signals emitted from the QHA are too weak for detection at the orbiter around the apoapsis, restricting its use to close orbital ranges at approximately 26600 km. A conservative estimate of the total power required for the monofilar helical antenna is approximately 50W and 30W for the QHA during transmission mode. The values in the brackets correspond to watts, whereas the numbers outside of the brackets correspond to decibel-milliwatt (dBm). The calculated half-power beamwidth of the high-gain antenna is around 43°, which is sufficient to maintain LOS with the orbiter throughout the mission duration, accounting for retrograde rotation of 300° of Venus.

Encoding and modulation also play a key role in the performance of the uplink system. For the lander transceiver, Binary Phase Shift Keying (BPSK) is chosen as the modulation technique for its robustness against additive Gaussian white noise and simplicity in low data rate planetary missions [145, 146]. A conservative estimate for the measurement bandwidth of BPSK is around 300Hz. An additional advantage of BPSK is that it possesses the lowest required Eb/No for a target bit error rate (BER). A plot showing this for different modulation schemes can be seen in Figure 5.43. For this mission, a target BER of 1e-06 was chosen, which had a required energy-per-bit to noise-power spectral density ratio (Eb/No) of 10.5 dB. However, this is under ideal conditions where it operates in an Additive White Gaussian Noise (AWGN) channel. This value can further be decreased with Forward Error Correction (FEC) schemes, where the lower performance Reed-Solomon and Convolutional coding is used, mainly for its low computational power requirement [147]. This FEC scheme

[55] `https://deepspace.jpl.nasa.gov/dsndocs/810-005/`, accessed on 15/May/2025.

also has an impact on the data rates that can be achieved for the channel, as older schemes tend to have around 1.5dB loss (ca. 70% efficiency) compared to the theoretical maximum calculated with the Shannon-Hartley formula depicted in Equation 5.13. Due to the large volume of data generated by the lander's instruments, a large data rate is required; this means that for uplink to the orbiter, the channels' maximum capacity will be utilized at 915.9 bps for the HGA and 870.6 bps for the LGA.

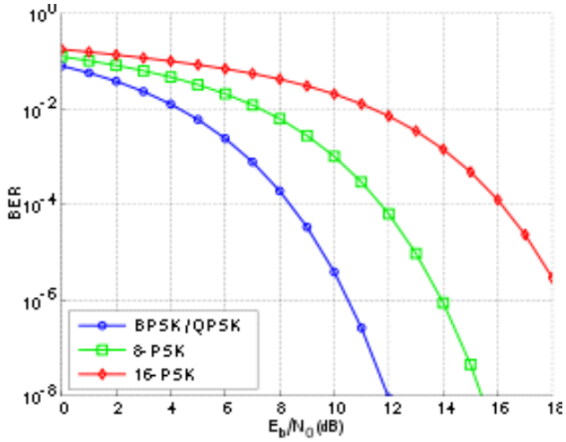

Figure 5.43: Eb/No vs BER for different modulation schemes [148].

$$R_D = B \cdot \log_2(1 + \text{SNR}) \tag{5.13}$$

where R_D is the data rate in bit/s, B is the channel bandwidth in Hz and SNR is the signal-to-noise ratio (linear).

Next, the downlink link budgets for the lander are calculated for both antennas, as seen in Table 5.35. The downlink link budget is for command downlink from the orbiter to the lander, such as changing the operational status of scientific instruments or requests for priority for certain measurements. The transmitting antenna has no detailed design or architecture as it will require extensive research, calibration, and trade-offs, all of which will be conducted in the following design phases. Additionally, the command packets are usually compact in size, usually 256 or 512 bits. For this reason, the communication channel for downlink does not need to operate at maximum capacity and is instead set to cap at around 400 bps, reducing cost, complexity, and increasing the link margin. The same modulation and FEC schemes will be used on the orbiter, with improved transmitter power, transmitter efficiency, and antenna efficiency due to the more manageable environment in space. It should be noted that since the antenna will endure ambient temperatures on the Venusian surface, the noise temperature of the receiver system will be significantly higher than the orbiter's, at around 800K, taking into account both the antenna temperature and the actively cooled transceiver temperature. With these constraints, the calculated link margin for the HGA is 3.74 dB, and 2.2 dB for the LGA, which will be sufficient for command downlinks.

Table 5.35: KYTHERA communication downlink link budgets.

(a) Primary high gain helical antenna downlink link budget.

General Parameters		
Frequency	1.2	GHz
Wavelength	0.250	m
Distance between antennas	65799800	m
Orbiter Transmitter		
Transmitter Power	46.58 (45.5)	dBm (W)
Transmitter Efficiency	0.7	—
Transmitter Cable Loss	-0.5	dB
Transmitted Power	46.08 (40.55)	dBm (W)
DC Power Supply	65	W
Modulation Scheme (BPSK) Measurement Bandwidth	300	Hz
FEC Performance Ideal (Convolutional + RS)	-1.5	dB
Data Rate Cap	400.00	bps
FEC Performance Real	-1	dB
Orbiter Trasmitting Antenna		
Antenna Efficiency	0.75	—
Gain (Log)	30	dBi
EIRP	74.08	dBm
Losses		
Free-Space Path Loss	190.39	dB
System Loss	2	dB
Atmospheric Loss	1	dB
Polarization Loss	0.2	dB
Lander Receiving Antenna		
Receiver Gain	11.97	dBi
Received Power	-105.54	dBm
Receiver Noise Temperature	800	K
Noise Power	-144.80	dBm
Signal-to-Noise Ratio	39.26	dB
Target Bit Error Rate	1.00E-06	—
Eb/N_0 (AWGN)	9.50	dB
Eb/N_0 (Actual)	13.24	dB
Link Margin	3.739	dB

(b) Secondary low gain quadrifilar helix antenna downlink link budget.

General Parameters		
Frequency	1.2	GHz
Wavelength	0.250	m
Distance between antennas	26596000	m
Orbiter Transmitter		
Transmitter Power	46.58 (45.5)	dBm (W)
Transmitter Efficiency	0.7	—
Transmitter Cable Loss	-0.5	dB
Transmitted Power	46.08 (40.55)	dBm (W)
DC Power Supply	65	W
Modulation Scheme (BPSK) Measurement Bandwidth	300	Hz
FEC Performance Ideal (Convolutional + RS)	-1.5	dB
Data Rate Cap	400	bps
FEC Performance Real	-1	dB
Orbiter Transmitting Antenna		
Antenna Efficiency	0.75	—
Gain (Log)	30	dBi
EIRP	74.08	dBm
Losses		
Free-Space Path Loss	182.52	dB
System Loss	2	dB
Atmospheric Loss	1	dB
Polarization Loss	0.1	dB
Lander Receiving Antenna		
Receiver Gain	2.467	dBi
Received Power	-107.07	dBm
Receiver Noise Temperature	800	K
Noise Power	-144.80	dBm
Signal-to-Noise Ratio	37.72	dB
Target Bit Error Rate	1.00E-06	—
Eb/N_0 (AWGN)	9.50	dB
Eb/N_0 (Actual)	11.70	dB
Link Margin	2.204	dB

System Parameters

The antenna sizing is determined through both link budget analysis and industry standards, while the transmitter is sized using off-the-shelf L-Band transmitter components[56], with partial modification for integration into the KYTHERA lander. The transmitter will be mounted on the top of the coldbox section and will be actively cooled. A custom coaxial cable will connect the transmitter to the antenna ground plate located on top of the drag plate, which operates at around ambient temperature. Initial designs proposed a single communication dome, but this was deemed not the most optimal due to the required antenna spacing larger than the wavelength (25 cm) for the selected bandwidth. Additionally, the high environmental tolerances of the antennas allow them to survive ambient conditions, apart from potential corrosion over the mission duration from the extremely high concentrated CO_2 on the Venusian surface, which can react with a multitude of materials to create corrosive compounds. To combat this, a silica coating will be applied to the exposed surfaces of both antennas, including the helix, ground plates, and parts of the coaxial cables. Silica is known for its high corrosion and temperature resistance, low permittivity, and dielectric loss. Table 5.36 shows all the subsystem parameters, and Table 5.37 is the overall budgets of the communication subsystem.

Table 5.36: KYTHERA communication subsystem parameters.

Main Helical Antenna			**Secondary Quadrifilar Antenna**			**Transmitter**		
Helix Height	37	cm	Helix Height	15.4	cm	Transmitter Length	19	cm
Helix Diameter	8	cm	Helix Diameter	10.6	cm	Transmitter Width	7	cm
Helix Windings	6	—	Helix Windings	2	—	Transmitter Height	3	cm
Helix Thickness	1	cm	Helix Thickness	1	cm	Trasmitter Mass	1.5	kg
Ground Plate Radius	20	cm	Ground Plate Radius	20	cm	**Main Antenna Mounting**		
Ground Plate Thickness	2	cm	Ground Plate Thickness	2	cm	Base Profile Length	17.8	cm
Coaxial Cable Length	80	cm	Coaxial Cable Length	80	cm	Base Height	6.6	cm
Coaxial Cable Outer Thickness	2	cm	Coaxial Cable Thickness	2	cm	Base Angle	10.4	deg
Cable Coating Thickness	0.03	mm	Cable Coating Thickness	0.03	mm	Mounting Length	19	cm
Main Antenna Mass	11.2	kg	Secondary Antenna Mass	4.2	kg			

[56] `https://www.everythingrf.com/search/microwave-rf-amplifiers/filters?page=1&country=global&manuid=;174;`, `https://www.safran-group.com/products-services/ewc36-band-transmitter`, accessed on 05/Jun/2025.

Table 5.37: KYTHERA communication subsystem budgets.

Mass (kg)	Power Transmission Mode (W)	Power Science Mode (W)	Cost (M€ FY2025)
16.9	50	30	7

The material selection is also crucial to ensure a long-living communication architecture. The antenna, ground plane, as well as part of the coaxial cable will be exposed to the harsh environment of the Venusian surface. The material selection for these components can be seen below in Table 5.38. The material selection procedure was focused on finding a balance between high survivability, thermal, corrosion resistance, and conductivity for minimal signal degradation. These choices will be tested and refined in the following design phases to ensure ideal compatibility and performance.

Table 5.38: Material selection for the antenna structure.

Component	Material	Justification
Helical Conductor - Base	Glidcop AL-15	High mechanical strength, good electrical conductivity, good corrosion resistance, easily formed and machined
Helical Conductor - Intermediate Layer	Alumina	Intermediate layer required as the thermal expansion coefficient between the base and coating are different
Helical Conductor - Coating	Fused Silica	Excellent corrosion resistance, high temperature tolerance, invisible to electromagnetic radiation
Ground Plane - Base	Glidcop AL-15	High mechanical strength, good electrical conductivity, good corrosion resistance, easily formed and machined
Ground Plane - Intermediate Layer	Alumina	Intermediate layer required as the thermal expansion coefficient between the base and coating are different
Ground Plane - Outer Coating	Fused Silica	Excellent corrosion resistance, high temperature tolerance, invisible to electromagnetic radiation
HGA Mounting - Base	Inconel 718	Excellent thermal tolerance, high corrosion and creep resistance
Coaxial Cable - Inner Conductor	Glidcop AL-15	High mechanical strength, good electrical conductivity, good corrosion resistance, easily formed and machined
Coaxial Cable - Dielectric Layer	Silicon Dioxide	High electrical insulation, low permittivity, high strength and chemically inert
Coaxial Cable - Outer Conductor	Silver-Plated Copper	High conductivity, silver provides good corrosion resistance high melting point
Coaxial Cable - Sheath	Inconel 718	Excellent thermal tolerance, high corrosion and creep resistance

Deployment, Pointing Mechanism and Relay Window

The orbiter will be in a polar orbit, meaning that the antenna's apoapsis will be above the North Pole of Venus, and in order to maximize data transmission capacity, the antenna will have to be pointed towards Venus's celestial north. Hence, a singular use pointing mechanism is developed to orient the antenna towards the north pole of Venus. The antenna alongside with the ground plate is preset to have an offset angle of around 20°, which is calculated through the difference between the north pole (90° N) and the landing site latitude (ca. 70° N). However, the spin of the lander around its vertical axis during EDL makes it unreliable to predetermine the azimuth, so the antenna cannot be preset to orient towards the orbiter. The developed pointing mechanism uses a short-lifetime motor, encased in a motor housing attached to the bottom of the ground plate mounting. The motor stage will be able to rotate the helical antenna by 180° in either direction. As the orbiter enters the apoapsis, ping signals are sent for the lander to pick up, and the lander will then assess the signal strength at different azimuths to find the optimal orientation of the lander. This process is done multiple times and averaged to determine a final orientation of the antenna. The motor then rotates the antenna to the target orientation and locks in place, after which the motor will be decommissioned and will thermally degrade over the following hours. A complete pointing mechanism flow diagram can be seen below in Figure 5.44.

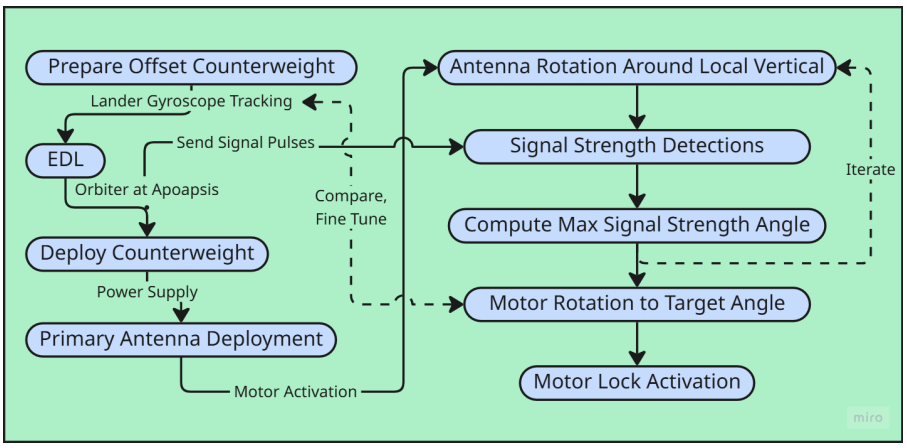

Figure 5.44: Pointing mechanism flow diagram.

From this, it is now possible to calculate the relay model, for which a simulation was made, and the results can be seen below in Figure 5.45. As can be seen from Figure 5.45, the primary antenna covers the apoapsis of the orbit where the orbiter has the slowest velocity in order to maximize the communication window. The secondary antenna provides additional relay time during science mode when the orbiter passes close to the lander and also acts as a redundancy measure in the event of primary antenna failure. The omnidirectional coverage is limited, as during most of the orbit near the periapsis, the lander and orbiter will not maintain LOS. The horizon plane displayed in the plot is directly affected by the lander location and can be optimized by increasing latitude or altitude when choosing landing sites. The omnidirectional coverage overlay shown is a preliminary approximation of the QHA radiation pattern, and a more realistic model will be generated in the coming design phases.

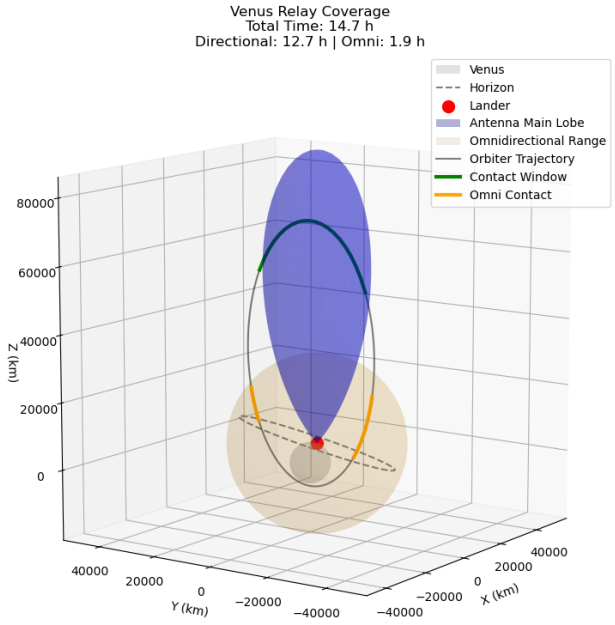

Figure 5.45: Relay window simulated model.

Now that the relay time is known per 24-hour orbit, through the Shannon-Hartley theorem, assuming 0.6 efficiency due to the harsh environments on the Venusian surface, the total transmission channel capacity can be calculated. The final maximum capacity data rates from both antennas are significantly higher than that of the previously suggested 300 bps data rate. These new values allow for more transmission capacity and ensure as much data is sent back to Earth for analysis as possible. The total capacity per 24 hours can be seen in Equation 5.14.

$$(915.9 \cdot 12.7 + 870.6 \cdot 1.9) \cdot 3600 = 47.83\text{Mbits} = 5.98\text{MB} \tag{5.14}$$

The lander is able to transmit around 6 MB per complete orbit, and this value will not be affected significantly by the

rotation of Venus. It will also be iterated as the simulations will be refined, and a more detailed design will be completed on the communication subsystem components.

Orbiter-Earth Communication Architecture

The communication subsystem onboard the orbiter plays a major role in the mission, serving as the relay between the lander and Earth ground stations. It possesses two key functions: uplinking all collected science and housekeeping data and downlinking commands from mission control. To accommodate these functions, the orbiter will be equipped with two antennas: an L-band (1.2 GHz) high-sensitivity parabolic dish antenna, serving as both the uplink and downlink antenna between the orbiter and the lander. The antenna employs a time-division duplexing scheme to efficiently switch between receiving and transmitting signals [149]. Additionally, the receiving/transmitting antenna must also be RHCP to have minimal polarization losses [150]. The second antenna will be a high-gain parabolic dish antenna capable of communication to the Estrack antennas on Earth. Both uplink and downlink will be done via X-band at 8.4 GHz.

5.4.5 Further Optimization and Considerations

The communication subsystem presents significant potential for further research, mainly in component selection, materials, and manufacturing processes. To optimize the transceiver's efficiency, a detailed design of all its components and electronics will be conducted. Since the transceiver will operate within the coldbox of the lander, its components do not require high temperature tolerance.

The partial cooling option of the antennas is still left to be explored. With the current configuration, the communication subsystem is able to maintain a communication link with the orbiter at ambient conditions, although much can still be optimized if partial cooling is employed. There will be reduced losses, improved antenna efficiency, and a drastically reduced thermal noise temperature. Concerns regarding the integration of such a partial cooling system include mechanical complexity, additional costs, and restrained freedom of movement in the coaxial cable.

The coaxial cable connecting the transmitter and the antennas will also be a key focus of further research. Currently, the cable will be coated with an extremely brittle ceramic, which will crack and shatter if exposed to strong loads. The pointing system requires the coaxial cable to have degrees of freedom of 180° in both directions. This might damage the coating and, in turn, induce corrosion and degradation of the cable. A potential mitigation procedure is researching and testing for a more compatible material that provides both corrosion resistance and flexibility. Furthermore, there are concerns regarding material compatibility, specifically in terms of thermal expansion. Large differences in thermal expansion coefficients result in deformation and fractures under high temperature changes, such as during descent. A way to minimize the effect of this is to include inter-layers with a thermal expansion coefficient between that of the main conductor and the coating.

A more detailed design of the orbiter's communication architecture will be developed in later phases of the KYTHERA mission. While the current design establishes the general framework, further study is needed for antenna selection, link budget analysis, and software optimization to maximize efficiency for both lander-orbiter links and orbiter-Earth links. For instance, advanced modulation schemes such as Quadrature Phase Shift Keying (QPSK) and FEC schemes such as Low-Density Parity-Check (LDPC) can be used to not only drastically increase theoretical maximum channel capacity, allowing for higher data transmission capacity but also higher efficiencies [151]. The communication flow diagram seen in Appendix D depicts a preliminary design for the entire communication process, and will be iterated and refined in subsequent design phases.

5.5 Command and Data Handling

The Command and Data Handling (CDH) system functions as the central intelligence of the lander, generating and coordinating a wide range of critical tasks across all onboard subsystems. As can be seen in the Data Handling Block Diagram shown in Figure 5.46, the CDH receives data from various inputs including scientific instruments, housekeeping sensors, the power and the thermal unit. These inputs are routed through the sensor interface, which ensures that all incoming signals are correctly interpreted and assigned to the appropriate processing streams. The command handling unit manages the distribution and execution of commands originating from the orbiter or generated autonomously by onboard systems. Meanwhile, the data processing unit organizes, formats, and prepares scientific data for downstream tasks, and this task is closely monitored by the instrument health monitoring system which continuously assesses the operational status and integrity of all connected instruments and sensors.

Once the data has been processed, it enters the data storage and handling section of the CDH. Here, the information is compressed to optimize storage and transmission efficiency, filtered to remove unnecessary or redundant content, and then packaged and scheduled for delivery. This delivery either goes toward long-term storage or toward the encoder interface for transmission back to the orbiter and then Earth. Here data and commands are encoded and decoded, and then sent to the communication interface where modulation and demodulation takes place before being sent to spacecraft. The following steps of communication are explained in more detail in the communications subsystem in Section 5.4.

The CDH also plays a crucial role in controlling the Entry, Descent, and Landing (EDL) phase of the mission. It interprets real-time input from EDL sensors and issues deployment commands to the parachute, the heat shield, and the aeroshell. Meanwhile, the fault handling unit within the CDH is responsible for fault detection and response. It monitors the system for anomalies and starts a transition to safe mode when necessary in order to preserve the lander's integrity and ensure mission survival.

The CDH system runs in coordination with the spacecraft's clock, which handles accurate timing and helps keep all activities and data properly aligned. This is important for keeping different parts of the lander working together without conflict. The CDH also communicates with the power system, which is responsible for how power is shared, when to activate the generator, and how to manage the batteries through their charging and discharging cycles. By staying connected to both timing and power systems, the CDH keeps the lander stable and able to respond on its own. This allows the mission to continue smoothly while keeping track of both operations and scientific tasks.

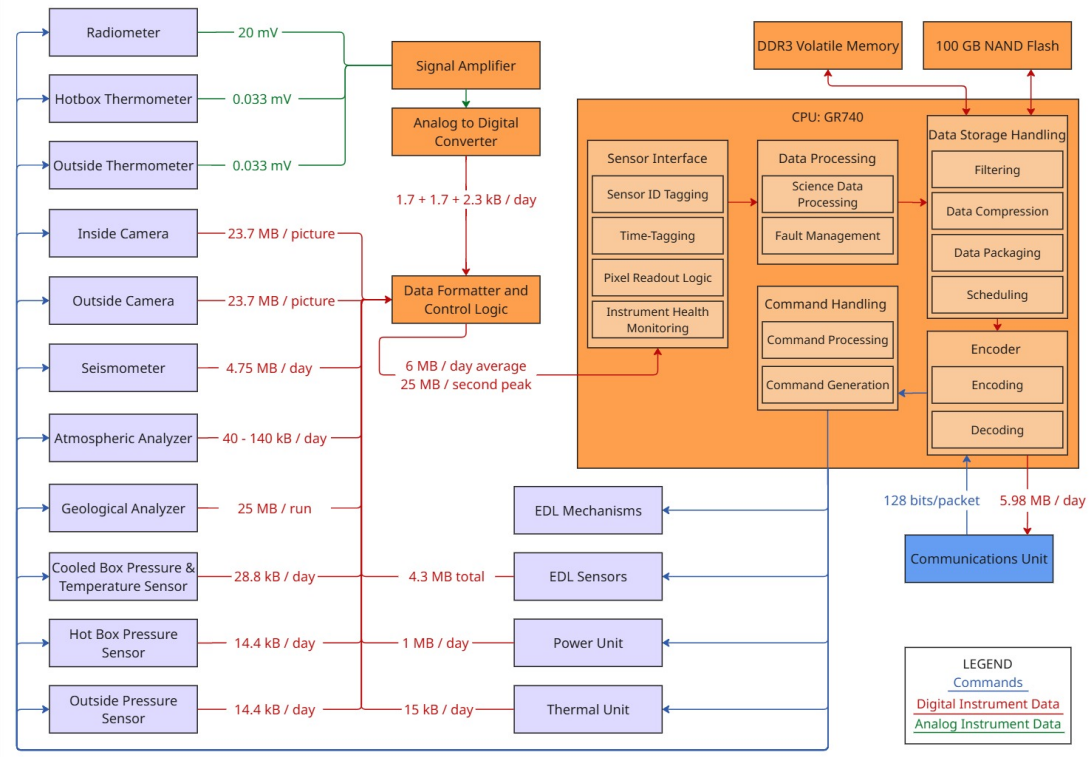

Figure 5.46: Data handling block diagram.

5.5.1 Requirements

Based on the previously mentioned functions, a set of requirements for the CDH system has been generated. Some of the most driving ones can be found below, in Table 5.39. Other less relevant requirements can be found in the Baseline and Midterm Report.

Table 5.39: Requirement compliance of command and data handling.

ID	Requirement Description	Verification	RC
CDH-1	The CDH subsystem shall validate telecommands received from the orbiter.	V-TST-FUN	✓
CDH-2	The CDH subsystem shall dispatch validated commands to the appropriate subsystem for execution.	V-DEM-TSK	✓
CDH-3	The CDH subsystem shall acquire, time tag, and store scientific and housekeeping data.	V-DEM-TSK	✓
CDH-6	The CDH subsystem shall support a data acquisition rate of at least 100 MBps from payload instruments.	V-DEM-TSK	✓
CDH-7	The CDH subsystem shall store a minimum of 100 GB of scientific and housekeeping data.	V-DEM-TSK	✓
CDH-9	The CDH subsystem shall format telemetry according to the CCSDS packet telemetry standard.	V-INS-SFT	✓
CDH-10	The CDH subsystem shall provide timestamping accurate to within ±1 ms using onboard clock synchronization.	V-DEM-TSK	✓
CDH-14	The CDH subsystem shall autonomously enter a safe state in response to predefined fault conditions.	V-DEM-TSK	✓
CDH-15	All CDH software shall be developed according to DO-178C or ECSS-E-ST-40C software engineering standards.	V-INS-SFT	✓

The description of verification method IDs are found in Table 4.1.

5.5.2 Subsystem Hardware

The GR740 processor was selected as the CPU model to serve as the central interactive element within the CDH system, managing the coordination between volatile and non-volatile memory resources to ensure reliable operation and efficient data handling. It interfaces directly with high-speed DDR3 volatile memory, which is used to support real-time computing tasks, such as data buffering, instrument control, and temporary storage of telemetry packets awaiting transmission. This dynamic memory enables the GR740 to run the onboard software, process commands, and respond to time-sensitive inputs from sensors with low latency. In parallel, the GR740 communicates with a non-volatile memory unit, in this case the NAND flash managed by an external controller, which is used for storing persistent mission data including science observations, logs, and system states. This memory interaction allows the GR740 to write long-term data asynchronously while maintaining active engagement with the live systems of the lander. Together, these two forms of memory enable the GR740 to function as an intelligent hub, capable of managing both immediate operations and long-duration data preservation in a seamless and coordinated manner. The budgets for the different components of the CDH can be found in Table 5.40. The GR740 CPU chip itself is very lightweight, weighing less than 20 grams. However, most of the mass accounted for the CPU, approximately 1 kg, comes from estimating the weight of the complete Single Board Computer, which includes the processor along with supporting components such as memory chips, power regulators, connectors, and the printed circuit board.

Table 5.40: Budget breakdown and dimensions of the CDH.

	Power (W)	Mass (kg)	Cost (M€ FY2025)	Dimensions
GR740	5 [57]	1	0.1 [58]	96 mm x 120 mm [59]
DDR3 [60]	3	0.1	0.1	133 mm x 30 mm
NAND Flash	0.5	0.450	1 [61]	15 mm x 20 mm

5.5.3 Generated Data

When designing the CDH subsystem, it is important to have an overview of all the data that the different instruments will be feeding into it, and their respective sizes. For this reason, an estimation has been performed. It is important to note that only a part of this data will get sent back to earth due to the limitations of communication.

- Cameras: The cameras have a resolution of 3840 by 2160 pixels, resulting in a total of 8,294,400 pixels using 3 bytes each for red, blue and green values. This means every picture will have a raw size of 23.7 MB. A minimum of 10 pictures shall be taken during landing and a minimum of 4 shall be taken on the surface.
- Seismometer: Because of the limited amount of technical information available about the NASA Glenn seismometer, the amount of generated data has been approximated by looking at seismometers used during similar missions. The seismometer used during the InSight mission to Mars for instance, stands out as a good analog example, and has a documented data production of 4.75 MB per day[62]. The seismometer will be recording continuously throughout the whole mission.
- For each atmospheric sampling run, the Venus Mass Spectrometer is expected to generate approximately 5.5 megabytes of data. This estimate is based on a configuration that uses 5000 mass bins per spectrum to achieve the resolution necessary for accurate identification of trace gases and isotopic ratios. Each bin is recorded with a depth of 2 bytes to provide sufficient dynamic range. Assuming 500 spectra are collected per run, the total raw data volume amounts to 5 megabytes. An additional 10 percent is included to account for metadata such as timing information, system status, and calibration data, resulting in a total of approximately 5.5 megabytes. This data volume is well aligned with the scientific objectives of the instrument and aligns within the expected limitations of onboard storage and data handling resources.
- Geological Analyzer: Assuming each chemical analysis using LIBS and time-resolved Raman spectroscopy generates approximately 25 MB of data, performing 20 analyses would produce a total of around 500 MB. This estimate is based on heritage data from NASA's SuperCam and ChemCam instruments, where the spectrometer unit collects hundreds of spectra per analysis, with about 15 MB for LIBS and 10 MB for Raman depending on the number of spectra and resolution.
- Pressure meter: Assuming a size of 4 bytes per pressure reading, the use of 3 pressure meters (one inside the cool box, one inside the hotbox and one outside), and a sampling rate of once every minute results in a total size of 43.2 kB per day.

[57] https://www.gaisler.com/products/gr740#downloads, accessed on 17/Jun/2025.
[58] https://www.ebay.com/itm/256939579411?, accessed on 17/Jun/2025.
[59] https://www.gaisler.com/products/gr740#downloads, accessed on 17/Jun/2025.
[60] https://media.digikey.com/pdf/Data%20Sheets/Micron%20Technology%20Inc%20PDFs/MT41J256M4,128M8,64M16.pdf, accessed on 15/Jun/2025.
[61] https://nl.rs-online.com/web/p/flash-memory/2737510, accessed on 17/Jun/2025.
[62] https://agupubs.onlinelibrary.wiley.com/doi/full/10.1029/2018EA000536, accessed on 02/Jun/2025.

- Thermometer: Again a size of 4 bytes per reading can be assumed as well as a time interval of one minute and the use of 3 thermometers resulting in the same amount of 43.2 kB per day.
- Radiometer: Assuming a 1-minute sampling interval, 4 channels, 16-bit resolution, and continuous operation, a data production rate of approximately 46.1 kB per day can be expected.

5.5.4 Image Compression

Images from the Sony IMX317 sensor, which has a high resolution and limited color depth, produce raw files around 23 megabytes. Given the restricted bandwidth available for sending data back from Venus, compressing these images is important. Past missions like Venera have shown that the Venus surface typically appears with low contrast and few color variations, which allows for more efficient compression. Lossless formats such as PNG and WebP are therefore well suited to this kind of content, reducing file sizes to around 1.2 to 2 megabytes while keeping the important visual details intact.

In situations where more compression is needed, lossy formats like JPEG and WebP can reduce the file size much further. JPEG brings it down to a few hundred kilobytes, though it tends to lose small features that might be important for scientific analysis. WebP's lossy mode offers a better balance, keeping more detail at similar sizes. Newer formats like HEIC can shrink files even more, but their performance with low-color images is less reliable. The lander will choose the best method based on the data link at the time, prioritizing image quality when possible, but still able to deliver useful pictures even under tight transmission limits.

5.5.5 Scientific Data Compression

It is required for the CDH system to perform compression of the raw scientific data generated by the lander's instruments to ensure that the information can be transmitted within the limited upload budget available. Each instrument produces a different amount of data in its raw form as previously listed. To reduce these volumes, the CDH uses a combination of compression methods. Lossless compression techniques such as Huffman coding and entropy encoding are used when data integrity is important, allowing file sizes to be reduced by removing statistical redundancies without losing any quality. For data generated by intruments for which some quality loss is allowed, such as spectrometer data, the CDH applies lossy compression algorithms, where compression rates and preservation of key spectral features is balanced. Downsampling and bit-depth reduction can be used by lowering the sampling frequency for slower changing measurements or by reducing the number of bits per sample when full resolution is unnecessary. These methods can reduce data sizes by factors of two to ten or more depending on the instrument and data type. For example, the 4.75 megabytes of seismometer data can realistically be compressed to about one to two megabytes per day, the 5.5 megabytes from the mass spectrometer might be lowered to around one and a half to three megabytes, and the large 500 megabytes from the geological analyzer could be compressed to between fifty and one hundred fifty megabytes. Smaller datasets such as the 46.1 kilobytes of radiometer data or 43.2 kilobytes of pressure and temperature readings can be compressed to just a few kilobytes.

5.6 Structures and Materials

When designing and sizing a complex structure such as KYTHERA, an iterative process is essential to arrive at the most optimal configuration. This process is driven by the load cases experienced throughout the mission, and their implications on material choice, geometry, and load paths. The following section outlines the requirements of this subsystem, load cases that define KYTHERA's structural design and the strategies used to withstand them, materials that can sustain the loads and environment, followed by the steps taken to size the lander components. The next steps to achieve a more optimized design is then detailed at the end of this section.

5.6.1 Requirements

Based on the functions for the mission and the subsystem, a number of requirements were formed. Table 5.41 lists the key and driving requirements for this subsystem. This table includes the requirement ID, its description, verification method, and whether the requirement compliancy (RC) was met.

Table 5.41: Requirement compliance of structures and materials.

ID	Requirement Description	Verification	RC
SMS-ENV-1	The external structure shall withstand external pressure loads of 93 bar with a safety factor.	V-DEM-PRE	✓
SMS-ENV-2	The structure and materials exposed to the Venusian atmosphere shall be fully operational at ambient temperatures of up to 464 °C.	V-DEM-TEM	✓
SMS-MAT-1	All structure and materials exposed to the Venusian atmosphere shall be corrosion-resistant in hot SO_2 atmosphere with ≤10 µm/year degradation.	V-DEM-COR	✓
SMS-MAT-2	CTE mismatch between adjacent bonded materials shall be $\leq 5\times10^{-6}$/K.	V-ANA-DOC	X
SMS-MAT-3	The energy-absorbing structure shall be made of foam and/or honeycomb materials.	V-ANA-DOC	✓
SMS-INT-1	The structure shall maintain an IP68-equivalent sealing integrity for the duration of the mission.	V-DEM-TSK	✓
SMS-INT-2	Subsystem components shall be integrated without obstructing other subsystems (e.g., cameras, instruments).	V-DEM-TSK	✓
SMS-LV-2	The structure shall survive landing shock loads at a terminal velocity of 8.5 m/s.	V-ANA-FEM, V-ANA-SIM	✓
SMS-LV-3	The natural frequency of the structure shall be ≥ 15 Hz.	V-ANA-SIM	✓
SMS-LV-4	The maximum acceleration during impact shall be less than the maximum acceleration during entry.	V-ANA-SIM	✓
SMS-LV-5	Structure shall be able to withstand a load of 120 g during the EDL phase.	V-ANA-FEM, V-ANA-SIM	✓
SMS-LV-6	All SMS structures shall be validated by FEA for buckling, creep, and fatigue.	V-ANA-FEM, V-ANA-SIM	X
SMS-LV-7	All SMS structures shall be validated by physical tests for buckling, creep, and fatigue.	V-DEM-TSK	X
SMS-BG-1	Total mass of SMS shall not exceed 190 kg with contingency.	V-INS-WEI	X
SMS-BG-2	Total cost of SMS shall not exceed 40M Euros with contingency.	V-ANA-CST	X

The description of verification method IDs are found in Table 4.1.

From the table, it can be seen that not all of the requirements have been complied with. The reasoning behind this will be discussed in more detail as they come up in the subsections that follow.

5.6.2 Defining Load Cases

KYTHERA experiences a variety of load cases across its mission timeline, from launch through entry, descent, landing, and extended surface operation. Each phase presents unique mechanical and environmental challenges that influence the structure's geometry, mass distribution, and material selection.

During launch, the lander is subjected to a range of loads due to interactions with the launch vehicle. These are categorized into quasi-static, dynamic, and shock loads. Quasi-static loads arise from the vehicle's acceleration and are present as continuous axial forces that compress the structure. Dynamic loads, including vibrations and acoustic excitation from rocket engines, can excite the lander's natural frequencies and must be accounted for, especially for slender or lightly damped members. Shock loads occur during discrete events such as stage separation , introducing transient impulses that may damage brittle components or overstress interface joints. To accommodate these loads, KYTHERA's structure is designed with high stiffness and appropriate safety factors, ensuring that its natural frequencies remain decoupled from expected excitation bands. Energy-absorbing materials and acoustic insulation are integrated to minimize damage from shock and acoustic loads during separation events.

The entry, descent, and landing (EDL) phase is structurally critical due to the intense mechanical and thermal environment during atmospheric entry. KYTHERA is expected to experience a peak deceleration of 120 g during entry. While the aeroshell absorbs a portion of this load, the internal structure of the lander must be capable of carrying the residual axial compression without local buckling, yielding, or failure at critical joints. Additionally, pyrotechnic separation events introduce localized shock loads. These are mitigated using reinforced load paths and energy-dissipating interfaces between the aeroshell and lander structure. Following entry, landing impact is another key load case. Despite atmospheric drag, the lander is expected to touch down at a vertical velocity of up to 10 m/s, including margin. This generates a high impulse shock concentrated on the impact ring and landing legs. To manage this, the impact ring will incorporate a foam structure to absorb impact energy and isolate the payload from excessive shock.

Once on the surface, KYTHERA must survive Venus's extreme environment for an extended duration. The primary load types during this phase include static structural loads, thermal loads, chemical exposure, and ambient pressure. The static loads arise from the lander's own weight under Venusian gravity, which is approximately 90 percent that of Earth. This means that as long as the structure can support its weight on Earth, it will be structurally intact under Venus gravity. The thermal loads stem from Venus's high surface temperature of 464 °C, which over time can induce thermal expansion, creep, and fatigue in structural members. These thermal effects are mitigated through the use of materials with low thermal expansion coefficients and high resistance to long-term heat exposure, as will be detailed in the materials section. In addition, as detailed in Section 5.3, the heat transfer in the system is taken into account to limit thermal loads. Chemical degradation is another concern due to Venus's CO_2-rich and sulfuric atmosphere. All externally exposed structural materials must be corrosion resistant or appropriately coated to withstand this harsh environment. Finally, Venus's surface pressure of approximately 93 bar acts on all exposed surfaces. Pressurized compartments, such as the electronics bay, must be designed as sealed pressure vessels with adequate wall thickness and geometry to resist external collapse, while maintaining safety

margins throughout the mission duration. In addition, the legs are designed to maintain stability on inclined or uneven terrain, up to a 10° slope. Although landing site selection partially mitigates this risk, worst case conditions must still be accounted for. Additionally, a one-leg-failure (OLF) condition is included in the design margins, ensuring that the structure remains stable and functional even if one landing leg fails structurally during touchdown.

Throughout all mission phases, KYTHERA's structure must be robust enough to endure extreme loads while remaining mass and volume efficient. This demands an iterative structural design process, beginning with definition of worst-case load cases, followed by sizing of key components through analytical and numerical methods, and then verified against criteria such as stress limits, buckling resistance, thermal stability, and corrosion durability. In accordance with SMAD [92], the structure will be designed for its load requirements, then verified to check if its natural frequency is agreeable. Therefore, loads that depend on dynamics reactions, structural vibrations in specific, will not be emphasized in the process, rather, the quasistatic and impact loads will mainly drive the decisions for component geometry, material selection, and safety margins, ultimately producing a design that is resilient, lightweight, and reliable throughout the entirety of the mission.

5.6.3 Material Allocation

Each of the components of the lander needs to be made out of a well-chosen material. This depends on the load case of that component - whether it needs to be strong in tension, strong in compression, stiff, etc. It also depends on the conditions this component will face during the mission - e.g. high temperatures, exposure to acids or humidity. In order to make a selection out of the thousands of materials available, a shortlist of engineering materials was made during the Midterm phase. An overview of these materials and their properties was made in a table, which was expanded continuously throughout the design up until this final report. The "materials master table" currently contains 43 materials and a selection of their physical, thermal, mechanical, electrical, corrosion and sustainability properties.

For the materials selection, the software ANSYS Granta was used [152]. This program contains a database of various engineering and non-engineering metals, ceramics, polymers and composites. It shows information about the materials' composition and use case, as well as the physical, mechanical, thermal, electrical and optical properties. It even includes sustainability, durability and processing characteristics. Next to the database function, ANSYS Granta also allows to plot materials charts, allowing easy comparison between subgroups of materials and visualization of such comparisons. The software proved an invaluable tool in the materials selection process for the different components of KYTHERA.

For each of the main components of the lander, materials trade-offs were performed. First, some "killer" criteria were defined: any materials in contact with Venus air must be operational in 464 °C. Additionally, for any structural component, a fracture toughness of at least 15 MPa $m^{1/2}$ is needed according to Ashby et al [153]. Hence, all materials that did not meet these two criteria were not considered for the trade-offs.

The criteria for the trade-offs, in general, were then as follows, although small deviations were made in some of the trade-offs to cater to the specific needs of each component:

- **Mass (Weight 3)**, incorporated as a density-based material index: a value for a certain material property or combination of properties that needs to be optimized for a certain load case. Since KYTHERA has a tight mass budget, this criterion has a high weight.
- **Cost (Weight 1)**, incorporated as a cost-based material index, i.e. the density-based material index multiplied by the cost per unit mass of the material. It should be noted that this is purely the material cost. Manufacturing cost is influenced by the manufacturability. Since material cost is not expected to be dominant, this criterion has a low weight.
- **Corrosion (Weight 3)**, a qualitative grade given to the corrosion behavior of the material in media relevant for Venus (sulphuric acid, SO_2, high-temperature). Since corrosion of materials can dangerously harm the mission, this criterion has a high weight, although coatings are available that might mitigate bad corrosion behavior of a material that otherwise scores well.
- **Sustainability (Weight 1)**, a qualitative grade based on information found in the safety datasheets of the material providers on the market. This includes both a human toxicity and an environmental hazard aspect. Since the design space for KYTHERA is narrow enough on its own, a low weight has been given to this criterion.
- **Manufacturability (Weight 2)**, a qualitative grade based on the processing properties given in ANSYS Granta, where necessary augmented with information from material providers. Materials that cannot be manufactured or welded cause delays in the design process and might require a redesign, causing this criterion to have a medium-high weight.

Most of the subsystems engineers performed their own materials selection. The materials for communication components are described in Section 5.4, and the thermal insulation and power materials are selected in Section 5.3. The structural component trade-offs, that is, those for the landing legs, landing ring, cooled and hotbox shells, windows and drag plate, are discussed here.

For the landing ring, the main priority is energy absorption. This can be achieved by a honeycomb or a foam. Since the exact load paths during landing are hard to predict (e.g. one of the lander's sides might hit the ground or a rock earlier), the isotropy of the foam was opted for. The superiority of foam was revealed in a trade-off in the Midterm report. However, it turned out to be hard to find information about metal foams. ANSYS Granta only contained information about aluminum foams, which do not have a high enough operating temperature to survive on Venus. During a Google Scholar search, steel foams were found. Such steel foam was used in the structural calculations, because it was the only option that could be found. The main disadvantage of steel foam is that not all steels are corrosion-resistant. This can be mitigated by using some form of liquid coating, using a foam based on a corrosion-resistant steel, or overdesigning the foam thickness and accepting that it will degrade over time (since its main function is fulfilled shortly after landing). Hence, further research is needed.

For the landing legs, a strong material needs to be selected. These legs will be loaded in compression. The material index in this case is $\frac{\rho}{\sigma_c}$ for mass optimization, and $\frac{C_m \rho}{\sigma_c}$ for cost optimization, with material density ρ, compression strength σ_c, and cost per unit mass C_m. However, thermal expansion should also be taken into account. Hence, for simplicity, the preliminary material for the legs was also set to steel, more specifically Stainless Steel 316. A proper trade-off was performed later, as discussed in Subsection 5.6.6, but there was no time left to still implement this material change in the design. Hence, for now, Stainless steel 316 is chosen for the lander legs, despite being suboptimal.

The next component is the cooled box shell. This is not a structural component, as there is no pressure difference or any other type of loading this shell has to withstand. The shell still needs to be there, however, to hold the instruments and provide protection against radiative heat transfer. The trade-off table for the cooled box material is shown in Table 5.42. The highest-scoring material is Stainless Steel 316. It scores well across the different criteria, being somewhat heavy but showing good cost and manufacturability properties. Additionally, it is reasonably sustainable. Hence, Stainless Steel 316 was chosen as the material for the cooled box shell.

Table 5.42: Materials trade-off for cooled box shell.

	Cost	**Manufacturability**	**Strength-to-Density**	**Conductivity**	**Thermal Tolerance**	**Sustainability**	
Weight	2.5	2.5	2	1	1	1	**Score**
Inconel 718	4	4	8	6	6	4	52
Inconel 625	2	6	6	8	8	4	52
Stainless Steel 316	10	10	2	4	10	6	74
Ti–6Al–4V	4	8	8	10	4	8	68
Invar 36	6	10	5	8	2	8	68
Hastelloy X-alloy	2	6	4	4	8	10	50
Zirconium Carbide	4	2	10	2	8	10	55

The material for the hotbox shell, as opposed to that for the coldbox, does need to withstand loads, a large pressure difference (93 bar), Venus temperatures, and corrosion by SO_2. Hence, some reshuffling in the trade-off criteria took place to put emphasis on what is important in this case. Table 5.43 shows the trade-off table for the hotbox material. Inconel 718 beats all other materials with an exceptionally high score of 80. It is very resistant against corrosion, very strong, and has acceptable sustainability, manufacturability and cost properties. Hence, Inconel 718 will be chosen for the hotbox shell material.

Table 5.43: Materials trade-off for hotbox shell.

	Corrosion	**Strength-to-Density**	**Thermal Resistance**	**Sustainability**	**Manufacturability**	**Cost**	
Weight	3	3	2	0.5	1	0.5	**Score**
Inconel 718	10	10	6	4	4	4	80
Inconel 625	10	6	8	4	6	2	73
Stainless Steel 316	4	2	10	6	10	10	56
Ti–6Al–4V	6	10	2	8	8	4	66
Hastelloy X-alloy	10	4	8	10	6	2	70

The final trade-off of this section is that for the drag plate. The drag plate was designed for stiffness rather than strength. It needs to maintain its shape in order to perform its function. Additionally, it needs to survive Venus temperatures and corrosion. The drag plate carries heavy components, namely the two Stirling generators and antennas, but the required load-bearing capacity will be provided through struts rather than by the plate itself. Hence, strength is not a design factor, and the relevant material indices are $\frac{\rho}{E^{1/3}}$ for mass optimization and $\frac{C_m \rho}{E^{1/3}}$ for cost optimization, with Young's modulus E. Table 5.44 shows the trade-off table for the drag plate material. The highest-scoring material is Hastelloy, followed by Inconel 718 and Titanium alloy Ti-5Al-2.5Sn-0.5Fe. However, Ti-5Al-2.5Sn-0.5Fe has outperforms Hastelloy vastly in

the stiffness-to-density and cost categories. It is not very corrosion resistant, but this can be solved with a coating. Hence, Ti-5Al-2.5Sn-0.5Fe will be chosen as the material for the drag plate.

Table 5.44: Materials trade-off for drag plate.

	Stiffness-to-Density	Cost	Sustain-ability	Corrosion	Manufacturability	
Weight	3	1	1	3	2	**Score**
Tungsten	4	1	5	8	7	56
Molybdenum	7	2	2	2	7	45
Stainless steel 316	7	6	1	2	9	52
Ti-5Al-2.5Sn-0.5Fe	10	10	5	3	6	66
Irridium	2	1	5	10	7	56
Inconel 625	7	4	3	6	5	56
Inconel 718	7	5	3	10	4	67
Hastelloy	7	4	8	10	5	73

As mentioned before, the materials selection for the communications subsystem has been discussed in Section 5.4. However, the communication components need to be protected from Venus' supercritical CO_2. The initial idea for this was to put the components in a protecting dome. This dome would need to be made out of a material that lets through signals, meaning it cannot be a metal (metals are not dielectric), while preventing gas leaks into the dome and keeping the desired pressure inside. Hence, it was decided to apply protective coating on the communications components.

To select a material to use, only Venus temperature-resistant, dielectric materials were considered. The relevant material indices are $\varepsilon_r \tan\delta\ \rho$ for mass and $\varepsilon_r \tan\delta\ \rho C_m$ for cost optimization, where ε_r is the material's dielectric constant and $\tan\delta$ is its dissipation factor. Silica scores very well in terms of mass, transmission, and cost. It also has acceptable sustainability and corrosion properties. It scores significantly better than all other considered materials. Hence, silica will be chosen as the coating for the communications components.

In conditions similar to Venusian, silica's corrosion rate is 0.5 µg/cm^2 hr [154]. Considering a 200 days (4800 hr) mission length, 2400 µg/cm^2 of silica will be lost by the planned end-of-life. Silica has a density of 2200 kg/m^3, allowing to calculate that $1.09 \cdot 10^{-3}$ cm^3/cm^2 or 0.0109 mm of silica will corrode over the lander's lifetime. A coating thickness of 0.03 mm hence provides a safety factor of almost 3, while still being incredibly thin and lightweight. This coating will protect the communications subsystem while still allowing it to function.

Table 5.45: Materials trade-off for communications dome/coating.

	Electromagnetic Transmission-to-Density	Cost	Sustain-ability	Corrosion	
Weight	3.25	2.25	1.25	3.25	**Score**
Alumina	1	4	8	10	38.5
Silica	10	10	5	5	65
Silicon Carbide	3	1	3	5	21
Silicon Nitride	6	2	6	4	36
Quartz	8	7	4	5	50.5
Glass Fiber (silica based)	8	6	3	6	47

In order for the instruments to be able to do their measurements, optically transparent windows will be needed. Four spectrometers and four cameras will each need a window on the coldbox, with four windows needed on the hotbox. Some of the materials options for these windows are: translucent alumina, silica, sapphire (with either 99.9% or 100% purity), and quartz. For thermal considerations, the emissivity of these windows needs to be low. Hence, sapphire was the best option, with an emissivity of 0.48[63]. Considering that the cost of pure sapphire is an order of magnitude higher than that of 99.9% sapphire [152] without significantly improved properties, the 99.9% purity version will be chosen for the windows.

That concludes the discussion of the materials selection. The relevant trade-offs have been discussed above. Their results and the chosen materials for the other subsystem components are summarized in Table 5.46. The properties of each of the used materials are shown in Table 5.47 and 5.48.

Some notes on the material properties tables need to be made.

- Unless otherwise specified, the properties are taken from the ANSYS Granta software [152].
- The properties of steel foam were taken from [155, 156]. The Young's modulus was not reported, but can be calculated according to $E_{foam} = E_{original}\left(\frac{\rho_{foam}}{\rho_{original}}\right)^2$ [153]. Some other data is missing for the steel foam, but these properties are not used in the design.

[63] `https://www.engineeringtoolbox.com/emissivity-coefficients-d_447.html`, accessed on 12/Jun/2025.

- Ceramics cannot yield, therefore their yield stress is indicated as ”N/A” (not applicable). Metals are conductors, therefore their dielectric constant is 1. For vacuum, most of the properties are also not relevant, hence these are also indicated as ”N/A”.
- The power system uses an unspecified nickel alloy and a material called Graphalloy for which no data is publicly available. These have hence not been taken up in the properties tables.

Table 5.46: Materials assigned to each of the subsystem components.

Subsystem	Component	Material	Subsystem	Component	Material
COM	Helix conductor	Gold plated gildcop AL15	SMS	Landing legs	Stainless steel 316
COM	Helix conductor	Aluminium oxide	SMS	Landing ring	Steel foam
COM	Helix conductor	Fused silica	SMS	Cooled box shell	Stainless steel 316
COM	Ground plane	Gold plated gildcop AL15	SMS	Hotbox shell	Inconel 718
COM	Ground plane	Aluminium oxide	THM	Insulation	Vacuum
COM	Ground plane	Fused silica	EDL	Drag plate	Ti-5Al-2.5Sn-0.5Fe
COM	Coaxial cable	Gold plated gildcop AL15	PAY	Windows	Sapphire 99.9
COM	Coaxial cable	Silica	POW	Stirling generator hot end	Molybdenum
COM	Coaxial cable	Inconel 718	POW	Stirling refrigerator components	Inconel X-750
COM	Coaxial cable	Silver-plated copper	POW	Stirling generator cold end	Inconel X-750
COM	Quarter-wave impedance transformer	Gold plated gildcop AL15	POW	Generator and cooler rejection radiator	Nickel
COM	Quarter-wave impedance transformer	Fused silica	POW	Generator and cooler regenerator matrix	Nickel alloy fiber (unspecified)
COM	Quarter-wave impedance transformer	Inconel 718	POW	Bearings/bushings	Graphalloy
COM	Coating on ground plane and helix	Fused silica	SMS	Connection rods between hot and coldbox	Silica glass fiber
COM	Cylindrical helix protection	Fused silica			
COM	Motor casing	Inconel 718			

Table 5.47: Properties of materials used on KYTHERA’s components.

Material	Density (kg/m^3)	Max T (K)	CTE (µm/m K)	κ (J/m K)	c_p (J/kg K)	σ_y (MPa)	σ_{ult} (MPa)	E (GPa)	Fracture toughness (MPa/m$^{1/2}$)	Fatigue strength, 10^7 cycles (MPa)
Aluminum oxide	3970	1840	8	26	775	N/A	300	373	3.3	276
(Fused) silica	2200	1373	0.57	2.21	1240	N/A	168	77.9	0.67	159
Gold plated gildcop AL15	8910	775	16.9	370	388	331	370	132	50	165
Inconel 718	8190	977	13	11.4	458	827	999	171	271	755
Inconel X-750	8290	1089	14	12.4	480	670	1140	191	116	660
Molybdenum	10220	2883	5.35	138	275	N/A	550	325	50	495
Nickel	8930	633	13.5	91	460	115	445	220	316	225
Steel foam	2300	823	14.5	N/D	N/D	67.5	192	13.72	N/D	N/D
Sapphire 99.9	3970	2223	5.6	43.5	768	N/A	273	460	1.5	246
Silica glass fiber	2190	1003	0.55	1.45	970	4890	5860	72.4	1	5270
Silver-plated copper	1050	463	19.9	422	240	300	340	73	64.9	170
Stainless steel 316	8000	1673	15.9	16.2	618	161	484	166	75	252
Ti-5Al-2.5Sn-0.5Fe	4510	593	9.88	13.8	662	420	546	89.3	100	450
Vacuum	0	N/A	N/A	0	N/A	N/A	N/A	N/A	N/A	N/A

Table 5.48: Properties of materials used on KYTHERA's components.

Material	Dielectric constant	Cost (€/kg)	Corrosion	Sustainability
Aluminum oxide	8 - 10	30.5 - 45.7	5	Not toxic to humans and environment. [157]
Fused silica	3.8	5.7 - 9.52	4; susceptible to corrosion when in contact with metals	Toxic when inhaled or ingested. Not carcinogenic. May have reproductive effects. Not expected to be a hazard to the environment.
Gold plated gildcop AL15	1	28.9 - 31.8	2; unacceptable in strong acids and oxidizes at 500°C	May cause irritation of skin, eyes and respiratory system. Not hazardous to humans and environment. Avoid release of dusts and fumes into environment though. [158]
Inconel 718	1	20.8 - 29.9	5	Nickel is toxic for humans and environment. Can cause cancer and/or fetal abnormalities.
Inconel X-750	1	27.7 - 37.1	5	Nickel is toxic for humans and environment. Can cause cancer and/or fetal abnormalities.
Molybdenum	1	59.6 - 65.4	2; susceptible to corrosion by strong alkalis and strong acids	Highly toxic to humans. Causes skin irritation and eye damage. Highly toxic to the aquatic environment. [159]
Nickel	1	19 - 27.2	4; slightly susceptible to corrosion by strong acids	Nickel is toxic for humans and environment. Can cause cancer and/or fetal abnormalities.
Steel foam	1	N/D	2; susceptible to corrosion by strong alkalis and strong acids, but more corrosion-resistant steels exist (e.g. 904L)	May cause allergic skin reactions, may cause cancer, causes damage to organs through prolonged or repeated exposure, not expected to be toxic to the environment.
Sapphire 99.9	7.5 - 11.5	2860 - 17100	5	Not toxic for humans. Highly toxic to the aquatic environment. [160]
Silica glass fiber	3.75	11.4 - 15.2	5; only corrodes in strong alkalis but that is not an issue on Venus	May cause cancer. Causes temporary irritation of eyes, skin and respiratory system. Not expected to be toxic to the environment. [161]
Silver-plated copper	1	573 - 748	3; good in all environments except in strong acids	Not expected to be toxic to humans or the environment. [162]
Stainless steel 316	1	5.48 - 8.65	3; susceptible to corrosion in contact with inorganic acids, alkalis, and sour oils and gases, fine otherwise	Toxic to humans and environment, suspected of causing cancer. [163]
Ti-5Al-2.5Sn-0.5Fe	1	19.9 - 26.9	4; good, but susceptible to stress corrosion cracking in chloride, halide, organic liquids, and N2O3	May cause irritation but fine apart from that. [164]
Vacuum	1	N/A	N/A	N/A

5.6.4 Component Design

With the load cases and materials for each component defined, the lander's structure can now be sized. This process is a rather iterative one, where certain parameters need to be predefined in order to get the dimensions desired. If these dimensions do not accommodate the conditions the lander needs to withstand, these initial conditions need to be redefined and the process is reiterated. The design and sizing of the components is done such that they abide by the design requirements and constraints while maintaining structural integrity.

Inner Sphere/Coldbox

The coldbox is the compartment of the lander that houses the components and payload which require active cooling. It does not have to hold any pressure, but must provide rigid mounting for the instruments and electronics. Additionally, the amount of heat leaking in must be minimized, mostly with the use of highly-reflective anti-infrared coatings, as explained in Section 5.3 and by reducing the size as much as possible. As shown in Section 6.2, this is constrained by its contents, which set a minimum diameter of 58 cm.

The bulk of the weight of the coldbox itself will come from the mounting and outer shell, payload and electronics excluded. As explained in Section 6.2, the design of the mounting of the instruments is outside the scope of this report, and is included as a recommendation for the future design of KYTHERA. This means that an estimation for the weight of the coldbox is difficult by itself. However, the Space Mission Analysis Handbook [92] provides a value for the ratio between structural mass and spacecraft mass:

$$m_{structures} \approx 0.12 m_{spacecraft} \tag{5.15}$$

Since this equation was derived for a use case far from KYTHERA's application, a very conservative stance is taken by doubling this ratio to 25%. In this case, Equation 5.15 is interpreted as follows: $m_{structures}$ is the mass of the coldbox itself, including mountings and the outer shell, but excluding payload and electronics, and $m_{spacecraft}$ is the mass of all the contents of the coldbox. As shown in Table 5.49, the total mass of the coldbox contents is $\sim$ 24 kg. Applying this methodology, a structural mass of $m_{structures} = 8$ kg is obtained.

	VMS	Cameras	Geochemical Analysis	CDH	Comms	Pressure sensor	Gyro & accelerometer	Total
Mass (kg)	5	1.4	14.7	0.5	1	0.3	0.8	23.7

Table 5.49: Masses of the items contained in the coldbox.

The material selection for the coldbox structure is explained in Table 5.42. In short, stainless steel is chosen for its low cost, very good manufacturability and excellent knowledge base of exploitation. The structure of the coldbox will consist of one or more decks, on which the instruments are mounted. It will be covered by a thin shell or a foil that is coated with the aforementioned highly reflective anti-infrared coating which will be supported by a grid structure. This is reviewed in Section 6.2.

Outer Sphere/Hotbox

In contrast to the coldbox, the shell of the hotbox is subjected to a significant external pressure of 93 bar by the dense Venusian atmosphere. This makes external pressure loading the dominant mechanical stress on the hotbox shell.

The mean diameter of the hotbox is constrained to 64 cm, such that there is a 6 cm difference in diameter between the coldbox and hotbox providing insulation between the two components. Given that the coldbox uses a radius of 58 cm with a thin wall, it is reasonable to expect that the hotbox will follow the thin-wall assumption as well. This assumption is later verified. While the hotbox will require a thicker shell to withstand the higher pressure, the wall thickness will still be small compared to the radius. This justifies applying the thin-wall approximation, allowing the use of the thin-walled hoop stress equation to estimate the required thickness:

$$\sigma_y = \frac{\Delta p \cdot D}{2 \cdot t} \cdot FS \tag{5.16}$$

Here, σ_y is the yield strength of the material taken from Table 5.47, Δp is the pressure difference (93 bar), D is the outer diameter of the shell, t is the wall thickness, and FS is the factor of safety, taken here as 1.5.

Rearranging this equation and solving for t yields a required thickness of approximately 5.340 mm. Since the radius-to-thickness ratio is still much greater than 10, the thin-wall assumption holds. For manufacturability and to provide additional margin, the thickness is rounded up to 5.5 mm. This thickness ensures that the hoop stress does not exceed the material's yield strength, even under worst-case loading.

It is important to note that the thin-wall hoop stress equation makes several simplifying assumptions: it assumes the stress is uniform through the wall thickness, and that the material behaves as linearly elastic, isotropic, and homogeneous. These assumptions may not fully hold under real-world conditions, meaning the calculated thickness could deviate from the true requirement.

In addition to withstanding pressure, the hotbox shell must resist buckling for the full mission duration. This is particularly important due to potential material degradation and creep at high temperatures. To ensure structural integrity, the critical buckling pressure must exceed the external pressure by a factor of at least 1.5. The critical buckling pressure for a spherical shell is given by Hutchinson [165]:

$$p_{cr} = \frac{2E}{\sqrt{3(1-\nu^2)}} \left(\frac{t}{r}\right)^2$$

where E is the Young's modulus, ν is Poisson's ratio of inconel 718 found to be 0.28 at 650 °C [166], and r is the mean radius. Using this expression, the ratio $\Delta p / p_{cr}$ is calculated to be approximately 1.65, satisfying the safety requirement and confirming that buckling is not expected to occur under the mission conditions.

Connection for Cold and Hotbox

The connection between the coldbox and the hotbox is a crucial element of the lander's structure. Its design can not only make the difference between keeping the instruments safe and catastrophically losing the mission but also substantially impact the power budget via heat conduction from the hotbox and the coldbox. Several options were considered, including a direct connection with a radial bolt and welding pin connectors between the two boxes. However, these options lead to very high heat fluxes due to conduction. Ultimately, a so-called *suspension rod* design was chosen, consisting of a simple rod specialized for one stress direction with a lengthened long side in order to slow down heat conduction. This is shown in Figure 5.47. The material chosen for this application was glass fiber due to its extremely high tensile strength and good insulating properties (see Table 5.47). Rods are attached to the equator of the coldbox with the use of mechanical fasteners helped by epoxy, and, on the other end, are attached through simple bolt, nut and washer fastening to hooks on the inside of the hotbox. Epoxy cannot be used on the hotbox because typical maximum temperatures of epoxies are below ~ 200

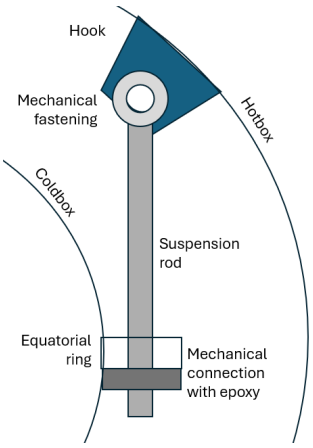

Figure 5.47: Illustration of one suspension rod between the hotbox and the coldbox.

°C [152]. The hemisphere will be cast with the hooks in its mould in order to maximize strength. This configuration is shown in Figure 5.47.

As will be explained in more detail in Equation 5.6.4, the number of landing legs will be 8. For the purposes of minimizing asymmetries and stress concentrations, an identical number of suspension rods will be used in the hotbox-coldbox connection. By using $F = \sigma A$, it is possible to find the total area of the suspension rods. The highest loads during the entire mission cycle will be $\approx 120\ g$, as explained in Section 5.1. As shown in Subsection 5.6.4, the total mass of the coldbox, including its shell and contents, will be 32 kg. This gives a total force $F = 376.7$ kN, and using $\sigma = 4890$ MPa from Table 5.47, an area of $A = 7.7 \cdot 10^{-6}$ m^2. For 8 rods, this gives an individual rod diameter of 3.2 mm.

Drag Plate

As discussed in the Midterm Report, a drag plate will be used as a speed retardation device. As per requirement OPS-EDL-FD-V-1, the maximum allowable landing speed is 8.5 $\mathrm{m\,s^{-1}}$. The required drag plate size was calculated by setting the terminal velocity at the landing site altitude (above reference level) to 8.5 $\mathrm{m\,s^{-1}}$. Equation 5.17 was used to estimate the coefficient of drag [167]:

$$C_D(r_{\text{DP}}) \approx 0.0112 \cdot (90^\circ - \zeta) \cdot \left(\frac{r_{\text{DP}} - r_{\text{HB}}\sqrt{1-\eta^2}}{r_{\text{DP}}} \right)^{0.6} + 0.16 \tag{5.17}$$

where r_{DP} and $r_{\text{HB}} = 0.32$ m are the radii of the drag plate and the hotbox, respectively. ζ is the drag plate angle and η is the mounting parameter of the drag plate ($\eta = 1$ for a drag plate mounted on the top of the hotbox, 0 for a drag plate mounted in the middle, and it linearly varies in-between). Giving a shallow conical shape to the drag plate is beneficial because the surface of the plate gets continuously washed by the airflow. An η value of close to 1 is preferable because it increases the stability of the lander during descent. The values for ζ and η are selected to be 2.5° and 0.9, respectively.

At terminal velocity, the drag equals the weight of the lander ($g = 8.87\ \mathrm{m\,s^{-2}}$, $S = r_{\text{DP}}^2\pi$):

$$F_D = \frac{1}{2}\rho V_{\text{td}}^2 C_D S = mg \tag{5.18}$$

$$\frac{1}{2}\rho V_{\text{td}}^2 C_D(r_{\text{DP}}) r_{\text{DP}}^2 \pi = mg \tag{5.19}$$

To comply with requirement GSYS-2, the mass of the lander is assumed to be 350 kg. Then Equation 5.19 can be solved iteratively for r_{DP}. As it was discussed in Section 3.2, the landing site is at most 3.2 km above the reference altitude. To be more conservative, the density calculated by Venus-GRAM at 5 km was used. With these assumptions, the necessary drag plate radius was found to be 0.74 m.

Legs and Impact Ring

Although the landing legs and impact ring differ significantly in structural design and load-bearing mechanisms, their sizing and design processes are closely interconnected, as will be demonstrated in this following section. All equations and relations used in his design process are derived from courses taught at TU Delft including but not limited to Mechanics of Materials, Structural Analysis and Design, and Vibrations.

Unlike the outer sphere, the landing legs and impact ring lack defined dimensional constraints, making their sizing inherently more complex. Consequently, the design of these components follows an iterative approach, where initial dimensions are assumed and subsequently refined based on their load-bearing performance.

The constants and mission parameters used in the design, based on mission constraints, atomspheric properties, and conventional constants [92] are as follows:

- Lander mass $m_{lander} = 350$ kg
- Earth's gravitational acceleration $g_0 = 9.81$ m/s^2
- Venus' gravitational acceleration $g = 8.87$ m/s^2
- Pressure difference $\Delta p = 9.3$ MPa
- Touchdown velocity $V_{td} = 10$ m/s
- Launch acceleration - axial: $3g_0$
- Launch acceleration - lateral: $0.5g_0$
- Dynamic shock factor $DS = 1.5$
- Factor of Safety $FS = 1.5$

It is to be noted that the touchdown velocity of 10 m/s is used instead of 8.5 m/s as defined by the EDL subsystem and drag-plate sizing to maintain conservative margins. In addition, dynamic effects, such as local stress concentrations during impact, are not modeled explicitly but are partially accounted for by the applied safety factor.

Initial estimates must be made for the dimensional variables of each component. For the landing legs, which are modeled as hollow cylinders primarily under axial loading, the following variables are defined:

- Number of legs n
- Leg angle from vertical θ
- Outer diameter D_{leg}
- Inner diameter d_{leg}
- Length of leg l_{leg}

With these values and the material properties (as defined in Subsection 5.6.3), the following structural properties are computed:

- Cross-sectional area A_{leg}
- Volume V_{leg}
- Total mass of the legs m_{legs}
- Second moment of area $I_{leg} = \frac{\pi \cdot (D_{leg}^4 - d_{leg}^4)}{64}$

The impact ring, also modeled as a hollow cylinder, is similarly defined by initial geometric and material parameters:

- Outer diameter D_{ring}
- Inner diameter d_{ring}
- Cross-sectional area A_{ring}
- Crush strength σ_{crush}

The crush strength of the foam is estimated as $\sigma_{crush} = 0.2\sigma_y$ [168].

The sizing process begins with the touchdown event. Upon landing, the kinetic energy (see Equation 5.20 of the lander must be dissipated through deformation of the impact ring. For a touchdown velocity of 10 m/s, this yields 17,500 J.

$$KE = \frac{1}{2} m_{lander} V_{td}^2 \tag{5.20}$$

This energy is assumed to be absorbed entirely by the foam in the impact ring [169], leading to the equivalence:

$$KE = \sigma_{crush} \cdot v_{crushed} = \sigma_{crush} \cdot A_{ring} \cdot h_{ring} \tag{5.21}$$

where $v_{crushed}$ is the crushed foam volume. Rearranging to solve for the minimum required height of the ring:

$$h_{ring} = \frac{KE}{\sigma_{crush} \cdot A_{ring}} \tag{5.22}$$

A factor of safety is applied to account for uncertainties and ensure that energy absorption remains within elastic deformation limits.

Although the foam absorbs most of the impact energy, a residual force is transmitted into the legs, The maximum reaction force and stress per leg are shown in Equation 5.23 and Equation 5.24 respectively.

$$F_{crush} = \frac{\sigma_{crush} \cdot A_{ring}}{n} \tag{5.23}$$

$$\sigma_{crush,leg} = \frac{F_{crush}}{A_{leg}} \tag{5.24}$$

This stress is compared to the yield strength of the leg material. Material yield is used as the failure criterion, assuming ductile behavior and no local instability before yield. To satisfy the safety requirement:

$$FS_{crush} = \frac{\sigma_{yield}}{\sigma_{crush,leg}} \geq FS \tag{5.25}$$

If this condition is not met, the leg cross-sectional area is increased until the required factor of safety is achieved.

With the ring height known, further properties are computed for later calculations:

- Cross-sectional area $A_{ring,cs}$
- Second moment of area
$$I_{ring} = \frac{h_{ring}^3 \cdot (D_{ring} - d_{ring})}{24} \tag{5.26}$$
- Volume v_{ring}
- Mass m_{ring}

With preliminary mass values for all major components (ring, legs, hotbox, coldbox, drag plate, and struts), the center of gravity (CG) position can be estimated:

$$x_{CG} = \frac{\sum x_{CG,component} \cdot m_{component}}{\sum m_{component}} \tag{5.27}$$

The datum is taken at the ground. While a lower CG is desirable for stability, it was not explicitly optimized in this process, though indirectly influenced by the mass and configuration of structural components.

The landing legs are subjected to several loading scenarios. During launch, both axial and lateral accelerations apply. The axial load on each leg is:

$$F_{axial} = \frac{m_{lander} \cdot 3g_0}{n \cdot \cos\theta} \tag{5.28}$$

where n is the number of legs and θ is the angle between the leg and the horizontal. The corresponding axial stress is:

$$\sigma_{axial} = \frac{F_{axial}}{A_{leg}} \tag{5.29}$$

Lateral acceleration induces a bending moment in each leg. The total lateral force on the lander is:

$$F_{lateral} = m_{lander} \cdot 0.5g_0 \tag{5.30}$$

The bending stress from this moment is:

$$\sigma_{bending} = \frac{M \cdot c}{I_{leg}} = \frac{F_{lateral} \cdot (x_{CG} - h_{ring}) \cdot (D_{leg}/2)}{I_{leg}} \tag{5.31}$$

where c is the maximum distance from the neutral axis in the structure. The combined launch-induced stress is:

$$\sigma_{launch} = \sigma_{axial} + \sigma_{bending} \tag{5.32}$$

This value must satisfy:

$$FS_{launch} = \frac{\sigma_y}{\sigma_{launch}} \geq FS \tag{5.33}$$

During the EDL phase, the lander undergoes significant deceleration. The maximum deceleration is defined as:

$$a_{EDL} = a_{max} \cdot g_0 \tag{5.34}$$

$$F_{EDL} = m_{lander} \cdot a_{EDL} \tag{5.35}$$

The axial force on a single leg is, with a dynamic shock factor:

$$\sigma_{EDL} = \frac{F_{EDL,leg} \cdot DS}{A_{leg}} \tag{5.36}$$

This stress is evaluated against:

$$FS_{EDL} = \frac{\sigma_{yield}}{\sigma_{EDL}} \geq FS \tag{5.37}$$

If not satisfied, the leg geometry is modified to increase A_{leg} accordingly. The total axial force from EDL is transmitted through the legs into the ring:

$$F_{ring,EDL} = F_{EDL,leg} \cdot n \tag{5.38}$$

The resulting axial stress in the ring is, with a corresponding safety factor:

$$FS_{axial,ring} = \frac{\sigma_{yield}}{\sigma_{axial,ring}} \geq FS \tag{5.39}$$

If necessary, $A_{ring,cs}$ is increased to meet this requirement.

After landing, the lander remains stationary, supported by its legs. While static loads are smaller, they act continuously. A worst-case one-leg-failure (OLF) scenario is considered. While OLF is considered for surface loads, redundancy during touchdown is not explicitly addressed and assumes all legs are intact. The static load per leg is:

$$F_{static} = \frac{m_{lander} \cdot g}{n \cdot \cos\theta} \tag{5.40}$$

Under OLF:

$$F_{static,eff} = \frac{m_{lander} \cdot g}{(n-1) \cdot \cos\theta} \tag{5.41}$$

The resulting stress is:

$$\sigma_{static} = \frac{F_{static,eff}}{A_{leg}} \tag{5.42}$$

Which must satisfy:

$$\frac{\sigma_{yield}}{\sigma_{static}} \geq FS \tag{5.43}$$

Adjustments are made to leg geometry as required. In addition to the aforementioned conditions, the leg struts are also tested to withstand loads at an inclination of 10°, though not explicitly mentioned in this report due to having minimal impact on the design as a whole.

Due to their slenderness, the legs are also vulnerable to buckling. Euler buckling is used due to the high slenderness ratio of the legs and assumption of elastic behavior within loading limits. Using Euler's formula for a fixed-pinned column:

$$F_{cr} = \frac{\pi^2 \cdot E \cdot I_{leg}}{(C \cdot l_{leg})^2} \tag{5.44}$$

with $C = 0.7$ [92]. To ensure buckling does not occur:

$$\frac{F_{cr}}{F_{max}} \geq FS \tag{5.45}$$

where F_{max} is the greatest compressive load experienced (e.g., from launch or EDL). If this condition fails, I_{leg} is increased by adjusting diameter or wall thickness. This ensures the legs remain stable under all mission phases and loading conditions.

Results

After a number of iterations with the process previously outline, the final dimensions are determined. Table 5.50 outlines these results along with their respective masses.

Table 5.50: SMS components dimensions and masses.

Component	Dimensions [m]	Mass [kg]
Coldbox	Outer Diameter: 0.58	8
Hotbox	Outer Diameter: 0.65 Thickness: 0.005	56.3
Legs	Outer Diameter: 0.08 Inner Diameter: 0.035 Length: 0.25 Angle: 20° Number of Legs: 8	Single leg: 8.1 All eight legs: 65
Impact Ring	Outer Diameter: 0.7 Inner Diameter: 0.45 Height: 0.1	51.9
Drag Plate	Diameter: 1.44	37.54
Struts	Outer Diameter: 0.08 Inner Diameter: 0.035 Length: 0.53 Angle: 52.5° Number of Struts: 4	20
TOTAL	**0.64**	**238.78**

In Figure 5.51, the main forces, stresses, and their corresponding safety factors in design are highlighted. Following that, the loading diagrams for the forces acting on the legs are presented in Figure 5.49. A diagram showing the sign conventions used in the loading diagram is shown in . Given an applied load F, the forces colored in green represent the internal forces and their indicated direction is the positive direction taken for the loading diagrams. In the case of a normal force diagram, the sign conventions are defined such that tension is positive, and compression is negative.

Figure 5.48: Sign conventions used in the loading diagrams.

Table 5.51: Forces, stresses, and safety factors for legs and impact ring.

Force	Value [N]	Stress [MPa]	Safety Factor
LEGS			
F_{crush}	381040.83	93.75	1.71
F_{axial}	2230.13	6.19	26
$F_{lateral}$	1716.75		
$F_{EDL,leg}$	59469.96	21.95	7.34
RING			
F_{crush}	3048326.62	13.5	5
F_{EDL}	475759.51	38.06	1.77

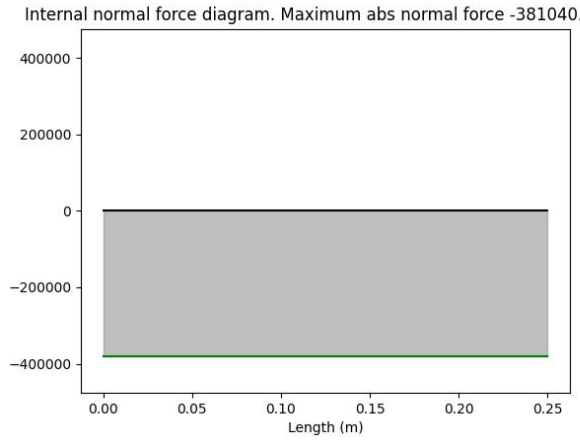

(a) Internal normal force for F_{crush}.

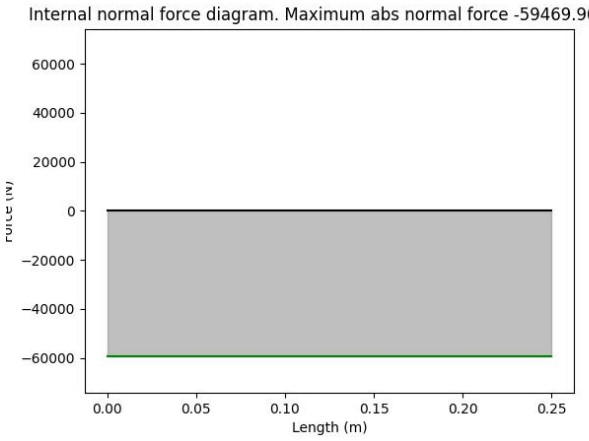

(b) Internal normal force for $F_{EDL,leg}$.

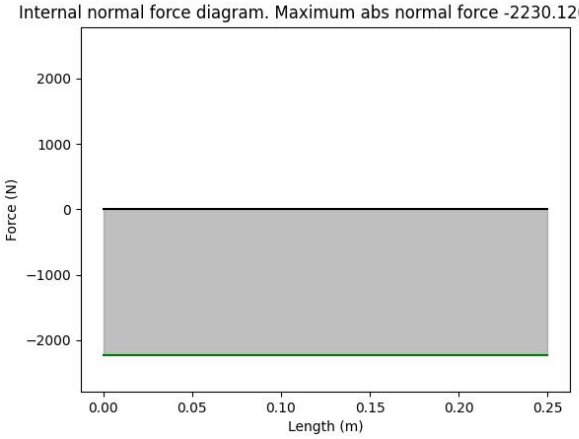

(c) Internal normal force for F_{axial}.

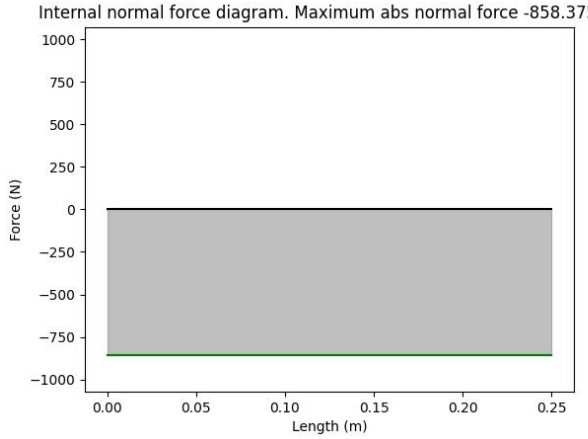

(d) Internal normal force for vertical segment of $F_{lateral}$.

Figure 5.49: Loading diagrams for leg strut.

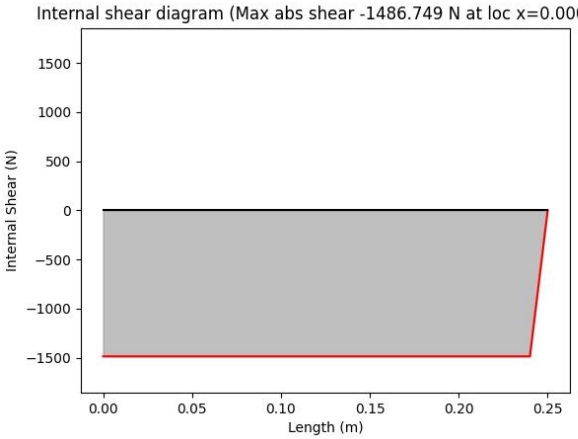

(e) Internal shear force for $F_{lateral}$.

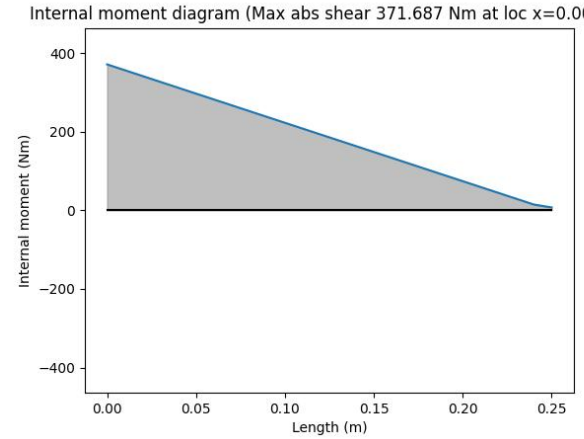

(f) Internal moment for $F_{lateral}$.

Figure 5.49: Loading diagrams for leg strut. (continued).

Natural Frequency

As discussed in Subsection 5.6.2, it is essential to account for vibrational loads to ensure the structure avoids resonance at various mission stages, from the launch vehicle during ascent to dynamic events such as stage separation. To estimate the natural frequency f_n of the lander, several assumptions and simplifications are made.

The hot and coldboxes are modeled as a single lumped mass concentrated at their combined center of gravity. The dynamic behavior of the lander is simplified to a single-degree-of-freedom system undergoing purely vertical motion, thereby

neglecting rotational and lateral dynamics. Furthermore, the system is assumed to behave linearly, with the landing legs and impact ring treated as linear springs connected in series to the lumped mass. This goes hand in hand with the assumption of small angle vibrations, which assumes that the displacements are small enough that linear approximations hold true.

While the impact ring could be modeled as a dashpot in a mass-spring-damper system, it is more accurately represented as a spring. This is because the foam in the ring deforms plastically, rather than viscously, as a dashpot would. Thus, the impact ring is approximated as a linear spring for the purpose of this vibration analysis. In addition, since the landing legs are inclined, only the vertical component of their stiffness contributes to the overall stiffness of the system.

Additional assumptions made in for the vibration analysis include an ideal load transfer and distribution for the legs; it is assumed that all legs are equally loaded in static equilibrium, such that they react the in the same way to the load applied. This assumption may not necessarily stand true, especially in the case of an inclined landing, as described in previously in the description of the lander legs calculation.

The stiffness of each leg, behaving as an axial spring is given by the formula

$$k_{leg} = \frac{EA}{L} \tag{5.46}$$

Considering only the vertical component, the total vertical stiffness from all legs becomes

$$k_{legs} = n \cdot \frac{EA}{L} \cos^2(\theta) \tag{5.47}$$

The stiffness of the impact ring k_{foam} is derived using energy equivalence. Assuming the foam behaves as a linear spring, the stiffness of the foam can be modelled using Equation 5.20 where E represents the kinetic energy, and δ is the height of the ring. Rearranging this formula, k_{foam} can be found using Equation 5.48.

$$k_{foam} = \frac{2 \cdot KE}{\delta^2} \tag{5.48}$$

$$f_n = \frac{1}{2\pi}\sqrt{\frac{k_{eff}}{m_{lander}}} \tag{5.49}$$

Because the legs and impact ring are in series, the effective stiffness of the lander suspension system is given by Equation 5.50, and the natural frequency of the lander is calculated using Equation 5.51.

$$\frac{1}{k_{eff}} = \frac{1}{k_{legs}} + \frac{1}{k_{foam}} \tag{5.50}$$

$$f_n = \frac{1}{2\pi}\sqrt{\frac{k_{eff}}{m_{lander}}} \tag{5.51}$$

The natural frequency comes to approximately 16 Hz. This lies within the acceptable limits for launch vehicle environments as detailed in SMAD [92].

5.6.5 Sensitivity Analysis

As outlined throughout this section, the structural sizing and verification process for the KYTHERA lander is highly iterative, due to the extensive interdependence between variables across both system and subsystem levels. While earlier sections addressed how variations in individual parameters influence the overall design, it is equally important to highlight how the constants, especially those defined or constrained by other teams, can significantly affect the Structures and Materials design process. This subsection elaborates on the most impactful drivers on the Structures and Materials subsystem.

One example of this is the pressure loading on the outer sphere. The design calculations assume a pressure differential of 93 bar, corresponding to Venus' surface conditions at sea level, and incorporate a factor of safety of 1.5. However, as discussed in Section 3.2, KYTHERA is intended to land on elevated terrain where the atmospheric pressure and temperature are substantially less extreme. Despite this, the team made a decision to size the structure for the more extreme sea-level conditions. This conservative approach serves two purposes. First, it ensures robustness against any unforeseen landing deviations, such as a failed targeting maneuver that results in a lower-elevation touchdown. Second, it provied the lander's structural design with potential future missions that may aim to explore lower, harsher regions of Venus' surface. Consequently, this decision had an effect on material selection and wall thickness calculations, ultimately resulting in a more resilient, albeit heavier outer structure.

Another structural consideration was the inclusion of a OLF scenario and an assumed initial tilt angle of $10°$ during landing. This was evaluated in the analysis of the legs and impact ring, where worst case loading distributions were examined. Interestingly, this case did not prove to be the primary sizing driver. It was initially expected that the maximum 120 g axial

loading during the EDL phase would dictate the structural design, and while that stands true for the impact ring, it is not the case for the legs; ultimately, the touchdown velocity that emerged as the most critical factor for leg design.

The touchdown velocity directly determines the kinetic energy that must be absorbed upon landing. This energy must be dissipated through deformation of the foam within the impact ring. As shown in Equation 5.20, this energy sets the required minimum height of the ring. Once the ring has compressed to absorb this energy, the residual load is transferred to the legs as a concentrated axial force. The magnitude of this force, as determined in Equation 5.23, was found to induce the highest stress in the leg structure across all examined loading scenarios.

This finding had significant implications for both the leg geometry and material utilization. The touchdown velocity case yielded a factor of safety of approximately 1.7 which was the lowest among all considered conditions, yet still compliant with the design threshold of 1.5. Importantly, this indicates that any increase in touchdown velocity beyond 15 m/s (1.5 times the design value of 10 m/s) would result in leg failure. While the expected nominal touchdown velocity is 8.5 m/s, the use of a 10 m/s design value ensures that the legs, and by extension the entire landing system, retain a buffer against unforeseen obstacles in descent dynamics or terrain interaction.

The main design drivers for the Structures and Materials subsystem were not simply the most extreme static forces or pressures, but rather dynamic conditions such as impact energy and subsystem failures. The use of conservative estimates for key variables, particularly those that are mission dependent or subject to uncertainty, enabled a structurally robust lander design that maintains a favorable safety margin without overconstraining the system.

5.6.6 Next Steps for More Accurate Design

Updates to Current Design

The current configuration of the coldbox-hotbox connection is extremely strong in the vertical direction, but is possibly vulnerable to side loads. It might happen that lateral accelerations from turbulence, manufacturing errors or other sources might overwhelm the current configuration and allow the two boxes to touch. If violent enough, this could damage the contents of the coldbox, possibly compromising the mission. Next steps for the structures subsystem should take this into account and design for lateral loads as well, depending on estimations from EDL about possible turbulence or other sources of sideways accelerations.

In the landing ring and legs of the lander, steel alloys are used. However, not all steel alloys are resistant to corrosion in Venus conditions. This will need to be mitigated, either by switching to another material, such as nickel foam (this may have a large impact on the design), using a corrosion-resistant steel type to make the foam, or by means of a liquid coating that can cover the entire foam structure.

Apart from the specific case of steel, research into coatings for other parts of the structure may also help reduce the system's mass. More lightweight materials that do not resist corrosion can be complemented by coatings to improve performance. Due to time constraints, the team did not look in depth into coatings and how their mechanics (e.g. thermal expansion, brittleness) work.

In addition, the inclusion of cutouts in both the inner and outer spherical structures introduces localized stress concentrations that can compromise mechanical performance, particularly under pressure or impact loading. These stress concentrations arise because the cutouts disrupt the uniform stress distribution, causing elevated local stresses around their edges, which can increase the risk of crack initiation, fatigue failure, and structural deformation. Choosing circular cutouts helps mitigate some of these effects, since their rounded geometry allows stress to flow more smoothly around the hole, reducing the intensity of stress concentrations compared to sharp-edged openings. Circular shapes also limit crack propagation since there are no corners to act as crack initiation points. However, despite this geometric advantage, circular cutouts still reduce the local stiffness and strength of the structure and will be addressed through targeted reinforcement for the upcoming report. This can be accomplished by locally thickening the shell material, increasing the load-bearing capacity and reducing peak stresses. Reinforcement rings or collars can also be used to redistribute stress away from the edges of the cutouts and back into the stronger surrounding material. In some cases, higher-strength materials can be applied selectively in these regions to improve resistance to local failure modes. Additional stress-relief features, such as small chamfers or radii at cutout edges, can further smooth stress transitions and enhance durability. These strategies, the detrimental effects of cutouts can be effectively managed without compromising the functional or thermal requirements that necessitate the openings in the first place.

Finally, the thermal expansion between the windows and the box shells may cause problems. The difference in the coefficient of thermal expansion (CTE) between the Inconel 718 on the hotbox shell and Sapphire on the windows is 7.4 μm/mK which is higher than the 5 μm/mK requirement that was initially set. This CTE disrepancy will need to be mitigated, for which further research is necessary, since e.g. leaving a gap is not an option if vacuum needs to be maintained.

Future Optimizations

After the completion of the preliminary design phase and the development of detailed Computer Aided Design (CAD) models, the next critical step involves conducting a Finite Element Method (FEM) analysis and applying topology opti-

mization techniques. FEM analysis serves not only as a means of verification and validation but also a tool for enhancing the design through structural refinement. While analytical calculations and CAD design provide a strong foundation, FEM enables a simulation of how the structure will behave under actual mission conditions, specifically with the loads detailed in Subsection 5.6.2.

One of the key advantages of FEM is its ability to discretize complex geometries into fine mesh elements, allowing engineers to simulate stress and strain distributions with high spatial resolution. The mesh can be selectively refined in regions expected to experience high stress concentrations, such as structural joints, load transfer paths, or cutouts in the hotbox and coldbox. These simulations help identify localized weaknesses or potential failure points that may not be evident through simpler analytical models [170]. Evaluating how loads are distributed across the structure during various mission phases allows to reinforce critical areas, adjust material distribution, or modify geometries to improve load paths.

In addition to static stress analysis, FEM facilitates modal analysis, which is essential for understanding the dynamic behavior of the structure. Identifying the natural frequencies of the system is crucial, especially during events such as launch and landing shocks where vibration loads are significant. If any of the natural frequencies of the structure align with the dominant frequencies of external excitation, resonance could occur, amplifying vibrations and potentially causing structural damage or instrument malfunction. By detecting and mitigating these resonant frequencies, modifications can be made such that KYTHERA remains structurally robust throughout its mission.

FEM also provides the baseline data needed for topology optimization, whichcan redistribute material in a way that maximizes the stiffness-to-weight ratio while still meeting all performance requirements. Once regions of low stress are identified, unnecessary mass can be removed, resulting in a structure that is both lighter and more efficient. Depending on the design and constraints, topology optimization has been shown to reduce structural mass by anywhere from 10% to over 50% [171], without compromising safety or functionality, which would ultiminately decrease the lander mass such that it stays well within the budget. Implementing these tools will not only result in a structurally optimized and mass efficient design for KYTHERA but also enhance its performance, reliability, and scientific return.

6

Integrated Design

This chapter will put together all the subsystems described in the previous chapter and show the integrated design of the KYTHERA lander. It starts with a brief overview of the overall configuration in Section 6.1, and then explains the design process of the coldbox and its results in Section 6.2. Next, the hotbox is described in Section 6.3, followed by an explanation of instrument integration in Section 6.4. Then, the drag plate design is elaborated in Section 6.5, and finally the connection between the EDL subsystem and the lander is detailed in Section 6.6.

6.1 Overall Configuration

Figure 6.1 is an annotated illustration of the integrated design of the KYTHERA lander. Its main components are: the hotbox, the landing ring, the landing struts, the drag plate, the Stirling generators, and the coldbox hidden within the hotbox.

The resulting design bears resemblance to previous designs, in particular the Venera landers (see Section 2.2), but also other concept studies. The reason behind this similarity is the extremely strict conditions stemming from the harsh environment of Venus; an optimal design has been reached, with an inner pressure-loading sphere, an impact-absorbing ring, and a drag plate that replaces parachutes. However, this similarity is superficial only, as on the inside the different design concepts are virtually all different, as is KYTHERA.

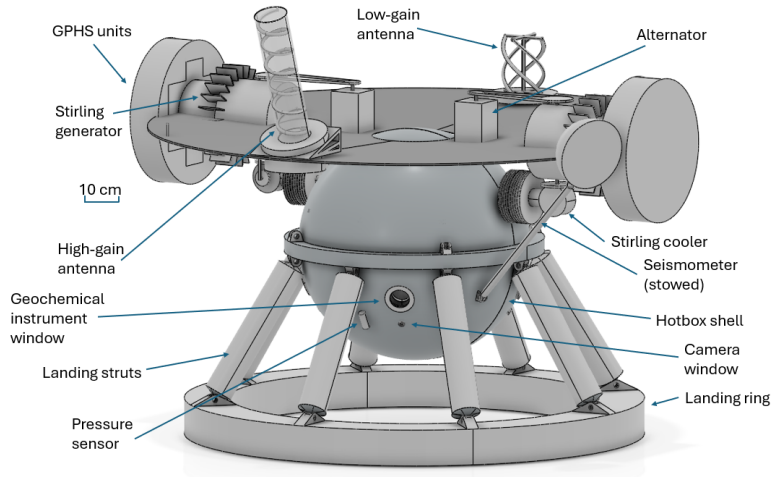

Figure 6.1: KYTHERA overall configuration.

6.2 Coldbox Configuration

The coldbox is the cooled compartment of the spacecraft. Its purpose is two-fold: to provide a structure for the delicate instruments to be mounted on, and to maintain a stable, lowered temperature for the electronics to function nominally. The second function is particularly critical, as cooling power requirements tend to be driving for the entire design; as a result, a minimal coldbox size is desirable for optimum heat management. Since it has no structural function save for mounting the payload, the size of the compartment is directly determined by its contents. The following is a list of all items that the coldbox must contain:

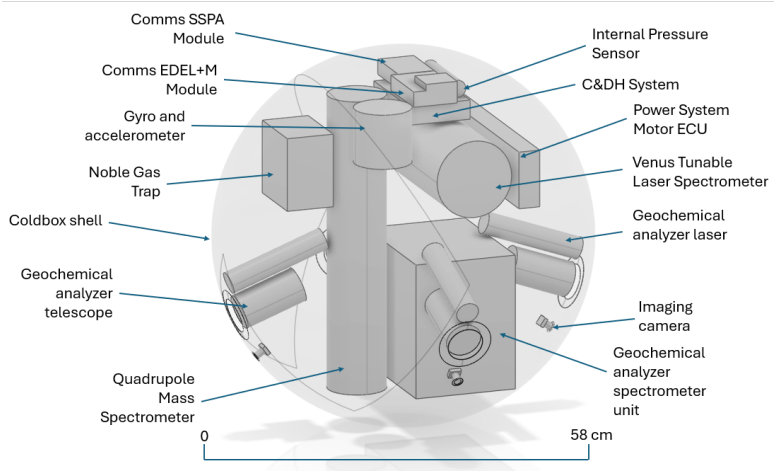

Figure 6.2: Coldbox contents configuration.

- The VMS, including the QMS, VTLS and NGT
- The geological analyzer instruments, including the geochemical analyzer spectrometer unit and the 4 telescope with laser pairs
- The 4 imaging cameras
- The CDH subsystem
- Communications modules
- Internal pressure sensors
- Gyro and accelerometer
- Power subsystem motor electonic control unit
- Batteries
- Pressure and temperature sensor

In order to size the coldbox, a manual two-step packing procedure was undertaking in CATIA. The first step consisted of all components being constructed and added to an assembly one by one and fit into place as tightly as possible, while keeping at least 1 cm clearance. The goal of this first step is to fit all components into a spherical volume of minimal diameter. The second step was iteration: the components were taken apart and placed together again, but with the new knowledge of how they best fit together. The end result was a sphere of 58 cm diameter that could encapsulate all previously listed items. This is shown in Figure 6.2.

Designing the mounting structure of the payload inside coldbox is outside the scope of this report and should be investigated in future design steps. However, the payload mountings will be made according to the contents of the coldbox, based on a main deck installed around the equator of the coldbox sphere. This main deck also pokes out of the spherical shape in order to provide mounting points of the suspension rods described in Subsection 5.6.4 that provide the connection with the hotbox. This is shown in Figure 6.3.

Since purpose of the shell of the coldbox is solely to reflect infrared radiation from the hotbox inner wall, it can be as thin as a reflective film. For this reason, the structure of the coldbox itself will be a grid pattern structure designed to let a foil neatly cover its entirety. It is important to note that the struts running across the coldbox's meridians and parallel are meant to bear no more weight than their own during EDL, as with this, the coldbox can achieve a lowered mass.

The coldbox will also feature several windows through which instruments can look to the outside of the spacecraft. These windows will be made of sapphire as it has a low emissivity and can insulate the coldbox better than a simple hole. Another feature of the exterior of the coldbox are portholes through which inlets for the VMS can transport Venusian air. These are not shown in Figure 6.3. Note that the actual inlets are placed on the hotbox.

6.3 Hotbox Design

The next component in the integrated design is the hotbox. The hotbox is the outer shell of the spacecraft, intended to keep a vacuum inside itself for minimization of heat conduction and convection. For this reason, it is spherical in shape, and will be made of a strong but lightweight material. The chosen material is Inconel 718, and, as explained in Subsection 5.3.4, it will have a diameter of 64 cm. Its thickness will be 5.34 mm, as shown in Subsection 5.6.4.

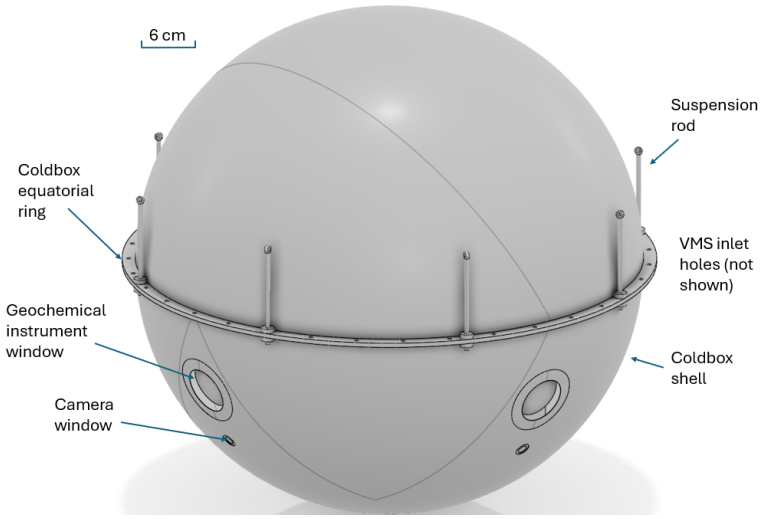

Figure 6.3: Exterior of the coldbox, showing the equatorial ring and the suspension rods.

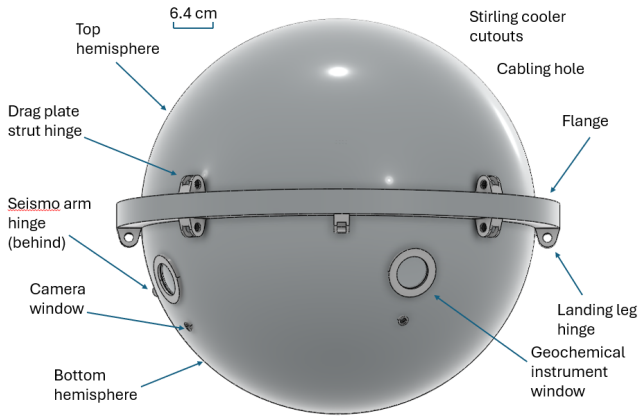

Figure 6.4: Hotbox exterior configuration. Stirling cooler and cabling holes not shown.

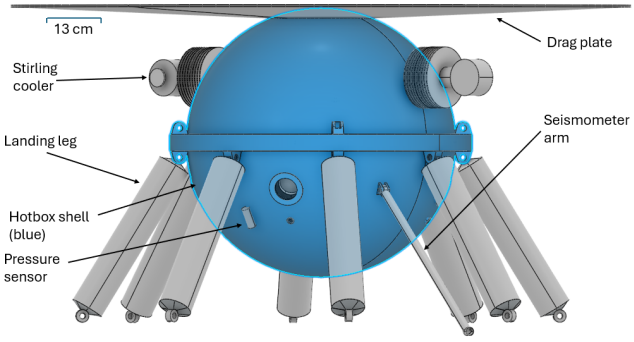

Figure 6.5: Exterior connections of the hotbox. The hotbox is highlighted in blue.

Some important features of the hotbox are its holes and cutouts. These are the windows and portholes for the instruments, which are explained more in detail in Section 6.4. On the top side of the interior of the hotbox, there will be hooks for the coldbox suspension rods to attach to, and there will be a small exterior pressure sensor on the bottom half of the hotbox.

The hotbox will be made of two hemispheres with flanges at their lips. These flanges will be used to bolt the two hemispheres together as well as keep the vacuum seal. They will also be used as the mounting points for the landing legs and the drag plate struts, whose role is explained in Section 6.5. The top hemisphere will be manufactured together with the suspension rod hooks in order to minimize stress concentrations. The connection between the hotbox and the coldbox is shown in Figure 6.6.

A hinge will be attached to the side of the hotbox, approximately 25 degrees below the flanges. This hinge will serve as the mounting point for the seismometer arm mechanism. Its location allows for the arm to be as long as possible while stowed to the side of the drag plate and still reach the ground with sensible tolerance. Another feature that the hotbox will have is cutouts for the Stirling coolers to penetrate through to the coldbox. These cutouts will be integrated and sealed together with the coolers. The last cutout will be a small hole near the top of the hotbox through which signal, power and communications cables can pass through.

Finally, the drag plate is mounted at the top of the hotbox, at a height of 90% of its radius. This will likely be done via welding so as to not introduce more cutouts into the structure.

The configuration of the hotbox is shown in Figure 6.4. Due to time constraints the holes for the Stirling coolers, the VMS inlets and cabling holes are not shown. The seismometer arm hinge is behind the hotbox in this view, but is identical in shape to the other hinges shown. Exterior connections of the hotbox are shown in Figure 6.5.

6.4 Instrument Integration

In order to conduct some of the measurements the instruments need to be have contact with the outside. This is the case

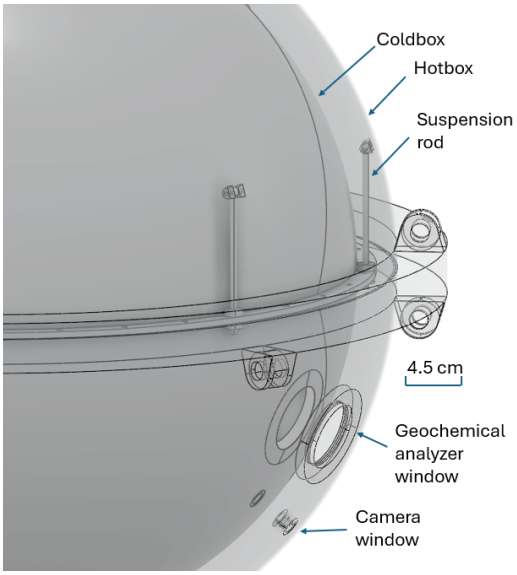

Figure 6.6: The connection between the hotbox and the coldbox. The hotbox is transparent.

for the geochemical analyzer, the camera and the atmospheric analyzer. The geochemical analyzer needs to send a laser to the target rock material and receive the radiation coming back from it through a telescope. In the case of the camera a view to the outside is simply required to take pictures. Lastly, the atmospheric analyzer has to collect atmosphere samples and push them back to the outside after analysis. All of the above instruments require cooling, which is why they are placed inside the coldbox.

For the atmospheric analyzer there will be one sample inlet, which connects the instrument in the coldbox, via the hotbox, to the Venus environment. This is the same for the sample outlet.
The lander contains four windows such that a $360°$ panoramic view from the surface and horizon can be captured by the camera. To maximize the scientific yield it is preferred by the team to allow the geochemical analyzer to have a view in four directions as well. This resulted in three design options on how to establish a view through the windows in four directions. The first option is to have one window in the coldbox and four in the hotbox. For this it is needed for the coldbox to be able to rotate about its vertical axis from one window to another. The second design option is to have the geochemical analyzer and the camera mounted onto a rotating arm. For this option, both the hot and coldbox contain four windows and the arm rotates the set of instruments horizontally from window to window. The last design option is to simply place the set of instruments in front of each window, which means having a total of four cameras and four geochemical analysis instruments (specifically the laser and telescope).
The first design option was rejected quickly because it would be too complex to for example organize the cabling and other connections to make it work. Design options two and three were both considered viable options. Option two has the advantage that no extra cost and mass is added as the minimum amount of instruments required can be used. The disadvantages, however, are that there will be an extra cost for developing the rotating arm and that the arm requires a significant amount of free volume in order to rotate. The third option has the advantage that less volume is needed and that there is redundancy for the instruments. The drawbacks are that there is an extra cost for the manufacturing of the additional instruments, but this is expected to be low. Since minimizing the volume of the coldbox is important for thermal cooling and there also need to be a lot of instruments placed inside the coldbox, volume was considered the most important criteria when selecting one of the design options. Therefore, the design option of having the set of instruments on each of the four windows was chosen.

As can be seen in Figure 6.2 and Figure 6.3 the geochemical analyzer and the camera have a separate window. This was done to keep the window size as small as possible in order to limit the amount of heat leaking into the coldbox. In between the cold and hotbox the windows will be made of sapphire, which is heat resistant and transparent for all the wavelengths needed. This is the case for both the camera and geochemical analyzer windows.
In between the hotbox and the exterior there will be fisheye lens for the camera. This allows the camera to have a field of view of $100°$. The fisheye lens is connected via optical cables to the rest of the camera inside the cold box. The camera sapphire window and fisheye lens will both have a diameter of 11.25 mm.
For the geochemical analyzer there will be placed a concave lens in between the hotbox and the Venus environment, which maximizes the field of view. The dimensions of the geochemical analyzer sapphire window and concave lens are both 55 mm diameter.

6.5 Drag Plate Planform Configuration

The drag plate is placed 290.52 mm vertically above the center of the hot and coldbox. Several components are placed on the drag plate. Firstly, two Stirling generators are placed 180° from each other. They are placed at the drag plate because the temperature of the GPHS modules can reach up to 1200 °C. Although there are thick insulation layers placed over the GPHS module, they should be placed far out from the rest of the lander structure as much as possible such that the heat from them does not affect other components or the structure. The Stirling generator is connected to an alternator which is also placed on top of the drag plate. Although not shown in the figures, additional struts from the flange to the drag plate will be needed to support the mass of the Stirling generator. Two struts per Stirling generator will be needed for this and they will be placed adjacent to each other. This means that a total of four struts, that are not currently visible, shall be added in the future. It may also be beneficial to place housing over the chain sprockets that connect the Stirling generator and cooler/alternator, to protect it from ambient, but this is left as a recommendation for future work. Furthermore, the low and high-gain antennas are placed on top of the drag plate to establish communication with the orbiter. The components are positioned such that they do not impact the center of gravity location or the spin stability of the lander. Lastly, a wind sensor and radiometer on placed on the drag plate as well, but are not visible on the figures.

6.6 EDL - Lander Connection

The lander must be integrated into the entry capsule and connected to the coasting stage. There will be holes in the backshell interface plate to accommodate the thermal (LHP piping), mechanical (the spring separator system) and electrical (cabling) connections. These connections will be cut when the coasting stage separates. There will be internal struts and a cup connecting the bottom of the lander to the aeroshell and the main heat shield structure, respectively. The high strength of the lander structure will be utilized during entry by incorporating it into the load path during entry and reduce the stresses in the EDL support structure. The cup carries the deceleration loads during entry from the lander directly to the heat shield. To reduce the loads imposed onto the drag plate during entry and prevent potential unwanted vibrations, the RSG modules and the drag plate are supported by additional struts connected to the aeroshell. The rigid connections are cut using pyrotechnic devices.

The LHP system will be mechanically attached to the aeroshell, placed above the drag plate. Its hot side will be thermally connected to the heat exchanger of the RSGs by high-conductivity brushes, so that the lander can freely slide out when it separates from the aeroshell. The paraffin wax container, that is to be used after coasting stage separation, is located beneath the drag plate. It is mechanically connected to the main heat shield (otherwise it would collide with the drag plate when the lander is released from the aeroshell), and is thermally connected to the RSG heat exchangers by paraffin heat switches, which activate by additional thermally expanding paraffin wax inside them when a limit temperature is reached.

The configuration of the lander within the EDL structure is shown in Figure 6.7a. Note that supporting structure such as the support cup, supporting struts and cruise stage subsystems are not shown. Figure 6.7b shows the Coasting Stage configuration.

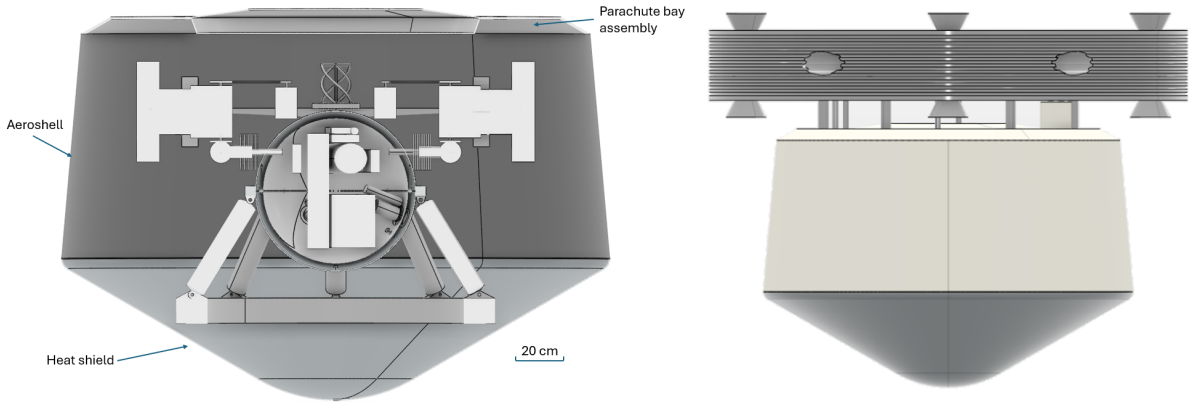

(a) EDL-lander configuration.

(b) Entry capsule with the Coasting Stage.

Figure 6.7: EDL configuration..

7

Conclusion

Author: Maurizio

This report has presented the preliminary design of KYTHERA: an extended duration robotic lander mission to Venus. A unique mission, it builds on the heritage of decades of Venus exploration by returning to the surface and surviving for 200 days, enhancing our understanding of Earth's closest planetary neighbor.

The lander will be capable of conducting several scientific experiments, analyzing the chemical composition of Venus's surface and lower atmosphere, taking images of the landing area both while descending and across the duration of the mission, and monitoring atmospheric properties throughout its lifetime. For this, several instruments have been included in its payload, including the Venus Mass Spectrometer, the Venus Tunable Laser Spectrometer, the SuperCam instrument from the Mars 2020 rover, a purpose-built Venus Seismometer, thermometers, barometers and radiometers. These are encased in a highly insulated vacuum capsule to protect them from the extremely hostile environment of Venus.

The subsystems required for bringing and sustaining this payload at its destination were developed in this report, including Power, Thermal, Communications, Command & Data Handling subsystems, as well as Entry, Descent and Landing (EDL) and Structures. A preliminary landing site was chosen for KYTHERA in Lakshmi Planum, but the final choice will be left up to a professional group of scientists after this stage of its design.

Certain requirements, however, have not been met. Unexpected circumstances has made the Power system's budget be substantially underestimated and thus the 200 million euro budget will be overrun to around 300 million euros. This overrun will be mitigated by reducing cooling requirements and seeking cost reductions in other subsystems.

Nonetheless, special attention was given to systems engineering tools, with an entire chapter being dedicated to them. These included mechanical block diagrams, concept of operations, risks, system requirements, budgets, and many more.

This report has detailed KYTHERA's preliminary design. However, many steps are still to be taken before the mission is ready for launch. A detailed design stage needs to be undertaken, as well as substantial optimization of several of its subsystems. Still, KYTHERA's strength lies in its uniqueness - as a relatively lightweight, low complexity interplanetary lander capable of sustaining operations on the surface of Venus for the better part of an Earth year, it could change our understanding of the Morning Star.

8

Resources and Acknowledgments

This report was made possible by valuable input, support, and resources from many individuals, institutions, and tools. This chapter highlights key contributors and resources who aided the project from concept to technical validation.

8.1 Acknowledgements

We would like to sincerely thank everyone who helped with this project by giving us their time, knowledge, and assistance. First and foremost, we would like to express our gratitude to Edgar Steenstra, our tutor, for his constant support, practical debates, and direction throughout the entire project. His guidance was crucial in determining the focus and scope of our work. We also thank Yun-Ching Lin and Ernst Schrama, our coaches, for their insightful counsel and insightful criticism, which significantly improved the quality of our design and analysis. We would especially like to thank Colin Wilson for kindly sharing his knowledge of Venus missions, which added important technical depth and context. We also appreciate the insights of Jasper Bouwmeester, whose guidance on thermal system design helped us refine a core aspect of the mission architecture. We would like to acknowledge Richard Strahan for his expert input on power systems and for providing access to key technical resources that supported our design process. Furthermore, we are thankful to Prof. Stefano Speretta for his advice and reflections on designing the communications system. We would like to thank Robin Bornoff for his valuable insights on the implementation of heat pipes in the design. Finally, we sincerely thank Prof. Erwin Mooij for his guidance on the sizing and cost estimation of the entry, descent, and landing system, which enabled us to develop a more robust and realistic mission profile. Their collective contributions were invaluable, and we are deeply appreciative of their support.

8.2 Resources

A wide range of resources were used throughout the project to ensure the technical depth and accuracy of the work. A basis of knowledge was built through the use of scientific papers accessed via online academic databases. These were used in combination with a variety of textbooks available at the Aerospace Engineering faculty, as well as more specialized books sourced from the TU Delft Library. These offered deeper insights into spacecraft subsystems, thermal control, and mission architecture. To support the analytical and design processes, several industry-standard tools and software packages were utilized. Simulink was used to model and simulate both power and thermal systems, allowing for dynamic performance assessments and optimization under mission-specific conditions. For atmospheric modeling, NASA's Venus-GRAM (Global Reference Atmospheric Model) provided vital environmental data tailored to the Venusian context, enabling more accurate trajectory and system-level analyses. Venus QuickMap was used to visualize surface features and assess terrain conditions, helping in the selecting potential landing sites and mission constraints. The ANSYS Granta software was also used and proved important data in the materials comparison and selection process. Practical and visual understanding of spacecraft configuration and subsystem integration was improved by visiting physical exhibits and models available in the faculty, more specifically in the space departement. These resources contributed to the development of more realistic and feasible system concepts. Additionally, technical datasheets obtained from manufacturer websites and component suppliers played a role in performing hardware selection. Finally, artificial intelligence tools such as ChatGPT were used in some instances to more effectively research topics or to improve the quality of the text. The use of these tools was documented in the AI statement submitted to the OSSA. Together, these resources formed a the basis for the project's design, analysis, and validation, supporting a well-informed approach throughout all phases of development.

References

[1] J. A. Cutts et al. *Roadmap for Venus Exploration*. Tech. rep. VEXAG Venus Exploration Roadmap Focus Group, 2019.

[2] E. S. Steenstra. "Project Guide Design Synthesis Exercise: An Extended Duration Robotic Lander Mission to Venus". In: *Design Synthesis Exercise* (2025).

[3] L. S. Glaze et al. "Future of Venus Research and Exploration". In: *Space Science Reviews* 214.5 (July 2018), p. 89. ISSN: 1572-9672. DOI: 10.1007/s11214-018-0528-z. URL: https://doi.org/10.1007/s11214-018-0528-z.

[4] T. Kremic et al. "Long-duration Venus lander for seismic and atmospheric science". In: *Planetary and Space Science* 190 (2020), p. 104961. DOI: https://doi.org/10.1016/j.pss.2020.104961.

[5] M. S. Gilmore et al. "Mineralogy of the Venus Surface". In: *Space Science Reviews* 219 (7 Oct. 2023). DOI: 10.1007/s11214-023-00988-6.

[6] A. H. Treiman. "Geochemistry of Venus' surface: Current limitations as future opportunities". In: *Geophysical Monograph-American Geophysical Union* 176.7 (2007).

[7] T. Widemann et al. *Venus: Evolution Through Time*. Springer Dordrecht, 2025. ISBN: 978-94-024-2269-6.

[8] J. Kargel et al. "The Volcanology of Venera and VEGA Landing Sites and the Geochemistry of Venus". In: *Icarus* 103.2 (June 1993), pp. 253–275. DOI: 10.1006/icar.1993.1069.

[9] A. Strezoski and A. H. Treiman. "The "Snow Line" on Venus's Maxwell Montes: Varying Elevation Implies a Dynamic Atmosphere". In: *The Planetary Science Journal* 3.12 (Dec. 2022), p. 264. DOI: 10.3847/PSJ/ac9f3a.

[10] E. V. Shalygin et al. "Active volcanism on Venus in the Ganiki Chasma rift zone". In: *Geophysical Research Letters* 42.12 (2015), pp. 4762–4769. DOI: https://doi.org/10.1002/2015GL064088.

[11] S. E. Smrekar et al. "Recent Hotspot Volcanism on Venus from VIRTIS Emissivity Data". In: *Science* 328.5978 (2010), pp. 605–608. DOI: 10.1126/science.1186785.

[12] R. C. Ghail et al. "Volcanic and Tectonic Constraints on the Evolution of Venus". In: *Space Science Reviews 2024 220:4* 220 (4 Apr. 2024), pp. 1–65. DOI: 10.1007/S11214-024-01065-2.

[13] National Research Council et al. *Vision and Voyages for Planetary Science in the Decade 2013-2022*. National Academy of Sciences, 2013. DOI: 10.17226/13117.

[14] Venus Exploration Analysis Group. "VEXAG, goals, objectives, and investigations, 2019." In: *vexag* (May 2014). URL: https://www.lpi.usra.edu/vexag/reports/GOI-Space-Physics-Update-0816.pdf.

[15] E. Marcq et al. "Variations of sulphur dioxide at the cloud top of Venus's dynamic atmosphere". In: *Nature Geoscience* 6.1 (Dec. 2012), pp. 25–28. ISSN: 1752-0908. DOI: 10.1038/ngeo1650. URL: http://dx.doi.org/10.1038/ngeo1650.

[16] A. Seiff et al. "Models of the structure of the atmosphere of Venus from the surface to 100 kilometers altitude". In: *Advances in Space Research* 5.11 (1985), pp. 3–58. DOI: https://doi.org/10.1016/0273-1177(85)90197-8.

[17] D. Senske et al. "Development of the Venera-D Mission Concept, from Science Objectives to Mission Architecture". In: *49th Lunar and Planetary Science Conference*. 2018.

[18] VENERA-D JOINT SCIENCE DEFINITION TEAM. *Venera-D: Phase II final report*. Tech. rep. Space Research Institute of the Russian Academy of Sciences, 2019.

[19] X. Dong et al. "Venus Volcano Imaging and Climate Explorer Mission". In: *Chinese Journal of Space Science* 42 (6 July 2024), pp. 1047–1059. DOI: 10.11728/CJSS2022.06.YG33.

[20] CAS National Space Science Center. *National Mid- and Long-term Plan for Space Science in China (2024-2050) –National Space Science Center, CAS*. Accessed on 01/05/2025. Aug. 2024. URL: http://english.nssc.cas.cn/pub/202410/t20241028_692867.html.

[21] Sauder et al. *Automaton Rover for Extreme Environments*. Tech. rep. Jet Propulsion Laboratory, California Institute of Technology, 2017.

[22] L. Campbell. "Rocket Lab Venus Probe Thermal Protection System – Design, Development, and Future Applications". In: *International Planetary Probe Workshop*. 2023.

[23] R. French et al. "Rocket Lab Mission to Venus". In: *Aerospace* 9.8 (2022). DOI: 10.3390/aerospace9080445.

[24] T. Kremic, G. W. Hunter, and L. Nero. *Long-Lived In-Situ Solar System Explorer (LLISSE)*. 2017.

[25] COSPAR Panel on Planetary Protection. *Editorial to the New Restructured and Edited COSPAR Policy on Planetary Protection*. Tech. rep. COSPAR, Mar. 2024.

[26] ECSS-U-ST-20C Working Group. *Space sustainability: Planetary protection*. Tech. rep. ESA Requirements and Standards Division ECSS-U-ST-20C, Aug. 2019.

[27] C. V. M. Pradon et al. "Global Three-Dimensional Emission Inventory for Launch Vehicles from 2009 to 2018". In: *Journal of Spacecraft and Rockets* 60 (3 May 2023), pp. 716–727. DOI: 10.2514/1.A35385.

[28] D. Stevenson et al. *Probing the Interior Structure of Venus*. Tech. rep. Keck Institute for Space Studies, Apr. 2015.

[29] M. S. Gilmore et al. "Investigation of the application of aerobot technology at Venus". In: *Acta Astronautica* 56 (4 Feb. 2005), pp. 477–494. DOI: 10.1016/j.actaastro.2004.06.005.

[30] M. Amato and D. Williams. "Accessing the Venus Lower Atmosphere and Surface - from Venera and Pioneer Venus to VISE and VITaL". In: *Inner Solar System: Prospective Energy and Material Resources*. Springer International Publishing, 2015, pp. 193, 319, 376–377.

[31] A. Gülcher et al. "Corona structures driven by plume–lithosphere interactions and evidence for ongoing plume activity on Venus". In: *Nat. Geosci.* 13 (2020), pp. 547–554. DOI: https://doi.org/10.1038/s41561-020-0606-1.

[32] S. A. Bledsoe and C. K. and. "Global distribution of canali on Venus". In: *Journal of Maps* 21.1 (2025), p. 2465669. DOI: 10.1080/17445647.2025.2465669. eprint: https://doi.org/10.1080/17445647.2025.2465669. URL: https://doi.org/10.1080/17445647.2025.2465669.

[33] S. Lebonnois et al. "Superrotation of Venus' atmosphere analyzed with a full general circulation model". In: *Journal of Geophysical Research (Planets)* 115.E6, E06006 (June 2010), E06006. DOI: 10.1029/2009JE003458.

[34] S. Lebonnois, N. Sugimoto, and G. Gilli. "Wave analysis in the atmosphere of Venus below 100-km altitude, simulated by the LMD Venus GCM". In: 278 (Nov. 2016), pp. 38–51. DOI: 10.1016/j.icarus.2016.06.004.

[35] A. Martinez et al. "Exploring the variability of the venusian thermosphere with the IPSL Venus GCM". In: 389, 115272 (Jan. 2023), p. 115272. DOI: 10.1016/j.icarus.2022.115272.

[36] M. A. Ivanov and J. W. Head. “Global geological map of Venus”. In: *Planetary and Space Science* 59.13 (2011). Exploring Phobos, pp. 1559–1600. ISSN: 0032-0633. DOI: https://doi.org/10.1016/j.pss.2011.07.008. URL: https://www.sciencedirect.com/science/article/pii/S0032063311002297.

[37] H. Apgar. “Cost Estimating”. In: *Space Mission Engineering: The New SMAD*. Ed. by J. R. Wertz, D. F. Everett, and J. J. Puschell. Microcosm Press, 2011, pp. 297–299.

[38] R. Leigh and S. Sherry. *NASA Cost Estimating Handbook*. 4th Edition. Provides guidance on cost estimating at NASA, suitable for both new and experienced cost estimators. Updates: Reflects policy changes since the 2008 edition. City, State or Country: National Aeronautics and Space Administration, 2015.

[39] C. Preyssl, R. Atkins, and T. Deak. “Risk management at ESA”. In: *ESA bulletin* 97 (1999), pp. 64–68.

[40] D. H. Mitchell. *Flight Separation Mechanisms*. Tech. rep. NASA Tech. Rep., 1970.

[41] D. G. Gilmore, ed. *Spacecraft Thermal Control Handbook, Volume 1: Fundamental Technologies*. 2nd. El Segundo, California: The Aerospace Press, 2002. ISBN: 1-884989-11-2.

[42] D. Mishkinis et al. “Development of Propylene LHP for European Mars Rover Applications”. In: *VII Minsk International Seminar on Heat Pipes, Heat Pumps, Refrigerators, Power Sources*. Sept. 2008.

[43] W. R. Humphries and E. I. Griggs. *A design handbook for phase change thermal control and energy storage devices*. Tech. rep. NASA, 1977.

[44] P. N. Desai et al. “Entry, descent, and landing operations analysis for the Stardust entry capsule”. In: *Journal of Spacecraft and Rockets* 45.6 (2008), pp. 1262–1268.

[45] R. G. Wilmoth, R. A. Mitcheltree, and J. N. Moss. “Low-density aerodynamics of the stardust sample return capsule”. In: *Journal of spacecraft and rockets* 36.3 (1999), pp. 436–441.

[46] R. A. Mitcheltree et al. “Aerodynamics of Stardust sample return capsule”. In: *Journal of Spacecraft and Rockets* 36.3 (1999), pp. 429–435.

[47] W. J. Marko. *Static aerodynamic characteristics of three blunted sixty-degree half-angle cones at Mach numbers from 0.60 to 1.30*. Tech. rep. 1968.

[48] B. Walker and R. W. Weaver. *Static aerodynamic characteristics of blunted cones in the Mach-number range from 2.2 to 9.5*. Tech. rep. 1967.

[49] S. Sepka and J. A. Samareh. “Thermal Protection System Mass Estimating Relationships For Blunt-Body, Earth Entry Spacecraft”. In: *45th AIAA Thermophysics Conference* (2015). DOI: 10.2514/6.2015-2507. eprint: https://arc.aiaa.org/doi/pdf/10.2514/6.2015-2507. URL: https://arc.aiaa.org/doi/abs/10.2514/6.2015-2507.

[50] H. L. Justh, A. M. D. Cianciolo, and J. Hoffman. *Venus-GRAM User Guide*. Tech. rep. NASA Marshall Space Flight Center and NASA Langley Research Center, 2021.

[51] K. Sutton and R. A. Graves Jr. *A general stagnation-point convective heating equation for arbitrary gas mixtures*. Tech. rep. NASA, 1971.

[52] J. Casoliva et al. “Robust guidance via a predictor-corrector algorithm with drag tracking for aero-gravity assist maneuvers”. In: *AIAA Guidance, Navigation and Control Conference and Exhibit*. 2008, p. 6816.

[53] M. Pavanello. “CFD modelling of Venus aerocapture flow”. MA thesis. Universita degli Studi di Padova and Instituto Superior Tecnico, 2022.

[54] M. E. Tauber, G. E. Palmer, and D. K. Prabhu. *Stagnation point radiative heating relations for Venus entry*. Tech. rep. 2012.

[55] E. Mooij. *Re-entry Systems*. Springer Nature Switzerland, 2024. ISBN: 9783031621741. DOI: 10.1007/978-3-031-62174-1. URL: http://dx.doi.org/10.1007/978-3-031-62174-1.

[56] A. Seiff et al. “Measurements of thermal structure and thermal contrasts in the atmosphere of Venus and related dynamical observations: Results From the four Pioneer Venus Probes”. In: *Journal of Geophysical Research: Space Physics* 85.A13 (1980), pp. 7903–7933. DOI: https://doi.org/10.1029/JA085iA13p07903. eprint: https://agupubs.onlinelibrary.wiley.com/doi/pdf/10.1029/JA085iA13p07903. URL: https://agupubs.onlinelibrary.wiley.com/doi/abs/10.1029/JA085iA13p07903.

[57] W. H. T. Loh. *Re-entry and Planetary Entry Physics and Technology: I / Dynamics, Physics, Radiation, Heat Transfer and Ablation*. Ed. by W. H. T. Loh. Berlin, Heidelberg: Springer Berlin Heidelberg, 1968. ISBN: 978-3-642-48927-3. DOI: 10.1007/978-3-642-48927-3_3. URL: https://doi.org/10.1007/978-3-642-48927-3_3.

[58] D. Ellerby. “Different Classes of TPS Architectures and the Influence of Material and Architecture on Failure Mode Evolution”. In: *The 10th Ablation Workshop, Burlington, VT*. 2018.

[59] United Kingdom Health and Safety Executive. *Control of exposure to silica dust: A guide for employees*. Tech. rep. 2024.

[60] Peraton Engineering. *Acusil® Thermal Protection System Product Suite*. Tech. rep. 2022.

[61] A. Distante. “Venus Surface and Atmospheric Sample Return Mission: Preliminary Design”. Supervised by Manuela Battipede. Joint program with University at Buffalo, The State University of New York. Master’s thesis. Turin, Italy: Politecnico di Torino, 2020. URL: https://webthesis.biblio.polito.it/12091/.

[62] T. W. Knacke. *Parachute recovery systems: design manual*. Para Pub., 1991.

[63] J. A. Shannon Lipp Mary Albrecht. *Spacecraft Fluidic Thermal Control Subsystem Reliability: An Open-Source Analysis*. Tech. rep. US Air Force Research Laboratory / Space Vehicle Directorate, 2022.

[64] H. Culling. *Statistical Methods Appropriate for Evaluation of Fuze Explosive-Train Safety and Reliability*. Tech. rep. US Naval Ordnance Laboratory, 1953.

[65] C. E. Stewart. *Spacecraft Parachute Recovery System Testing from a Failure Rate Perspective*. Tech. rep. NASA Johnson Space Center, 2013.

[66] J. K. Wayer, J.-F. Castet, and J. H. Saleh. “Spacecraft attitude control subsystem: Reliability, multi-state analyses, and comparative failure behavior in LEO and GEO”. In: *Acta Astronautica* 85 (2013), pp. 83–92. ISSN: 0094-5765. DOI: 10.1016/j.actaastro.2012.12.003. URL: https://www.sciencedirect.com/science/article/pii/S0094576512004833.

[67] L. L. Dai, E. J. Garnero, and J. Lyons. *Development of a Rugged Seismometer for Venus Surface Deployment*. 2023. URL: https://techport.nasa.gov/projects/96536 (visited on 05/15/2025).

[68] W. Brinckerhoff and P. Mahaffy. “Investigating the Origin and Evolution of Venus with Descent Probe Mass Spectrometry”. In: ().

[69] M. G. Trainer et al. *THE DAVINCI VENUS MASS SPECTROMETER INVESTIGATION*. 2024. URL: https://www.hou.usra.edu/meetings/lpsc2024/pdf/2436.pdf (visited on 05/15/2025).

[70] M. G. Trainer et al. “THE DAVINCI VENUS MASS SPECTROMETER INVESTIGATION.” In: *Lunar and Planetary Science Conference*. Vol. 55. Mar. 2024.

[71] P. Mahaffy, C. Webster, and M. e. a. Cabane. “The Sample Analysis at Mars Investigation and Instrument Suite”. In: *Space Sci Rev* 170 (2012), pp. 401–478. DOI: \url{https://doi.org/10.1007/s11214-012-9879-z}.

[72] K. T. T. et al. “Simulation of a Miniature, Low-Power Time-of-Flight Mass Spectrometer for In Situ Analysis of Planetary Atmospheres”. In: *SPIE Defense and Security Symposium*. 2008.

[73] Christopher R. Webster and Paul R. Mahaffy. *Measuring Methane and its Isotopic Ratios 13C/12C and D/H with the Tunable Laser Spectrometer (TLS) on SAM for the Mars Science Laboratory (MSL) Mission*. https://sci.esa.int/documents/33745/35957/1567259793745-Methane2009_Session8_2_TLS_Webster.pdf. Retrieved: 2025-06-17. 2009.

[74] S. Rafkin et al. "A LOW COST TUNABLE LASER SPECTROMETER FOR MARS WATER VAPOR, TRACE GASES, AND EDDY FLUX MEASUREMENTS". In: *Planetary In Situ Surface-Atmosphere*. June 2022.

[75] J. Brückner et al. "Refined data of Alpha Proton X-ray Spectrometer analyses of soils and rocks at the Mars Pathfinder site: Implications for surface chemistry". In: *Journal of Geophysical Research: Planets* 108.E12 (2003). DOI: https://doi.org/10.1029/2003JE002060. eprint: https://agupubs.onlinelibrary.wiley.com/doi/pdf/10.1029/2003JE002060. URL: https://agupubs.onlinelibrary.wiley.com/doi/abs/10.1029/2003JE002060.

[76] R. Rieder et al. "The new Athena alpha particle X-ray spectrometer for the Mars Exploration Rovers". In: *Journal of Geophysical Research: Planets* 108.E12 (2003). DOI: https://doi.org/10.1029/2003JE002150. eprint: https://agupubs.onlinelibrary.wiley.com/doi/pdf/10.1029/2003JE002150. URL: https://agupubs.onlinelibrary.wiley.com/doi/abs/10.1029/2003JE002150.

[77] R. Arevalo Jr, Z. Ni, and R. M. Danell. "Mass spectrometry and planetary exploration: A brief review and future projection". In: *Journal of Mass Spectrometry* 55.1 (2020), e4454. DOI: https://doi.org/10.1002/jms.4454. eprint: https://analyticalsciencejournals.onlinelibrary.wiley.com/doi/pdf/10.1002/jms.4454. URL: https://analyticalsciencejournals.onlinelibrary.wiley.com/doi/abs/10.1002/jms.4454.

[78] P. Wurz et al. "Mass Spectrometric Analysis in Planetary Science: Investigation of the Surface and the Atmosphere". In: *Solar System Research* 46 (Dec. 2010), pp. 408–422. DOI: 10.1134/S003809461206007X.

[79] I. Mitrofanov et al. "Laboratory demonstration of space experiment for spectrometry of planetary gamma-rays with tags of Galactic Cosmic Rays producing them". In: *Nuclear Instruments and Methods in Physics Research Section A: Accelerators, Spectrometers, Detectors and Associated Equipment* 1003 (2021), p. 165286. ISSN: 0168-9002. DOI: https://doi.org/10.1016/j.nima.2021.165286. URL: https://www.sciencedirect.com/science/article/pii/S0168900221002709.

[80] D. A. Senske and J. A. Cutts. *Venus Flagship Mission Study: Report of the Venus Science and Technology Definition Team*. Tech. rep. 2009.

[81] R. Harmon and G. Senesi. "GGR Handbook of Rock and Mineral Analysis Chapter 13 Laser□Induced Breakdown Spectroscopy (LIBS)". In: *Geostandards and Geoanalytical Research* 48 (Nov. 2024), pp. 763–792. DOI: 10.1111/ggr.12560.

[82] R. C. Wiens et al. "Combined remote mineralogical and elemental identification from rovers: Field and laboratory tests using reflectance and laser-induced breakdown spectroscopy". In: *Journal of Geophysical Research: Planets* 107.E11 (2002), FIDO 3-1-FIDO 3–14. DOI: https://doi.org/10.1029/2000JE001439. eprint: https://agupubs.onlinelibrary.wiley.com/doi/pdf/10.1029/2000JE001439. URL: https://agupubs.onlinelibrary.wiley.com/doi/abs/10.1029/2000JE001439.

[83] *The SuperCam Instrument Suite on the NASA Mars 2020 Rover: Body Unit and Combined System Tests*. Feb. 2021. DOI: 10.1007/s11214-020-00777-5.

[84] G. Klingelhoefer et al. "The Alpha Particle X-Ray Spectrometer APXS on Rosetta Philae". In: Jan. 2015.

[85] C. Kuenzer and S. Dech. *Remote Sensing and Digital Image Processing Thermal Infrared Remote Sensing*. URL: http://www.springer.com/series/6477.

[86] R. C. Wiens et al. *The SuperCam Instrument Suite on the NASA Mars 2020 Rover: Body Unit and Combined System Tests*. Feb. 2021. DOI: 10.1007/s11214-020-00777-5.

[87] J. Thapa, M. P. Buric, and B. T. Chorpening. *Non-contact high-temperature measurement using Raman spectroscopy*. Tech. rep. US Department of Energy.

[88] C. Bodie et al. "High temperature X-ray and γ-ray spectroscopy with a diamond detector". In: *Nuclear Instruments and Methods in Physics Research Section A: Accelerators, Spectrometers, Detectors and Associated Equipment* 1058 (2024), p. 168882. ISSN: 0168-9002. DOI: https://doi.org/10.1016/j.nima.2023.168882. URL: https://www.sciencedirect.com/science/article/pii/S0168900223008732.

[89] P. R. Christensen et al. "Miniature Thermal Emission Spectrometer for the Mars Exploration Rovers". In: *Journal of Geophysical Research: Planets* 108.E12 (2003). DOI: https://doi.org/10.1029/2003JE002117. eprint: https://agupubs.onlinelibrary.wiley.com/doi/pdf/10.1029/2003JE002117. URL: https://agupubs.onlinelibrary.wiley.com/doi/abs/10.1029/2003JE002117.

[90] S. Maurice et al. *The SuperCam Instrument Suite on the Mars 2020 Rover: Science Objectives and Mast-Unit Description*. Apr. 2021. DOI: 10.1007/s11214-021-00807-w.

[91] S. K. Sharma, A. K. Misra, and U. N. Singh. "Remote Raman spectroscopy of minerals at elevated temperature relevant to Venus exploration". In: *Lidar Remote Sensing for Environmental Monitoring IX*. Vol. 7153. SPIE, Dec. 2008, p. 715307. ISBN: 9780819473950. DOI: 10.1117/12.806371.

[92] W. J. Larson and J. R. Wertz. *Space Mission Analysis and Design*. Third. El Segundo, CA, USA, Norwell, MA, USA, and Dordrecht, Netherlands: Microcosm Press and Kluwer Academic Publishers, 1999. ISBN: 978-1-881883-10-4.

[93] G. Machin and J. Pearce. "Step change improvements in high-temperature thermocouple thermometry". In: Sept. 2012, pp. 637–643. ISBN: 978-1-4673-1559-3. DOI: 10.1109/CONTROL.2012.6334704.

[94] J. D. Wrbanek et al. *Development of a Venus Surface Wind Sensor Based on a Miniature Drag-Force Anemometer*. Tech. rep. NASA Glenn Research Center, 2020. URL: http://www.sti.nasa.gov.

[95] J. D. Wrbanek. *Development of a Venus Surface Wind Sensor*. Tech. rep. NASA Glenn Research Center. URL: www.nasa.gov.

[96] D. Pullan et al. "Beagle 2: the Exobiological Lander of Mars Express". In: *Mars Express: the Scientific Payload*. 2004.

[97] P. Fortescue and J. Stark. *Spacecraft Systems Engineering*. Second. Chichester, UK: John Wiley and Sons Ltd., 1995.

[98] G. A. Landis and K. C. Mellott. "Venus surface power and cooling systems". In: *Acta Astronautica* 61.11 (2007), pp. 995–1001. ISSN: 0094-5765. DOI: 10.1016/j.actaastro.2006.12.031. URL: https://www.sciencedirect.com/science/article/pii/S0094576507001208.

[99] R. Chang and R. Minck. "Sodium-sulfur battery flight experiment definition study". In: *Journal of Power Sources* 29.3 (1990), pp. 555–563. ISSN: 0378-7753. DOI: https://doi.org/10.1016/0378-7753(90)85025-8. URL: https://www.sciencedirect.com/science/article/pii/0378775390850258.

[100] Ibeos. *B28-275 28-Volt Modular Battery (8S2P)*. Tech. rep. Satsearch, 2024.

[101] I. M. Abdulagatov and P. V. Skripov. "Thermodynamic and Transport Properties of Supercritical Fluids. Part 2: Review of Transport Properties". In: *Russian Journal of Physical Chemistry B* 15 (7 Dec. 2021), pp. 1171–1188. DOI: 10.1134/S1990793121070022.

[102] Y. A. Cengel. *Property Tables and Charts (SI Units)*. 2015, pp. 898, 908.

[103] B. Hu, D. Wu, and R. Z. Wang. *Water vapor compression and its various applications*. Dec. 2018. DOI: 10.1016/j.rser.2018.08.050.

[104] B. A. Pint, K. L. More, and P. F. Tortorelli. "The Effect of Water Vapor on Oxidation Performance of Alloys Used in Recuperators". In: *Volume 1: Turbo Expo 2002*. ASMEDC, Jan. 2002, pp. 1045–1051. DOI: 10.1115/GT2002-30543.

[105] K. R. Anderson et al. "Venus lander electronics payload thermal management using a multistage refrigeration system". In: *Journal of Thermophysics and Heat Transfer* 32.3 (2018), pp. 659–668. DOI: 10.2514/1.T5286.

[106] K. Mellott. “Electronics and sensor cooling with a Stirling cycle for Venus surface mission”. In: *2nd International Energy Conversion Engineering Conference*. 2004, p. 5610.

[107] K. Mellott. “Power conversion with a Stirling cycle for Venus surface mission”. In: *2nd International Energy Conversion Engineering Conference*. 2004, p. 5622.

[108] R. Dyson et al. “Long-lived Venus lander conceptual design: how to keep it cool”. In: *7th International Energy Conversion Engineering Conference*. 2009, p. 4631.

[109] Y. A. Cengel et al. *Thermodynamics: An Engineering Approach*. 9th. New York, NY: McGraw-Hill Education, 2019.

[110] Y. Rodriguez. “Plutonium”. In: *Encyclopedia of toxicology* (2014), pp. 982–985.

[111] A. Rogalski. “Progress in focal plane array technologies”. In: *Progress in Quantum Electronics* 36.2-3 (2012), pp. 342–473.

[112] G. Walker and J. Senft. *Free Piston Stirling Engines*. Ed. by C.A.Brebbia and S. Orszag. Springer-Verlag, 1985.

[113] J. Meseguer, I. Pérez-Grande, and A. Sanz-Andrés. *Spacecraft thermal control*. Woodhead Publishing Limited, 2012.

[114] R. D. Karam. *Satellite Thermal Control for Systems Engineers*. Vol. 181. American Institute of Aeronautics and Astronautics, 1998.

[115] L. Dudzinski. “Radioisotope Power Systems (RPS) for Discovery 2010 Missions”. In: *Discovery Potential Bidders Conference*. 2010.

[116] D. F. Woerner. *Next-Generation Radioisotope Thermoelectric Generator Study Final Report*. Tech. rep. Jet Propulsion Laboratory, California Institute of Technology, 2017.

[117] T. G. George and D. Pavone. *General-purpose heat source safety verification test series: SVT-11 through SVT-13*. Tech. rep. Los Alamos National Lab. (LANL), Los Alamos, NM (United States), May 1986. DOI: 10.2172/5664400. URL: https://www.osti.gov/biblio/5664400.

[118] H. Diamond et al. “Half-lives of Pu-238 and Cm-242”. In: *Phys. Rev. C* 15 (1977), pp. 1034–1042. DOI: 10.1103/PhysRevC.15.1034.

[119] E. Novillo. *Nacelle cowl NExt generation Opening System*. Tech. rep. CESA, 2022.

[120] C. Ha et al. *Reliability Demonstration Approach for Advanced Stirling Radioisotope Generator*. Tech. rep. E-17367. Lockheed Martin Space Systems, NASA Glenn Research Center, Sunpower, Sest Inc., 2010. URL: https://ntrs.nasa.gov/citations/20100040438.

[121] Graphalloy. *Graphalloy® Technical Specifications and Design Information*. PDF provided via private communication by email with manufacturer on 23 June 2025, document might not be publicly accessible.

[122] Ecuadorian Space Agency (EXA). *TITAN-1 350Whr Power Bank Module*. Tech. rep. Satsearch, 2025.

[123] A. Sanchez-Torres. “Radioisotope Power Systems for Space Applications”. In: Oct. 2011. ISBN: 978-953-307-510-5. DOI: 10.5772/20928.

[124] M. R. Islam. “Chapter 7 - Field guidelines”. In: *Reservoir Development*. Ed. by M. R. Islam. Sustainable Oil and Gas Development Series. Gulf Professional Publishing, 2022, pp. 737–843. ISBN: 978-0-12-820053-7. DOI: https://doi.org/10.1016/B978-0-12-820053-7.00004-4. URL: https://www.sciencedirect.com/science/article/pii/B9780128200537000044.

[125] C. Tarau, K. L. Walker, and W. G. Anderson. *High Temperature Variable Conductance Heat Pipes for Radioisotope Stirling Systems*. Tech. rep. 1. Mar. 2009, pp. 22–29. DOI: 10.1063/1.3115500. eprint: https://pubs.aip.org/aip/acp/article-pdf/1103/1/22/12148057/22_1_online.pdf. URL: https://doi.org/10.1063/1.3115500.

[126] B. Häusler et al. “Venus Atmospheric, Ionospheric, Surface and Interplanetary Radio-Wave Propagation Studies with the VeRA Radio-Science Experiment”. In: *ESA Special Publication* 1295 (2006), pp. 1–30.

[127] T. Iida. *Satellite communications : system and its design technology*. Ohmsha ; IOS Press, distributor, 2000. ISBN: 9784274903793. URL: https://books.google.com/books/about/Satellite_Communications.html?id=v-OuSc4t7IQC.

[128] J. D. Kraus. *Antennas*. First edition. New York: McGraw-Hill, 1950. URL: https://durenberger.com/wp-content/uploads/2019/11/Kraus_antennas.pdf.

[129] C. A. Balanis. *Antenna Theory: Analysis and Design*. 4th ed. Hoboken, NJ: John Wiley & Sons, 2016. ISBN: 9781118642061. URL: https://cchgeu.ru/upload/iblock/29e/zeyes3wain7f8rphd73v6lcrhpp415qt/Balanis_Teoriya_Antenn.pdf.

[130] C. Edwards, Jr. et al. “Relay communications strategies for Mars exploration through 2020”. In: *Acta Astronautica* 59.1 (2006). Space for Inspiration of Humankind, Selected Proceedings of the 56th International Astronautical Federation Congress, Fukuoka, Japan, 17-21 October 2005, pp. 310–318. ISSN: 0094-5765. DOI: https://doi.org/10.1016/j.actaastro.2006.02.038. URL: https://www.sciencedirect.com/science/article/pii/S0094576506000816.

[131] D. D. Morabito et al. *Venus Surface AM Radio Link Analysis: Preliminary Study*. IPN Progress Report 42-236. NASA Contract Sponsor. Jet Propulsion Laboratory, California Institute of Technology, Feb. 2024. URL: https://ipnpr.jpl.nasa.gov/progress_report/42-236/236.pdf.

[132] G. Maral, M. Bousquet, and Z. Sun. *Satellite Communications Systems: Systems, Techniques and Technology*. 6th. Includes discussions on digital signal communication for space. John Wiley & Sons, 2017. URL: https://books.google.nl/books?id=0bVeDwAAQBAJ.

[133] J. G. Proakis and M. Salehi. *Digital Communications*. 5th. A foundational textbook comparing digital and analog communication, emphasizing noise immunity, error correction, and bandwidth efficiency. McGraw-Hill, 2008.

[134] NASA Communications Division. *Benefits of Digital Signal Processing in Space Communications*. Tech. rep. Discusses digital signal processing (DSP) efficiency in deep-space missions. NASA, 2012. URL: https://www.nasa.gov/directorates/heo/scan/engineering/technology/txt_accordion1.html.

[135] G. D. Hunter et al. *High-Temperature Electronics Progress White Paper*. Tech. rep. NASA/TM–2020-5004681. NASA Technical Memorandum. NASA Glenn Research Center, 2020. URL: https://ntrs.nasa.gov/api/citations/20205004681/downloads/High%20Temp%20Electronics%20Progress%20White%20paper%20Hunter%20NASA%20Glenn.pdf.

[136] NASA Jet Propulsion Laboratory. *NASA's Mission Operations and Communications Services (MOCS)*. Technical Report. Accessed on today. NASA / JPL, Oct. 2014. URL: https://deepspace.jpl.nasa.gov/files/6_NASA_MOCS_2014_10_01_14.pdf.

[137] M. Maldari. *Satellite Operations Center: An Integrated Approach*. Technical Report (SOC Q1 2008). Presented at Space Ops Conference Q1 2008; available at opsjournal.org. Aerospace Corporation, Mar. 2008. URL: https://opsjournal.org/DocumentLibrary/Uploads/2008Q1_SOC_Maldari.pdf.

[138] S. Miller, A. Wales, and E. Reid. “Long-Term Venus Lander”. Honors Theses Paper 3383. Honors Thesis. Western Michigan University, Apr. 2021. URL: https://scholarworks.wmich.edu/honors_theses/3383.

[139] E. J. Smith et al. *Venus Lander Mission Concept Study*. Technical Report NASA/TM-2016-219180. National Aeronautics and Space Administration (NASA), 2016. URL: https://ntrs.nasa.gov/api/citations/20160011272/downloads/20160011272.pdf.

[140] G. Slade. “The Basics of Quadrifilar Helix Antennas”. In: *RF Globalnet Newsletter* (Mar. 2015). URL: https://www.researchgate.net/publication/275828209_The_Basics_of_Quadrifilar_Helix_Antennas.

[141] W. Tomasi. *Electronic Communication Systems: Fundamentals through Advanced*. 5th. Comprehensive textbook covering analog/digital communication systems, modulation, and transmission technologies. Jurong, Singapore: Pearson Education South East Asia, 2004. ISBN: 981-247-093-X.

[142] F. Alimenti et al. “K/Ka-Band Very High Data-Rate Receivers: A Viable Solution for Future Moon Exploration Missions”. In: *Electronics* 8.3 (2019). ISSN: 2079-9292. DOI: 10.3390/electronics8030349. URL: https://www.mdpi.com/2079-9292/8/3/349.

[143] A. Grami. *Communication Networks*. Ed. by A. Grami. Chapter from the edited volume. Academic Press, 2016, pp. 457–491. ISBN: 9780124076822. DOI: 10.1016/B978-0-12-407682-2.00011-9. URL: https://doi.org/10.1016/B978-0-12-407682-2.00011-9.

[144] C. Diez et al. “GMAT: A Generic Mission Analysis Tool for Multiple Use Cases”. In: *Proceedings of the 8th International ESA Conference on Space Debris (SDC 2022)*. ESA. 2022. URL: https://conference.sdo.esoc.esa.int/proceedings/sdc8/paper/184/SDC8-paper184.pdf.

[145] NASA Jet Propulsion Laboratory. *DSN Telecommunications Link Design Handbook (810-005, Rev. E)*. https://deepspace.jpl.nasa.gov/dsndocs/810-005/. 2021. URL: https://deepspace.jpl.nasa.gov/dsndocs/810-005/.

[146] Consultative Committee for Space Data Systems (CCSDS). *Radio Frequency and Modulation Systems—Part 1: Earth Stations and Spacecraft (CCSDS 401.0-B-24)*. https://public.ccsds.org/Pubs/401x0b24.pdf. May 2019. URL: https://public.ccsds.org/Pubs/401x0b24.pdf.

[147] M. E. Al-Mualla, C. N. Canagarajah, and D. R. Bull. “Chapter 9 - Error-Resilience Video Coding Techniques”. In: *Video Coding for Mobile Communications*. Ed. by M. E. Al-Mualla, C. N. Canagarajah, and D. R. Bull. Signal Processing and its Applications. San Diego: Academic Press, 2002, pp. 205–229. ISBN: 978-0-12-053079-3. DOI: https://doi.org/10.1016/B978-012053079-3/50011-1. URL: https://www.sciencedirect.com/science/article/pii/B9780120530793500111.

[148] M. R. H. Proloy. “Design and Implementation of a Low Power Communication System for Wireless Sensor Networks”. Accessed: 2025-06-17. MA thesis. Khulna University of Engineering & Technology, 2013. URL: http://103.133.167.11:8080/bitstream/handle/123456789/2013/Md._Razaul_Hoq_Proloy.pdf?sequence=1&isAllowed=y.

[149] R. Esmailzadeh, M. Nakagawa, and E. Sourour. “Time-division duplex CDMA communications”. In: *IEEE Personal Communications* 4.2 (1997), pp. 51–56. DOI: 10.1109/98.590675.

[150] W. L. Stutzman and G. A. Thiele. *Antenna Theory and Design*. 3rd ed. Retrieved from Hungarian University of Agriculture and Life Sciences (formerly Széchenyi István University). Wiley, 2012. ISBN: 978-0-470-57664-9. URL: https://maxwell.sze.hu/~ungert/Radiorendszerek_satlab/Segedanyagok/Ajanlott_irodalom/antenna_theory_and_design_-_stutzman_,_thiele.pdf.

[151] H.-G. Zhang et al. “Low-density parity-check code (LDPC) schemes with BICM”. In: *International Conference on Communication Technology Proceedings, 2003. ICCT 2003.* Vol. 2. 2003, 1148–1151 vol.2. DOI: 10.1109/ICCT.2003.1209733.

[152] ANSYS Inc. *ANSYS Granta*. Software Package, Ver. 2024 R2. 2024.

[153] M. Ashby, H. Shercliff, and D. Cebon. *Materials: Engineering, Science, Processing and Design*. Fourth edition. Elsevier, 2019, p. 593.

[154] J. Lee et al. “Silica nanoparticles as copper corrosion inhibitors”. In: *Materials Research Express* 6 (8 June 2019). DOI: 10.1088/2053-1591/ab2270.

[155] N. Bekoz and E. Oktay. “High temperature mechanical properties of low alloy steel foams produced by powder metallurgy”. In: *Materials and Design* 53 (2014), pp. 482–489. DOI: 10.1016/j.matdes.2013.07.050.

[156] M. Tavares et al. “Mechanical behavior of steel and aluminum foams at elevated temperatures. Local buckling based approach toward understanding of the material system behavior”. In: *International Journal of Mechanical Sciences* 181 (Sept. 2020). DOI: 10.1016/j.ijmecsci.2020.105754.

[157] Sigma-Aldrich. *Safety Data Sheet Aluminum Oxide*. Tech. rep. Oct. 2021.

[158] Centerline. *Safety Data Sheet (SDS) CenterLine Glidcop Resistance Welding Electrodes and Material*. Tech. rep. May 2021.

[159] Carl Roth GmbH. *Safety Data Sheet Molybdenum Standard Solution -AAS 1000 mg/l Mo*. Tech. rep. Sept. 2024.

[160] Corteva Agriscience. *Safety Data Sheet Sapphire*. Tech. rep. Mar. 2022.

[161] Johns Manville. *Safety Data Sheet Amorphous High-Purity Silica Fiber*. Tech. rep. July 2024.

[162] Carl Roth GmbH. *Safety Data Sheet Silver ≥99,9 %, 0,5 mm as wire*. Tech. rep. Oct. 2024.

[163] TW Metals. *Safety Data Sheet Stainless Steel*. Tech. rep. Aug. 2022.

[164] LTS Research Laboratories Inc. *Material Safety Data Sheet Titanium Alloy Grade 5*. Tech. rep. Sept. 2014.

[165] J. W. Hutchinson. URL: https://groups.seas.harvard.edu/hutchinson/papers/RevisitingSphericalShells-2016.pdf.

[166] F. Alisafaei et al. *Nanoindentation based properties of Inconel 718 at elevated temperatures: A comparison of conventional versus additively manufactured samples*. May 2019. URL: https://www.sciencedirect.com/science/article/pii/S074964191830860X.

[167] K. Schroeder, J. Bayandor, and J. Samareh. “Structural sizing and synthesis of venera-class landers”. In: *Journal of Spacecraft and Rockets* 55.3 (2018), pp. 561–574.

[168] ERGAerospace. *Foam energy absorption: Duocel® foam*. URL: https://ergaerospace.com/energy-absorption/.

[169] J. Ying and X. Zhang. *Mechanical performance and cushioning energy absorption characteristics of rigid polyurethane foam at low and high strain rates*. Mar. 2022. URL: https://www.sciencedirect.com/science/article/pii/S0142941822000575.

[170] M. Orme and M. Ferrari. URL: https://www.researchgate.net/publication/318550709_Designing_for_Additive_Manufacturing_Lightweighting_Through_Topology_Optimization_Enables_Lunar_Spacecraft.

[171] X. Wang et al. *Topology optimization of aerospace part to enhance the performance by additive manufacturing process*. Feb. 2022. URL: https://www.sciencedirect.com/science/article/pii/S2214785322006460?.

Appendices

The Function Breakdown Structure, Function Flow Chart, post DSE Gantt chart and Communication Flow Diagram are shown on the following pages, in this order.

Appendix A

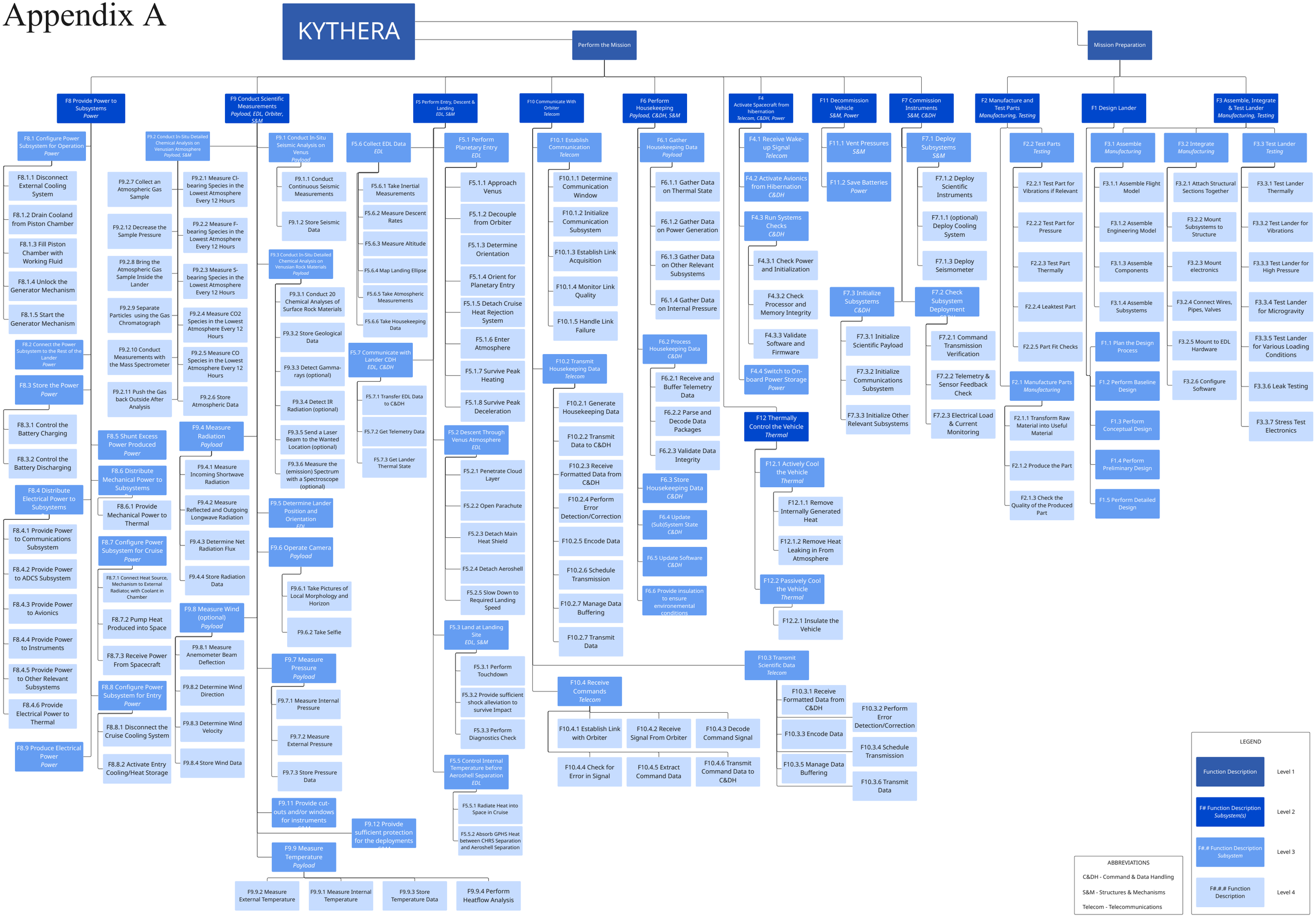
KYTHERA
Perform the Mission
Mission Preparation
F8 Provide Power to Subsystems
Power
F8.1 Configure Power Subsystem for Operation
Power
F8.1.1 Disconnect External Cooling System
F8.1.2 Drain Cooland from Piston Chamber
F8.1.3 Fill Piston Chamber with Working Fluid
F8.1.4 Unlock the Generator Mechanism
F8.1.5 Start the Generator Mechanism
F8.2 Connect the Power Subsystem to the Rest of the Lander
Power
F8.3 Store the Power
Power
F8.3.1 Control the Battery Charging
F8.3.2 Control the Battery Discharging
F8.4 Distribute Electrical Power to Subsystems
F8.4.1 Provide Power to Communications Subsystem
F8.4.2 Provide Power to ADCS Subsystem
F8.4.3 Provide Power to Avionics
F8.4.4 Provide Power to Instruments
F8.4.5 Provide Power to Other Relevant Subsystems
F8.4.6 Provide Electrical Power to Thermal
F8.5 Shunt Excess Power Produced
Power
F8.6 Distribute Mechanical Power to Subsystems
F8.6.1 Provide Mechanical Power to Thermal
F8.7 Configure Power Subsystem for Cruise
Power
F8.7.1 Connect Heat Source, Mechanism to External Radiator, with Coolant in Chamber
F8.7.2 Pump Heat Produced into Space
F8.7.3 Receive Power From Spacecraft
F8.8 Configure Power Subsystem for Entry
Power
F8.8.1 Disconnect the Cruise Cooling System
F8.8.2 Activate Entry Cooling/Heat Storage
F8.9 Produce Electrical Power
Power
F9 Conduct Scientific Measurements
Payload, EDL, Orbiter, S&M
F9.2 Conduct In-Situ Detailed Chemical Analysis on Venusian Atmosphere
Payload, S&M
F9.2.7 Collect an Atmospheric Gas Sample
F9.2.12 Decrease the Sample Pressure
F9.2.8 Bring the Atmospheric Gas Sample Inside the Lander
F9.2.9 Separate Particles using the Gas Chromatograph
F9.2.10 Conduct Measurements with the Mass Spectrometer
F9.2.11 Push the Gas back Outside After Analysis
F9.2.1 Measure Cl-bearing Species in the Lowest Atmosphere Every 12 Hours
F9.2.2 Measure F-bearing Species in the Lowest Atmosphere Every 12 Hours
F9.2.3 Measure S-bearing Species in the Lowest Atmosphere Every 12 Hours
F9.2.4 Measure CO2 Species in the Lowest Atmosphere Every 12 Hours
F9.2.5 Measure CO Species in the Lowest Atmosphere Every 12 Hours
F9.2.6 Store Atmospheric Data
F9.4 Measure Radiation
Payload
F9.4.1 Measure Incoming Shortwave Radiation
F9.4.2 Measure Reflected and Outgoing Longwave Radiation
F9.4.3 Determine Net Radiation Flux
F9.4.4 Store Radiation Data
F9.8 Measure Wind (optional)
Payload
F9.8.1 Measure Anemometer Beam Deflection
F9.8.2 Determine Wind Direction
F9.8.3 Determine Wind Velocity
F9.8.4 Store Wind Data
F9.1 Conduct In-Situ Seismic Analysis on Venus
Payload
F9.1.1 Conduct Continuous Seismic Measurements
F9.1.2 Store Seismic Data
F9.3 Conduct In-Situ Detailed Chemical Analysis on Venusian Rock Materials
Payload
F9.3.1 Conduct 20 Chemical Analyses of Surface Rock Materials
F9.3.2 Store Geological Data
F9.3.3 Detect Gamma-rays (optional)
F9.3.4 Detect IR Radiation (optional)
F9.3.5 Send a Laser Beam to the Wanted Location (optional)
F9.3.6 Measure the (emission) Spectrum with a Spectroscope (optional)
F9.5 Determine Lander Position and Orientation
EDL
F9.6 Operate Camera
Payload
F9.6.1 Take Pictures of Local Morphology and Horizon
F9.6.2 Take Selfie
F9.7 Measure Pressure
Payload
F9.7.1 Measure Internal Pressure
F9.7.2 Measure External Pressure
F9.7.3 Store Pressure Data
F9.11 Provide cut-outs and/or windows for instruments
F9.12 Proivde sufficient protection for the deployments
F9.9 Measure Temperature
Payload
F9.9.2 Measure External Temperature
F9.9.1 Measure Internal Temperature
F9.9.3 Store Temperature Data
F9.9.4 Perform Heatflow Analysis
F5 Perform Entry, Descent & Landing
EDL, S&M
F5.6 Collect EDL Data
EDL
F5.6.1 Take Inertial Measurements
F5.6.2 Measure Descent Rates
F5.6.3 Measure Altitude
F5.6.4 Map Landing Ellipse
F5.6.5 Take Atmospheric Measurements
F5.6.6 Take Housekeeping Data
F5.7 Communicate with Lander CDH
EDL, C&DH
F5.7.1 Transfer EDL Data to C&DH
F5.7.2 Get Telemetry Data
F5.7.3 Get Lander Thermal State
F5.1 Perform Planetary Entry
EDL
F5.1.1 Approach Venus
F5.1.2 Decouple from Orbiter
F5.1.3 Determine Orientation
F5.1.4 Orient for Planetary Entry
F5.1.5 Detach Cruise Heat Rejection System
F5.1.6 Enter Atmosphere
F5.1.7 Survive Peak Heating
F5.1.8 Survive Peak Deceleration
F5.2 Descent Through Venus Atmosphere
EDL
F5.2.1 Penetrate Cloud Layer
F5.2.2 Open Parachute
F5.2.3 Detach Main Heat Shield
F5.2.4 Detach Aeroshell
F5.2.5 Slow Down to Required Landing Speed
F5.3 Land at Landing Site
EDL, S&M
F5.3.1 Perform Touchdown
F5.3.2 Provide sufficient shock alleviation to survive Impact
F5.3.3 Perform Diagnostics Check
F5.5 Control Internal Temperature before Aeroshell Separation
EDL
F5.5.1 Radiate Heat into Space in Cruise
F5.5.2 Absorb GPHS Heat between CHRS Separation and Aeroshell Separation
F10 Communicate With Orbiter
Telecom
F10.1 Establish Communication
Telecom
F10.1.1 Determine Communication Window
F10.1.2 Initialize Communication Subsystem
F10.1.3 Establish Link Acquisition
F10.1.4 Monitor Link Quality
F10.1.5 Handle Link Failure
F10.2 Transmit Housekeeping Data
Telecom
F10.2.1 Generate Housekeeping Data
F10.2.2 Transmit Data to C&DH
F10.2.3 Receive Formatted Data from C&DH
F10.2.4 Perform Error Detection/Correction
F10.2.5 Encode Data
F10.2.6 Schedule Transmission
F10.2.7 Manage Data Buffering
F10.2.7 Transmit Data
F10.3 Transmit Scientific Data
Telecom
F10.3.1 Receive Formatted Data from C&DH
F10.3.2 Perform Error Detection/Correction
F10.3.3 Encode Data
F10.3.4 Schedule Transmission
F10.3.5 Manage Data Buffering
F10.3.6 Transmit Data
F10.4 Receive Commands
Telecom
F10.4.1 Establish Link with Orbiter
F10.4.2 Receive Signal From Orbiter
F10.4.3 Decode Command Signal
F10.4.4 Check for Error in Signal
F10.4.5 Extract Command Data
F10.4.6 Transmit Command Data to C&DH
F6 Perform Housekeeping
Payload, C&DH, S&M
F6.1 Gather Housekeeping Data
Payload
F6.1.1 Gather Data on Thermal State
F6.1.2 Gather Data on Power Generation
F6.1.3 Gather Data on Other Relevant Subsystems
F6.1.4 Gather Data on Internal Pressure
F6.2 Process Housekeeping Data
C&DH
F6.2.1 Receive and Buffer Telemetry Data
F6.2.2 Parse and Decode Data Packages
F6.2.3 Validate Data Integrity
F6.3 Store Housekeeping Data
C&DH
F6.4 Update (Sub)System State
C&DH
F6.5 Update Software
C&DH
F6.6 Provide insulation to ensure environemental conditions
F4 Activate Spacecraft from hibernation
Telecom, C&DH, Power
F4.1 Receive Wake-up Signal
Telecom
F4.2 Activate Avionics from Hibernation
C&DH
F4.3 Run Systems Checks
C&DH
F4.3.1 Check Power and Initialization
F4.3.2 Check Processor and Memory Integrity
F4.3.3 Validate Software and Firmware
F4.4 Switch to On-board Power Storage
Power
F12 Thermally Control the Vehicle
Thermal
F12.1 Actively Cool the Vehicle
Thermal
F12.1.1 Remove Internally Generated Heat
F12.1.2 Remove Heat Leaking in From Atmosphere
F12.2 Passively Cool the Vehicle
Thermal
F12.2.1 Insulate the Vehicle
F11 Decommission Vehicle
S&M, Power
F11.1 Vent Pressures
S&M
F11.2 Save Batteries
Power
F7.3 Initialize Subsystems
C&DH
F7.3.1 Initialize Scientific Payload
F7.3.2 Initialize Communications Subsystem
F7.3.3 Initialize Other Relevant Subsystems
F7 Commission Instruments
S&M, C&DH
F7.1 Deploy Subsystems
S&M
F7.1.2 Deploy Scientific Instruments
F7.1.1 (optional) Deploy Cooling System
F7.1.3 Deploy Seismometer
F7.2 Check Subsystem Deployment
F7.2.1 Command Transmission Verification
F7.2.2 Telemetry & Sensor Feedback Check
F7.2.3 Electrical Load & Current Monitoring
F2 Manufacture and Test Parts
Manufacturing, Testing
F2.2 Test Parts
Testing
F2.2.1 Test Part for Vibrations if Relevant
F2.2.2 Test Part for Pressure
F2.2.3 Test Part Thermally
F2.2.4 Leaktest Part
F2.2.5 Part Fit Checks
F2.1 Manufacture Parts
Manufacturing
F2.1.1 Transform Raw Material into Useful Material
F2.1.2 Produce the Part
F2.1.3 Check the Quality of the Produced Part
F1 Design Lander
F3.1 Assemble
Manufacturing
F3.1.1 Assemble Flight Model
F3.1.2 Assemble Engineering Model
F3.1.3 Assemble Components
F3.1.4 Assemble Subsystems
F3.2 Integrate
Manufacturing
F3.2.1 Attach Structural Sections Together
F3.2.2 Mount Subsystems to Structure
F3.2.3 Mount electronics
F3.2.4 Connect Wires, Pipes, Valves
F3.2.5 Mount to EDL Hardware
F3.2.6 Configure Software
F3.3 Test Lander
Testing
F3.3.1 Test Lander Thermally
F3.3.2 Test Lander for Vibrations
F3.3.3 Test Lander for High Pressure
F3.3.4 Test Lander for Microgravity
F3.3.5 Test Lander for Various Loading Conditions
F3.3.6 Leak Testing
F3.3.7 Stress Test Electronics
F1.1 Plan the Design Process
F1.2 Perform Baseline Design
F1.3 Perform Conceptual Design
F1.4 Perform Preliminary Design
F1.5 Perform Detailed Design
ABBREVIATIONS
C&DH - Command & Data Handling
S&M - Structures & Mechanisms
Telecom - Telecommunications
LEGEND
Function Description
Level 1
F# Function Description
Subsystem(s)
Level 2
F#.# Function Description
Subsystem
Level 3
F#.#.# Function Description
Level 4

Appendix B1

F1 Design Lander

F2 Manufacture and Test Parts *Manufacturing, Testing*

F3 Assemble, Integrate, and Test Lander *Manufacturing, Testing*

F4 Activate Spacecraft from hibernation *Telecom, C&DH, Power*

F5 Perform EDL Procedure *EDL, S&M,C&DH*

F6 Perform Housekeeping *Payload, C&DH*

F7 Commission Instruments *S&M, C&DH*

F8 Provide Power to Subsystems *Power*

F9 Conduct Scientific Measurements *Payload, EDL, Orbiter*

F10 Communicate with Orbiter *Telecom*

F11 Decommission vehicle *S&M, Power*

F12 Thermally Control the Vehicle *Thermal*

F2.1 Manufacture Parts *Manufacturing*

F2.1.1 Transform Raw Material into Useful Material

F2.1.2 Produce the Part

F2.1.3 Check the Quality of the Produced Part

F2.2 Test Parts *Testing*

F2.2.1 Test Part for Vibrations if Relevant

F2.2.2 Test Part for Pressure

F2.2.3 Test Part Thermally

F2.2.4 Part Leaktests

F2.2.5 Part Fit Checks

F1.1 Plan the Design Process

F1.2 Perform Baseline Design

F1.3 Perform Conceptual Design

F1.4 Perform Preliminary Design

F1.5 Perform Detailed Design

F3.1 Assemble *Manufacturing*

F3.1.1 Assemble Flight Model

F3.1.2 Assemble Engineering Model

F3.1.3 Assemble Components

F3.1.4 Assemble Subsystems

F3.2 Integrate *Manufacturing*

F3.2.1 Assemble structural Sections Together

F3.2.2 Mount subsystems to Structure

F3.2.3 Mount Electronics

F3.2.4 Connect Wires, Pipes, Valves

F3.2.5 Mount vehicle to EDL Hardware

F3.2.6 Configure Software

F3.3 Test Lander *Testing*

F3.3.1 Test Lander Thermally

F3.3.2 Test Lander for Vibrations

F3.3.3 Test Lander for High Pressure

F3.3.4 Test Lander for Microgravity

F3.3.5 Test Lander for Various Loading Conditions

F3.3.6 Leak Testing

F3.3.7 Stress Test Electronics

F5.5 Control Internal Temperature before Aeroshell Separation *EDL*

F5.5.1 Radiate Heat into Space in Cruise

F5.5.2 Absorb GPHS Heat between CHRS Separation and Aeroshell Separation

F5.1.3 Determine Orientation

AND

F5.1 Perform Planetary Entry *EDL*

F5.1.1 Approach Venus

F5.1.2 Decouple from Orbiter

AND

F5.1.4 Orient for Planetary Entry

F5.1.5 Detach Cruise Heat Rejection System

F5.1.6 Enter Atmosphere

F5.1.7 Survive Peak Heating

F5.1.8 Survive Peak Deceleration

F5.2 Descent Through Venus Atmosphere *EDL*

F5.2.1 Penetrate Cloud Layer

F5.2.2 Open Parachute

F5.2.3 Detach Main Heat Shield

F5.2.4 Detach Aeroshell

F5.2.5 Slow Down to Required Landing Speed

AND

F5.3 Land at Landing Site *EDL, S&M*

AND

F5.3.1 Perform Touchdown

F5.3.3 Perform Diagnostics Check

F5.3.2 Provide sufficient shock alleviation to survive Impact

AND

F5.7 Communicate with Lander C&DH *EDL, C&DH*

AND

F5.7.2 Get Telemetry Data

F5.7.3 Get Lander Thermal State

F5.7.1 Transfer EDL Data to C&DH

F5.6 Collect EDL Data *EDL*

AND

F5.6.1 Take Inertial Measurements

F5.6.2 Measure Descent Rates

F5.6.3 Measure Altitude

F5.6.5 Take Atmospheric Measurements

F5.6.6 Take Housekeeping Data

F5.6.4 Map Landing Ellipse

F6.6 Provide insulation to ensure environemental conditions S&M

AND

F6.1 Gather Housekeeping Data *Payload*

AND

F6.1.3 Gather Data on Internal Pressure

F6.1.3 Gather Data on Other Relevant Subsystems

F6.1.2 Gather Data on Power Generation

F6.1.1 Gather Data on Thermal State

F6.2 Process Housekeeping Data *C&DH*

F6.2.1 Receive and Buffer Telemetry Data

F6.2.2 Parse and Decode Data Packages

F6.2.3 Validate Data Integrity

F6.3 Store Housekeeping Data *C&DH*

OR

F6.4 Update (Sub)System State *C&DH*

F6.5 Update Software *C&DH*

F7.1 Deploy Subsystems *S&M*

AND

F7.1.1 (optional) Deploy Cooling System

F7.1.2 Deploy Scientific Instruments

F7.1.3 Deploy Seismometer

F7.2 Check Subsystem Deployment *C&DH*

F7.2.1 Command Transmission Verification

F7.2.2 Telemetry & Sensor Feedback Check

F7.2.3 Electrical Load & Current Monitoring

F7.3 Initialize Subsystems *C&DH*

F7.3.1 Initialize Scientific Payload

F7.3.2 Initialize Communications Subsystem

F7.3.3 Initialize Other Relevant Subsystems

F4.1 Receive Wake-up Signal *Telecom*

F4.2 Activate Avionics from Hibernation *C&DH*

F4.3 Run Systems Check *C&DH*

F4.4 Switch to On-board Power Storage *Power*

F4.3.1 Check Power and Initialization

F4.3.2 Check Processor and Memory Integrity

F4.3.3 Validate Software and Firmware

ABBREVIATIONS

C&DH - Command & Data Handling

S&M - Structures & Mechanisms

Telecom - Telecommunications

LEGEND

F# Function Description *Subsystem(s)* — Level 2

F#.# Function Description *Subsystem* — Level 3

F#.#.# Function Description — Level 4

Level 4 does not have explicitly indicated subsystems. Its subsystem is the one in the corresponding Level 3 function.

Appendix B2

F1 Design Lander

F2 Manufacture and Test Parts *Manufacturing, Testing*

F3 Assemble, Integrate, and Test Lander *Manufacturing, Testing*

F4 Activate Spacecraft from hibernation *Telecom, C&DH, Power*

F5 Perform EDL Procedure *EDL, S&M,C&DH*

F6 Perform Housekeeping *Payload, C&DH*

F7 Commission Instruments *S&M, C&DH*

F8 Provide Power to Subsystems *Power*

F9 Conduct Scientific Measurements *Payload, EDL, Orbiter*

F10 Communicate with Orbiter *Telecom*

F11 Decommission vehicle *S&M, Power*

F11.1 Vent Pressures *S&M*

F11.2 Save Batteries *Power*

F12 Thermally Control the Vehicle *Thermal*

AND

F12.1 Actively Cool the Vehicle *Thermal*

F12.1.1 Remove Internally Generated Heat *Telecom, Thermal*

F12.1.2 Remove Heat Leaking in from Atmosphere *Thermal*

F12.2 Passively Cool the Vehicle *Thermal*

F12.2.1 Insulate the Vehicle *Thermal*

F8.7 Configure Power Subsys. for Cruise Generation *Power*

F8.7.1 Connect Heat Source, Mechanism to External Radiator, with Coolant in Chamber

AND

F8.7.2 Pump Heat Produced into Space

F8.7.3 Receive Power From Mother Probe

F8.8 Configure Power Subsys. for Entry *Power*

F8.8.2 Activate Entry Cooling/Heat Storage

F8.8.1 Disconnect Cruise Cooling

F8.1 Configure Power Subsystem for Operation *Power*

F8.1.1 Disconnect Entry Cooling

F8.1.2 Drain Coolant from Piston Chamber

F8.1.3 Fill Piston Chamber with Working Fluid

F8.1.4 Unlock the Generator Mechanism

F8.1.5 Start the Generator Mechanism

F8.2 Connect Power Subsystem to the rest of the Lander *Power*

F8.3 Produce Electrical Power *Power*

AND

F8.4 Distribute Electrical Power to Subsystems *Power*

AND

F8.4.1 Provide Power to Communications Subsystem

F8.4.2 Provide Power to ADCS Subsystem

F8.4.3 Provide Power to Avionics

F8.4.4 Provide Power to Instruments

F8.4.5 Provide Power to Other Relevant Subsystems

F8.4.6 Provide Electrical Power to Thermal

F8.5 Shunt Excess Power *Power*

OR

F8.3 Store the Electrical Power *Power*

AND

F8.3.1 Control the Battery Discharging

F8.3.1 Control the Battery Charging

F8.6 Distribute Mechanical Power to Subsystems *Power*

F8.6.1 Distribute Mechanical Power to Thermal

AND

F9.1 Conduct In-situ Seismic Analysis on Venus *Payload*

F9.1.1 Conduct Continuous Seismic Measurements

F9.1.2 Store Seismic Data

F9.3 Conduct In-Situ Detailed Chemical Analysis on Venusian Rock Materials *Payload*

F9.3.1 Conduct 20 Chemical Analyses of Surface Rock Materials

OR

F9.3.5 Measure the (emission) Spectrum with a Spectroscope (optional)

F9.3.5 Send a Laser Beam to the Wanted Location

F9.3.3 Detect Gamma-rays (optional)

F9.3.4 Detect IR Radiation (optional)

F9.3.2 Store Geological Data

F9.5 Determine Lander Position and Orientation *EDL*

F9.2 Conduct Chemical Analysis on Venusian Lower Atmosphere *Payload*

F9.2.7 Collect an Atmospheric Gas Sample

F9.2.12 Decrease the Sample Pressure

F9.2.8 Bring the Atmospheric Gas Sample Inside the Lander

F9.2.9 Separate Particles using the Gas Chromatograph

F9.2.10 Conduct Measurements with the Mass Spectrometer

AND

F9.2.1 Measure Cl-bearing Species

F9.2.2 Measure F-bearing Species

F9.2.3 Measure S-bearing Species

F9.2.4 Measure CO2 Species

F9.2.5 Measure CO Species

F9.2.6 Store Atmospheric Data

F9.2.11 Push the Gas back Outside After Analysis

Repeat Every 12 Hours

F9.4 Measure Radiation *Payload*

AND

F9.4.1 Measure Incoming Shortwave Radiation

F9.4.2 Measure Reflected and Outgoing Longwave Radiation

F9.4.3 Determine Net Radiative Flux

F9.4.4 Store Radiation Data

F9.6 Operate Camera *Payload*

OR

F9.6.2 Take Selfie

F9.6.1 Take Pictures of Local Morphology and Horizon

F9.7 Measure Pressure *Payload*

AND

F9.7.1 Measure Internal Pressure

F9.7.2 Measure External Pressure

F9.7.3 Store Pressure Data

F9.8 Measure Wind (optional) *Payload*

F9.8.1 Measure Anemometer Beam Deflection

AND

F9.8.2 Determine Wind Direction

F9.8.3 Determine Wind Velocity

F9.8.4 Store Wind Data

F9.9 Measure Temperature *Payload*

AND

F9.9.1 Measure Internal Temperature

F9.9.2 Measure External Temperature

F9.9.3 Store Temperature Data

F9.9.4 Perform Heatflow Analysis

F9.11 Provide Cut-Outs and/or Windows for Instruments *S&M*

F9.12 Provide Sufficient Protection for the Deployments *S&M*

F10.1 Establish Communication *Telecom*

F10.1.1 Determine Communication Window

F10.1.2 Initialize Communication Subsystem

F10.1.3 Establish Link Acquisition

F10.1.4 Monitor Link Quality

F10.1.5 Handle Link Failure

F10.2 Transmit Housekeeping Data *Telecom*

F10.2.1 Generate Housekeeping Data

F10.2.2 Transmit Data to C&DH

F10.2.3 Receive Formatted Data from C&DH

F10.2.4 Perform Error Detection/Correction

F10.2.5 Encode Data

F10.2.6 Schedule Transmission

F10.2.7 Manage Data Buffering

F10.2.8 Transmit Data

F10.3 Transmit Scientific Data *Telecom*

F10.3.1 Receive Formatted Data from C&DH

F10.3.2 Perform Error Detection/Correction

F10.3.3 Encode Data

F10.3.4 Schedule Transmission

F10.3.5 Manage Data Buffering

F10.3.6 Transmit Data

F10.4 Receive Commands *Telecom*

F10.4.1 Establish Link with Orbiter

F10.4.2 Receive Signal from Orbiter

F10.4.3 Decode Command Signal

F10.4.4 Check for Error in Signal

F10.4.5 Extract Command Data

F10.4.6 Transmit Command Data to C&DH

ABBREVIATIONS

C&DH - Command & Data Handling

S&M - Structures & Mechanisms

Telecom - Telecommunications

LEGEND

F# Function Description *Subsystem(s)* — Level 2

F#.# Function Description *Subsystem* — Level 3

F#.#.# Function Description — Level 4

Level 4 does not have explicitly indicated subsystems. Its subsystem is the one in the corresponding Level 3 function.

Appendix C

Post DSE Gantt Chart

Task ID	Task	Start Date	End Date
P	**Preliminary Design**	**01/Jul/2025**	**31/Dec/2025**
P.1	Complete Preliminary Design Iterations		
P.2	Finalize Lander Architecture		
P.R1	Preliminary design review	31/Dec/2025	
D	**Detailed Design**	**01/Jan/2026**	**31/Mar/2028**
D.1	Detailed Interface Definition		
D.2	Orbiter System Level Design		
D.3	Order long lead items		
D.4	Orbiter Subsystem level Design		
D.5	Life Cycle Assessment		
D.6	Build Engineering Model (BBM & EM)		
D.7	Breadboard Testing		
D.8	Rebaselining	31/Sep/2027	
D.9	Complete COSPAR Documentations		
D.10	Plan Assembly & Integration Testing		
D.11	Documentation		
D.R1	Critical Design Review	31/Mar/2028	
QV	**Qualification/Verification and Production**	**01/Apr/2028**	**30/Jun/2034**
QV.1	Build Qualification Hardware		
QV.2	Qualification Subsystem Level Testing		
QV.3	Software Testing		
QV.4	Rebaselining	31/Sep/2029	
QV.5	Integrate Qualification Hardware		
QV.6	Qualification System level Testing		
QV.7	Build Flight Hardware		
QV.8	Acceptance Testing		
QV.R1	Flight Acceptance Review	30/Jun/2034	
QV.R2	Flight Readiness Review	08/Mar/2036	
-----	**Schedule Margin**	**Duration: 20 months**	
OPS	**Operations and Utilization**	**08/Mar/2036**	**17/Jan/2037**
OPS.M1	Launch	08/Mar/2036	-----
OPS.1	Transfer Orbit	08/Mar/2036	-----
OPS.2	Cruise Phase to Venus	08/Mar/2036	28/Jun/2036
OPS.M2	Commission Orbiter	28/Jun/2036	-----
OPS.3	Venus Lander Coasting	28/Jun/2036	30/Jun/2036
OPS.M3	Perform Lander EDL	30/Jun/2036	-----
OPS.M4	Commission Lander	30/Jun/2036	-----
OPS.4	Science Phase	01/Jul/2036	17/Jan/2037
EL	**End-of Life and Disposal**	**18/Jan/2037**	**31/Jun/2037**
EL.1	Final Data Downloading		
EL.2	Decommisionning		
EL.3	Make Mission Closeout Report		
EL.4	Make Lesson Learned Report		
EL.R1	Mission Close-out Review	30/Sep/2037	

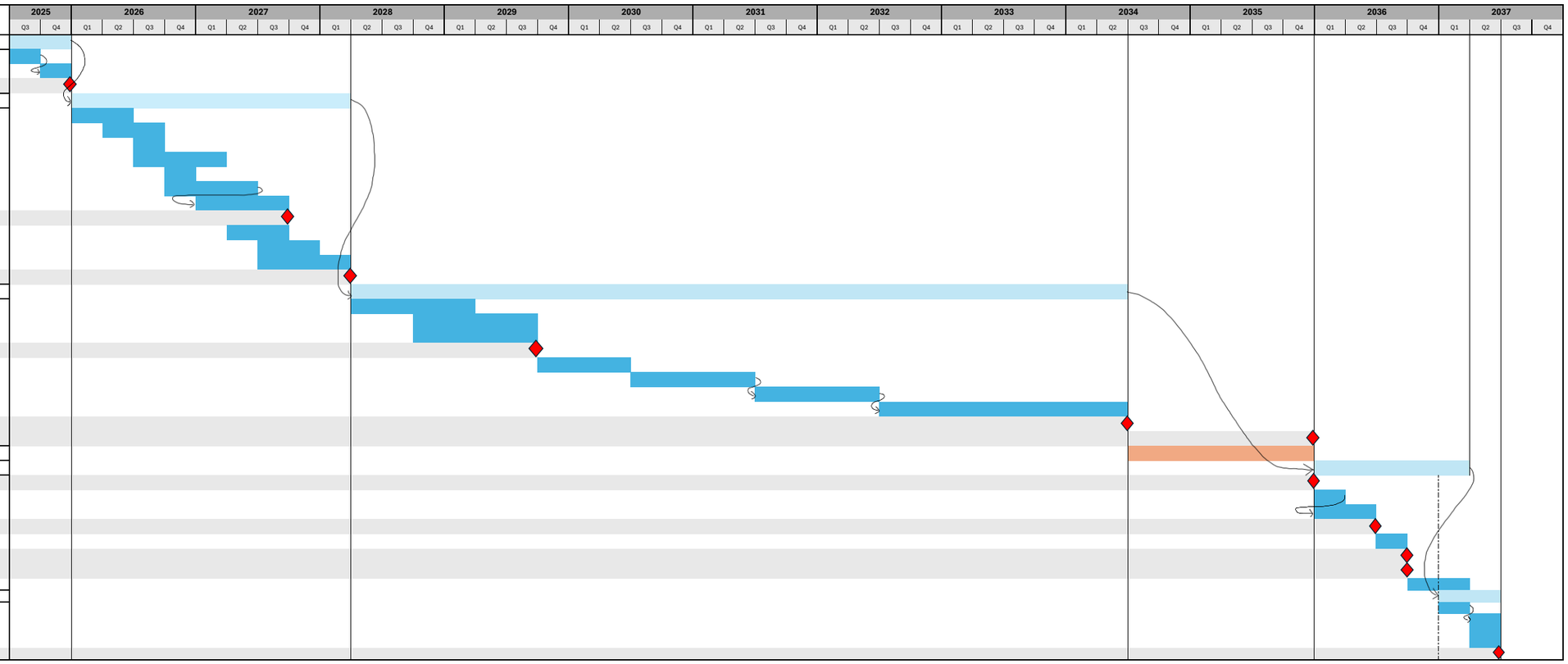

Appendix D

Communication Flow Diagram

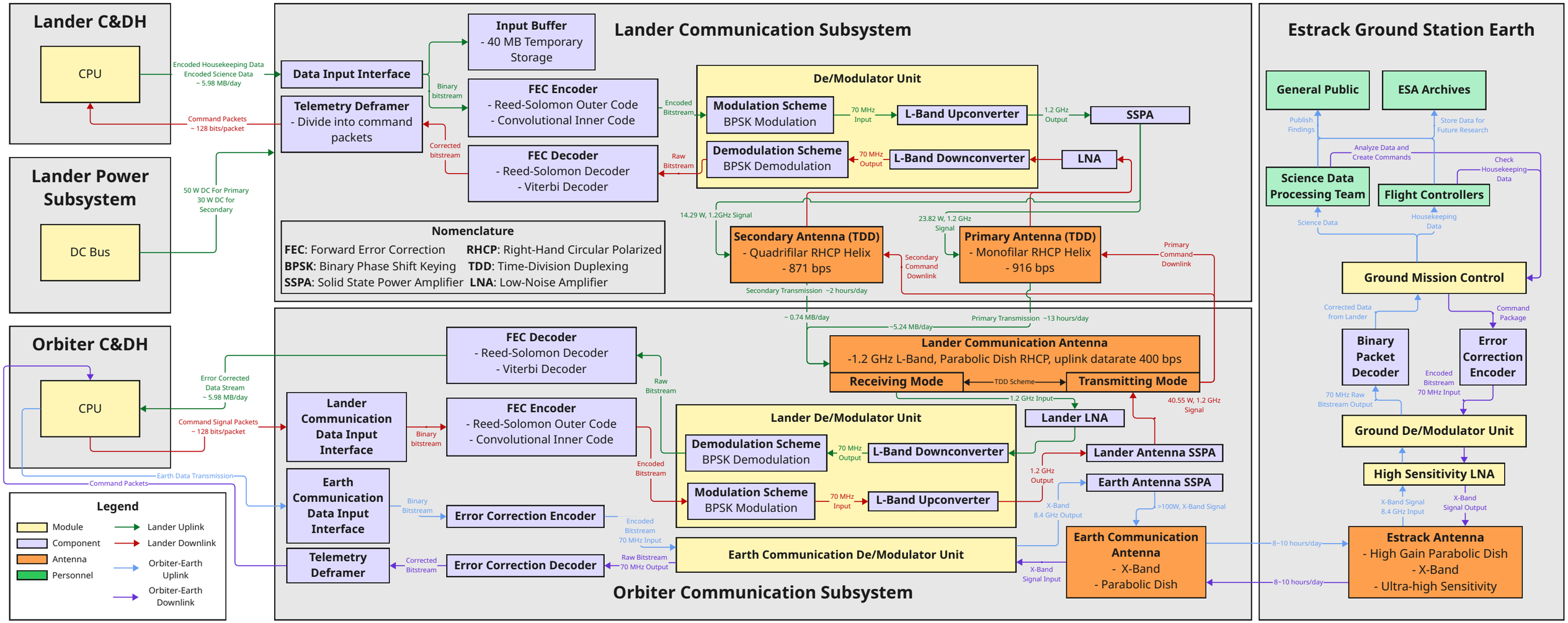

Appendix E

Requirement Deviation Request for Requirement GSYS-1 – Cost Budget

Project Name: KYTHERA

Date: 18/06/2025

Submitted by: Thomas Wijgerse, on behalf of DSE group 12

Requirement ID: GSYS-1

Requirement Description: Total lifetime cost, excluding the EDL system, shall not exceed 200 million EUR.

Description of Deviation

We request a deviation to the above requirement to allow the total cost ceiling to exceed the specified limit of 200 million EUR by 100 million EUR, resulting in a new total cost of 300 million EUR.

Justification

The aforementioned cost overrun is caused a much higher than anticipated cost in the Electrical Power Subsystem. 170 million EUR cost that is currently estimated versus a 40 million EUR allocated cost.

The aforementioned cost overrun is primarily due to:

- The unique mission environment and scope of the KYTHERA mission leading to an inaccurate cost estimation in the conceptual design phase.
- The required power system still being developed by external parties made it hard to pinpoint an accurate cost estimate until now.
- The requirement for a doubling of the required electrical power, due to higher than expected cooling power requirements.

Because of this, the requirement in question was incorrectly not designated as a killer requirement, and therefore was not re-baselined during the baseline review to a more realistic value.

Impact:

- Technical: No impact. Design does not change.
- Schedule: No impact. Procurement has not started yet.
- Cost: System level cost will increase.

Mitigation:

The team proposed to mitigate this cost overrun by:

- Seeking cost reductions in other systems.
- Seeking reduction of cooling requirements to allow for a cheaper electrical power subsystem.

This deviation request has been review and endorsed by:

Electrical Power Lead: Luka Lorenci

Systems Engineer: Thomas Wijgerse